NASA CR-54711
EOS Report 6954-Summary

ELECTRON BOMBARDMENT CESIUM ION ENGINE SYSTEM

by

G. Sohl, V. V. Fosnight, and S. J. Goldner

prepared for

NATIONAL AERONAUTICS AND SPACE ADMINISTRATION

CONTRACT NAS3-7112

ELECTRO-OPTICAL SYSTEMS, INC.
A Subsidiary of Xerox Corporation
300 N. Halstead St., Pasadena, California, 91107 · (213) 449-1230

Requests for copies of this report should be referred to

National Aeronautics and Space Administration
Office of Scientific and Technical Information
Attention: AFSS-A
Washington, D.C. 20546

NASA CR-54711
EOS Report 6954-Summary

SUMMARY REPORT

ELECTRON BOMBARDMENT CESIUM ION ENGINE SYSTEM

by

G. Sohl, V. V. Fosnight, and S. J. Goldner

prepared for

NATIONAL AERONAUTICS AND SPACE ADMINISTRATION

April 1967

CONTRACT NAS3-7112

Technical Management
National Aeronautics and Space Administration
Lewis Research Center
Cleveland, Ohio
James Wolters

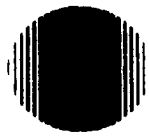

ELECTRO-OPTICAL SYSTEMS, INC.
A Subsidiary of Xerox Corporation

ABSTRACT

Development of a 1-kilowatt ion engine system is reported. This system, including a discharge neutralizer and "zero-gravity" feed system, produced 6.7 millipounds thrust at 5000 seconds specific impulse. Two systems were life tested for 3700 and 8200 hours, respectively, until exhaustion of their cesium supplies. A permanent magnet engine designed for operation at the same level as the life test engines and weighing only 1.6 lb is described. A fourth engine, which was built around the concept of an ac discharge, and controls for this engine, which automatically regulated the discharge power at its optimum level, are also reported.

SUMMARY

This summary report for the period 3 May 1965 to 16 December 1966 describes the work performed under Contract NAS3-7112, "Modification, Fabrication, Extended Testing, and Evaluation of Electron-Bombardment Cesium Ion Engine Systems." The engine developed under prior Contract NAS3-5250 was modified to provide increased thrust at lower specific impulse. Neutralizers were developed and included in the systems tested, along with "zero gravity" feed systems. At the design level of 1 kilowatt system power and 5000 seconds specific impulse the system power-to-thrust ratio was to be less than 160 kilowatts per pound.

Two systems were to be tested for durations of 2000 and 4000 hours. These systems operated at power-to-thrust ratios of 152.3 and 150.7 kilowatts per pound for 3700 and 8200 hours, respectively. Both systems were in excellent condition at the end of the tests, which were terminated by exhaustion of the cesium supplies.

A third engine system was fabricated and delivered to the NASA, Lewis Research Center. During tests at that center, performance obtained was identical to that of the life test engine systems.

Further effort on permanent magnet engine development resulted in an engine which weighed only 1.6 pounds. This engine, designed for the same operating level as the life test engines, was not operated. However, tests were conducted which verified the mechanical and magnetic features of the design.

Finally, an ac discharge engine was designed and tested. Performance was equal to that of the dc discharge engines. Automatic control of the discharge power was developed for this engine which maintained the discharge operation at the point of maximum engine efficiency.

CONTENTS

CONTENTS (Contd)

ILLUSTRATIONS

ILLUSTRATIONS (contd)

ILLUSTRATIONS (contd)

ILLUSTRATIONS (contd)

SECTION 1

INTRODUCTION

The work described in this report was performed under Contract NAS3-7112 administered by the National Aeronautics and Space Administration's Lewis Research Center. This program was a follow-on to Contract NAS3-5250 and consisted primarily of extended life testing of engine systems using an engine similar to the Model DF engine developed and tested under that contract. This report describes the development of the Model DG engine system and life tests of two DG engine systems of 3700 and 8200 hours. Design of a permanent magnet engine and development of an ac discharge engine with automatic control are described.

1.1 BACKGROUND

This was the fourth program in a series which covered development of the high-efficiency, long-lived, cesium electron-bombardment ion engine following its proposal by Forrester and Speiser in 1961. They proposed this approach after Kaufman of NASA-LeRC demonstrated the feasibility of the use of a low-density mercury plasma as a source of ions for electric propulsion in 1960.

The Kaufman source (Ref. 1,2), using mercury as propellant, consists of a thermionic cathode placed inside a cylindrical anode with a magnetic field parallel to the axis of the system. A plasma is generated within the cylinder, and those ions which drift to one end are extracted through apertures in a screen by an accelerating electrode.

The feasibility of the use of cesium for the propellant was demonstrated at EOS under Contract NAS8-2511 (Ref. 3). The source tested under that program utilized the first cesium autocathode. This cathode, which has been a key to long life and high efficiency, emits electrons from a tantalum surface over which the cesium is passed into the chamber. Cesiated-tantalum cathodes are capable of one ampere per square centimeter emission currents at only 600°C. The temperatures required are low enough to use only ion bombardment and radiation from the plasma to maintain operation, and external heat is required only for starting. The long lifetime is due, in part, to the low bombarding ion energies and resultant lack of sputtering. Other advantages of the use of cesium are the absence of doubly-charged ions, low magnetic fields, and a high degree of ionization.

Under a follow-on contract (Contract NAS3-2516) a 12.5-centimeter diameter source was developed. This engine, designated Model DE, operated at a power-to-thrust ratio of 200 kilowatts per pound at 7000 seconds specific impulse. Two engine systems including "zero gravity" feed systems and laboratory power supplies and control systems were developed and delivered to NASA-LeRC (Ref. 4).

In the third program, Contract NAS3-5250, continued research and development resulted in the Model DF engine which operated at a power-to-thrust ratio of 182 kilowatts per pound at 7000 seconds specific impulse (Ref. 5,6). This engine, Model DF-1, was operated in three consecutive tests for a total time of 2610 hours. A modified permanent magnet version of the engine was built utilizing a cylindrical permanent magnet which also functioned as the engine shell.

1.2 PROGRAM OBJECTIVES

In early 1965 when this program was begun, it was apparent that practical lightweight power was not to be realized as early as previously hoped. This meant that lower specific impulse, even with reduced efficiency, would be required to reduce total power and hence the weight for a given system. The goals of this program were set at a power-to-thrust ratio of 160 kilowatts per pound or less at a specific impulse of 5000 seconds. A 1-kilowatt power level was selected which was an increase of about 30 percent over the capability of the DF engine at 5000 seconds specific impulse. Two complete systems, including "zero gravity" feed systems and plasma bridge neutralizers were to be tested for 2000 and 4000 hours, respectively.

Permanent magnet engine development was pursued and an engine which utilized an alternating current power source for the discharge was evaluated.

1.3 ORGANIZATION OF REPORT

Development of the Model DG engine systems for life testing is described in Section 2 followed by a description of the life tests in Section 3. A third engine system, described in Section 4, was built and delivered to NASA-LeRC. Section 5 covers the work done on permanent magnet engines. The ac discharge engine development and its automatic control system are described in Section 6. The quality assurance system used in conjunction with the life testing is described in Section 7.

The authors wish to acknowledge the assistance of Mr. F. A. Barcatta and Mr. G. E. Trump, who provided the feed systems support for this program, and Mr. R. H. Vernon, Mr. K. G. Wood, Mr. T. R. Dillon, and Mr. L. J. Olinger, who performed much of the work on the DG-3 and DGA systems. Mr. D. P. West did another fine job of design, and the quality assurance support of Mr. S. Zafran was very effective. It would be difficult to list the name of each person whose contributions had a direct effect upon the success of this program. The total cooperation achieved was due in large measure to the excellent program management provided by Mr. R. C. Speiser.

SECTION 2

DG ENGINE SYSTEM DEVELOPMENT

The starting point for the program was the DF engine, which had been tested in three consecutive runs for a total of 2610 hours at 10 millipounds thrust and at a specific impulse of 7000 seconds (Ref. 5). While the DF engine had been operated over a specific impulse range of 3000 to 8000 seconds, the thrust obtainable at 5000 seconds was about 6 millipounds. That level of thrust required a high negative accelerator potential nearly equal to the positive source potential) which was not desirable from the standpoint of long lifetime. Since the efficiency of the DF engine was already high, no increase in engine efficiency was anticipated under the present program, but an increase in thrust was sought.

The DF engine with the 750-hour feed system (approximately 5-pound capacity) is shown in Fig. 1. This engine incorporated distributed geometry, high-perveance electrodes which promised lifetimes in excess of 20,000 hours as extrapolated from the 2610-hour test results. No erosion of the cathode had occurred during those tests but the reliability of the internal heater had not been firmly established.

2.1 DG ENGINE DEVELOPMENT

The first requirement of the DG engine design was for higher electrode perveance. The aperture-diameter distribution function found to be successful with the DF engine was used. The aperture diameters were reduced about 80 percent. To obtain a good fit to the distribution function four aperture diameters were used on the new electrodes. By thus reducing aperture diameters and by decreasing aperture spacings, the number of apertures was increased by 67 percent. To maintain the same ion optics focusing, the spacing between the electrodes was also reduced. The result of increasing the number of apertures and decreasing the gap was a significant increase in overall electrode perveance (the ratio of maximum beam current to the 3/2 power of the potential difference between the electrodes). This increase in perveance allowed an increase in the beam current along with a reduction of the accelerator electrode potential to a low enough value to maintain the lifetime of the DF engine.

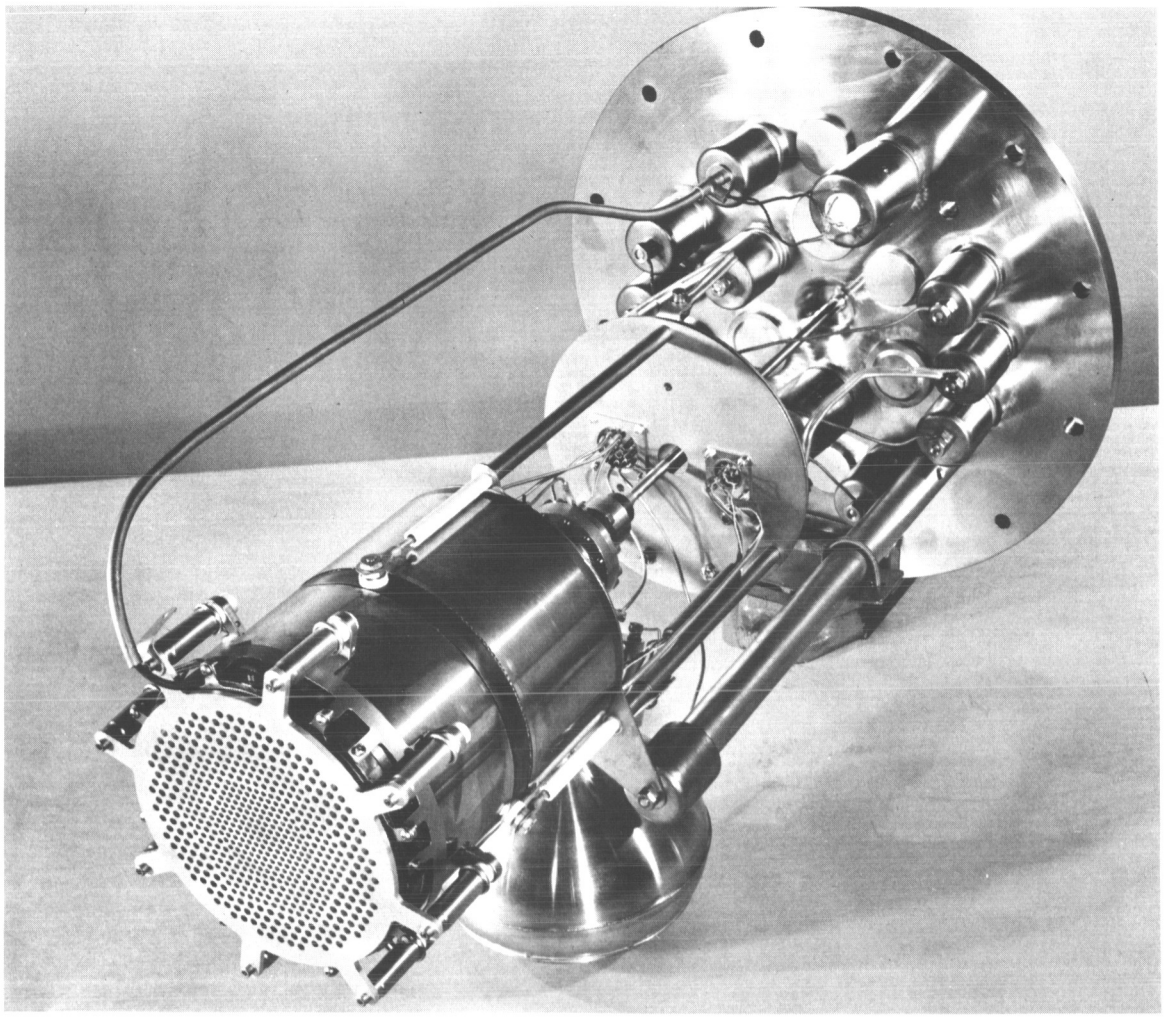

Figure 1. DF Engine with 750-Hour Feed System

Figure 2 shows the prototype screen electrode with the new aperture pattern. The transparency of this electrode was increased by about 10 percent. This created web areas between apertures which were too small for conventional machining techniques. In order to fabricate this new electrode it was necessary to machine oversize and chemically etch the part down to the desired dimensions. This process proved successful.

Figure 3 shows the perveance of the DG electrodes compared with that of the DF electrodes. Performance data for a DF engine using each of these electrode systems are listed in Table I. The goal of increased thrust and reduced accelerator potential was achieved with the DG electrodes.

The second major change in the engine consisted of redesigning the cathode. A solid tantalum structure was designed to replace the internally heated emitter of the DF cathode and the starting heater was placed on the outside of the cathode. The two cathodes are shown schematically in Fig. 4. While the cathode heating time was increased slightly, no difficulty in initiating the discharge was encountered with the new cathode. Source efficiency with the new cathode was as good as that with the DF engine cathode.

In addition to the changes described above, some minor design modifications were made in the engine configuration. Most significant among these was the elimination of four of the accelerator electrode support insulators. This was made possible by the weight reduction obtained when the accelerator electrode was changed from 0.062 inch thick copper to 0.125 inch thick aluminum under Contract NAS3-5250 (Ref. 5).

Efficiency of the DG engine is equivalent to that of the DF engine. An increase in mass efficiency at 5000 seconds due either to increased electrode transparency or to the new cathode was offset by a slightly higher drain current. While the electrode spacing was reduced (lower voltages), the thickness of the accelerator was not changed. This required more precise ion trajectories to prevent interception near the downstream end of the accelerator apertures. Therefore, higher accelerator drain current was expected initially, but this current was expected to decrease as the apertures erode on the downstream side during any extended test.

2.2 FEED SYSTEMS

To fulfill the requirements of this program, three different zero-g cesium feed systems were used. Two were new designs and the third was a modification of a feed system developed under Air Force Contract

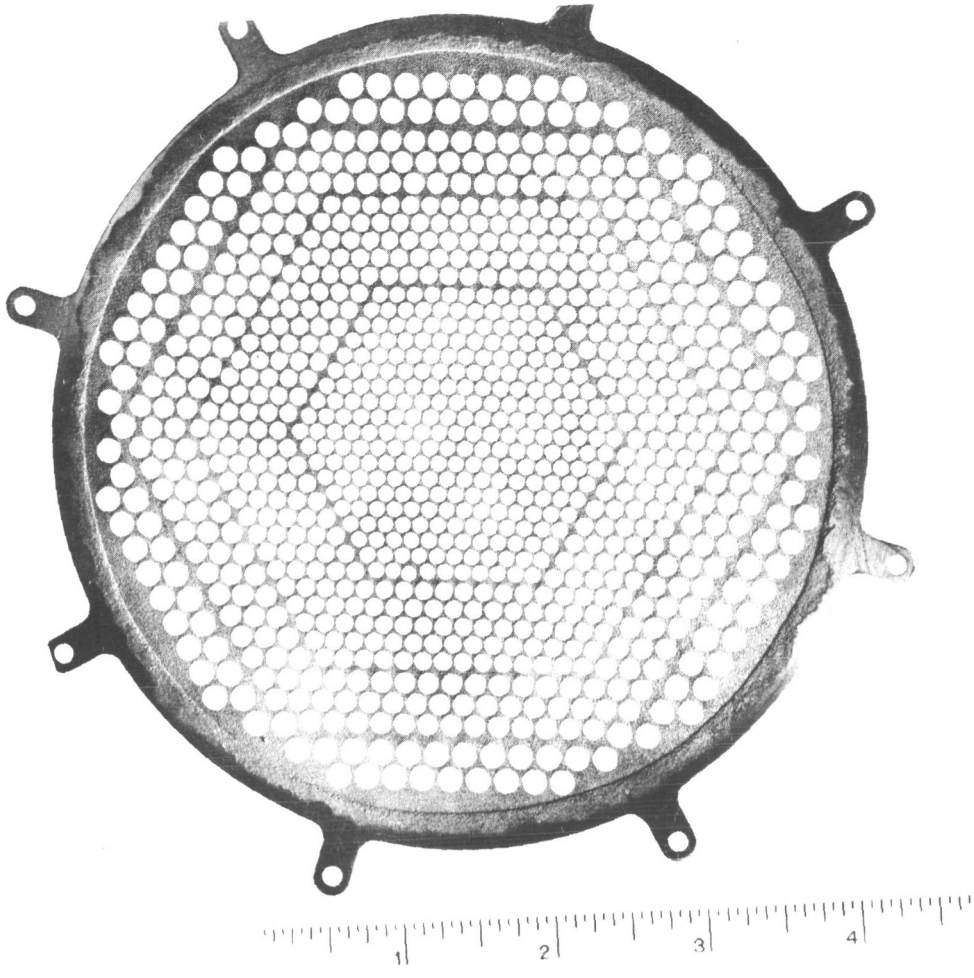

Figure 2. Prototype DG Screen Electrode

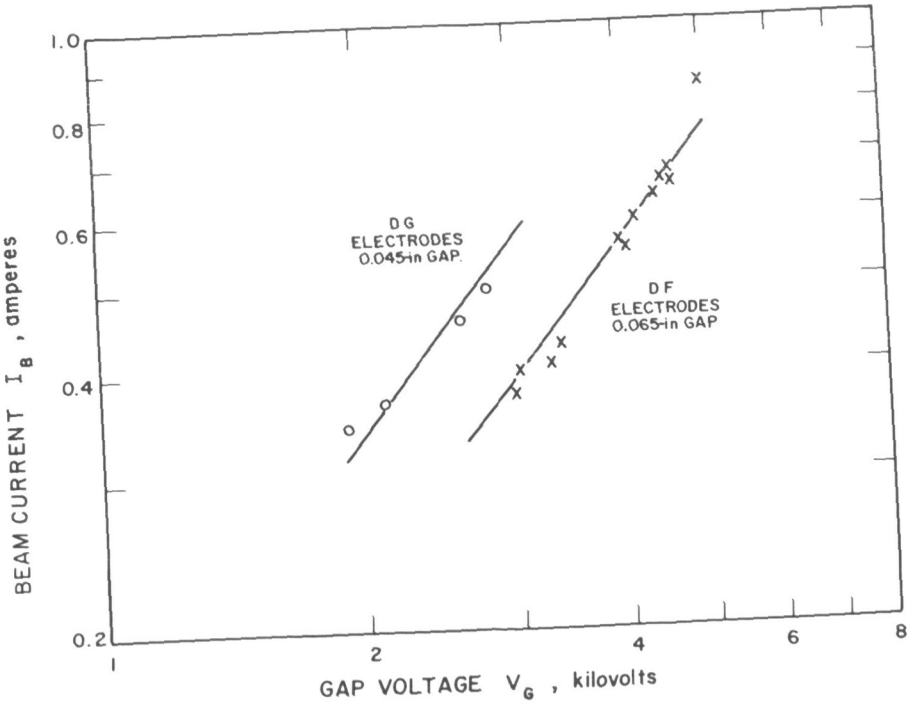

Figure 3. Perveance of DF and DG Electrodes

TABLE I

DF ENGINE PERFORMANCE WITH DF AND DG ELECTRODES

	DF	DG
Positive High Voltage, V_+ (kV)	2.05	2.0
Negative High Voltage, V_- (kV)	1.7	0.7
Negative HV Current, I_- (A)	0.0060	0.0063
Beam Current, I_B (A)	0.355	0.402
Arc Voltage, V_A (V)	6.5	7.7
Arc Current, I_A (A)	17.5	18.0
Magnet Current, I_M (A)	2.3	2.2
Beam Power, P_B (kW)	0.728	0.804
Drain Power, P_D (kW)	0.023	0.017
Magnet Power, P_M (kW)	0.013	0.012
Arc Power, P_A (kW)	0.114	0.139
Total Power, P_E (kW)	0.878	0.972
Thrust, T (mlb)	6.05	6.77
Power-to-Thrust Ratio, P/T (kW/lb)	145.1	144.0
Power Efficiency, η_p (%)	82.9	82.7
Mass Efficiency, η_M (%)	92.0	92.2
Overall Engine Efficiency, η_E (%)	76.3	76.2
Specific Impulse, I_{sp} (sec)	5099	5050
Ratio of Drain Current to Beam Current, I_-/I_B (%)	1.69	1.57
Source Energy per Ion, P_A/I_B (keV/ion)	0.321	0.346

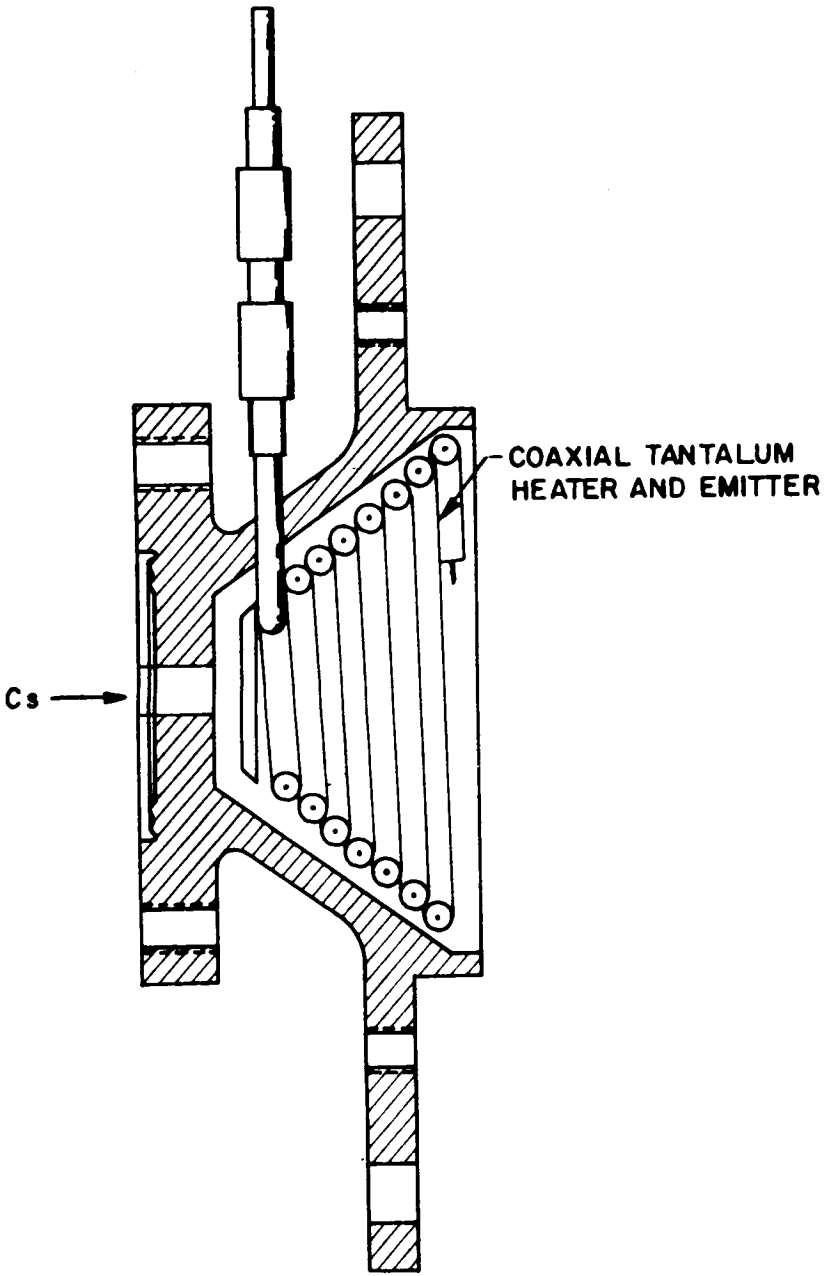

a. INTERNAL HEATER CATHODE (DF)

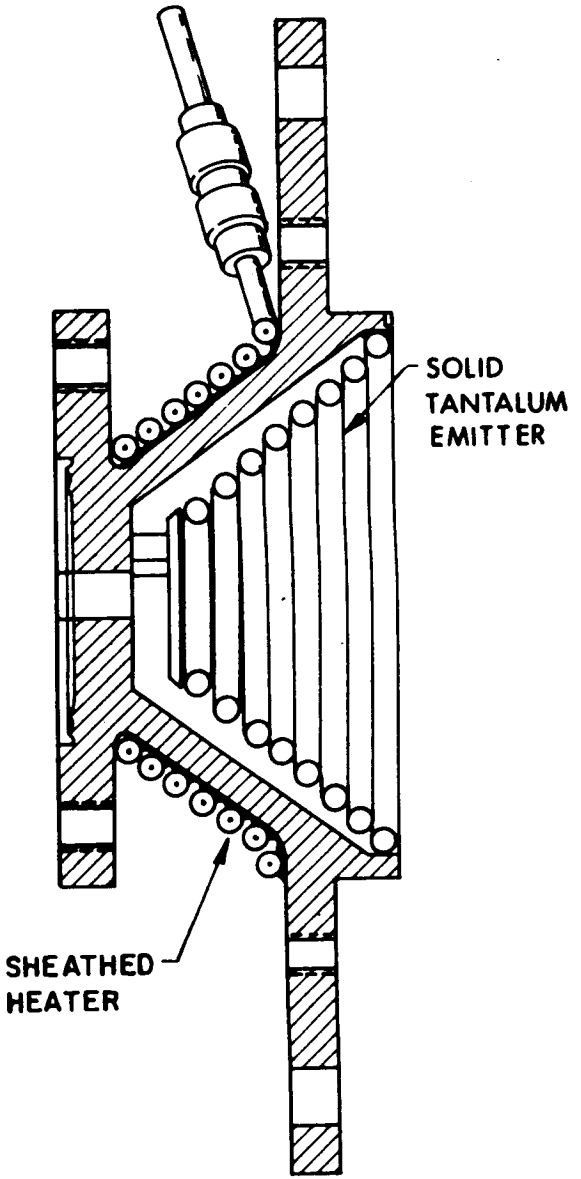

b. EXTERNAL HEATER CATHODE (DG)

Figure 4. DF and DG Cathode Designs

AF 33(657)-10980 (Ref. 7). All three feed systems depend solely upon surface tension forces to separate the liquid and vapor phases within the storage volume and to deliver cesium to the vaporizer (Ref. 8). Controllable feed is obtained from the vaporizer by heating and resultant evaporation. Each feed system consists of a storage volume broken into tapered cells which bring cesium to a porous nickel wick on the reservoir axis. One end of this wick forms the vaporizer surface from which the cesium is evaporated.

2.2.1 THE 20-POUND FEED SYSTEM

This feed system, shown in Fig. 5, had a manually operated feed valve and an electrically operated port valve. These valves were used to protect the cesium from the atmosphere and resultant contamination during handling in the laboratory. This system (less the manual valve) was developed under the above mentioned Air Force program.

The manual valve (shown in Fig. 6) was opened at the start of engine testing and closed before the system was removed from the vacuum chamber. The actuating rod was retracted during engine operation to allow for high voltage isolation.

Figure 7 shows the reservoir port valve used to evacuate the reservoir ullage during pumpdown of the test facility. An electromagnet actuation system was used here since this valve is allowed to close and remain closed during engine operation.

Figure 8 shows the test assembly for the 2000-hour test. A U-shaped tube was incorporated to reduce the total system height for installation into the vacuum chamber. The reservoir heater shown in Fig. 8 is used only to heat the reservoir before operating the engine to ensure that the cesium wets the reservoir fins and the porous nickel wick. This function is unnecessary for flight systems, as will be apparent from the discussion in Subsection 2.2.3 (Neutralizer Feed Systems).

The actual capacity of the 20-pound feed system was slightly over 18 pounds of cesium. Some of this capacity would be expended by startups and performance mapping, but a comfortable margin existed to cover possible false starts.

2.2.2 THE 40-POUND FEED SYSTEM

For the 4000-hour test a feed system with about twice the capacity of the 20-pound feed system was designed. This system had a capacity of 42 pounds of cesium and is illustrated in Fig. 9.

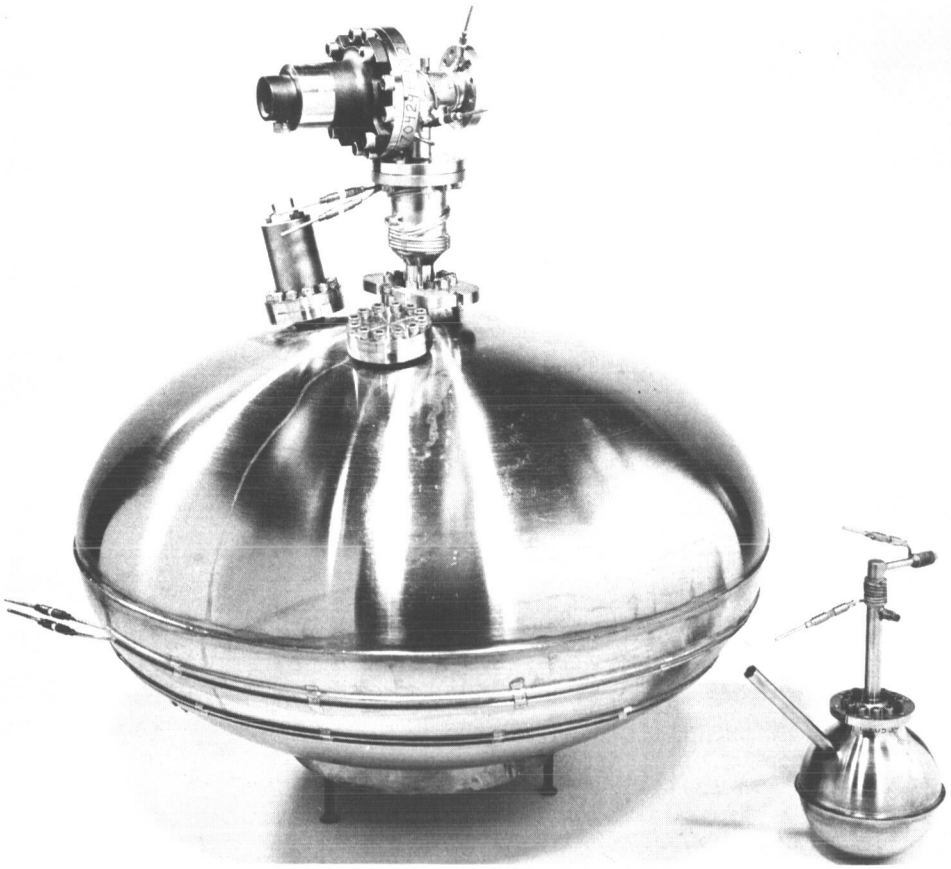

Figure 5. The 20-Pound Feed System

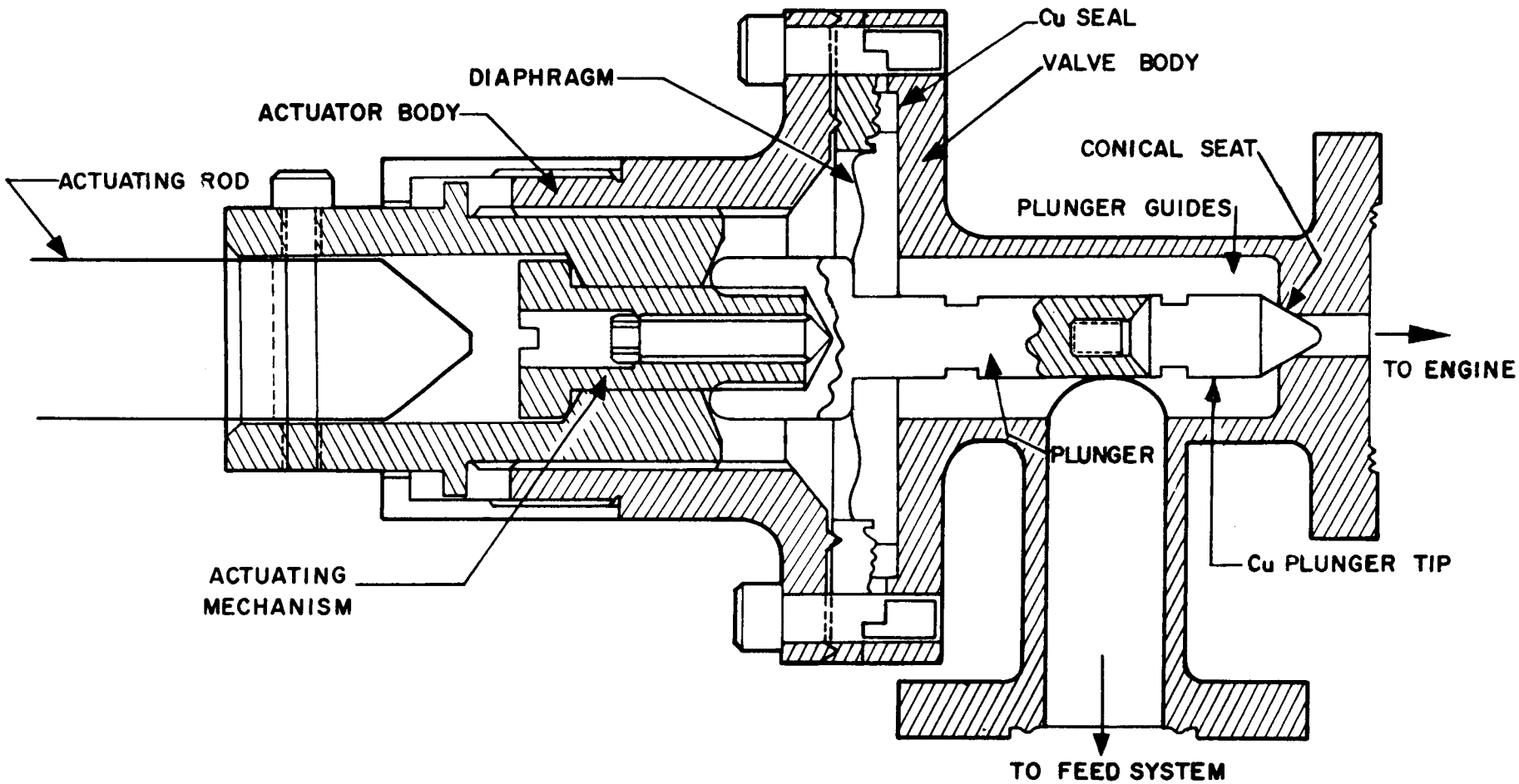

Figure 6. Manual Valve Design

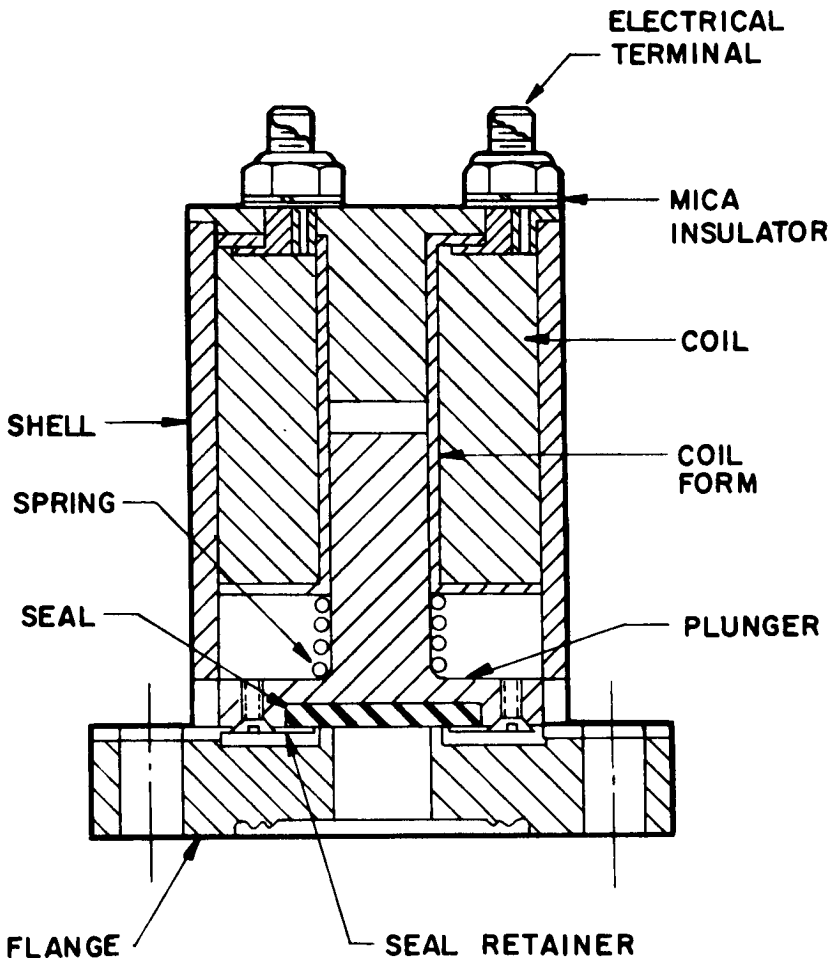

Figure 7. Port Valve Design

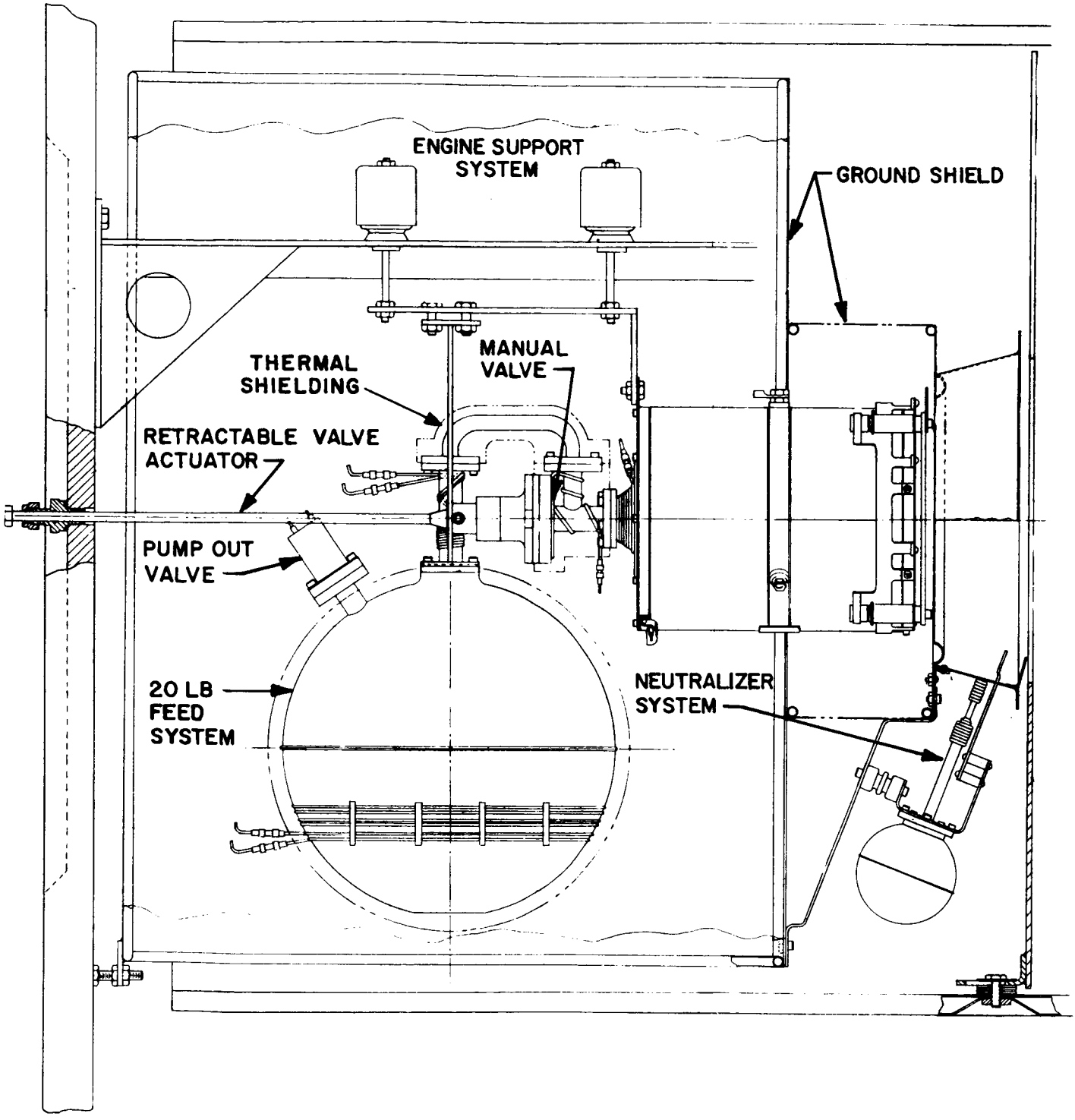

Figure 8. The 2000-Hour Test Assembly

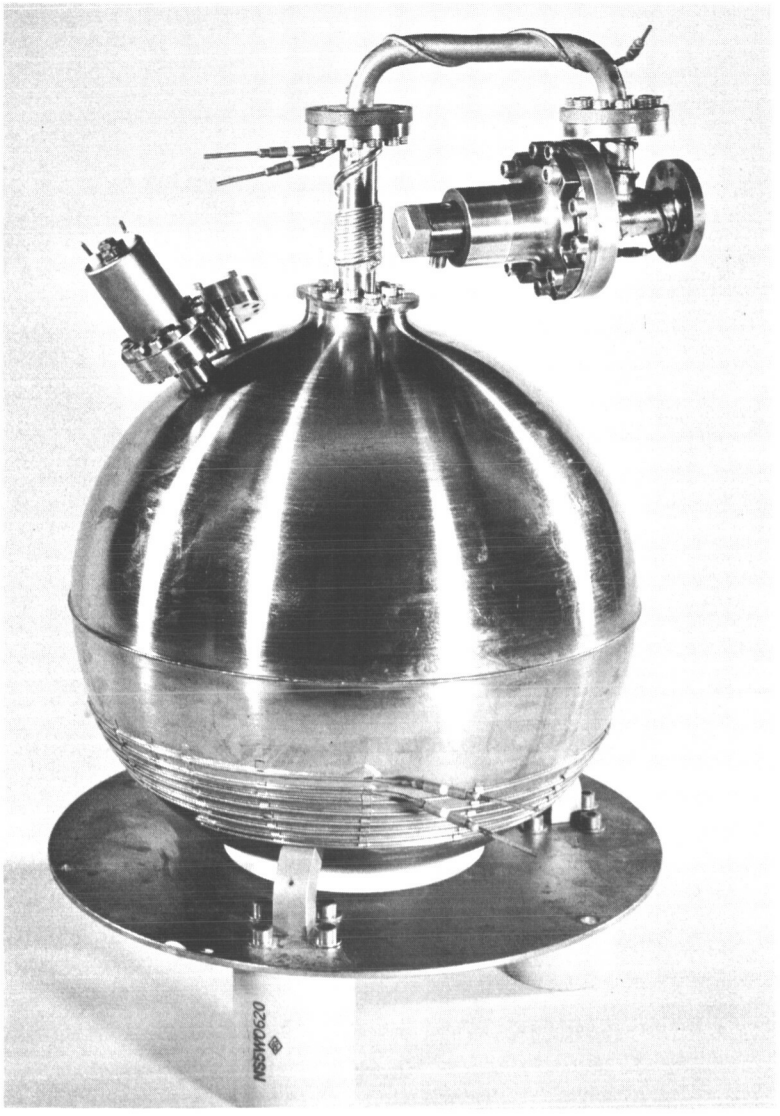

Figure 9. The 40-Pound Feed System and 10,000-Hour Neutralizer

In order to reduce the height (significant only for testing in a 1-g environment) of the porous rod, it was decided to shape the reservoir in the form of an oblate spheroid. The resultant height of the porous rod was 8 inches, approximately the same as that of the 20-pound system. The reservoir had a minor diameter of 8 inches and a major diameter of 13 inches.

To help minimize the feed system weight, only 90 fins were placed in the reservoir storage volume. This then required expansion of the vaporizer section to a diameter of 1 inch in order that the location of the liquid could be stabilized in a theoretical zero-g environment.

2.2.3 NEUTRALIZER FEED SYSTEM

The third feed system was the 1/2-pound neutralizer feed system designed to operate the neutralizer for 10,000 hours. Figures 10 and 11 show exploded and assembled views of this feed system. The reservoir is 2-1/2 inches in diameter and has fin structure consisting of 72 fins. A porous nickel rod inserted along the central axis delivers liquid cesium to the vaporizer (shown in Fig. 12).

Unlike the other feed systems, which used a port valve to evacuate the reservoir ullage after loading and during pumpdown of the vacuum chamber, this system entered the vacuum chamber completely evacuated and with the porous rod wetted with cesium. The neutralizer with its orifice sealed with cadmium was attached to the reservoir and the system was then leak-checked, loaded with cesium, evacuated, and sealed by melting shut the end of the fill tube in the electron-beam welding machine. The sealed system was then heated in an oven to 200°C to wet the porous rod. The first time the neutralizer cathode was heated after evacuation of the chamber, the cadmium orifice seal evaporated and the feed system was ready for operation.

2.3 NEUTRALIZERS

Early in 1965 a new neutralizer concept was developed at Electro-Optical Systems under Air Force Contract AF 33(615)-1530 (Ref. 9). This device promised long life at high efficiencies, so tests of the new neutralizer approach were started immediately under Contract NAS3-5250 (Ref. 5). These tests were continued in this program, and a neutralizer and neutralizer control system were developed for use on the long tests.

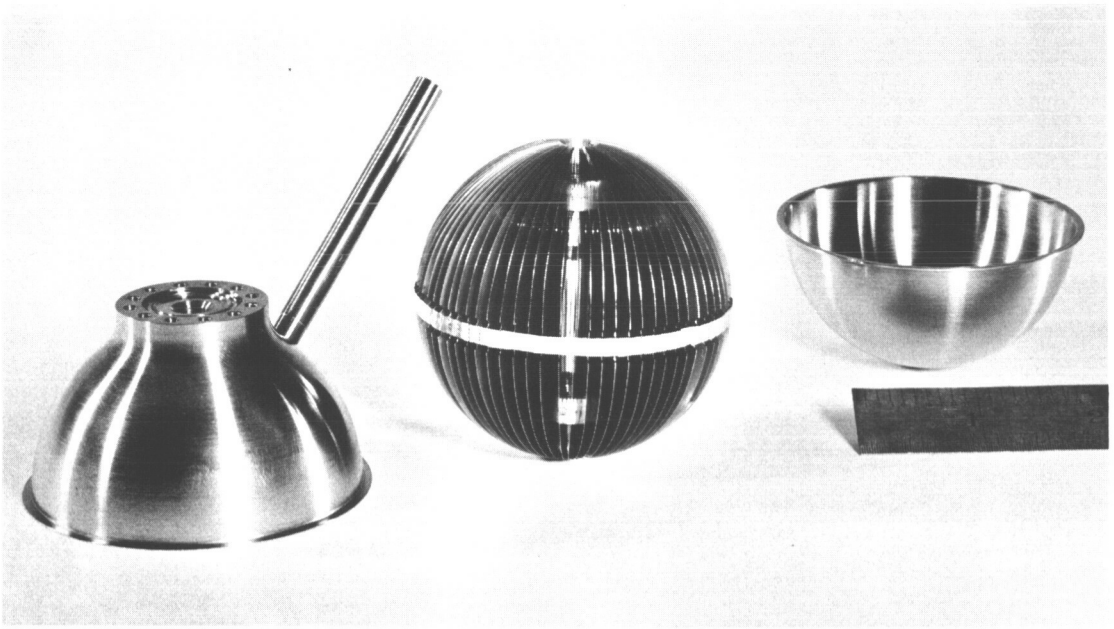

Figure 10. The 1/2-Pound Feed System Reservoir - Disassembled

Figure 11. The 1/2-Pound Feed System Reservoir - Assembled

86543
86541

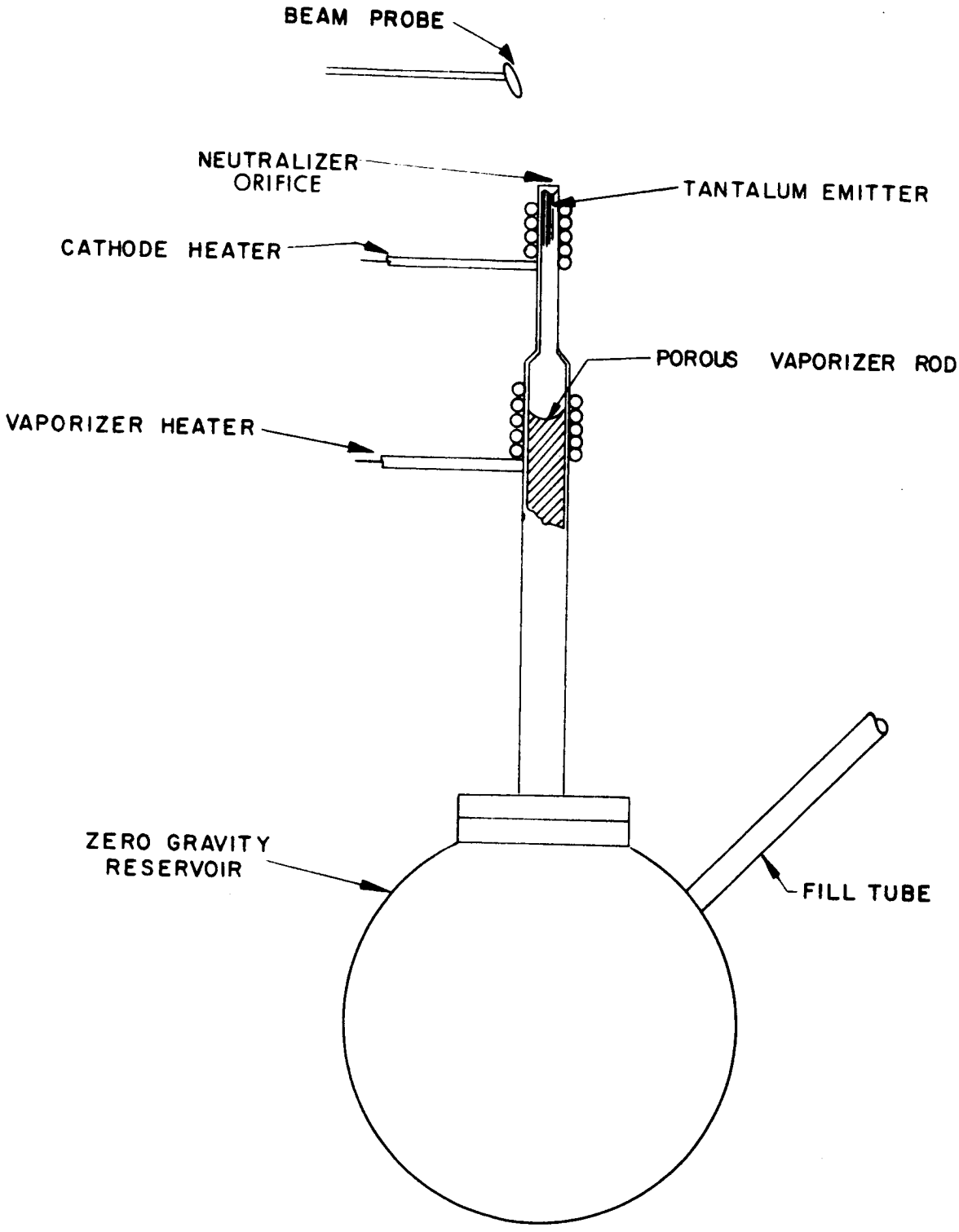

Figure 12. Prototype Neutralizer

2.3.1 NEUTRALIZER OPERATION

Figure 13 is a cutaway of the DG prototype neutralizer. Electrons are emitted by an externally heated, cesiated tantalum cathode similar in operating principle to the DG engine cathode. Cesium vapor is supplied to the emitter surfaces from a "zero gravity" feed system. The cathode chamber is heated to about 500°C by a sheathed external heater. A small orifice in the cathode chamber, typically 0.007 inch in diameter, faces the ion engine beam.

A discharge is established between the grounded neutralizer and the ion beam which, if unneutralized, floats to a positive potential. From this discharge, the ion beam acquires the electrons it needs for neutralization. The beam potential required to sustain the discharge is typically 4 to 8 volts, much lower than had been obtainable with conventional thermionic neutralizer cathodes. The neutralizer could be mounted several inches from the beam even at these low beam potentials because ions that formed in the discharge helped overcome space charge effects.

The continuous cesium loss with this neutralizer reduces the system specific impulse. This can be corrected by slightly increasing the engine specific impulse from its original level. Properly contained cathodes of this type have demonstrated emission ratios of over 100 electrons per cesium atom, so the loss of cesium from the neutralizer was expected to be less than 1 percent of the engine flow rate. Flow rates for these neutralizers were found to be nominally 0.80 percent of the engine flow rates on the life tests.

The neutralizer requires power for the cathode and the vaporizer heaters. Both of these could have been heat shielded but the total power consumption was only 10 watts during the life tests.

2.3.2 NEUTRALIZER CONTROL SYSTEM

Cathode heater power for the "plasma bridge" neutralizer may be preset. It was anticipated, however, that the large changes in cesium flow rate that could be obtained with small vaporizer temperature changes would not be tolerable for long-duration testing and that some vaporizer control would be required.

Control of the vaporizer power required some form of information feedback. The system parameter which was most dependent upon the cesium flow rate through the neutralizer was the beam potential, approximated by the potential of a floating collector in the vacuum facility.

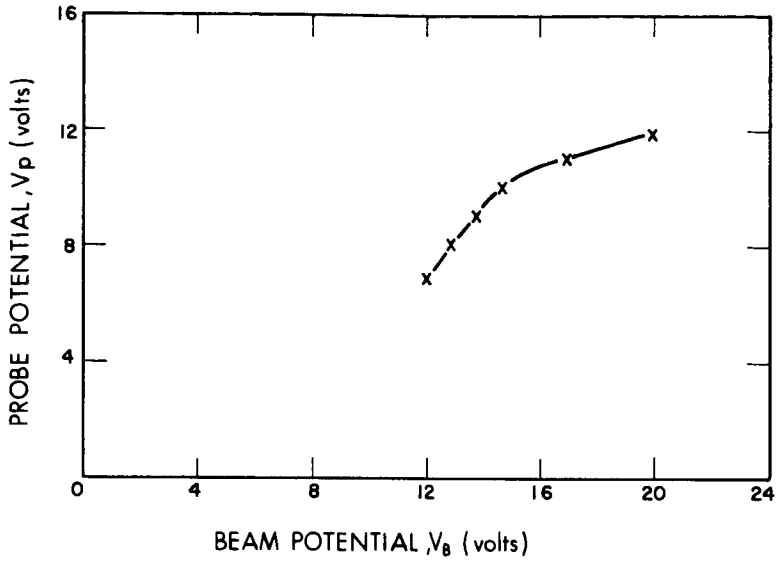

Figure 13. "Plasma Bridge" Probe Characteristics

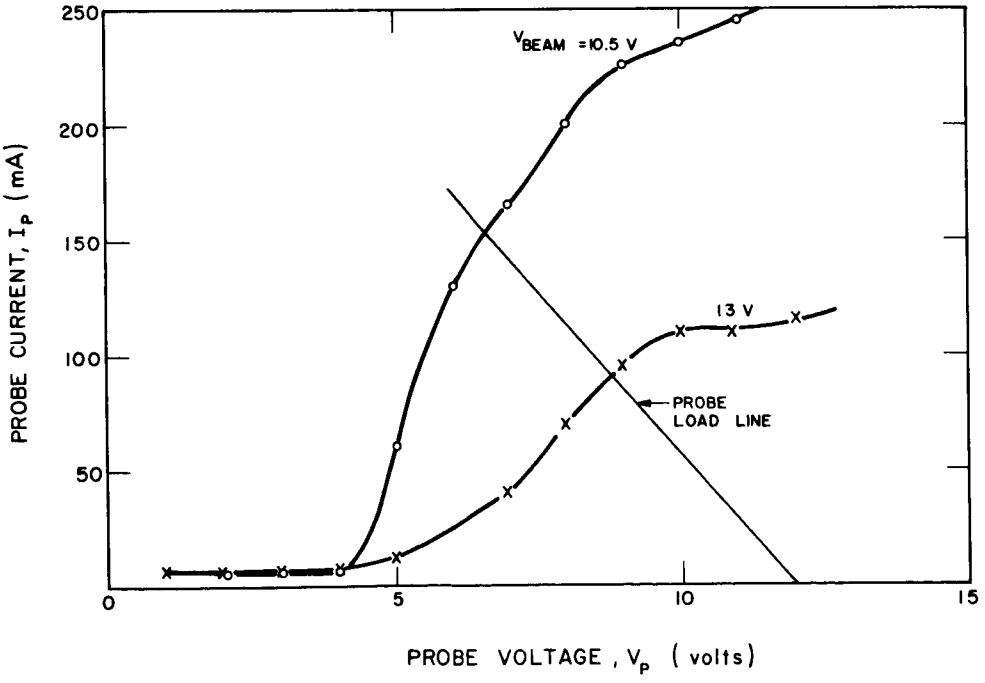

Figure 14. Probe Potential Correlation

Increasing the flow rate reduced the beam potential. Thus, it was possible to adjust the vaporizer power to maintain a given beam potential. However, for a control system to be realistic, the collector could not be used as the feedback sensor.

Beam Potential Probe

Since a plasma will attach itself to the most positive object it contacts, the "plasma bridge" was assumed to be at or near the beam potential. Langmuir probing of the low-energy "plasma bridge" would then yield beam potential information. This probe would not sputter away during long-term operation as would a probe immersed in the ion beam. Figure 13 shows probe I-V characteristics taken for two values of "beam" potential with an operating neutralizer. The "beam" for this experiment was a copper screen located about 2 inches from the neutralizer. The probe used was similar to that shown in Fig. 16.

A probe biased through a 33-ohm resistor from a 12-volt supply would operate along the load line shown in Fig. 13. While a probe operated in this manner will not measure true plasma potential, positive correlation between the probe and beam potentials can be obtained. Figure 14 shows the correlation obtained with a 400 milliamperes constant current source applied to the "beam". These data were taken as the vaporizer was allowed to cool, causing the "beam" potential to rise. An automatic vaporizer feedback control was synthesized based on the results of these tests.

2.3.3 PROTOTYPE NEUTRALIZER

The prototype neutralizer is shown in Fig. 15. A long narrow vaporizer section was used to minimize heat losses. This neutralizer, shown in Fig. 16 with the probe, was tested with the DG engine. Table II lists the operating parameters obtained and the net effect on engine performance. The cesium loss was converted to an equivalent power loss and the power associated with accelerating electrons to the beam was included. This "perveance" power is offset by the initial acceleration of ions from plasma potential to the potential of the screen electrode. Since these powers are small and nearly equal they are usually neglected; perveance power is shown here to allow comparison with other neutralizers.

As shown the effective cost of neutralization was about 20 watts or 2 percent of the DG system power of 1 kilowatt. This was far superior to any other available neutralizer.

Figure 15. Prototype Neutralizer

Figure 16. Neutralizer Assembly

TABLE II

NEUTRALIZER OPERATING PARAMETERS
AND TOTAL EQUIVALENT POWER

Cathode Heater Power, P_K	3.9 watts
Vaporizer Heater Power, P_V	10.2 watts
Emission Current, I_N	0.4 ampere
Beam Potential,[1] V_B	9.5 volts
Perveance Power,[2] $V_B I_N$	3.8 watts
Cesium Flowrate[3] (percent of Engine Flowrate), η_{cs}	1.0 percent
Slope of Engine P/T vs I_{sp} Curve at 5000 seconds, ^{sp}K	17 watts/pound-second
Engine Thrust, T	6.77 millipounds
Engine Specific Impulse, I_{spE}	5050 seconds
Neutralizer Flowrate Penalty in Equivalent Power, (η_{cs} K T I_{sp} x 10^{-5}), P_{cs}	5.8 watts
Total Neutralizer Power, P_N	23.9 watts
Neutralizer P/T Penalty, P/T_N	3.5 kilowatts/pound

[1] Correlation between engine beam current and neutralizer emission current was within 5 percent.

[2] Potential of isolated collector in the vacuum system.

[3] Estimated from previous tests.

SECTION 3

EXTENDED TESTS

Two extended tests were performed under the contract. Both tests were run with DG engines. The DG-1 engine was used on the 2000-hour (nominal) test and the DG-2 engine was used on the 4000-hour test. The second test was begun before the first had terminated. These tests were run for 3700 and 8200 hours, respectively, with no loss of vacuum in either test.

3.1 THE 2000-HOUR, DG-1 ENGINE SYSTEM TEST

The DG-1 engine system, test facility, control system, extended test, and analysis are described in the following subsections.

3.1.1 THE DG-1 ENGINE SYSTEM

The DG engine was described in Section 2. The system tested (Fig. 17) included the DG-1 engine, a 20-pound capacity cesium feed system, and the two plasma-bridge neutralizers of the type mentioned in Subsection 2.7. The complete system with ground screen is shown in Fig. 18. Two neutralizers were included as any failure modes had not yet been accurately determined. It was planned to use one only and keep the second for a spare. This was done and one neutralizer functioned throughout the test.

The 20-pound feed system previously described was used on this test. The design engine flow rate was 2.16 grams per hour of operation. The reservoir was loaded with just over 18 pounds of cesium. This would provide 3600 to 3800 hours of operation at design levels. About 2 grams of cesium were to be used for startup and 30 grams for initial performance mapping of the engine. The neutralizer was expected to expel cesium at a rate of 1 percent of the rate of the engine flow. About 215 grams of cesium, enough for over 10,000 hours of operation, was loaded into each neutralizer. Thus a wide safety margin was provided with respect to the fulfillment of the required 2000-hour test period.

Careful attention was paid to the provision of adequate ground shielding to prevent electrons reaching the engine from the neutralizer. Any such "backstreaming" causes erroneously high beam current readings and engine efficiency calculations.

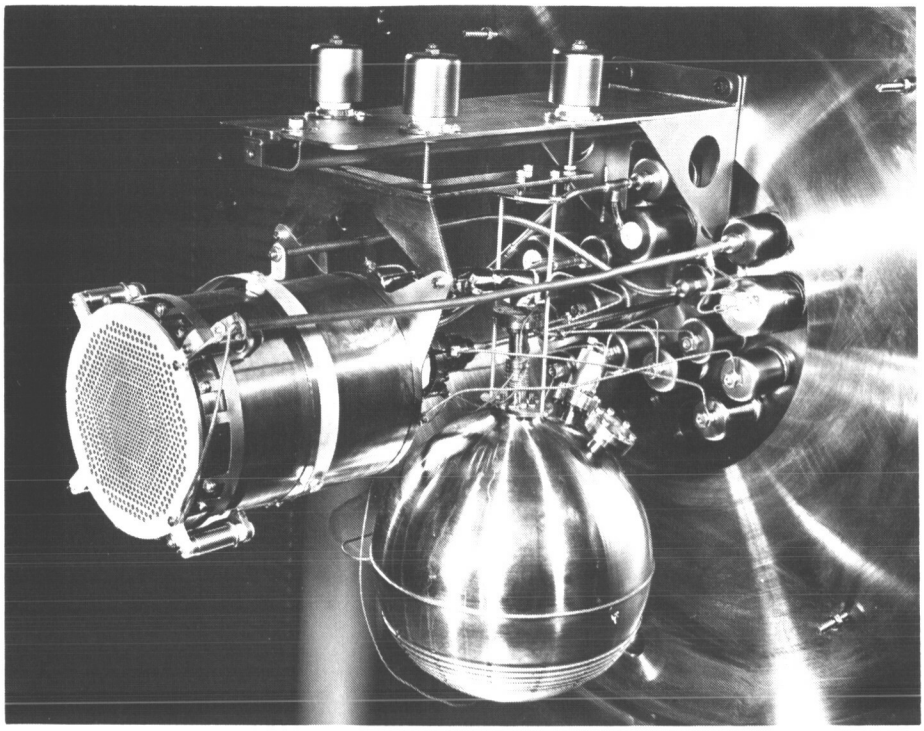

Figure 17. DG-1 Engine and Feed System

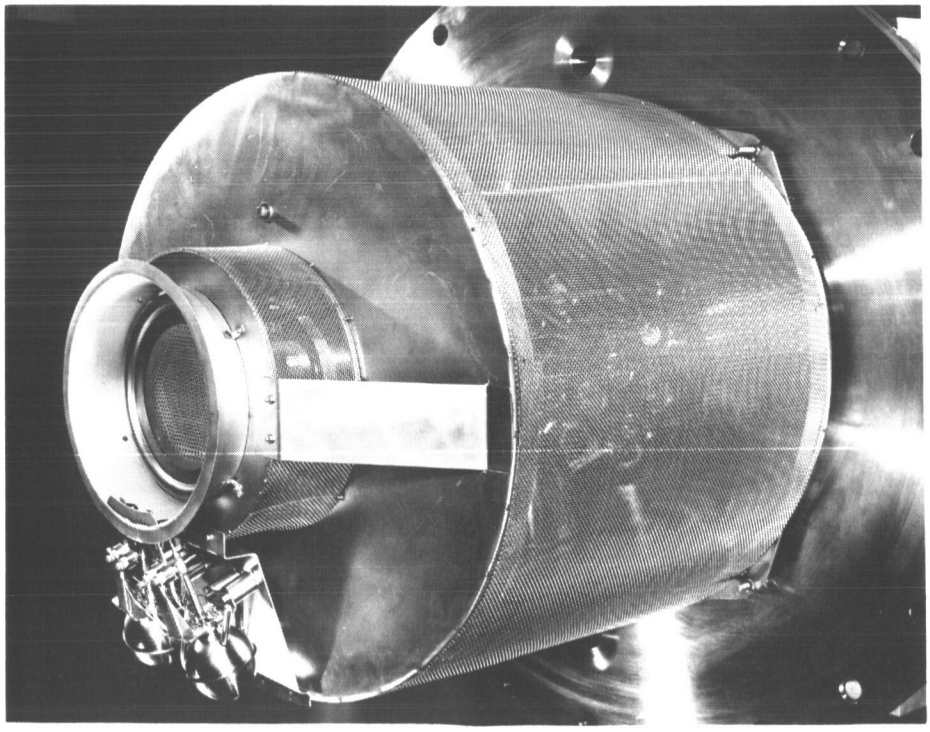

Figure 18. 2000-Hour Engine System

3.1.2 TEST FACILITY

The facility used for the 2610 hours of testing under Contract NAS3-5250 (Ref. 5) was used for the 2000-hour test. This facility is shown in Fig. 19. The engine was mounted in a tank section 28 inches in diameter and 3-1/2 feet long. This section had a 2-foot-diameter, stainless-steel, liquid-nitrogen-cooled liner and was pumped by a 10-inch diffusion pump with a 6-inch standby pump. Both pumps had liquid-nitrogen-cooled baffles. Mounted in this section was a neutral cesium detector which, because it extended so far down into the beam, was removed after performance mapping and prior to the start of the continuous portion of the 2000-hour test. There was also a mass spectrometer tube in the engine section for residual gas analysis. The collector section of the facility was 28 inches in diameter and 5 feet long. The liner in this section was made of copper and was cooled by liquid-nitrogen coils. Improved liner baffles were made for the collector section. They were of larger inside diameter to decrease sputtering from the liner. A 1-1/2 inch thick copper collector of honeycomb design was used because of its effectiveness in trapping sputtered material. A pressure below 5×10^{-7} torr was maintained during the test.

Extensive precautions were taken to insure that a failure in any support equipment did not cause termination of the test. For example, should the 10-inch diffusion pump have failed, the 6-inch pump, which was kept warmed up at all times, would have automatically taken over and the 10-inch pump would have been valved off from the chamber. In the event of a power failure the 10-inch pump would have been valved off from the facility and the 6-inch pump would have automatically taken over on emergency generator power. In case of a water failure from the cooling tower to the diffusion pumps a switch to city water would have taken place. Bottled gas was kept ready to operate the diffusion pump gate valves in case of an air pressure failure.

As with the vacuum system, a power failure to the control system was to be met by generator power. All of these possible failure modes were thus unterlocked for automatic correction. Any such failure would also alert the local security guard, who would reach a member of the technical staff by phone. Delayed automatic shutdown sequences were used; for example, a pressure rise would have caused the ion gage to turn off and generate an alarm. The system was set to turn off automatically after a period of about 20 minutes if no one arrived to reset the alarm. In a similar way the high voltage overloads were counted. After 20 overload rest periods, an alarm was sounded. After 20 additional rest periods the system was automatically turned off unless the alarm was reset.

There was no backup system for a liquid nitrogen failure; however a liquid nitrogen high temperature alarm was installed on the facility.

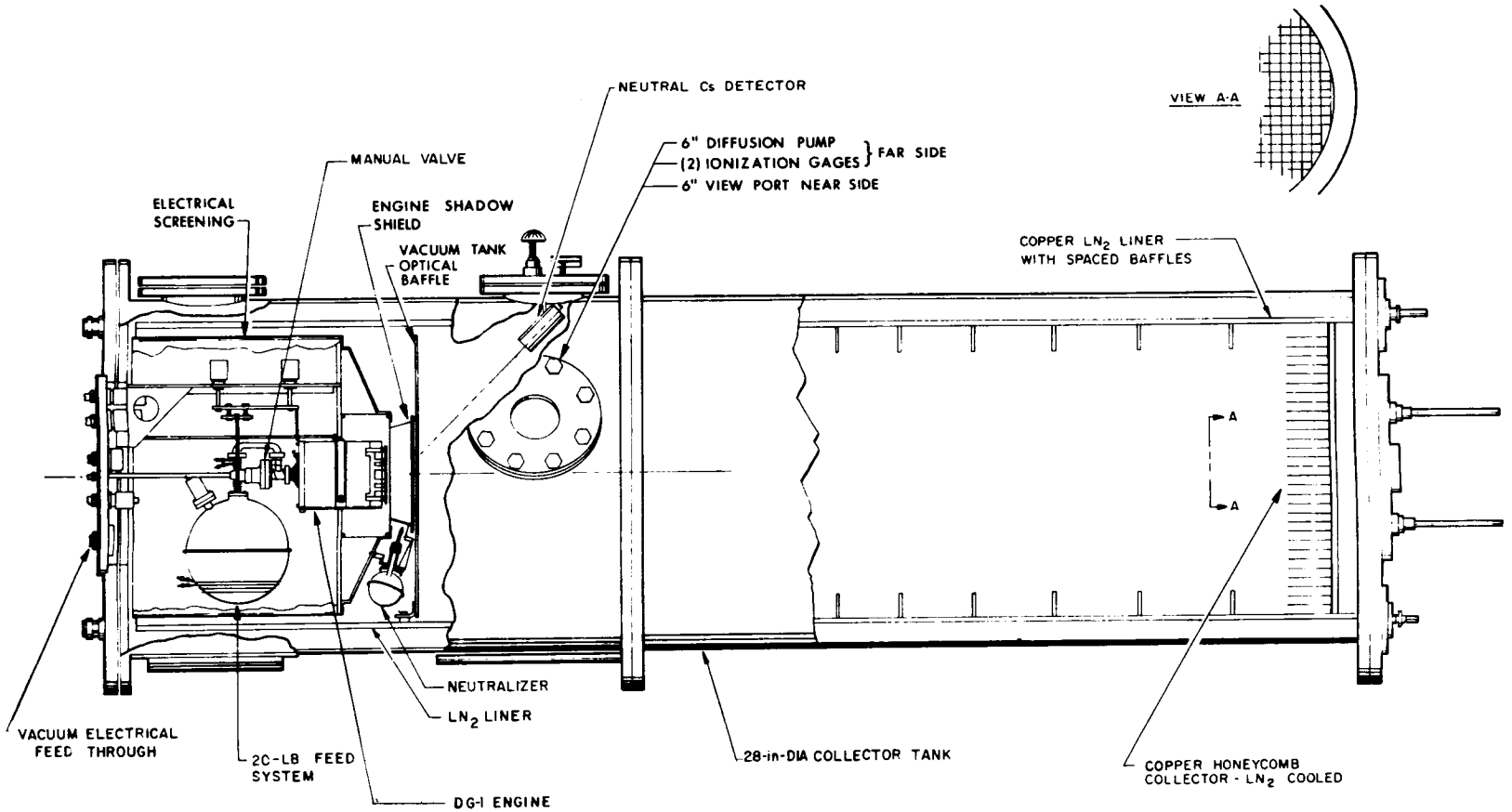

Figure 19. The 2000-Hour Engine System Test Facility

3.1.3 CONTROL SYSTEM

The engine for the 2000-hour test was operated by a control system developed under Contract NAS3-2516 (Ref. 3), and modified under Contract NAS3-5250 and the present contract. It featured a cathode interlock to deliver power to the cathode heater only when the arc current fell below a preset level. Cathode heater power is unnecessary with normal arc levels since the emitter is heated by ion bombardment. The vaporizer power was also interlocked to turn off with the high voltage supplies to stop cesium feed to the engine when the high voltage was off. The vaporizer was regulated to maintain constant beam current during normal engine operation by means of a feedback control loop.

Modifications to the control system design included improved high voltage interlocking and the addition of a neutralizer control panel. Changes to enhance long-term operation were also incorporated.

One difficulty was not resolved; the turn-on characteristic of the high voltage power supplies was not well matched to the load. Whenever the electrode voltages were low and the beam current was high enough to exceed the perveance limit, the plasma could not be restrained within the discharge chamber. In such a case the plasma filled the gap between the electrodes and acted as a low impedance between the positive and negative high voltage supplies. When the turn-on rate of rise of voltage was slow, this low impedance was sensed by the supplies, an overload was signalled, and the supplies turned back off. This caused a continuous overload cycling condition to follow almost any overload. To recover from this condition, the vaporizer and high voltages were held off for a "rest cycle" whenever six rapid consecutive overloads were detected. This allowed the plasma density to drop, reducing the current flow during turn-on.

In order to increase the reliability of the power and the control system, the circuitry was simplified. Superfluous meter ranges and adjustment provisions were eliminated. The overload detection circuits were redesigned to use more reliable components and the overload cycling for the two high-voltage supplies was paralleled at the detection level, reducing the number of components for these circuits by about 50 percent.

The programmer was redesigned to eliminate self-latching relays and other components that were found to be affected by transients. In the process of this redesign, the automatic start and stop programs were eliminated, allowing further simplification and adding to the expected long-term reliability of the laboratory power and control system.

The neutralizer control system provided an integral system of power supplies for the cathode and vaporizer heaters, a beam probe bias supply, and a feedback control loop to regulate the vaporizer power to the beam potential as indicated by the beam probe. With this system the cathode heater could be set for one power level before start-up and another for continuous running. A provision was made to bias the neutralizer negative with respect to ground in the event that the liner or collector of the vacuum system became shorted to ground.

3.1.4 PERFORMANCE MAPPING

METHODS OF MEASUREMENT, CALCULATION, AND ANALYSIS

The basic electrical schematic for DG engine system is shown in Fig. 20, which has been drawn to include all of the heaters used on the long test. The U-tube (feed line) heater, manual valve heater, and reservoir heaters would not be necessary for a flight system.

The engine system operating parameters measured directly were the positive and negative high voltages, the beam current, the negative high voltage supply drain current, the arc voltage, the arc current, the magnet supply voltage, the magnet current, the vaporizer supply voltage, the vaporizer current, the neutralizer vaporizer current, the neutralizer cathode current, the collector voltage, and the neutralizer emission current.

The low sides (ground returns) of both high voltage supplies were joined together and returned through a current meter to ground. This meter thus read the difference between the positive and negative supply currents, that is the net positive current leaving the engine, which is the beam current. This measurement of the beam current should be lower, if anything, than the actual energetic particle flow out of the engine since fast neutrals formed by charge exchange are not counted in the beam current and electrons going from the accelerating electrode to ground are subtracted from the beam current. Electrons going from the accelerating electrode to the screen electrode or ions going from the ion source to the accelerating electrode do not affect the beam current measurement. Care was taken to prevent stray electron current from ground to those parts of the engine which were at high positive potentials.

The vaporizer voltage and current were measured on ac meters located between the power supply and the power feedthroughs on the vacuum flange.

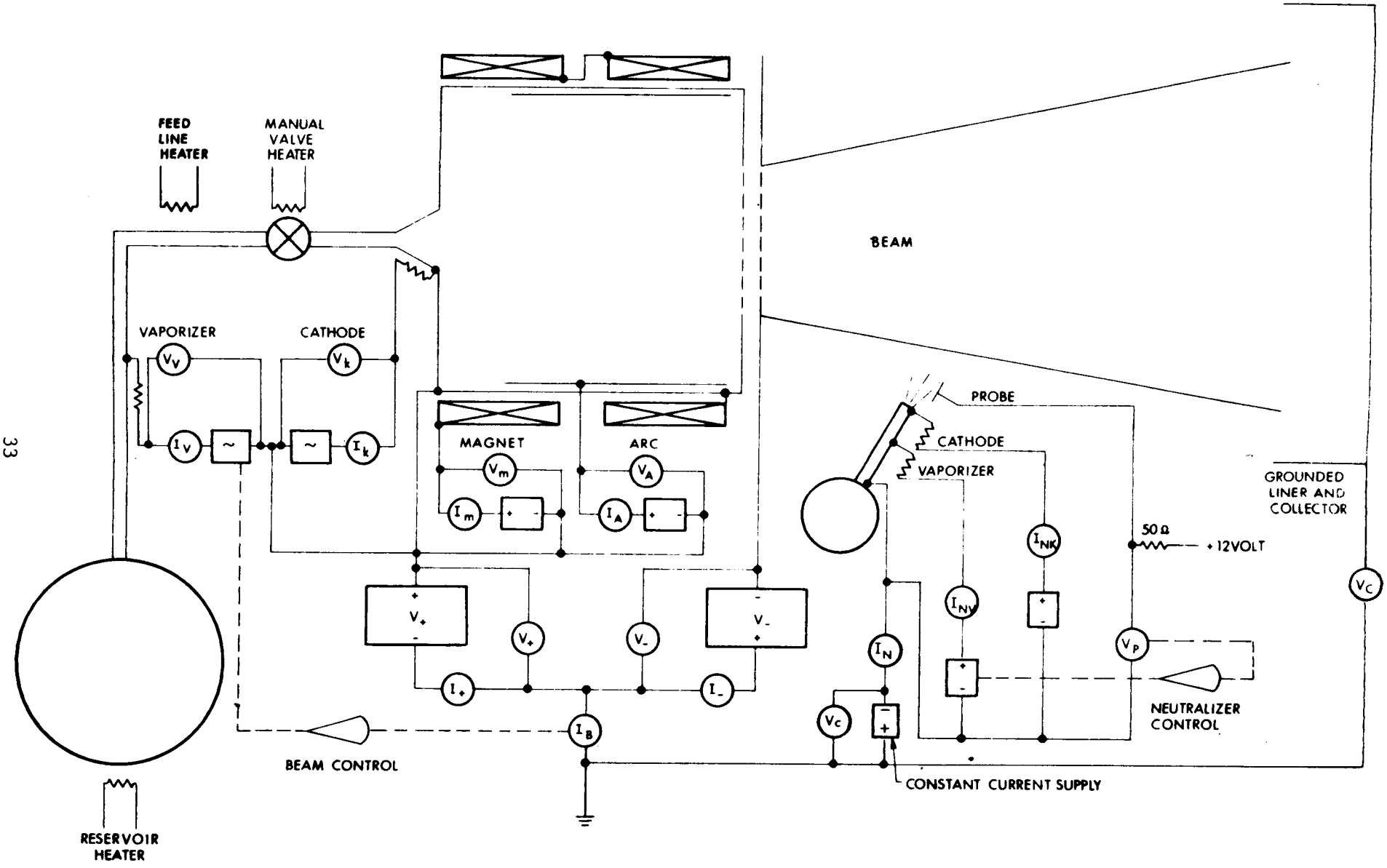

Figure 20. Electrical Schematic for DG-1 Engine System

The neutralizer vaporizer and cathode currents were measured between the power supplies and the vacuum feedthroughs with dc meters. The neutralizer emission current was measured on a dc meter between the neutralizer common and system ground outside the vacuum facility. The collector potential was measured with a dc meter between the isolated collector and liners and ground.

The total flow rate was determined by means of a neutral cesium detector. This detector has an entrance portion in which electric fields deflect ions and prevent them from entering the detector. Neutral cesium atoms entering the detector are ionized at a hot tungsten filament and a fraction of these ions are collected and measured. A mechanical shutter which prevents any particles from entering the detector allows determination of the background signal level which is subtracted from the detector reading.

The angular acceptance entrance area and the distance of the detector from the engine are such that the ratio of neutral particles to neutral particles sampled is of the order of 10^6.

The total flow rate is determined for each performance point by calibrating the neutral detector signal in terms of a total equivalent neutral efflux current. The vaporizer power is set manually and when steady state conditions are reached the beam current, I_B, and the neutral cesium detector signal, I_{NCD}, are recorded. Keeping the vaporizer power (and, therefore, the feed rate) unchanged, the arc power is then reduced and a lower beam current, I_B', and a higher neutral detector signal, I_{NCD}', are measured.

The change in the neutral detector signal, $\Delta I_{NCD} = I_{NCD}' - I_{NCD}$, corresponds to an increase of the total neutral efflux of $\Delta I_B = I_B - I_B'$ since the flow rate was held constant. The neutral particle current equivalent (I_{Cs}) of the neutral detector signal I_{NCD} is therefore

$$I_{Cs} = I_{NCD}(\Delta I_B/\Delta I_{NCD})$$

And the total flow rate (in current equivalent) is

$$I_o = I_B + I_{Cs}.$$

Performance Calculations

The total power into the engine is the sum of the beam power, the accelerator drain power, the arc power, and the magnet power. The currents and voltages are designated as

Symbol	Meaning
V_+	positive high voltage
V_-	negative high voltage
I_B	beam current
I_-	negative HV supply current (drain current)
V_A	arc voltage
I_A	arc current
V_M	magnet voltage
I_M	magnet current

The associated powers are

Power	Symbol	How Calculated
Beam power	P_B	$V_+ I_B$
Drain power	P_D	$(V_+ + \lvert V_- \rvert) I_-$
Arc power	P_A	$V_A I_A$
Magnet power	P_M	$V_M I_M$

The total power into the engine, P_E, is, therefore,

$$P_E = P_B + P_D + P_A + P_M$$

The total system power is defined to be the sum of the total engine power, the feed system power, and the total neutralizer power. The total neutralizer power is defined as the sum of the powers of the vaporizer heater, cathode heater, and perveance loss. The voltages, currents, and resistances are designated as

Symbol	Meaning
V_V	vaporizer voltage
I_V	vaporizer current
I_{NV}	neutralizer vaporizer current
R_{NV}	neutralizer vaporizer resistance
I_{NK}	neutralizer cathode current
R_{NK}	neutralizer cathode resistance
V_c	collector voltage
I_N	neutralizer emission current

The associated powers are

Power	Symbol	How Calculated
Feed system power	P_F	$V_V I_V$
Neutralizer vaporizer power	P_{NV}	$I_{NV}^2 R_{NV}$
Neutralizer cathode power	P_{NK}	$I_{NK}^2 R_{NK}$
Perveance loss	P_p	$V_c I_N$

(Since the perveance power is not associated with a power supply but is part of the power supplied by the high voltage supply, accurate system power is determined without the perveance power.) The total neutralizer power, P_N, is therefore

$$P_N = P_{NV} + P_{NK}$$

The total power into the engine system, P_S, is therefore

$$P_S = P_E + P_F + P_N$$

The thrust, T, is calculated from the beam current, I_B, and the net accelerating voltage, V_+. The ions leave the engine with a velocity $v_+ = (2eV_+/M_{Cs})^{1/2}$ where e is the elctronic charge and M_{Cs} is the mass of a cesium ion. The number of ions leaving the engine per second is $N_+ = I_B/e$ and since each ion has the mass M_{Cs} the flow rate of accelerated ions is

$$\dot{m}_+ = M_{Cs} I_B / e$$

The thrust is then given by

$$T = \dot{m}_+ v_+ = I_B \left(\frac{2M_{Cs} V_+}{e}\right)^{1/2}$$

For I_B in amps and V_+ in kilovolts this is

$$T = 11.9\ I_B\ V_+^{1/2}\ \text{mlb}$$

The power-to-thrust ratio for the engine is defined to be the total power input to the engine, P_E, divided by the thrust, T. It is usually calculated using total engine power in kilowatts and thrust in pounds to get the power-to-thrust ratio in kilowatts/pound.

The system power-to-thrust ratio is expressed as the total system input power, P_S, divided by the thrust, T. This is also given in kilowatts/pound.

The engine power efficiency, η_{PE}, is defined to be the ratio of power in the beam to the total power being fed into the engine or

$$\eta_{PE} = P_B/P_E$$

Likewise, the system power efficiency, η_{PS}, is defined as the ratio of the beam power to the total power input to the system

$$\eta_{PS} = P_B/P_S$$

The engine mass utilization efficiency, η_{ME}, is defined to be the ratio of the ion efflux from the engine to the total efflux from the engine (ions plus neutral particles) or

$$\eta_{ME} = I_B/I_o$$

The system mass utilization efficiency is defined as the ratio of the beam current to the total cesium mass flow rate from the system (engine flow rate, I_o, plus neutralizer mass flow rate, I_{oN}). No means were available for rapid measurement of I_{oN}, but the flow rate of a prototype neutralizer had been found by measurement of the cesium weight loss after an extended run with a beam current of 0.475 amp to be 0.85 percent of the engine feed rate. Thus the effect of the neutralizer is to lower η_M by at most one percent. Therefore, the system mass efficiency was taken to be

$$\eta_{MS} = \eta_{ME} - 1\%$$

At the conclusion of the life tests the neutralizer flow rates were found to be 0.80 percent of the engine flow rates.

The overall system efficiency, η_S, is the product of the system power efficiency and the system mass utilization efficiency,

$$\eta_S = \eta_{PS}\,\eta_{MS}$$

To calculate the engine specific impulse, I_{sp}, the neutral efflux is assumed to have negligible velocity. The specific impulse is defined to be the thrust, in pounds, divided by the total flow rate of propellant to the engine in lb/sec, or

$$I_{sp} = T/\dot{W} = T/\dot{m}g = \frac{\dot{m}_+ v_+}{\dot{m}\, g}$$

where $\dot{m}$ is the total mass flow rate to the engine and g is the acceleration due to gravity at the earth's surface.

Since

$$\eta_{ME} = \frac{\dot{m}_+}{\dot{m}}$$

then

$$I_{sp} = \eta_{ME}\, v_+/g$$

$$= (\eta_{ME}/g) \quad (2eV_+/M_{Cs})^{1/2}$$

For V_+ in kV, the specific impulse is given by

$$I_{sp} = 3.88 \times 10^3\, \eta_{ME}\, V_+^{1/2} \text{ seconds}$$

The system specific impulse is found by everywhere replacing the mass flow rate to the engine, $\dot{m}$, with $\dot{m} + \dot{m}_N$ where $\dot{m}_N$ is the cesium flow rate to the neutralizer, and by replacing the engine mass utilization efficiency, η_{ME}, with the system mass efficiency, η_{MS}. For V_+ in kV, the system specific impulse in seconds is

$$I_{spS} = 3.88 \times 10^3\, \eta_{MS}\, V_+$$

Qualifying Remarks

The source of the ions is a plasma at anode potential. This means that the true energy gained by an ion is e $(V_+ + V_A)$ if it is accelerated to ground potential. Since the ions are accelerated to the collector potential their energy is e $(V_+ + V_A - V_c)$. V_A is nearly equal to V_c so no significant error in ion velocity results from the use of an energy eV_+.

The arc power should also be calculated as $V_A(I_A - I_B)$. The perveance power $V_c I_N$ is in this case about equal to $V_A I_B$ and could be neglected if the arc power were calculated as $V_A I_A$. The arc powers presented in this report were calculated as $V_A I_A$ for convenience but the perveance power was left in for the DG-1 performance mapping to show the efficiency of the neutralizer. The error in arc power is generally less than 3 percent or 0.5 percent of the system power.

Analysis

For purposes of analysis the arc power per beam ion, P_A/I_B, is of interest.

For a given positive high voltage and beam current there is a trade-off between power efficiency and mass utilization efficiency. If the arc power is raised, more particles are ionized and the beam current is maintained with a lower total flow rate. The thrust and beam power remain unchanged and the mass utilization efficiency is increased. If the arc power is reduced, the power efficiency is increased but the mass utilization efficiency is decreased. In either case, the overall engine efficiency may be increased or decreased.

At optimum operating parameters, the mass utilization and power efficiencies trade off in such a way as to leave the overall engine efficiency relatively unchanged. The arc power per beam ion and the mass utilization efficiency give an indication of whether the operating point is near the optimum. Since the major power loss is the arc power, the power efficiency is close to (but less than) $V_+/(V_+ + P_A/I_B)$. The relation between η_M and P_A/I_B around a given operating point thus indicates how η_E can be optimized. For higher specific impulses, overall engine efficiency is obtained with higher mass efficiency and source energy expenditures in eV/ion. The power efficiency is approximately given by the ratio of positive high voltage, V_+, to V_+ plus the eV/ion expended in the source. As V_+ is reduced to reduce the specific impulse, the power efficiency becomes the predominant factor in overall efficiency. At lower specific impulses it therefore becomes desirable to reduce both the source eV/ion and mass efficiency to increase the power efficiency and obtain the maximum overall engine efficiency.

For a long life test it is necessary to run with low accelerator drain current and a low accelerating voltage since the only known lifetime limitation is erosion of the accelerator by charge exchange sputtering. As mentioned above the high perveance DG electrode system not only provides an increase in thrust while maintaining a low percentage of drain current to beam current but allows a significant decrease in the accelerating electrode potential to a level compatible with long life. As with previous engines the optimum overall performance generally occurs in the DG engine with minimum accelerator potential and drain current.

3.1.5 PERFORMANCE DATA

The DG-1 engine was performance mapped over a wide range of optimum and nonoptimum operating levels. The measurements and reduced data are presented in Table III.

Because of possible difficulty of obtaining dependable mass efficiency data with the neutralizer in operation the engine was performance mapped with an unneutralized beam. In order to include neutralizer power levels for each point of the performance data the data in Table IV were taken. It shows the neutralizer performance data for different emission current levels. From this data the curve of Fig. 21 was drawn showing the total neutralizer power as a function of the neutralizer emission current. A conservative extrapolation was made. From this curve the total neutralizer power was taken for the beam current of each performance point in Table III.

In a similar manner, the feed system power for each performance point was taken from the curve in Fig. 22; it was not feasible to bring the feed system reservoir to thermal equilibrium for each point, since this requires several hours. The response of reservoir temperature is too slow to cause any significant error in flow rate measurements at each point.

Figure 23 presents the overall efficiencies for the DF-1 engine (Contract NAS3-5250) and the DG-1 engine. The DG-1 engine system overall efficiency is also shown as a function of the system specific impulse. The upper curve shows the DG engine efficiency to be very similar to that of the DF engine with a slight improvement at lower specific impulse. The lower curve for the DG-1 engine system plotted against system specific impulse shows the effect of the feed system and neutralizer. These lower the overall efficiency by about 1.5 percent at 7000 seconds system specific impulse and about 5 percent at 3000 seconds. At 5000 seconds the overall efficiency is about 3 percent lower than that of the engine alone.

Figure 24 shows power-to-thrust ratio versus specific impulse curves for the DF-1 engine, the DG-1 engine, and the DG-1 engine system. The DG-1 engine system curve shows that the penalty for the neutralizer and feed system is about 4 kilowatts per pound thrust at 7000 seconds and about 9 kilowatts per pound at 3000 seconds. At the design level of 5000 seconds specific impulse the penalty is about 5 kilowatts per pound of thrust.

Figure 25 shows the thrust versus system specific impulse. There are two distinct curves shown representing the maximum and the optimum thrust. The maximum thrust curve represents a limit imposed by the

TABLE III

DG-1 ENGINE SYSTEM PERFORMANCE MAPPING

Parameter	Point Number 1	2	3	4	5	6	7	8	9	10	11	12	13	14	15	16	17	18
Positive High Voltage, V_+ (kV)	0.500	0.500	0.745	1.000	1.350	2.000	2.000	2.200	2.380	2.380	2.370	2.740	2.780	3.325	3.525	4.000	4.150	4.800
Negative High Voltage, V_- (kV)	1.605	1.625	1.825	1.350	1.560	1.000	0.540	0.600	0.440	0.460	0.470	0.430	0.470	0.400	0.325	0.335	0.325	0.385
Negative HV Current, I_- (amp)	0.0082	0.0075	0.0070	0.0061	0.0068	0.013	7.5	0.0051	0.0067	0.0062	0.0061	0.0125	0.0060	0.0065	0.0070	0.0108	0.008	0.010
Beam Current, I_B (amp)	0.265	0.252	0.290	0.260	0.378	0.499	0.392	0.400	0.435	0.439	0.429	0.630	0.478	0.460	0.530	0.415	0.580	0.700
Arc Voltage, V_A (volts)	6.4	6.3	6.5	6.5	6.8	6.7	7.1	6.8	7.1	7.1	7.1	7.2	7.1	7.0	7.0	7.2	7.0	7.0
Arc Current, I_A (amp)	12.3	12.3	15.5	12.7	17.8	22.0	19.0	20.0	20.0	21.0	22.0	33.5	22.5	23.8	24.0	21.0	26.5	32.0
Magnet Voltage, V_M (volts)	5.5	5.25	4.75	5.25	5.0	5.30	4.70	5.0	5.0	5.0	4.8	4.9	4.90	5.0	5.0	5.0	5.0	5.0
Magnet Current, I_M (amp)	23.5	2.25	2.05	2.25	2.15	2.35	2.05	2.05	2.15	2.15	2.05	2.05	2.05	2.0	2.15	2.0	2.05	2.0
Beam Power, P_B (kW)	0.132	0.126	0.216	0.260	0.511	0.998	0.784	0.880	1.035	1.045	1.018	1.725	1.370	1.529	1.868	1.660	2.405	3.360
Drain Power, P_D (kW)	0.017	0.016	0.018	0.014	0.020	0.039	0.019	0.014	0.019	0.018	0.017	0.040	0.019	0.024	0.028	0.047	0.036	0.052
Magnet Power, P_M (kW)	0.013	0.012	0.010	0.012	0.010	0.012	0.010	0.010	0.011	0.011	0.010	0.010	0.010	0.010	0.011	0.010	0.010	0.010
Arc Power, P_A (kW)	0.079	0.078	0.100	0.082	0.121	0.147	0.135	0.136	0.142	0.149	0.160	0.237	0.160	0.167	0.168	0.144	0.185	0.224
Total Engine Power, P_E (kW)	0.241	0.232	0.344	0.348	0.662	1.196	0.948	1.040	1.207	1.223	1.201	2.012	1.559	1.730	2.075	1.861	2.636	3.646
Feed System Power, P_F (kW)	0.021	0.021	0.021	0.021	0.023	0.025	0.023	0.023	0.024	0.024	0.024	0.028	0.024	0.024	0.026	0.023	0.027	0.031
Total Neutralizer Power, P_N (kW)	0.012	0.012	0.012	0.012	0.013	0.015	0.012	0.014	0.014	0.014	0.014	0.018	0.015	0.014	0.016	0.014	0.016	0.020
Total System Power, P_S (kW)	0.274	0.265	0.377	0.381	0.698	1.236	0.983	1.077	1.245	1.261	1.239	2.058	1.598	1.768	2.117	1.898	2.679	3.697
Thrust, T (mlb)	2.23	2.12	2.98	3.09	5.24	8.41	6.61	7.06	8.00	8.07	7.87	12.4	9.51	9.99	11.9	9.88	14.05	18.25
Engine Power-to-Thrust Ratio, $P_{E/T}$ (kW/lb)	108	109	115	113	126	142	143	147	151	152	153	162	164	173	175	189	188	200
System Power-to-Thrust Ratio, $P_{S/T}$ (kW/lb)	123	125	126	123	133	147	149	152	156	156	157	166	168	177	179	192	191	202
Engine Power Efficiency, η_{PE} (%)	54.9	54.5	62.8	74.6	77.3	83.3	82.8	84.6	85.8	85.4	84.6	85.8	87.8	88.4	90.0	89.1	91.4	92.2
System Power Efficiency, η_{PS} (%)	48.2	47.5	57.3	68.2	73.2	80.7	79.8	81.7	83.1	82.9	82.2	83.8	85.7	86.5	88.2	87.5	90.0	90.9
Engine Mass Efficiency, η_{ME} (%)	78.5	80.3	86.7	87.6	93.1	88.3	92.4	90.3	91.3	91.5	92.3	91.6	92.2	85.8	94.6	91.7	93.0	92.4
System Mass Efficiency, η_{MS} (%)	77.5	79.3	85.7	86.6	92.1	87.3	91.4	89.3	90.3	90.5	91.3	90.6	91.2	84.8	93.6	90.7	92.0	91.4
Overall Engine Efficiency, η_E (%)	43.1	43.7	54.4	65.2	72.0	73.6	76.6	76.3	78.6	78.2	78.1	78.6	81.1	75.8	85.1	81.7	85.0	85.0
Overall System Efficiency, η_S (%)	37.4	37.7	49.1	59.1	67.4	70.5	72.9	73.0	75.0	75.0	75.0	75.9	78.2	73.4	82.6	79.4	82.8	83.1
Engine Specific Impulse, I_{spE} (sec)	2150	2200	2905	3395	4190	4840	5060	5190	5455	5470	5510	5870	5960	6060	6895	7110	7345	7840
System Specific Impulse, I_{spS} (sec)	2125	2175	2870	3360	4150	4785	5010	5130	5400	5410	5450	5810	5900	5095	6810	7025	7260	7750
Ratio of Drain Current to Beam Current I_-/I_B (%)	3.09	2.97	2.42	2.34	1.80	2.60	1.91	1.27	1.54	1.41	1.42	1.98	1.25	1.41	1.32	2.61	1.38	1.43
Source Energy Per Ion, P_A/I_B (keV/ion)	0.337	0.306	0.346	0.315	0.320	0.295	0.344	0.341	0.326	0.340	0.364	0.377	0.334	0.363	0.317	0.347	0.319	0.320
Neutral Detector Current, I_{NCD} (10^{-9} amp)	28.5	28.0	15.5	15.5	12.0	19.5	1.1	11.0	11.0	10.8	10.0	12.5	11.0	9.5	10.0	10.0	10.0	12.5
Neutral Detector Current at I'_B, I'_{NCD} (10^{-9} amp)	67.5	67.5	50.5	57.5	43.0	48.5	4.3	36.0	37.0	37.0	38.5	34.0	49.0	22.0	33.0	38.0	32.5	44.5
Reduced Beam Current, I'_B (amp)	165	150	190	160	0.278	400	280	0.100	0.335	0.339	0.329	0.530	0.340	0.360	0.430	0.310	0.480	0.550
Total Cesium Flowrate, I_o (amp)	0.338	0.314	0.334	0.297	0.406	0.565	0.425	0.444	0.477	0.480	0.465	0.688	0.518	0.536	0.560	0.452	0.625	0.759

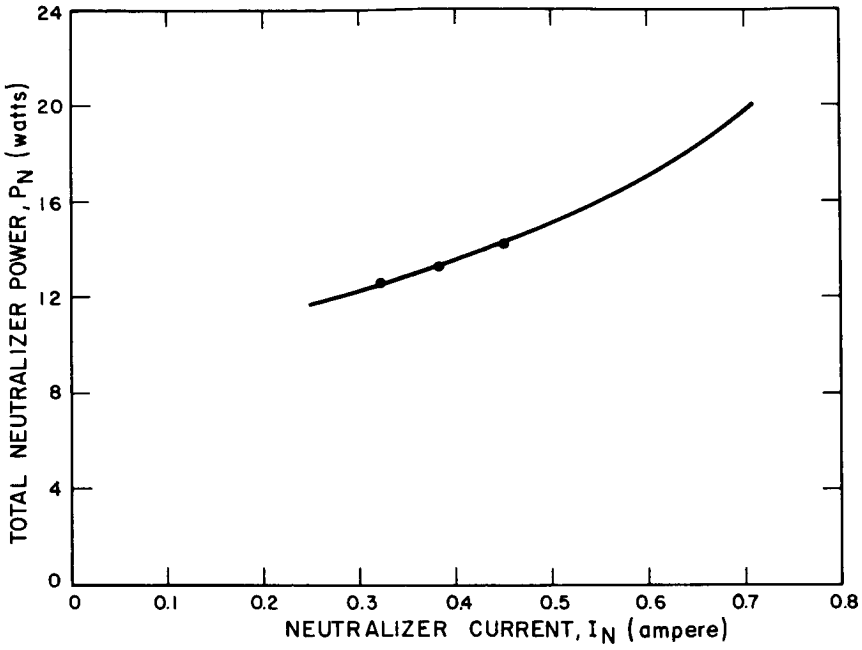

Figure 21. Total Neutralizer Power versus Neutralizer Emission Current

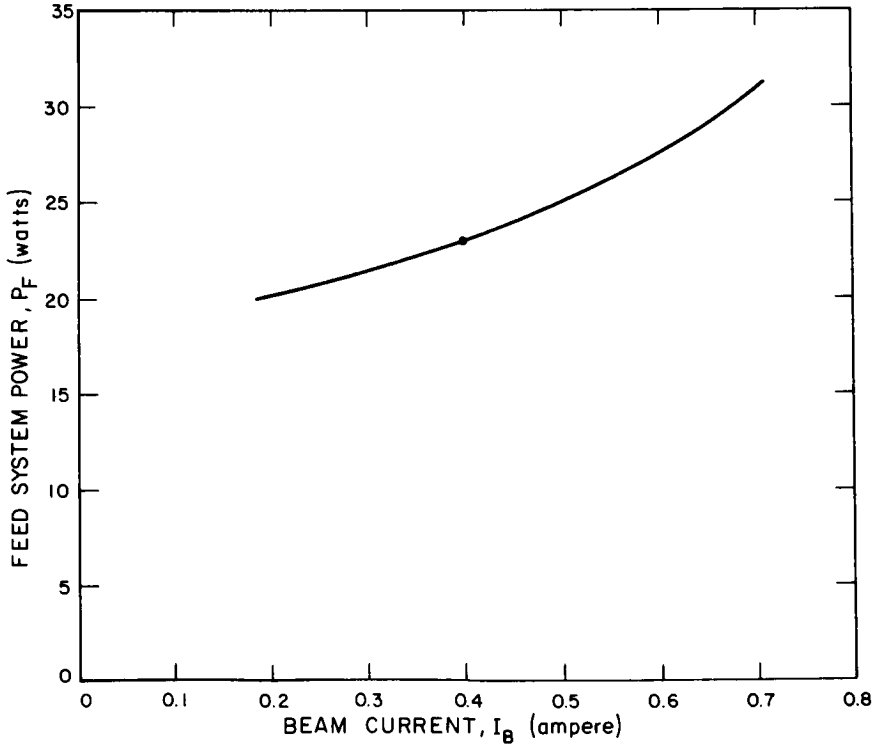

Figure 22. Feed System Power versus Beam Current

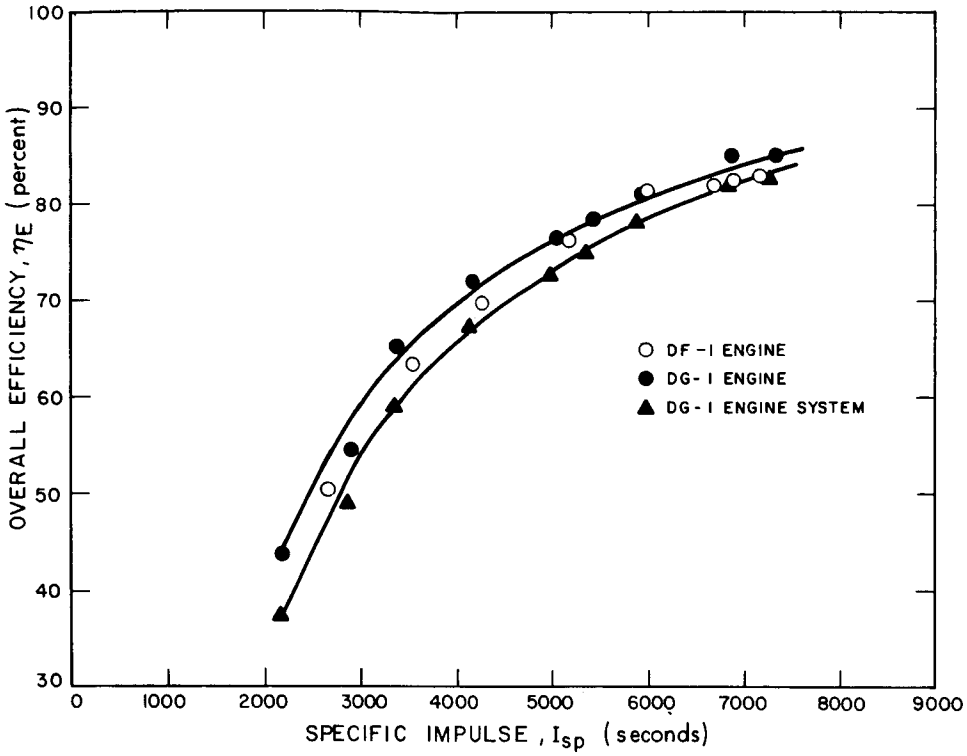

Figure 23. Overall Efficiency versus Specific Impulse

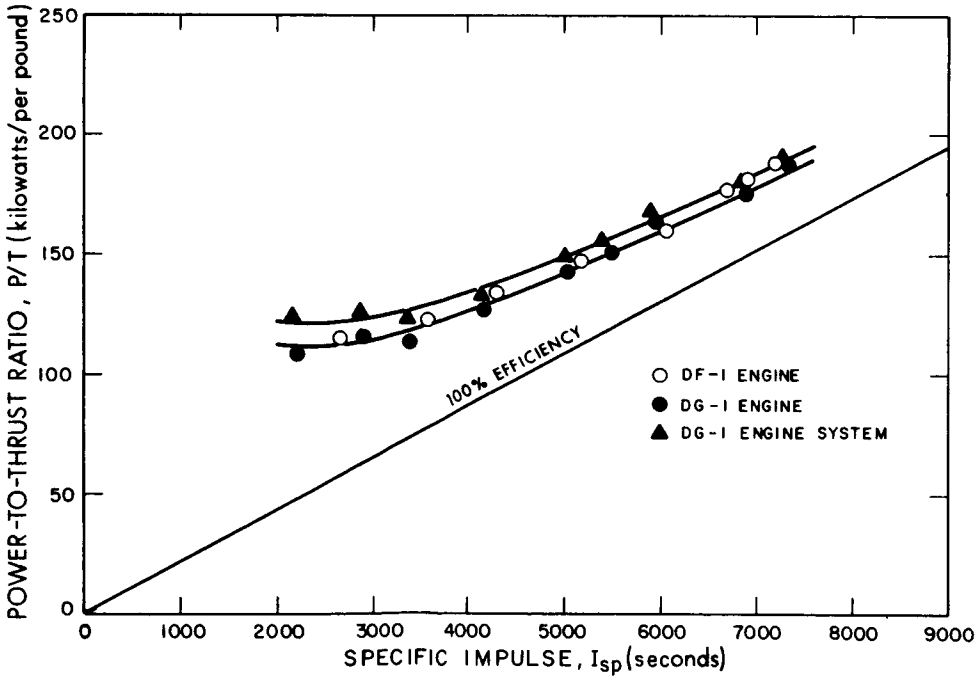

Figure 24. Power-to-Thrust Ratio versus Specific Impulse

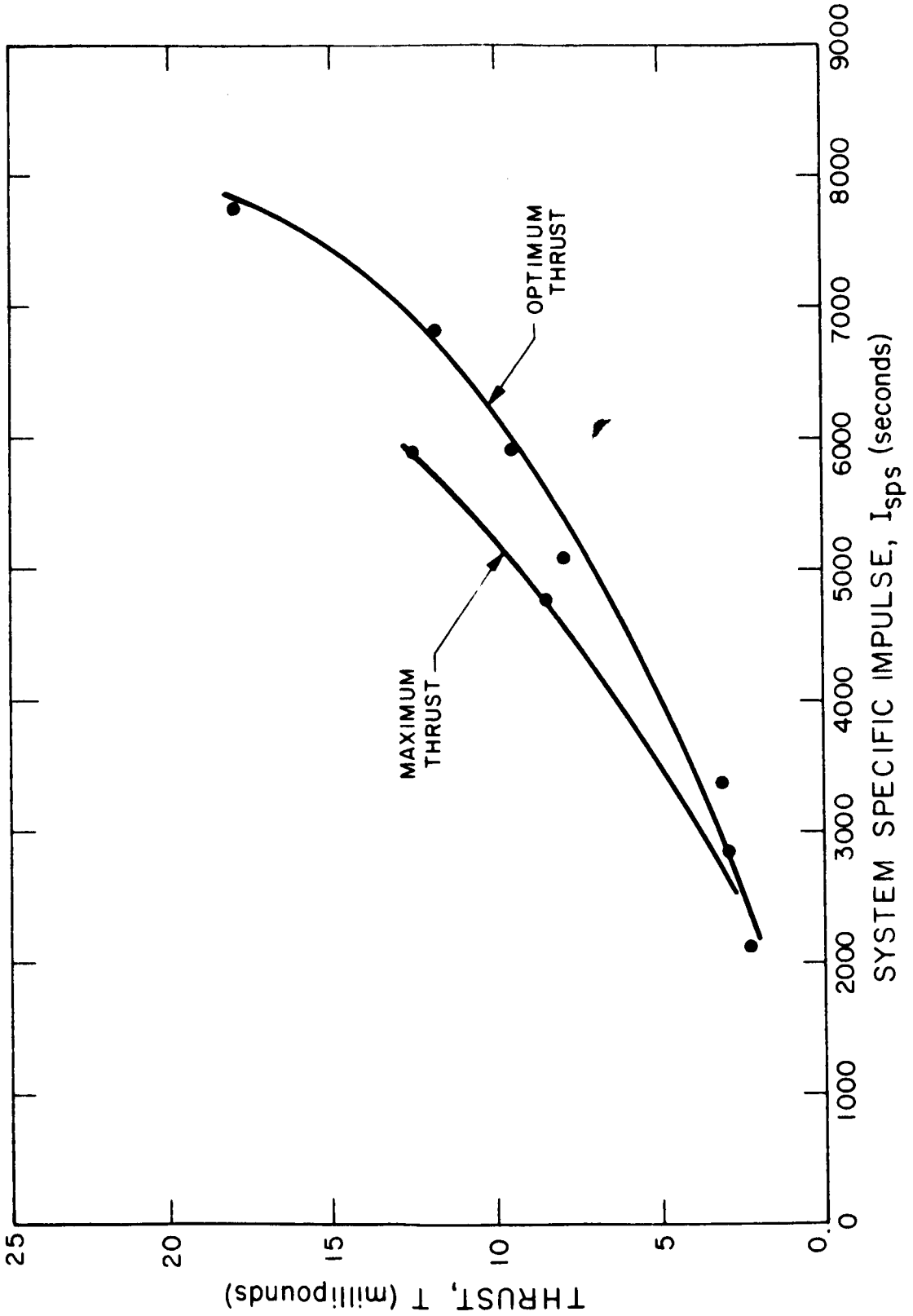

Figure 25. Thrust versus Specific Impulse

TABLE IV

NEUTRALIZER PERFORMANCE DATA
FOR THREE EMISSION CURRENT LEVELS

Emission Current, I_N (amp)	0.322	0.382	0.450
Collector Potential, V_c (volts)	8.0	8.4	10.1
Vaporizer Current, I_{NV} (amp)	1.55	1.56	1.52
Cathode Current, I_{NK} (amp)	1.54	1.53	1.52
Vaporizer Temperature, T_{NV} (^{o}C)	270	272	274
Cathode Temperature, T_{NK} (^{o}C)	462	462	462
Vaporizer Power, P_{NV} (watts)	6.2	6.3	6.0
Cathode Power, P_{NK} (watts)	3.8	3.7	3.7
Perveance Power Loss, P_p (watts)	2.6	3.2	4.5
Total Neutralizer Power, P_N (watts)	12.6	13.3	14.2

perveance and optics of the electrode system. The points on the maximum thrust curve have a lower overall system efficiency and a higher power-to-thrust ratio than points on the optimum curve for the same specific impulse. For example, the two points near 6000 seconds are similar in specific impulse, but while one point has a higher thrust the overall system efficiency is lower by more than 2 percent. The difference in the points, other than the higher drain power for the high thrust point, can be explained by the ratio of arc power to beam current which is much higher for the high thrust point even though the mass efficiency is lower. The reason for this is that the current density for the high thrust point requires a denser plasma and results in disproportionately increased losses in the arc.

Conclusions and Prediction Regarding Engine Performance

The following conclusions may be drawn from the performance mapping data:

a. For a given specific impulse, optimum overall engine efficiency is consistent with long lifetime. This follows from the fact that the only known lifetime limitation is that due to accelerator electrode sputtering by charge-exchanged ions and that optimum overall performance generally occurs with minimum accelerator potential and drain current.

b. Maximum overall efficiency is not necessarily obtained at maximum thrust.

c. At 5000 seconds system specific impulse optimum engine system performance can be obtained with a thrust of approximately 7 millipounds.

d. At 5000 seconds system specific impulse the system power-to-thrust ratio should be about 150 kilowatts per pound at an overall system efficiency of about 73 percent. The ratio of drain current to beam current should be well below 2 percent with an accelerator potential of about 500 volts.

3.1.6 2000-HOUR TEST PERFORMANCE

The objective of the 2000-hour test was operation of the engine system at a system power-to-thrust ratio below 160 kilowatts per pound at a nominal 5000 seconds specific impulse for 2000 hours or more. The feed system was loaded with 7976 grams of cesium prior to the start of the performance mapping. Deducting 33.0 grams for performance mapping and startups and estimating that 23 grams of cesium would remain trapped in the porous wick, 7920 grams of cesium should have been available to the engine for the test. Using the expected 92 percent mass efficiency for the engine the 7920 grams of cesium available should have allowed about 3650 hours of run time. At 5000 seconds specific impulse and a total system power of about one kilowatt, a thrust of 6.67 millipounds would give a system power-to-thrust ratio of about 150 kilowatts per pound. This operating level was chosen on the basis of the performance mapping.

The DG-1 engine had logged 57 hours of operating time prior to the start of the long test. Most of this time was logged with a different accelerator electrode than was used on the 2000-hour test. The only components replaced since the DG-1 engine was first run were the accelerator electrode and the neutralizers. No difficulty was encountered with the neutralizer seal system used with the DG-1 engine. While over two weeks elapsed between the time the neutralizers were sealed and the first neutralizer seal was opened, an almost negligible pressure rise was noted when the cadmium orifice seal evaporated. The second neutralizer remained sealed throughout the test as the first one did not fail.

The 2000-hour test was begun on 30 August 1965. Performance of the system at various times during the test is shown in Table V. As the data show, the penalty for neutralization and for the feed system totaled just over 6 kilowatts per pound at the start of the test. This was reduced to slightly over 5 kilowatts per pound after 32 hours. This reduction was primarily due to the attainment of equilibrium in the reservoir temperature for the engine and neutralizer feed systems. A significant increase in efficiency was also realized through the reduced accelerator drain power. This was anticipated as discussed in Subsection 2.1.

The discharge or arc power was increased during the first 750 hours. This was found to minimize the accelerator electrode drain current. The arc current did not change, however, suggesting that either a series impedance developed or a change in the cathode emitter surface condition occurred which caused an increase in arc impedance. This increase in arc impedance was observed during the 2610 hours of testing conducted under NASA Contract NAS3-5250.

At about 900 hours into the run, an increase in vaporizer temperature was noted (see Fig. 26). This was due either to blockage of the feed line or a change in the vaporizer characteristic. Whatever the cause of this change, the control system maintained the thrust level within 3 percent. Fluctuations in flow rate occurred subsequent to the change in vaporizer temperature. These fluctuations were on the order of ±2 percent. A long period (order of 4 hours) feed system heat imbalance was thought to have been the cause. The vaproizer temperature increase ceased at about 1400 hours of run time after attaining an average of 290^{o} centigrade.

The bottom plot of Fig. 27 shows the number of high voltage arcs accumulated on a counter between successive data points. Two significant characteristics of these arcs were noted in the laboratory: (1) Transients in the vacuum control and monitoring circuits occasionally interfered with the engine control circuits and actuated the high voltage overload cycling circuits. This was concluded after dozens of arcs occurred coincidentally with observed transients on vacuum gages caused by motion of loose connections. As a result, slamming a cabinet door initiated some of the engines arcs. (2) When a high voltage cycle occurred, the high voltage could not recover and the control system initiated an engine clean-up period (rest cycle). This involved shutting off high voltage and feed system power for 60 seconds. This time was not adequate, however, so no single arcs were counted; two or three arcs were counted each time a high-voltage breakdown occurred. Thus, the arc rate due to the engine was really only one-third that shown in Fig. 27. This was verified in later tests with the DG-2 engine at EOS and the DG-3 engine at NASA-LeRC.

TABLE V

DG-1 ENGINE SYSTEM PERFORMANCE ON LONG TEST

Run Time	0.0
Positive High Voltage, V_+ (kV)	2.0
Negative High Voltage, V_- (kV)	0.600
Negative HV Current, I_- (amp)	0.0090
Beam Current, I_B (amp)	0.398
Arc Voltage, V_A (volts)	7.0
Arc Current, I_A (amp)	19.5
Magnet Voltage, V_M (volts)	4.5
Magnet Current, I_M (amp)	2.0
Beam Power, P_B (kW)	0.796
Drain Power, P_D (kW)	0.023
Magnet Power, P_M (kW)	0.009
Arc Power, P_A (kW)	0.137
Total Engine Power, P_E (kW)	0.965
Feed System Power, P_F (kW)	0.027
Total Neutralizer Power, P_N (kW)	0.012
Total System Power, P_S (kW)	1.004
Thrust, T (mlb)	6.64
Engine Power-to-Thrust Ratio, $P_{E/T}$ (kW/lb)	145.3
System Power-to-Thrust Ratio, $P_{S/T}$ (kW/lb)	151.2
Engine Power Efficiency η_{PE} (%)	82.5
System Power Efficiency, η_{PS} (%)	79.2
Engine Mass Efficiency, η_{ME} (%)	~ 92.0
System Mass Efficiency, η_{MS} (%)	~ 91.0
Overall Engine Efficiency, η_E (%)	75.8
Overall System Efficiency, η_S (%)	72.1
Engine Specific Impulse, I_{spE} (sec)	5050
System Specific Impulse, I_{spS} (sec)	4993
Ratio of Drain Current To Beam Current, I_-/I_B (%)	2.3
Source Energy per Ion, P_A/I_B (keV/ion)	0.344

TABLE V

DG-1 ENGINE SYSTEM PERFORMANCE ON LONG TEST (contd)

Run Time	32.3	100.8	309.8	1000.85	1505.1
V_+ (kV)	2.0	2.02	2.01	2.02	2.03
V_- (kV)	0.600	0.597	0.540	0.535	0.525
I_- (amp)	0.0074	0.0070	0.0087	0.006	0.0057
I_B (amp)	0.405	0.398	0.402	0.393	0.390
V_A (volts)	6.6	6.7	6.95	7.45	7.3
I_A (amp)	20.0	20.1	20.7	20.0	20.0
V_M (volts)	4.7	4.8	4.85	5.1	5.05
I_M (amp)	2.03	2.08	2.1	2.2	2.21
P_B (kW)	0.810	0.804	0.808	0.794	0.792
P_D (kW)	0.019	0.018	0.022	0.015	0.015
P_M (kW)	0.009	0.010	0.010	0.011	0.011
P_A (kW)	0.132	0.135	0.144	0.149	0.146
P_E (kW)	0.971	0.967	0.984	0.969	0.964
P_F (kW)	0.023	0.023	0.022	0.025	0.026
P_N (kW)	0.010	0.010	0.009	0.009	0.010
P_S (kW)	1.004	1.000	1.015	1.003	1.000
T (mlb)	6.76	6.67	6.73	6.59	6.56
P_E/T (kW/lb)	143.6	145.0	146.3	147.1	146.9
P_S/T (kW/lb)	148.5	149.9	151.0	152.3	152.3
η_{PE} (%)	83.5	83.1	82.2	82.0	82.1
η_{PS} (%)	80.6	80.4	79.6	79.0	79.2
η_{ME} (%)	~ 92.0	~ 92.0	~ 92.0	~ 92.0	~ 92.0
η_{MS} (%)	~ 91.0	~ 91.0	~ 91.0	~ 91.0	~ 91.0
η_E (%)	76.7	76.4	75.6	75.4	75.5
η_S (%)	73.4	73.2	72.5	71.9	72.1
I_{spE} (sec)	5050	5070	5060	5070	5080
I_{spS} (sec)	4993	5018	5006	5018	5031
I_-/I_B (%)	1.8	1.8	2.2	1.5	1.5
P_A/I_B (keV/ion)	0.326	0.338	0.358	0.379	0.374

TABLE V

DG-1 ENGINE SYSTEM PERFORMANCE ON LONG TEST (contd)

Run Time	2006.3	2503.3	2927.5	3511.6
V_+ (kV)	2.02	2.01	1.99	2.01
V_- (kV)	0.525	0.535	0.525	0.530
I_- (amp	0.0063	0.0069	0.0069	0.0065
I_B (amp)	0.391	0.403	0.391	0.396
V_A (volt)	7.5	7.4	7.5	7.2
I_A (amp)	20.1	21.8	23.1	22.3
V_M (volt)	5.2	5.2	5.1	5.1
I_M (amp)	2.25	2.17	2.15	2.16
P_B (kW)	0.790	0.810	0.778	0.796
P_D (kW)	0.016	0.018	0.017	0.016
P_M (kW)	0.012	0.011	0.011	0.0110
P_A (kW)	0.151	0.161	0.173	0.161
P_E (kW)	0.969	1.000	0.979	0.984
P_F (kW)	0.0270	0.025	0.026	0.024
P_N (kW)	0.010	0.010	0.010	0.011
P_S (kW)	1.006	1.035	1.015	1.019
T (mlb)	6.56	6.74	6.51	6.62
P_E/T (kW/lb)	147.6	148.4	150.0	148.7
P_S/T (kW/lb)	153.2	153.6	156.0	153.7
η_{PE} (%)	81.5	81.0	79.5	81.9
η_{PS} (%)	78.5	78.2	76.7	78.2
η_{ME} (%)	~ 92.0	~ 92.0	~ 92.0	~ 92.0
η_{MS} (%)	~ 91.0	~ 91.0	~ 91.0	~ 91.0
η_E (%)	75.0	74.5	73.1	75.4
η_S (%)	71.4	71.2	69.8	71.2
I_{spE} (sec)	5070	5060	5036	5060
I_{spS} (sec)	5018	5006	4981	5006
I_-/I_B (%)	1.6	1.7	1.8	1.6
P_A/I_B (keV/ion)	0.386	0.400	0.440	0.406

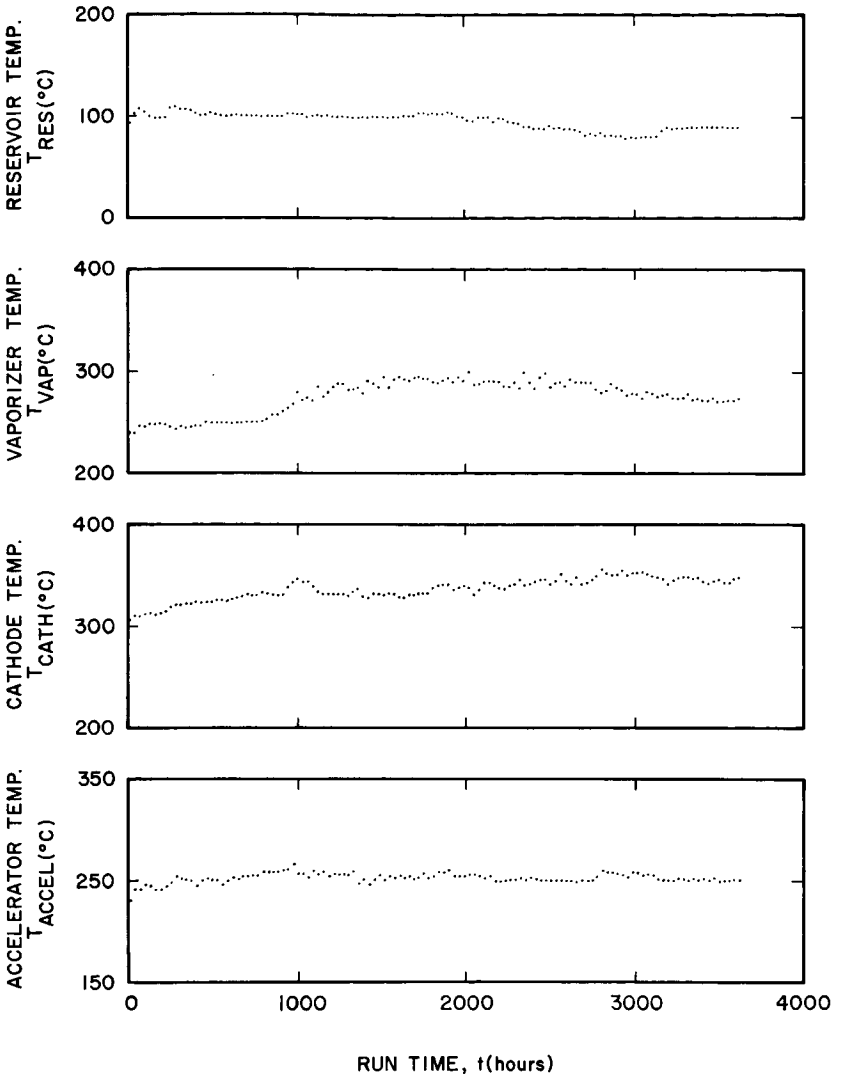

Figure 26. DG-1 Component Operating Temperatures

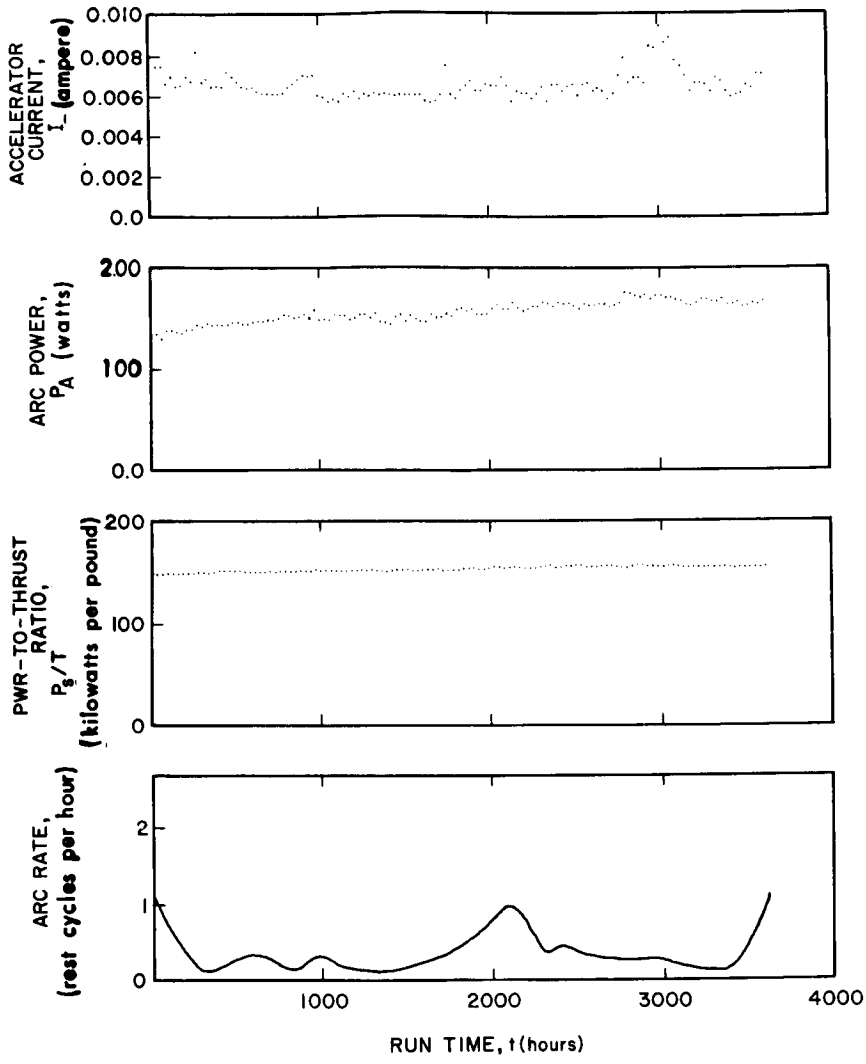

Figure 27. DG-1 System Operating Parameters

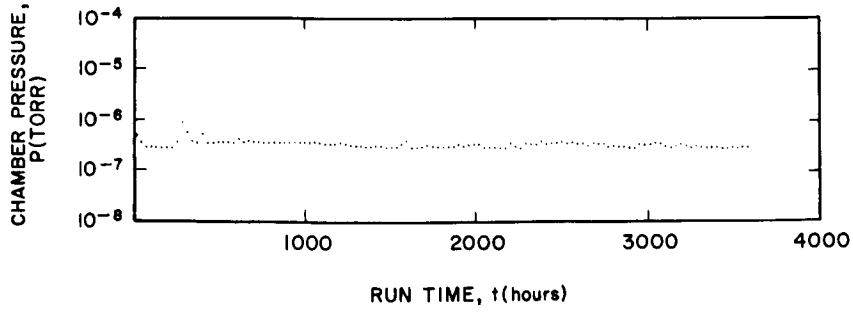

Figure 28. Chamber Pressure During DG-L Test

Two thousand hours of operation were completed on 21 November 1965. On 22 November the engine system was partially shut down for vacuum system maintenance; the high voltages, feed system powers, and neutralizer power were shut off for 5 hours. During this period the vacuum system was held at a pressure below 10^{-6} torr using the back-up diffusion pump, and the main diffusion pump was replaced. The only difficulty encountered was a slightly increased arc rate caused by backsputtered copper which peeled loose during the 5 hours the engine was off and cooling. The scope of the program was then increased to require operation until exhaustion of the cesium supply. Therefore operation was resumed and continued uninterrupted until 30 January 1966 when the cesium supply was exhausted. The engine system ran a total of 3625 hours during the test without loss of vacuum.

Performance of the DG-1 engine system throughout the test was excellent. The power-to-thrust ratio, including feed system and neutralizer power, was 152 ±4 kilowatts per pound, well below the goal of 160 kilowatts per pound. The specific impulse, corrected for neutral cesium losses from both the engine and neutralizer, was 5000 ±50 seconds. The thrust was maintained at 6.7 ±0.2 millipounds.

The engine duty cycle was excellent despite the multiple arc counting observed. Initially, the engine was off for only 0.5 percent of the elapsed time. This down time dropped, as the engine cleaned up, from 0.8 percent during the first 225 hours to 0.25 percent during the period after 500 hours. The down time for vacuum repair and subsequent increased arc rate after 2000 hours of operation raised the run average "down time" to 1.1 percent by the end of the test.

Vacuum was held quite low throughout the test as is shown in Fig. 28. A mass spectrometer analysis of the residual gas in the chamber near the start of the test showed 66 percent hydrogen, 13 percent water (mass 17, 18), and 0.14 percent oxygen (mass 32). The remainder was mostly nitrogen, carbon monoxide, and hydrocarbons. By the end of the test, oxygen content was below the detection limit of 2×10^{-12} torr and water vapor comprised only 0.15 percent of the residual gas. Over 92 percent was hydrogen and 6 percent was mass 28 (CO, N_2).

3.1.7 POST RUN ANALYSIS

The DG-1 engine performed excellently on the 2000-hour (nominal) test. A summary of its average performance during 3625 hours at design level thrust is given in Table VI. These results include only the time accumulated while the engine was under unbroken vacuum. The engine logged about 57 hours of run time during initial tests and performance mapping but this period is not included in the 3625 hours of run time summarized in the table. Average engine mass efficiency was 91.9 percent as calculated from beam current and weight loss.

TABLE VI

PARAMETRIC DG-1 TEST RESULTS

A. Results of Continuous Test	
Test duration	3665 hours
Time at 6.70 mlb average thrust	3625 hours
Duty cycle	98.9 percent
Cs consumed by engine	7865 grams
Initial load	7890 grams
Fraction consumed	99.7 percent
Cs consumed by neutralizer	68.2 grams
Initial load	214.4 grams
Fraction consumed (11,000-hour capacity)	31.6 percent
Neutralizer-to-engine flowrate ratio	0.0087
Specific impulse $\left(\frac{\text{thrust x time}}{\text{total weight loss}}\right)$	5001 seconds
Maximum power-to-thrust ratio	157.4 kW/lb
Average power-to-thrust ratio	152.3 kW/lb
Minimum power-to-thrust ratio	147.1 kW/lb
B. Total Operating Times (including performance mapping)	
Engine and feed system	3718 hours
Neutralizer	3666 hours

A complete electrical checkout of the engine system both prior to removal from the vacuum system and, where necessary, after removal, showed no deterioration throughout the test.

The DG-1 engine system and subassemblies are shown in Figs. 29 through 33 immediately after removal from the vacuum system. The contamination observed was due to backsputtered copper in the electrode region and carbon deposits left by breakdown by hydrocarbons by cesium in the vicinity of the neutralizers. Samples of deposits on the system were taken from various locations, as shown in Fig. 34. The quantitative analyses of these deposits are given in Table VII.

NOTE

A small sample size necessitated a qualitative analysis for some samples. The results of such analyses are not given in percent but show only the relative abundances of the element detected. The major elements in the sample are denoted by 1, and other elements, in decreasing order of abundance, are denoted by 2, 3, and 4. A dash denotes an element which was not detected in the analysis of a sample. Where an estimate of the lower detection limit for an undetected element was possible the limit is noted in the table by <, denoting "less than". That is, if tungsten were not detected in a sample and the analyst estimated the lower limit for detection to be 0.01 percent, this figure would be listed as < 0.01, denoting the known abundance of tungsten to be less than 0.01 percent.

The major deposit is copper which has been backsputtered from the vacuum facility liner and collector. Aluminum eroded from the accelerator electrode is also present. Other impurities are small and indicate only minor erosion of the engine components. Considerable contamination of the cathode was found; however, this was assumed to be a deposition of impurities from the cesium and was the most probable cause of the arc power increase. This suggested that thermal adjustments in the feed system and/or cathode could alleviate the problem by preventing buildup at the cathode. Results of analysis of the deposits in the DG-2 cathode indicate that the contamination may be material sputtered from the vacuum chamber and transported to the cathode by the discharge.

Weight loss measurements on the engine and feed system showed only a small weight loss from the reservoir. Weight loss from the accelerator electrode could not be measured accurately due to the difficulty of removing the backsputtered copper. Such a measurement must be very accurate since corrections must be made for the high mass around the electrode periphery in determining effective percentage weight losses. For this reason a detailed analysis of the location and extent of accelerator erosion was conducted. Other components of the engine system were essentially unchanged (see Table VIII).

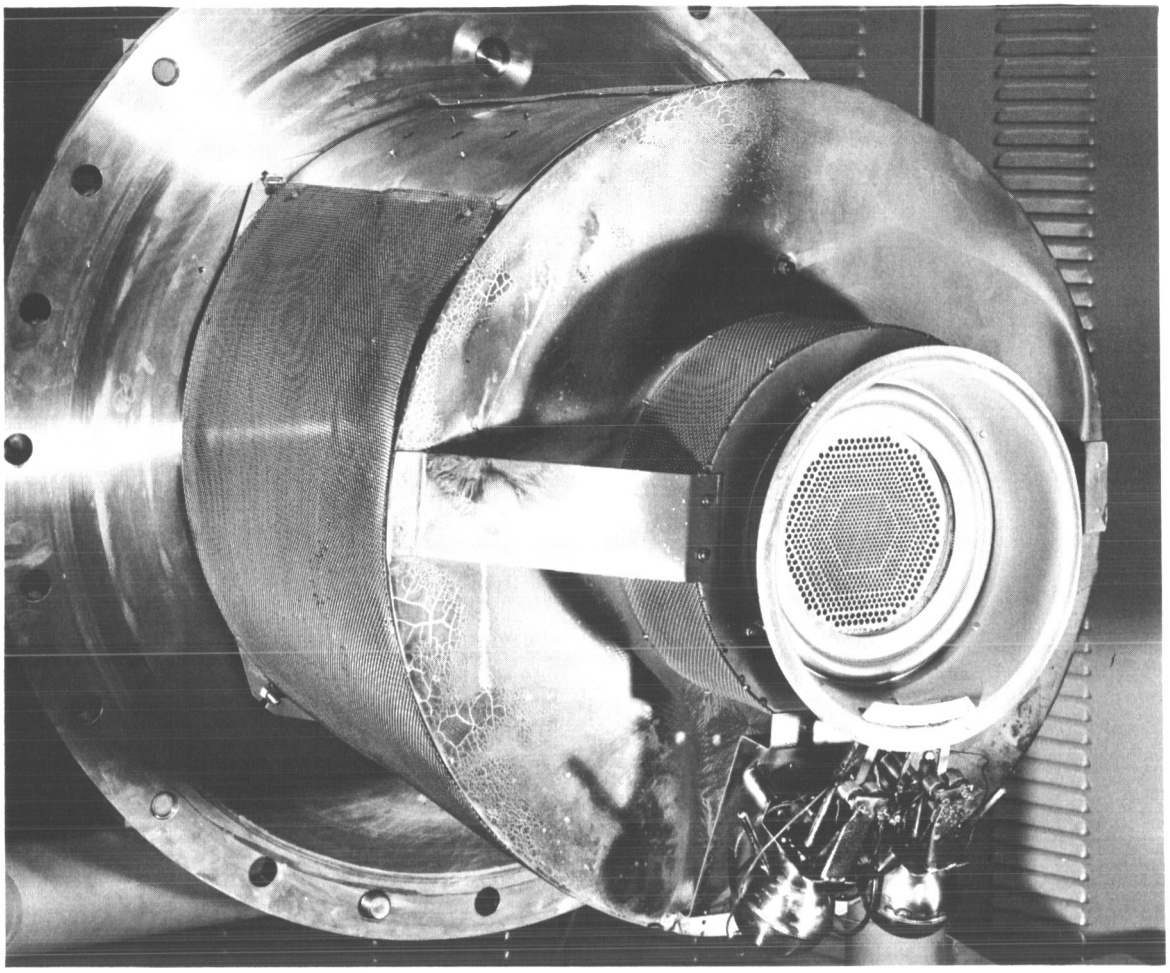

Figure 29. DG-1 Test Assembly After 3700-Hour Test

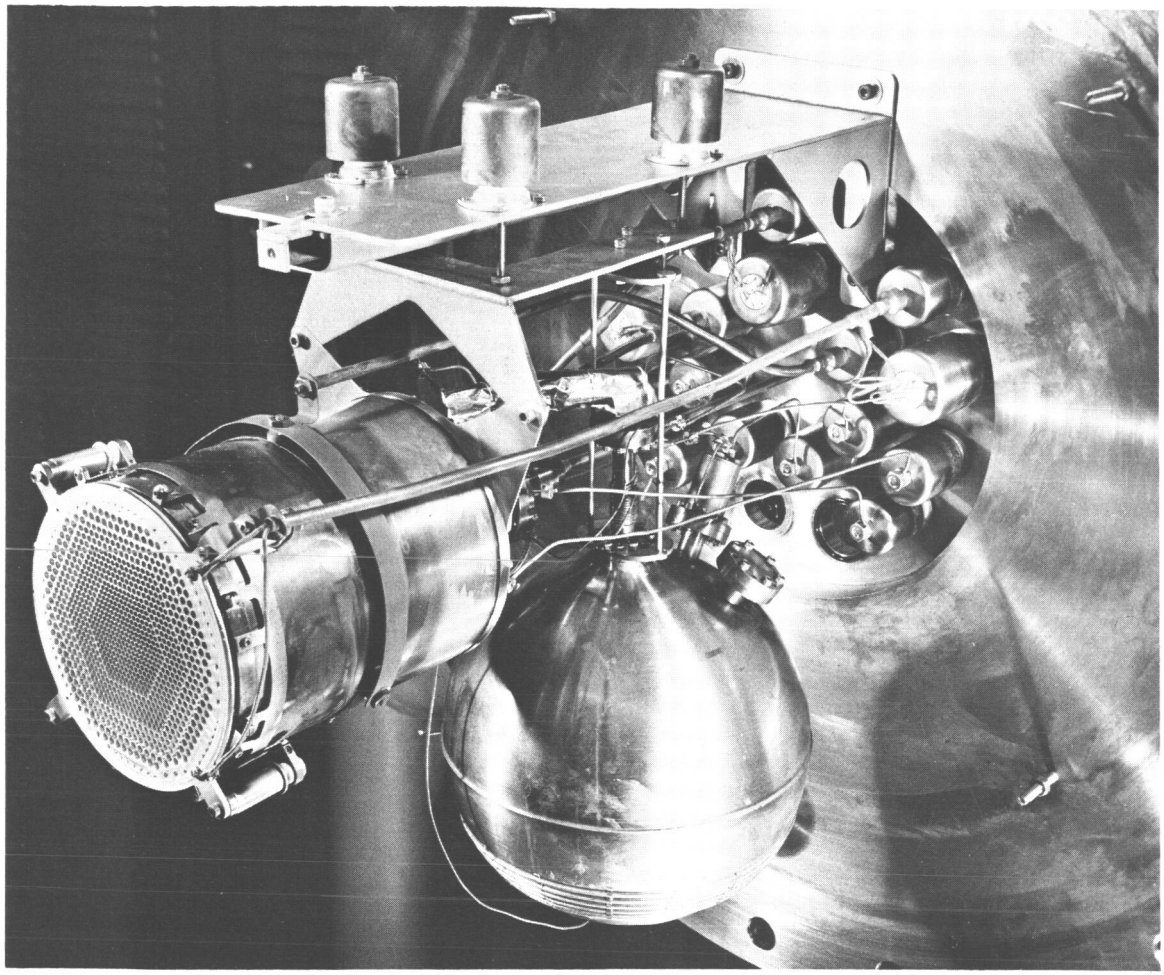

Figure 30. DG-1 Engine and Feed System After 3700-Hour Test

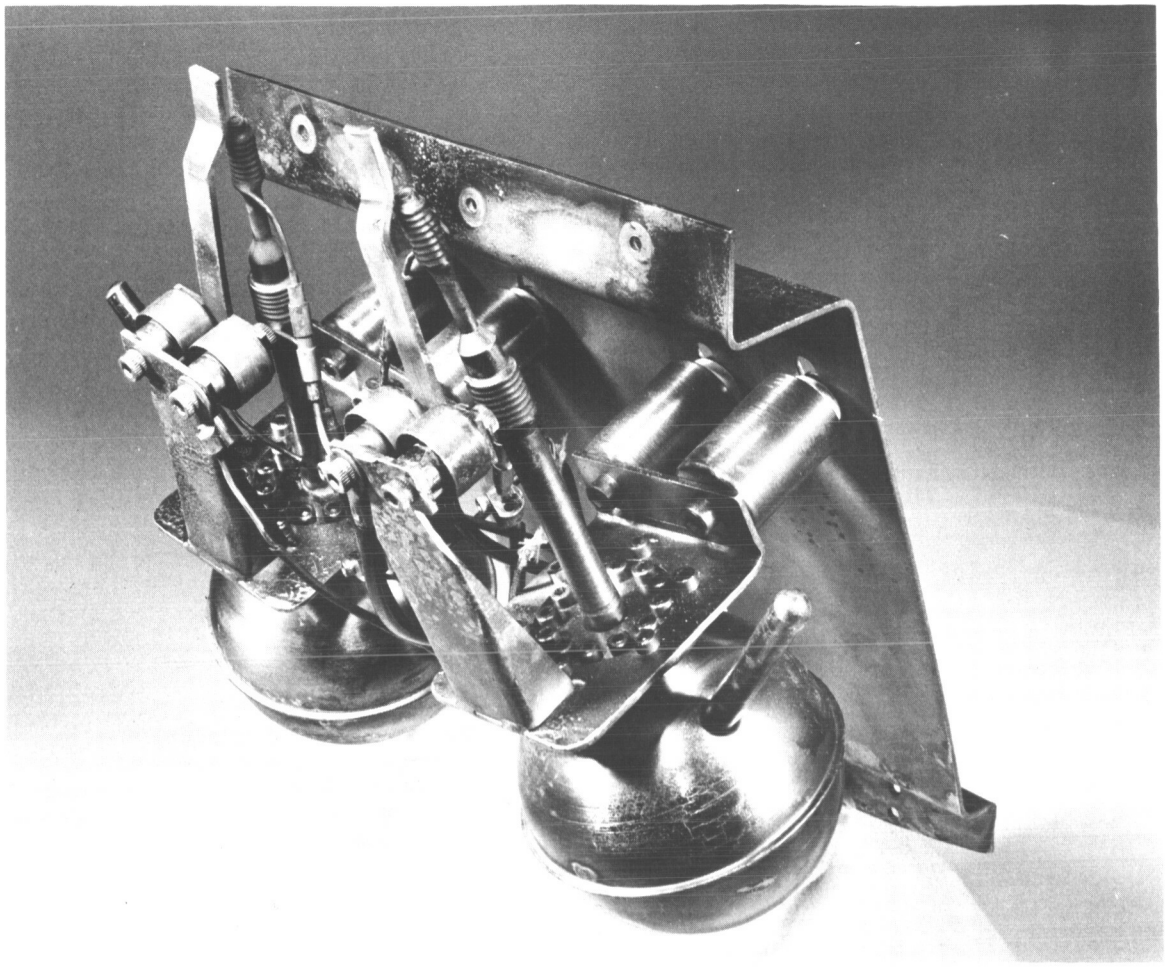

Figure 31. DG-1 Neutralizers (left-hand one used during 3700-hour test)

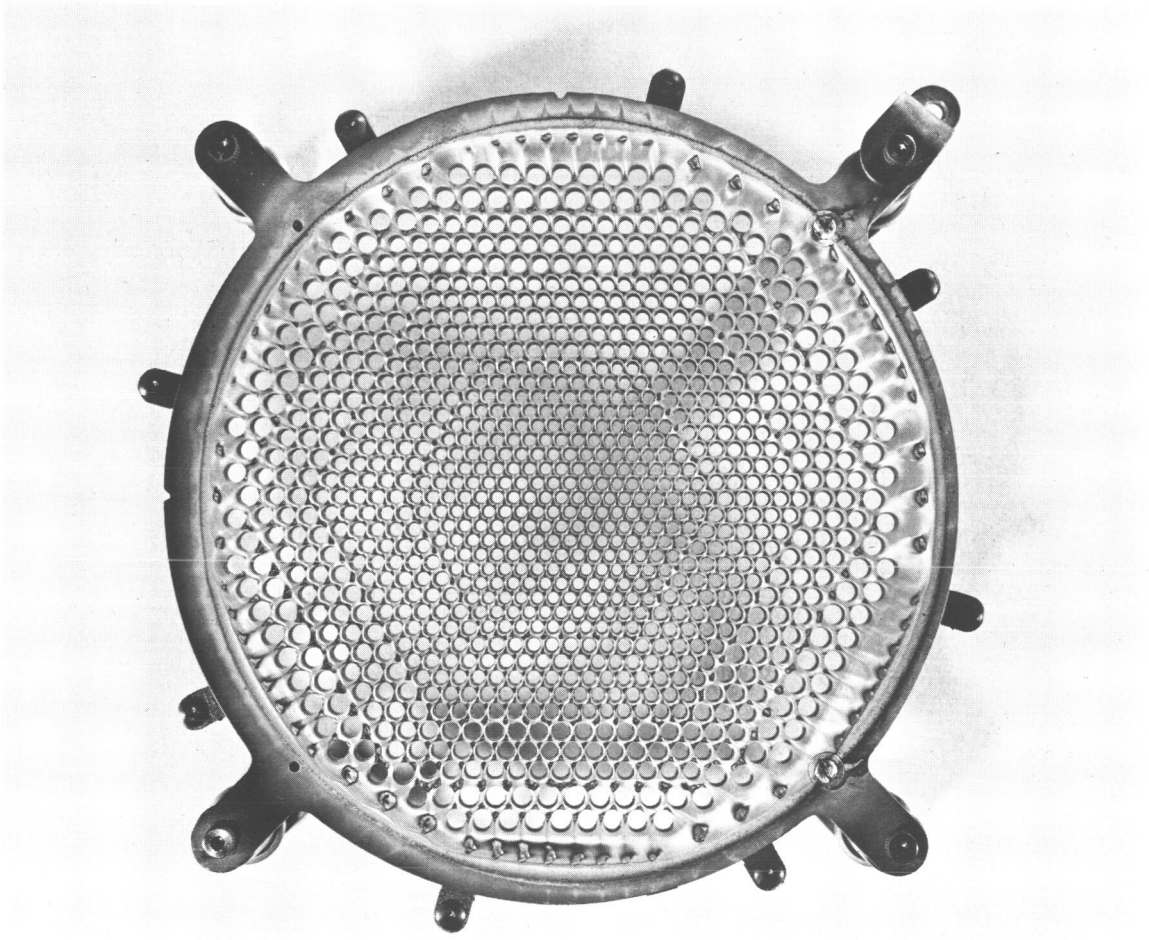

Figure 32. Electrode System (downstream side) After 3700-Hour Test

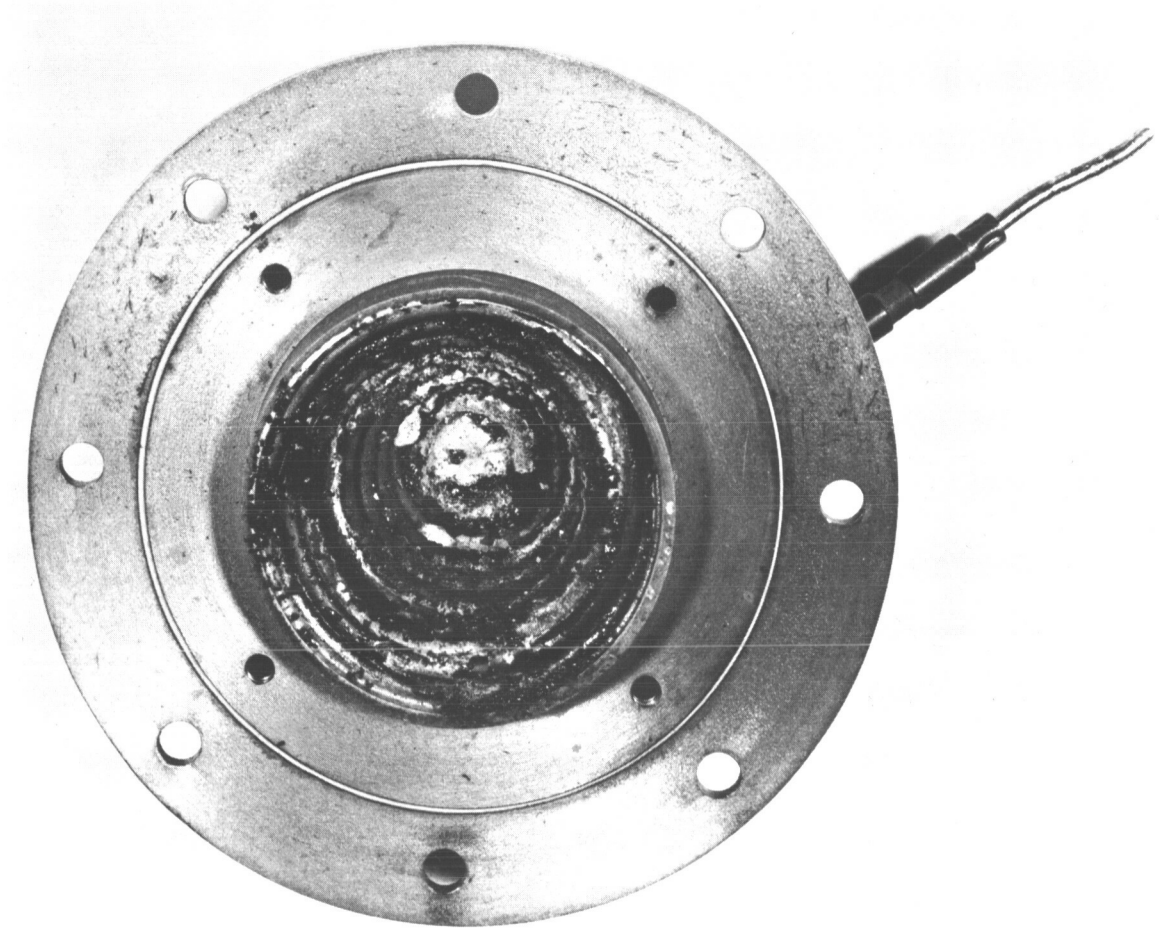

Figure 33. DG-1 Cathode After 3700-Hour Test

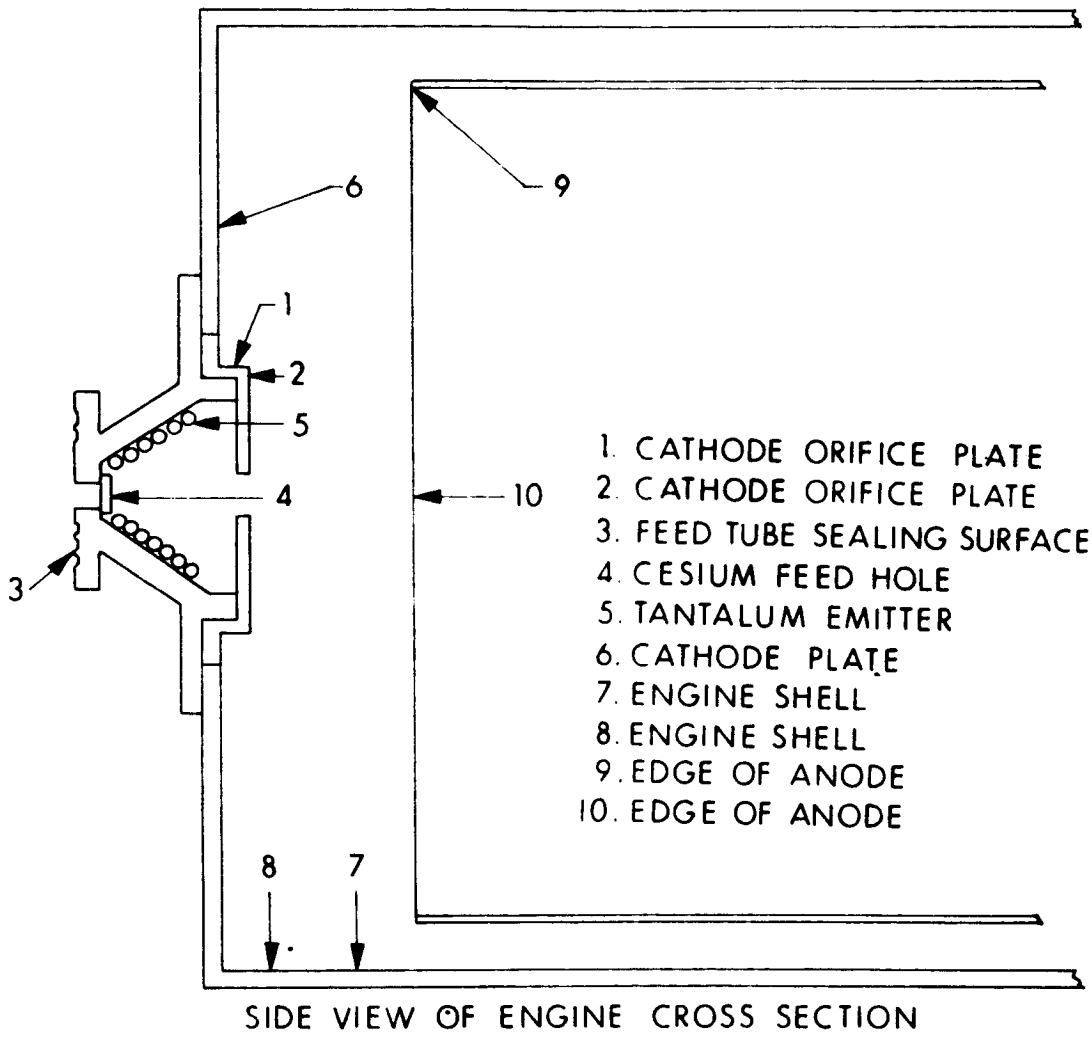

Figure 34. Deposits Sampled on DG-1 After 3700-Hour Test

TABLE VII

ANALYSIS OF DEPOSITS OF DG-1 AFTER LONG TEST*

Sample No. / Element	1 (%)	2 (%)	1	4 (%)	5 (%)	6 (%)	7 (%)	8 (%)	9	10
Al	23.0	10.0	4	0.10	0.10	15.0	25.0	17.0	2	2
Mg	0.006	0.007	4	—	—	< 0.005	< 0.006	< 0.003	4	4
Pb	< 0.004	0.005	–	—	—	0.009	< 0.006	< 0.003	–	4
Cr	0.02	0.02	3	—	—	0.05	< 0.01	< 0.006	4	4
Cu	Rem	Rem	4	0.10	0.10	Rem	Rem	Rem	1	1
Fe	0.08	0.15	3	0.004	0.004	0.2	0.1	0.06	3	3
Mn	0.004	0.002	4	—	—	0.002	0.003	0.001	3	4
Mo	0.04	0.05	1	3.2	3.2	0.05	0.03	0.01	4	2
Ni	0.04	0.10	–	0.005	0.005	0.05	0.2	0.01	–	4
Si	0.08	0.05	4	0.01	0.01	0.04	0.2	0.03	3	3
Ag	0.08	0.0005	4	0.005	0.004	0.0005	0.3	0.03	4	3
Ti	0.004	0.003	–	0.003	0.001	0.003	< 0.003	< 0.002	–	3
W	< 0.04	< 0.05	–	0.04	0.08	< 0.05	< 0.05	< 0.03	–	–
Ta	—	—	–	3.2	6.0	—	—	—	–	–
Cs	—	—	–	Rem**	Rem**	—	—	—	–	–
Na	—	—	–	—	—	—	—	—	–	3
Sn	—	—	–	—	—	—	—	—	–	4
B	—	—	–	—	—	—	—	—	–	4

*See Note, page 55, for explanation

**The sample was hygroscopic and as such contains water and anions in the balance.

TABLE VIII

DG-1 ENGINE COMPONENT WEIGHT AND DIMENSION CHANGES

Part	Weight Upon Assembly (grams*)	Weight After 3700-Hour Test (grams*)	Weight Change (grams**)
Engine Shell	719.79	718.05	-1.74
Anode	228.656	232.468	+3.812
Cathode Orifice Plate	34.221	35.115	-0.106
Cathode Body	183.140	185.841	+2.701
Cathode Plate (end of shell)	154.282	154.237	-0.045
Screen Electrode	46.041	48.460	+2.419
Accelerator Electrode	103.638	101.151	-2.487

*Uncertainty in last figure of each measurement is ±2 or less.

**Uncertainty in last figure of each measurement is ±4 or less.

The accelerator electrode was eroded similarly to that used on the 2610-hour test (Ref.1) of the DF engine. Erosion was nonexistent on the upstream side of the electrode and only a small increase in the aperture diameters was found on the downstream or exhaust side. The principal erosion occurred as well defined pits on the web area on the downstream side of the electrode. This erosion is due to impingement of slow ions formed in the beam plasma. These ions were focused by the shape of the plasma sheath near the accelerator electrode such that they impinged upon the web areas.

A measurement of the erosion pit depths on the accelerator was carried out using a binocular microscope and dial indicator. In the aluminum accelerator, which has a thickness of 0.125 inch, the deepest pit (0.068 inch) was found not in the web area but near the neutralizer where the cesium neutral density was increased due to the neutralizer cesium efflux. The pits in the web area were deepest in the transition region between aperture patterns. In these areas pit depths averaged about 0.030 inch or about one quarter of the electrode thickness. The deepest of these pits was 0.039 inch.

Backsputtered copper did not significantly mask accelerator erosion. A 0.005-inch layer of copper was deposited on the engine, and hence the accelerator, during the run. This effectively increased the accelerator thickness by only 0.002 inch with respect to sputtering as copper is sputtered off faster than aluminum. This effective increase is small in comparison to the pit depths; hence, where significant erosion occurred it was not strongly affected and erosion was masked only where it was insignificant. This is only true where a high contrast erosion such as this occurs.

An exact extrapolation of the time to breakthrough of the deepest pit is difficult as the erosion rate decreases with time due to the trapping nature of the pit shapes. Bearing this in mind, a figure of 20,000 hours to pit breakthrough is justified. Under Contract NAS3-5250 it was shown that breakthrough will not affect performance so the lifetime of this system eertainly appears to exceed requirements.

Feed System Post-Run Analysis

Upon completion of the 3718-hour test of the DG-1 engine the 20-pound feed system SN-1 was analyzed with respect to weight loss, cesium used, corrosion, and appearance. The other feed systems used were two 1/2-pound-capacity neutralizer feed systems SN-2 and SN-3. The SN-3 neutralizer feed system, although attached to the engine during the test, was not used and therefore no post-run analysis was performed. The SN-2 neutralizer feed system was not sectioned and analyzed. A weight loss measurement was taken, however, to determine the neutralizer cesium flow rate.

After removal from the engine the feed system was weighed. The weight of cesium remaining was 24.5 grams. This was approximately the amount required to fill the porous rod and none was available for chemical analysis. During the test, 99.7 percent of the cesium load was exhausted. The various engine feed system component weights are given in Table IX.

The manual valve was found to be in very good condition when disassembled. All parts were clean except for the diaphragm, which was covered with a thin film of orange colored material. The change in this material when exposed to air indicates that it was mostly cesium. This film has been seen after other long duration tests. However, the dark colored resinous deposits previously noted on the valve stem were absent.

The U-tube was exceptionally clean except for the same orange colored film on the flange next to the manual valve.

The porous rod was removed from the vaporizer and sectioned. Analysis of these sections as well as those from a section obtained during assembly are tabulated in Table X. SN-7, -8, and -9 are sections taken at the vaporizer end of the porous rod, SN-10 at the middle of the rod, and SN-11 at the reservoir end.

The vaporizer tube was sectioned. The interior showed only minor pitting and the tool marks from fabrication were plainly visible. Because of the obviously good condition, photomicrographs were not taken.

The port valve was clear of cesium deposits and the O-ring was still intact and capable of sealing the system.

After cleaning, the reservoir was cut apart and various components were accurately weighed. These weights taken before and after the test are tabulated in Table IX. The 8.6-gram weight loss of the fin assembly was unaccountable. However, the weight loss of the complete reservoir was found to be only 3 grams. The 5-gram difference could be an amount removed from the fin assembly and redeposited on the reservoir shell. Unfortunately the weld area around the reservoir was ground away in opening the shells and an accurate weight determination of the shells was not possible.

It was originally suspected that the material lost from the feed system could be accounted for in the deposits found on the cathode. However, the analysis of the cathode deposits showed only insignificant amounts of the constituents of stainless steel. The most abundant contaminant found, other than cesium, was molybdenum, the material used for the cathode housing.

TABLE IX

POST RUN ANALYSIS OF 20-POUND FEED SYSTEM

	Before (grams)	After (grams)	Wt. Change (grams)
Feed System Weights			
Control Fin	16.73185	16.64885	-0.08300
Fin Assembly	1818.0616	1809.4483	-8.6133
Reservoir Assembly	2617.5448	2614.4030	-3.1418
Port Valve Flange	33.51560	33.50115	-0.01445
Vaporizer	99.53370	99.25895	-0.27475
U-Tube	116.9830	116.8874	-0.0956
Manual Valve Body	231.2105	230.926	-0.2845
Manual Valve Diaphragm	64.11915	63.92035	-0.1988
Manual Valve Tip	4.61775	4.61855	+0.0008
Copper Seal Weights			
Port Valve	1.74085	1.7464	+0.00555
Blank Flange	1.73235	1.7322	-0.00015
Reservoir-Vaporizer	1.75575	1.7534	-0.00235
Vaporizer-U-Tube	1.73825	1.73887	+0.00062
U-Tube-Valve	1.76295	1.76315	+0.00020
Manual Valve	5.18235	5.1835	+0.00115
Valve-Cathode	1.7751	1.77535	+0.00025
Feed System Dimensions	(inch)	(inch)	(inch)
Control Fin Thickness	.005	.005	0
Vaporizer Base	.491	.491	0
Top Shell Thickness	.0210-.0220	.0210-.0220	0
Bottom Shell Thickness	.0155-.0180	.016-.018	0

TABLE X

POROUS ROD ANALYSIS 20-POUND FEED SYSTEM

Porous Rod	Before (%)	SN 7 (%)	SN 8 (%)	SN 9 (%)	SN 10 (%)	SN 11 (%)
Nickel	Rem.	Rem	Rem.	Rem.	Rem.	Rem.
Iron	0.39	1.18	1.16	0.34	0.33	0.28
Manganese	0.016	0.05	0.05	0.02	0.02	0.02
Silicon	0.09	0.22	0.08	0.08	0.19	0.10
Aluminum	0.003	0.02	0.03	0.01	0.005	0.005
Copper	0.12	0.03	0.03	0.02	0.02	0.02
Titanium	< 0.004	< 0.004	< 0.004	< 0.004	< 0.004	< 0.004
Cobalt	0.09	0.15	0.17	0.15	0.17	0.17
Chromium		0.03	0.01	0.01	0.01	0.01
Magnesium		0.002	0.004	0.002	0.003	0.003

TABLE XI

CONTROL FIN ANALYSIS 20-POUND FEED SYSTEM

Constituent	Before Duration of Test (%)	After Duration of Test (%)
Manganese	1.43	1.65
Silicon	0.51	0.30
Chromium	17.2	17.4
Nickel	12.8	10.6
Molybdenum	0.30	0.35
Columbium	0.60	0.86
Copper	0.44	0.48

A sample of the reservoir control fin was chemically analyzed and is compared with a previous analysis in Table XI. The control fin was arbitrarily designated and marked before the test so that this comparison could be made.

All portions of the feed system were in exceptionally good condition with no signs of corrosion. The feed system supplied propellant until the supply was exhausted with no problems encountered. It appears that this type of system could be used for periods many times the 3718 hours accumulated on this test.

3.2 THE 4000-HOUR DG-2 ENGINE SYSTEM TEST

The second long test run under the program was designated the 4000-hour test. After completion of 4000 hours the scope of the program was increased to require operation until exhaustion of the cesium supply. The DG-2 engine system tested ran 8133 hours at thrust under unbroken vacuum. The test system was identical to that used on the 2000-hour test of DG-1 except for a different thrustor feed system.

3.2.1 THE DG-2 ENGINE SYSTEM

The DG engine was described in Section 2. The 4000-hour test system included the DG-2 engine, a 40-pound capacity cesium feed system (Fig. 35), and two plasma bridge neutralizers of the type mentioned in Subsection 2.7 (entire assembly Fig. 36). As on the first long test, two neutralizers were included, one as a spare, because their lifetime had not been accurately determined. Also included was a ground screen surrounding the test assembly to provide electrostatic shielding. This prevented stray electrons from bombarding the engine and giving erroneous readings of beam current and, therefore, of efficiency.

The neutralizers were different than those used with DG-1. Modified neutralizer components were employed to facilitate mounting on the DG-2 assembly. Each had its cathode tube mounted at 90° to the vaporizer and feed tube section to allow the orifice to be oriented horizontally instead of vertically as on the previous long test. This mounting was used to prevent clogging of the neutralizer orifice if backsputtered material peeled off the ground screen or accelerator electrode. The expected length of the run prompted this consideration which was not taken in the shorter test of the DG-1 engine. Figure 37 shows one of the modified neutralizers.

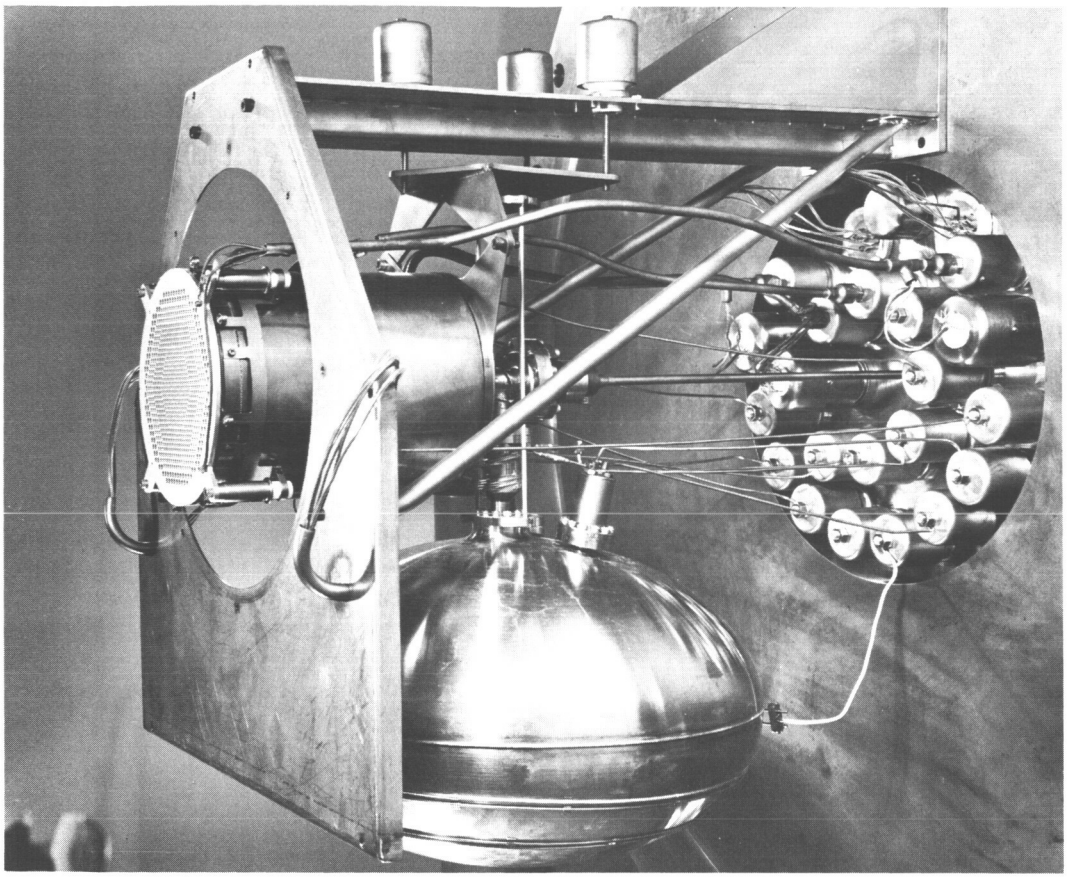

Figure 35. DG-2 Engine and Feed System

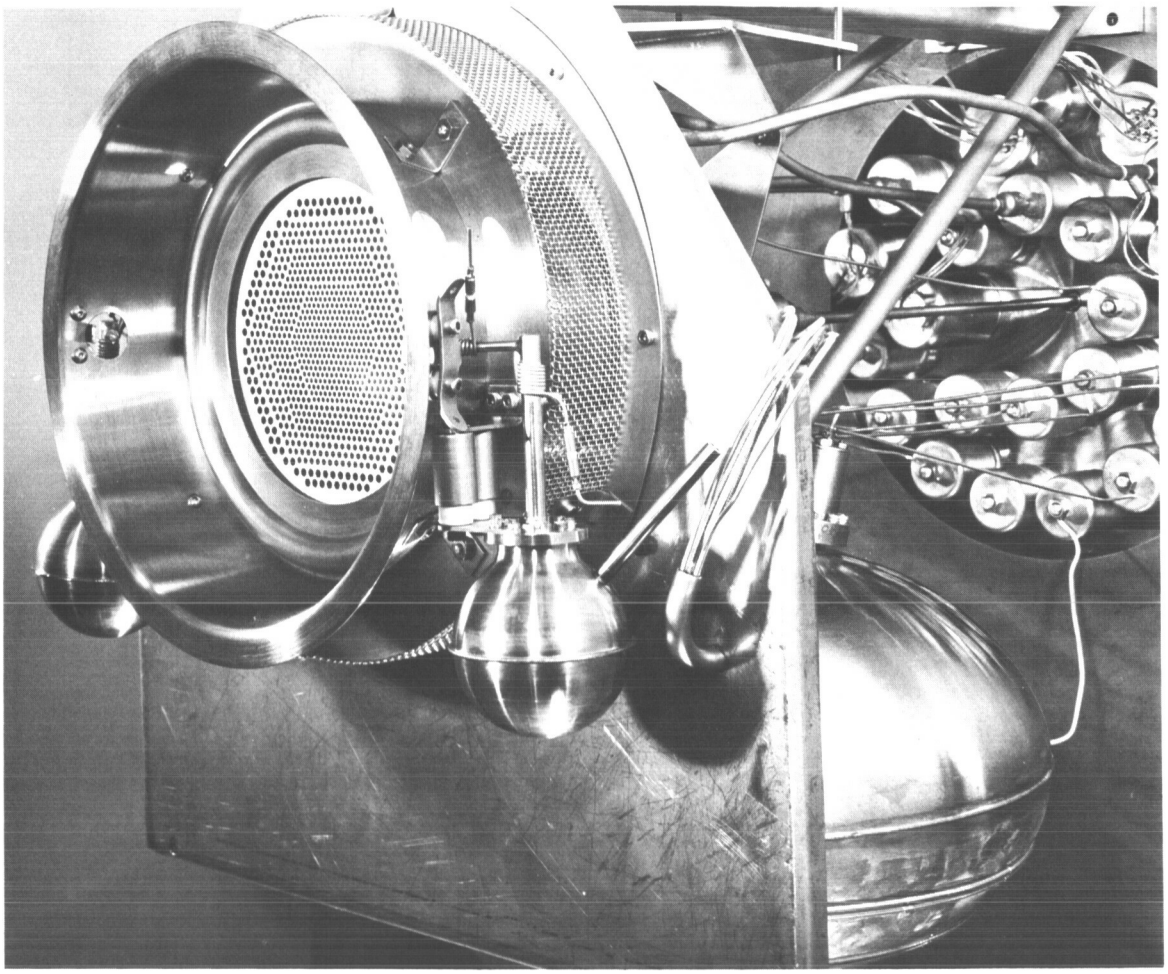

Figure 36. DG-2 Engine System With Neutralizers Mounted

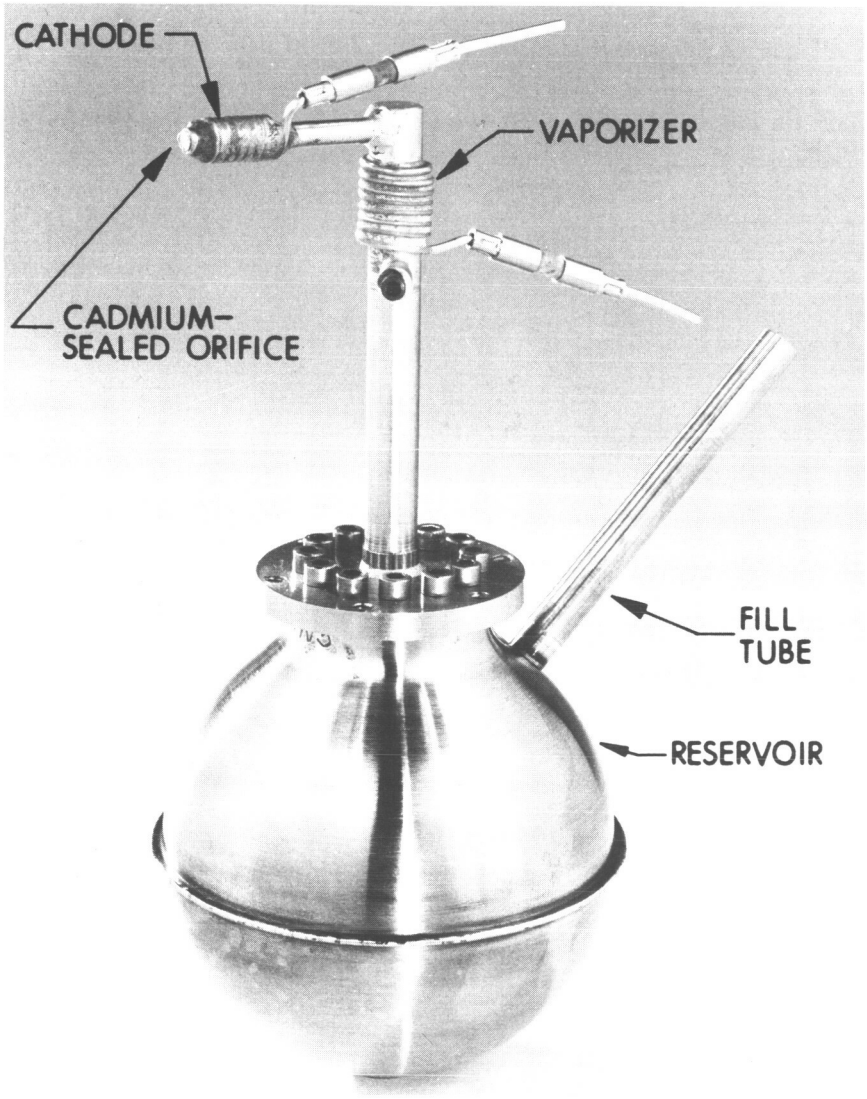

Figure 37. Plasma Bridge Neutralizer for DG-2

The 40-pound feed system was designed so that its manual feed valve connected directly to the engine cathode, saving the complication and power loss of the inverted U-tube as used with the DG-1 engine. This was possible with an oblate-spheroid shape of the reservoir which conserved height and allowed the system to fit into the test chamber.

As in the first test, the engine was expected to use about 2.16 grams of cesium per hour. The reservoir was loaded with approximately 41-1/2 pounds of cesium. Approximately two grams of cesium were to be used for startup and 33 grams for the performance mapping of the engine. The remainder was considered sufficient for 8500 to 8700 hours of operation at the design point. The neutralizer cesium flowrate was expected to be about 1 percent of the flowrate of the engine feed system. Approximately 215 grams (enough for 10,000 hours of operation) were loaded into each neutralizer. Again, a wide safety margin was provided with respect to the fulfillment of the contracted test period.

3.2.2 TEST FACILITY

A vacuum facility was modified as shown in Fig. 38 for extended test operation of the DG-2 engine system. A 3-foot diameter 2-1/2-foot long engine antechamber was added to the 2-foot diameter by 6-foot long facility. Aluminum was used for the collector and the liner baffles to reduce the rate of backsputtering of material to the engine.

A retractable neutral cesium detector was fabricated. This detector was lowered into the tank for performance checks at 1000, 2000, and 3000 hours.

Backup was provided in case of facility failure. Auxiliary power, water, and air supplies were interlocked to continue the test if the primary sources failed. A standby diffusion pump in continuous operation was to be gated onto the chamber in the event of main pump failure. The standby pump was capable of running on one-phase city power or on an emergency generator. Should any of these systems have failed, project personnel were to be notified by phone from an alarm service company.

A pressure of less than 10^{-6} torr was to be maintained throughout the duration of the test.

3.2.3 CONTROL SYSTEM

The control system was identical to that used on the 2000-hour (actually 3700 hour) test of DG-1. It is discussed in Subsection 3.1.3 of this report.

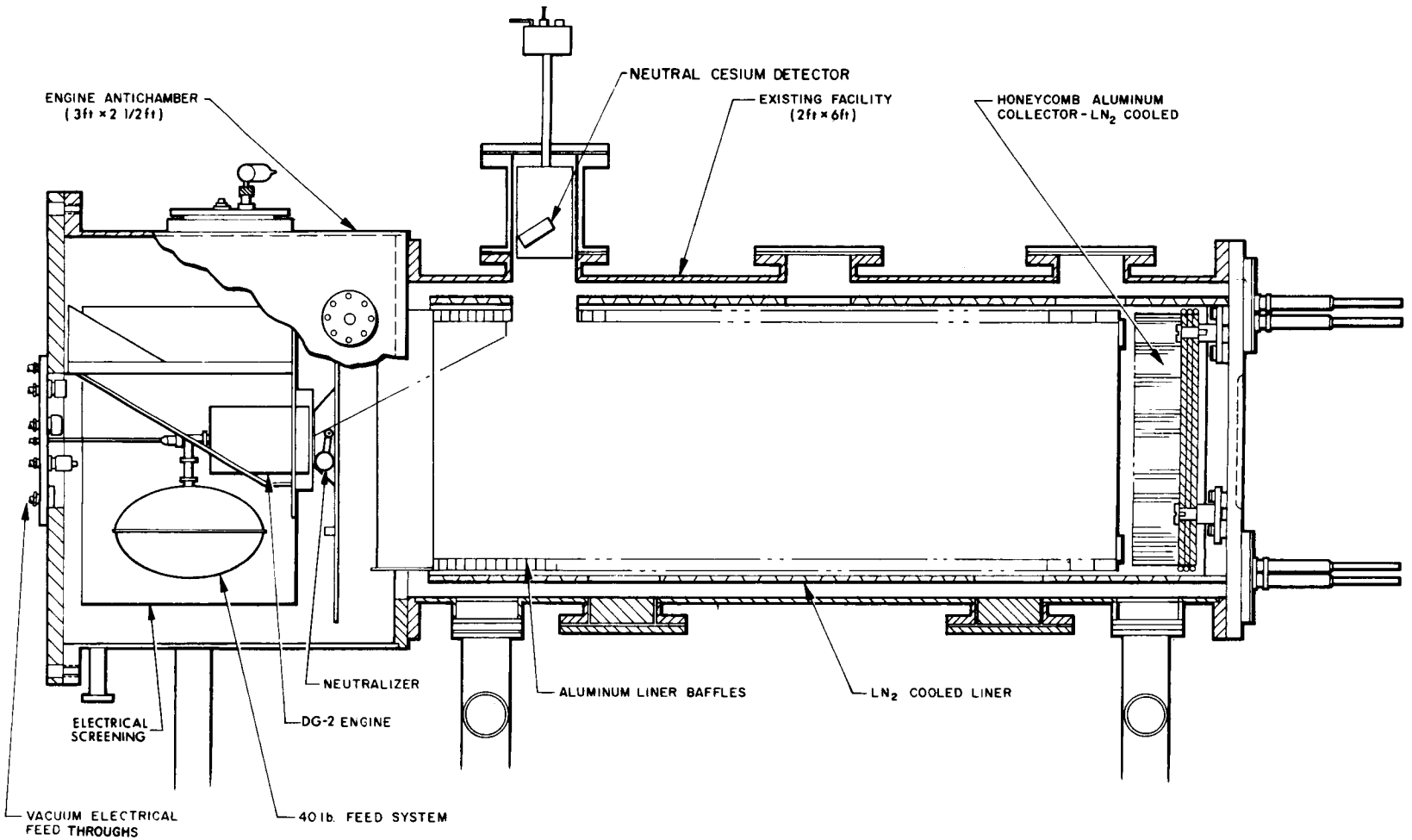

Figure 38. The 4000-Hour Test Facility

3.2.4 PERFORMANCE MAPPING

The performance mapping of the DG-2 engine was carried out in a manner similar to that of the DG-1 engine. These procedures and expectations may be found in Subsection 3.1.4. The electrical schematic, Fig. 20, applies to DG-2 as well as to DG-1.

3.2.5 PERFORMANCE DATA

The DG-2 engine was performance mapped over a wide range of optimum and nonoptimum operating levels. For a particular mass flow rate, operation at low, optimum, and high specific impulse was attempted. In this manner, the domain of optimum and nonoptimum engine operation was explored.

Since the feed system required many hours to reach an equilibrium temperature for any power input, the feed system power consumption necessitated for various stable beam currents was determined in a separate test of the feed system vaporizer.

Determinations of mass efficiency could be affected by cesium from the neutralizer, so the neutralizer was performance-mapped separately. In calculating the system power-to-thrust ratio and specific impulse, the separately determined feed system and neutralizer powers were added to the engine data.

The original data from the engine performance mapping are given in Table XII. Table XIII gives all data for the feed system and Table XIV shows the neutralizer data.

Figures 39 and 40 give plots of feed system power versus beam current and total neutralizer power versus neutralizer emission current, respectively. Powers taken from these graphs were used in calculating system performance. Table XV shows the corrected data and calculated performance for the engine and engine system in order by specific impulse.

Figure 41 shows engine and system overall efficiency versus specific impulse. The maximum efficiency was found with the highest attainable beam at any specific impulse, so the criterion of efficiency alone implied high-beam operation. When the effects of negative high voltage and drain current on lifetime were considered, a lower than maximum beam level was found desirable.

TABLE XII

DG-2 PERFORMANCE MAPPING ORIGINAL DATA

Data Point	Positive High Voltage, V_+ (kV)	Negative High Voltage, V_- (kV)	Negative HV Current, I_- (amp)	Beam Current, I_B (amp)	Arc Voltage, V_A (volts)	Arc Current, I_A (amp)	Magnet Voltage, V_M (volt)	Magnet Current, I_M (amp)	Neutral Detector Current, I_{NCD} (10^{-9} amp)	NCD Background, I_{NCD_o} (10^{-9} amp)	I_{NCD} at I_B, I'_{NCD} (10^{-9} amp)	Reduced Beam Current, I'_B (amp)
1	2.00	0.900	0.0080	0.490	7.5	22.5	4.4	2.1	6.5	2.5	22.0	0.340
2	1.5	1.4	0.0090	0.495	7.5	23.0	4.4	2.1	7.2	2.7	23.0	0.345
3	1.0	1.9	0.0150	0.490	7.5	23.0	4.4	2.1	8.6	3.0	26.0	0.340
4	2.35	0.600	0.0068	0.490	7.5	23.2	4.4	2.1	7.0	2.7	23.1	0.345
5	2.8	0.300	0.0070	0.490	7.6	23.0	4.4	2.1	6.8	2.7	24.0	0.340
6	3.25	0.400	0.120	0.485	7.6	23.2	4.4	2.1	6.5	2.7	24.0	0.330
7	3.7	0.300	0.0210	0.485	7.6	23.9	4.4	2.1	6.4	2.6	23.6	0.330
8	2.35	0.800	0.0082	0.590	7.5	30.8	4.4	2.1	7.2	2.8	19.0	0.465
9	2.00	1.1	0.0092	0.595	7.5	29.0	4.7	2.2	7.5	3.5	17.5	0.480
10	1.6	2.00	0.0170	0.590	7.5	27.0	4.7	2.2	8.5	3.6	18.5	0.490
11	1.3	2.20	0.0150	0.590	7.5	27.1	4.7	2.2	9.6	4.1	21.0	0.490
12	2.8	0.400	0.0083	0.600	7.5	27.6	4.7	2.2	9.0	4.3	20.0	0.490
13	3.25	0.350	0.0091	0.600	7.5	27.1	4.7	2.2	8.2	3.8	17.0	0.500
14	3.7	0.350	0.0144	0.600	7.5	29.4	4.7	2.2	8.0	4.0	18.2	0.500
15	4.25	0.400	0.0270	0.595	7.5	29.0	4.7	2.2	8.2	3.8	20.5	0.475
16	4.25	0.500	0.0200	0.730	7.7	35.5	4.6	2.1	8.2	4.0	16.5	0.630

TABLE XII

DG-2 PERFORMANCE MAPPING ORIGINAL DATA (contd)

Data Point	Positive High Voltage, V_+ (kV)	Negative High Voltage, V_- (kV)	Negative HV Current, I_- (amp)	Beam Current, I_B (amp)	Arc Voltage, V_A (volts)	Arc Current, I_A (amp)	Magnet Voltage, V_M (volt)	Magnet Current, I_M (amp)	Neutral Detector Current, I_{NCD} (10^{-9} amp)	NCD Background, I_{NCD_o} (10^{-9} amp)	I_{NCD} at I'_B I'_{NCD} (10^{-9} amp)	Reduced Beam Current, I'_B (amp)
17	4.8	0.500	0.0320	0.730	7.7	35.1	4.6	2.1	7.9	3.6	15.5	0.625
18	3.7	0.400	0.0143	0.730	7.7	36.1	4.9	2.2	7.5	4.9	14.6	0.605
19	1.5	0.400	0.0042	0.225	7.1	11.7	4.0	2.1	6.3	0.8	16.0	0.165
20*	1.1	0.700	0.0046	0.225	7.0				8.5	1.1	22.0	0.140
21	0.400	1.60	0.0150	0.200	7.0	11.3	3.6	2.0	8.2	1.5	18.5	0.130
22	0.400	1.20	0.0064	0.190	6.9	11.0	3.6	2.0	10.8	1.6	21.5	0.120
23	0.400	1.10	0.0060	0.180	6.9	10.1	3.6	2.0	12.5	1.6	22.3	0.115
24	0.600	1.10	0.0039	0.203	6.9	12.0	3.4	1.9	9.0	1.8	18.0	0.140
25	0.600	1.20	0.0042	0.203	7.0	11.4	3.6	2.0	8.8	1.9	19.0	0.135
26	0.800	1.10	0.0044	0.215	7.0	12.0	3.6	2.0	8.5	2.2	18.1	0.145
27	1.000	0.900	0.0044	0.215	7.0	12.1	3.6	2.0	8.0	2.2	19.5	0.135
28	1.300	0.600	0.0046	0.220	7.0	13.0	3.6	2.0	7.0	2.1	17.5	0.145
29	1.600	0.300	0.0046	0.215	7.0	12.1	3.6	2.0	7.3	2.0	17.6	0.140
30	2.00	0.100	0.0049	0.218	7.0	12.2	3.6	2.0	6.8	2.0	17.0	0.140
31	2.35	0.100	0.008	0.218	7.0	12.0	3.7	2.05	6.5	2.0	16.1	0.145
32	2.8	0.050	0.0126	0.215	7.1	12.0	3.8	2.05	6.3	2.0	13.6	0.160

*Data recording was interrupted.

TABLE XII

DG-2 PERFORMANCE MAPPING ORIGINAL DATA (contd)

Data Point	Positive High Voltage, V_+ (kV)	Negative High Voltage, V_- (kV)	Negative HV Current, I_- (amp)	Beam Current, I_B (amp)	Arc Voltage, V_A (volts)	Arc Current, I_A (amp)	Magnet Voltage V_M (volt)	Magnet Current, $I_{M'}$ (amp)	Neutral Detector Current, I_{NCD} (10-9 amp)	NCD Background, I_{NCD_o} (10-9 amp)	I_{NCD} at I'_B, I'_{NCD} (10-9 amp)	Reduced Beam Current, I'_B (amp)
33	3.25	0.050	0.0207	0.215	7.2	12.0	3.8	2.05	6.1	2.0	13.8	0.160
34	3.25	0.050	0.015	0.305	7.0	16.2	3.9	2.1	6.8	2.3	19.6	0.215
35	2.80	0.050	0.0087	0.310	7.0	15.3	3.9	2.1	8.0	2.6	22.4	0.205
36	2.8	0.050	0.0088	0.318	7.0	17.0	3.9	2.1	7.2	2.6	24.0	0.200
37	2.35	0.050	0.0080	0.325	7.0	17.1	3.9	2.1	7.9	2.7	22.5	0.220
38	2.00	0.300	0.011	0.325	7.0	17.6	4.0	2.1	8.0	2.9	22.0	0.225
39	1.6	0.600	0.013	0.322	7.0	17.2	4.0	2.1	8.4	2.9	22.0	0.225
40	2.35	0.400	0.0069	0.420	8.1	19.0	4.3	2.1	5.5	1.0	17.6	0.320
41	2.80	0.200	0.0088	0.408	8.1	17.7	4.3	2.1	6.0	1.2	17.3	0.040
42	3.25	0.100	0.012	0.428	8.2	18.1	4.3	2.1	5.8	1.3	19.5	0.320
43	2.0	0.700	0.0088	0.425	7.7	19.5	4.3	2.1	7.4	1.4	21.0	0.320
44	1.60	1.20	0.0115	0.425	7.6	19.2	4.3	2.1	8.7	1.6	23.5	0.315
45	1.3	1.50	0.020	0.425	7.5	19.8	4.2	2.1	9.9	1.7	25.0	0.315
46	2.0	0.680	0.0059	0.405	7.5	19.5	3.9	2.1	4.2	0.9	13.2	0.315
47	2.35	0.460	0.0058	0.405	7.9	19.0	3.9	2.1	4.1	0.6	11.6	0.320
48	2.8	0.220	0.008	0.400	7.6	19.5	3.9	2.05	3.8	0.6	12.1	0.320

TABLE XII

DG-2 PERFORMANCE MAPPING ORIGINAL DATA (contd)

Data Point	Positive High Voltage, V_+ (kV)	Negative High Voltage, V_- (kV)	Negative HV Current, I_- (amp)	Beam Current, I_B (amp)	Arc Voltage, V_A (volts)	Arc Current, I_A (amp)	Magnet Voltage, V_M (volt)	Magnet Current, I_M (amp)	Neutral Detector Current, I_{NCD} (10^{-9} amp)	NCD Background, I_{NCD_o} (10^{-9} amp)	I_{NCD} at I'_B, I_{NCD} (10^{-9} amp)	Reduced Beam Current, I'_B (amp)
49	3.25	0.220	0.0136	0.430	7.7	20.0	3.9	2.05	3.9	0.7	12.8	0.330
50	3.25	0.220	0.0136	0.410	8.0	18.1	4.2	2.1	3.9	0.7	12.0	0.320
51	3.7	0.120	0.020	0.410	7.9	19.1	4.2	2.1	4.1	0.6	13.1	0.310
52	3.7	0.120	0.0205	0.420	8.0	20.0	4.2	2.1	4.0	0.8	12.2	0.315
53	1.5	1.45	0.0075	0.400	7.7	20.8	4.1	2.1	4.3	0.8	13.0	0.300
54	1.0	1.65	0.0071	0.400	7.3	19.0	4.2	2.1	8.1	1.0	20.0	0.300
55	0.80	1.85	0.0094	0.405	7.4	20.0	4.2	2.1	7.3	1.0	22.1	0.305
56	1.0	1.71	0.0074	0.410	7.3	20.5	4.2	2.1	7.6	0.9	21.6	0.310
57	2.35	0.530	0.0062	0.420	7.3	21.2	4.2	2.1	4.5	0.6	15.2	0.320
58	2.35	0.600	0.0067	0.420	7.3	22.0	4.2	2.1	4.2	0.5	16.0	0.315
59	3.7	0.330	0.0215	0.425	7.3	22.0	4.2	2.1	4.5	0.5	16.5	0.320
60	2.0	0.440	0.0057	0.308	7.2	16.0	4.4	2.15	2.8	0.0	12.0	0.220
61	2.35	0.220	0.0058	0.310	7.1	16.0	4.2	2.1	3.1	0.0	11.3	0.230
62	1.6	0.800	0.0056	0.315	7.1	16.0	4.2	2.1	3.7	0.1	17.0	0.200
63	1.3	1.0	0.0058	0.305	7.2	15.8	4.2	2.1	4.7	0.3	15.0	0.220
64	1.0	1.33	0.0056	0.305	7.1	15.5	4.2	2.1	7.0	0.8	20.0	0.200

TABLE XII

DG-2 PERFORMANCE MAPPING ORIGINAL DATA (contd)

Data Point	Positive High Voltage V_+ (kV)	Negative High Voltage, V_- (kV)	Negative HV Current, I_- (amp)	Beam Current, I_B (amp)	Arc Voltage, V_A (volts)	Arc Current, I_A (amp)	Magnet Voltage, V_M (volt)	Magnet Current, I_M (amp)	Neutral Detector Current, I_{NCD} (10^{-9} amp)	NCD Background, I_{NCD} (10^{-9} amp)	I_{NCD} at I'_B, I'_{NCD} (10^{-9} amp)	Reduced Beam Current, I'_B (amp)
65	0.800	1.56	0.0061	0.305	7.2	16.0	4.0	2.05	7.0	1.0	21.3	0.205
66	0.600	1.64	0.0075	0.305	7.1	16.3	3.8	2.0	7.0	1.0	21.6	0.205
67	1.0	1.3	0.0053	0.305	7.1	16.8	3.8	2.0	6.7	1.1	18.0	0.215
68	1.0	1.34	0.006	0.300	7.1	16.5	4.0	2.1	6.7	1.2	22.0	0.180
69	3.5	0.100	0.0175	0.685	7.5	32.5	4.2	2.15	7.0	2.4	14.5	0.600
70	3.7	0.320	0.0105	0.690	7.5	34.1	4.2	2.1	6.5	2.4	16.5	0.590
71	4.25	0.120	0.0155	0.715	7.5	34.8	4.4	2.1	6.5	2.6	16.0	0.600
72	4.8	0.330	0.0238	0.715	7.9	34.2	4.6	2.1	6.3	2.9	16.3	0.600
73	3.25	0.575	0.0089	0.700	7.6	33.0	5.2	2.24	6.8	3.0	15.0	0.600
74	2.8	0.900	0.0084	0.665	7.5	32.6	4.8	2.23	6.8	3.0	15.0	0.565
75	2.35	1.3	0.009	0.710	7.6	37.3	4.1	2.20	7.1	3.2	14.5	0.600

TABLE XIII

FEED SYSTEM PERFORMANCE DATA

Point No.	Beam Current, I_B (amp)	Vaporizer Current, I_V (amp)	Vaporizer Voltage, V_V (volts)	Vaporizer Temperature, T_{vap} (°C)	Feed System Power, P_F (kW)
1	0.144	3.8	4.5	250	0.0171
2	0.187	4.0	4.8	250	0.0192
3	0.182	4.0	4.8	250	0.0192
4	0.207	4.1	4.9	252	0.0201
5	0.257	4.2	5.0	257	0.0210
6	0.304	4.3	5.1	260	0.0219
7	0.384	4.4	5.25	267	0.0231
8	0.504	4.6	5.4	275	0.0298
9	0.504	4.65	5.5	280	0.0256

TABLE XIV

NEUTRALIZER PERFORMANCE DATA

Emission Current, I_N (amp)	Collector Potential, V_c (volts)	Beam Probe Potential, V_P (volts)	Vaporizer Current, I_{NV} (amp)	Cathode Current, I_{NK} (amp)	Vaporizer Temperature, T_{NV} (°C)	Cathode Temperature, T_{NK} (°C)	Cathode Power, P_{NK} (watts)	Vaporizer Power, P_N (watts)	Total Power, P_N (watts)
0.150	9.5	8.7	1.62	1.55	272	440	3.8	6.8	10.6
0.190	8.2	8.9	1.40	1.62	272	448	4.2	5.1	9.3
0.200	8.2	8.7	1.46	1.61	275	445	4.1	5.5	9.8
0.215	8.3	8.5	1.38	1.63	273	450	4.3	5.0	9.3
0.270	8.7	8.5	1.36	1.60	274	450	4.1	4.8	8.9
0.312	9.0	8.3	1.4	1.57	282	450	3.9	5.1	9.0
0.390	10.0	8.2	1.4	1.61	289	462	4.1	5.1	9.2
0.496	11.5	9.0	1.46	1.51	297	440	3.6	5.5	9.1
0.590	12.3	8.7	1.49	1.48	306	465	3.5	5.8	9.3

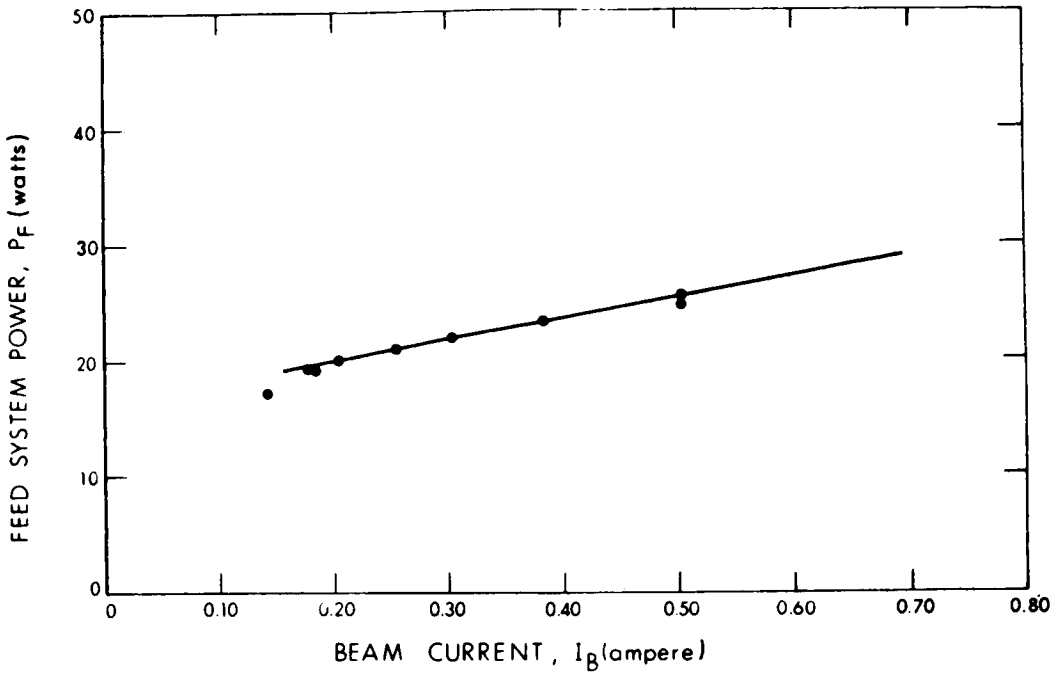

Figure 39. Feed System Power versus Beam Current

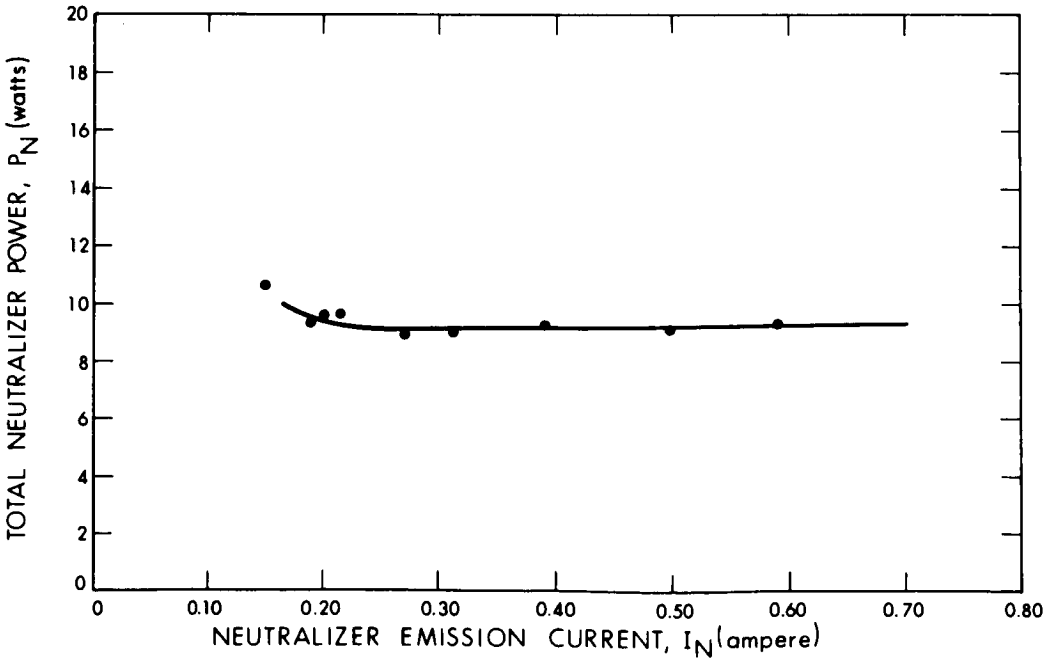

Figure 40. Neutralizer Power versus Neutralizer Emission Current

TABLE XV

CORRECTED AND REDUCED PERFORMANCE DATA

			21	24	25	66	26	65	55	27	64	54	67	68	16
Positive High Voltage, V_+ (kV)	0.400	0.400	0.400	0.600	0.600	0.60	0.800	0.80	0.80	1.00	1.00	1.00	1.0	1.0	4.36
Negative High Voltage, V_- (kV)	1.10	1.20	1.60	1.10	1.20	1.64	1.10	1.56	1.85	0.040	1.33	1.65	1.30	1.34	0.500
Negative HV Current, I_- (amp)	0.0060	0.0064	0.0150	0.0039	0.0042	0.0075	0.0044	0.0061	0.0094	0.0044	0.0056	0.0071	0.0053	0.006	0.0200
Beam Current, I_B (amp)	0.180	0.190	0.200	0.203	0.203	0.305	0.215	0.305	0.405	0.215	0.305	0.400	0.305	0.300	0.730
Arc Voltage, V_A (volts)	6.5	6.5	6.6	6.5	6.6	6.7	6.6	6.8	7.0	6.6	6.7	6.9	6.7	6.7	7.3
Arc Current, I_A (amp)	10.1	11.0	11.3	12.0	11.4	16.3	12.0	16.0	20.0	12.1	15.5	19.0	16.8	16.5	35.5
Magnet Voltage, V_M (volts)	3.6	3.6	3.6	3.4	3.6	3.8	3.6	4.0	4.2	3.6	4.2	4.2	3.8	4.0	4.6
Magnet Current, I_M (amp)	7.0	2.0	2.0	1.9	2.0	2.0	2.0	2.05	2.1	2.0	2.1	2.1	2.0	2.1	2.1
Beam Power, P_B, (kW)	0.072	0.076	0.080	0.1218	0.1218	0.183	0.1720	0.244	0.324	0.2150	0.0305	0.400	0.305	0.300	3.183
Drain Power, P_D (kW)	0.0090	0.0102	0.0300	0.0066	0.0076	0.0168	0.0084	0.0144	0.0249	0.0084	0.0130	0.0188	0.0122	0.140	0.0471
Magnet Power, P_M (kW)	0.0070	0.0070	0.0070	0.0063	0.0070	0.0074	0.0070	0.0080	0.0086	0.0070	0.0086	0.0086	0.0074	0.0082	0.0094
Arc Power, P_A (kW)	0.0657	0.0715	0.0746	0.0780	0.0752	0.1092	0.0792	0.1088	0.140	0.0799	0.1039	0.1317	0.1126	0.1106	0.2592
Total Engine Power, P_E (kW)	0.1537	0.1647	0.1916	0.2127	0.2116	0.3164	0.2666	0.3752	0.4975	0.3103	0.4305	0.5585	0.437	0.4328	3.549
Feed System Power, P_F (kW)	0.0195	0.0197	0.0199	0.0200	0.0200	0.0219	0.0201	0.0219	0.0237	0.0201	0.0219	0.0236	0.219	0.0218	0.0296
Neutralizer Power, P_N (kW)	0.0090	0.0090	0.0090	0.0090	0.0090	0.0091	0.0090	0.0091	0.0091	0.0090	0.0091	0.0091	0.0091	0.0091	0.0094
System Power, P_S (kW)	0.1822	0.1934	0.2205	0.2417	0.2406	0.3474	0.2957	0.4082	0.5303	0.3394	0.4615	0.5912	0.4682	0.4637	3.588
Thrust, T (mlb)	1.34	1.42	1.50	1.85	1.85	2.79	2.27	3.22	4.27	2.54	3.60	4.72	3.60	3.54	17.9
Engine Power-to-Thrust Ratio, P_E/T (kW/lb)	114.9	116.2	127.7	114.7	114.2	113.6	117.4	116.4	116.4	127.2	119.6	118.3	121.4	122.2	197.8
System Power-to-Thrust Ratio, P_S/T (kW/lb)	136.0	136.2	147.0	130.6	130.1	124.5	130.3	126.1	124.2	133.6	128.2	125.3	130.1	131.0	200.4
Engine Power Efficiency, η_{PE} (%)	46.8	46.1	41.8	57.3	57.6	57.8	64.5	65.0	65.1	69.3	70.8	71.6	69.8	69.3	89.7
System Power Efficiency, η_{PS} (%)	39.5	39.3	36.3	50.4	50.6	52.7	58.2	60.1	61.1	63.3	66.1	67.7	65.1	64.7	88.7
Engine Mass Efficiency, η_{ME} (%)	71.4	75.9	81.5	80.2	81.5	88.1	82.4	87.9	90.4	84.3	85.9	87.0	87.1	87.5	93.5
System Mass Efficiency η_{MS} (%)	70.4	74.9	80.5	79.2	80.5	87.1	81.4	86.9	89.4	83.3	84.9	86.0	86.1	86.5	92.5
Overall Engine Efficiency, η_E (%)	33.4	35.0	34.1	46.0	46.9	50.0	53.1	57.1	58.9	58.4	60.8	62.3	60.8	60.6	83.9
Overall System Efficiency, η_S (%)	27.8	29.4	29.2	39.9	40.7	45.9	47.4	52.2	54.6	52.7	56.1	58.2	56.1	56.0	82.0
Engine Specific,Impulse, I_{SPE} (sec)	1753	1863	2000	2410	2449	2648	2860	3051	3137	3270	3333	3376	3380	3395	7576
System Specific Impulse, I_{SPS} (sec)	1740	1840	1980	2390	2420	2620	2830	3020	3110	3240	3300	3340	3350	3360	7500
Ratio of Drain Current, I_-/I_B (%)	3.33	3.37	7.50	1.92	2.07	2.46	2.05	2.00	2.32	2.05	1.84	1.78	1.74	2.00	2.74
Source Energy per Ion, P_A/I_B (keV/ion)	0.365	0.376	0.373	0.384	0.371	0.358	0.368	0.357	0.346	0.371	0.340	0.328	0.369	0.368	0.355
Total Cesium Flowrate, I (amp)	0.252	0.250	0.246	0.253	0.249	0.346	0.261	0.347	0.448	0.255	0.355	0.460	0.350	0.343	0.781

TABLE XV

CORRECTED AND REDUCED PERFORMANCE DATA (contd)

	56	28	45	63	11	19	29	53	44	2	3	39	62	10	71
Positive High Voltage, V_+ (kV)	1.00	1.30	1.30	1.30	1.30	1.50	1.60	1.50	1.60	1.50	1.00	1.60	1.60	1.60	4.36
Negative High Voltage, V_- (kV)	1.71	0.600	1.50	1.00	2.20	0.400	0.300	1.45	1.20	1.40	1.90	0.0600	0.800	2.00	0.120
Negative HV Current, I_- (amp)	0.0074	0.0046	0.0200	0.0058	0.0150	0.0042	0.0046	0.0075	0.115	0.0090	0.0150	0.0130	0.0056	0.0120	0.0155
Beam Current, I_B (amp)	0.410	0.220	0.425	0.305	0.590	0.225	0.215	0.400	0.425	0.495	0.490	0.322	0.315	0.590	0.715
Arc Voltage, V_A (volts)	6.9	6.6	7.1	6.8	7.1	6.7	6.6	7.3	7.2	7.1	7.1	6.6	6.7	7.1	7.1
Arc Current, I_A (amp)	20.5	13.0	19.8	15.8	27.1	11.7	12.1	20.8	19.2	23.0	23.0	17.2	16.0	27.0	34.8
Magnet Voltage, V_M (volts)	4.2	3.6	4.2	4.2	4.7	4.0	3.6	4.1	4.3	4.4	4.4	4.0	4.2	4.7	4.4
Magnet Current, I_M (amp)	2.1	2.0	2.1	2.1	2.2	2.1	2.0	2.1	2.1	2.1	2.1	2.1	2.1	2.2	2.1
Beam Power, P_B, (kW)	0.410	0.2860	0.5525	0.3465	0.767	0.3375	0.3440	0.600	0.680	0.7425	0.490	0.5152	0.5040	0.944	3.117
Drain Power, P_D (kW)	0.0201	0.0087	0.0560	0.0133	0.0375	0.0080	0.0087	0.0221	0.0322	0.0261	0.0435	0.0286	0.0134	0.0312	0.0694
Magnet Power, P_M (kW)	0.0086	0.0070	0.0086	0.0086	0.0101	0.0082	0.0070	0.0084	0.0088	0.0090	0.0090	0.0082	0.0086	0.0101	0.0090
Arc Power, P_A (kW)	0.1415	0.0858	0.1406	0.1074	0.1924	0.0784	0.0799	0.1518	0.1382	0.1633	0.1633	0.1135	0.1072	0.1917	0.2471
Total Engine Power, P_E (kW)	0.5802	0.3875	0.7577	0.5258	1.007	0.4321	0.4396	0.7823	0.859	0.940	0.7058	0.6655	0.6332	1.177	3.443
Feed System Power, P_F (kW)	0.0238	0.0202	0.0241	0.0219	0.0270	0.0203	0.0201	0.0236	0.0241	0.0253	0.0252	0.0222	0.0221	0.0270	0.0293
Neutralizer Power, P_N (kW)	0.0091	0.0090	0.0092	0.0091	0.0093	0.0090	0.0090	0.0091	0.0092	0.0092	0.0092	0.0091	0.0091	0.0093	0.0093
System Power, P_S (kW)	0.6131	0.4167	0.7910	0.5568	1.043	4.350	0.4687	0.815	0.8925	0.9754	0.7402	0.6988	0.6644	1.213	3.482
Thrust, T (mlb)	4.84	2.96	5.72	4.11	7.94	3.25	3.21	5.78	6.35	7.15	5.70	4.81	4.70	8.81	17.7
Engine Power-to-Thrust Ratio, P_E/T (kW/lb)	119.9	130.7	132.4	128.1	126.8	132.8	136.8	135.3	135.4	131.6	122.1	138.4	134.7	133.6	194.5
System Power-to-Thrust Ratio, P_S/T (kW/lb)	126.7	140.8	138.3	135.5	131.4	133.8	146.0	141.1	140.6	136.4	129.9	144.9	141.4	137.7	196.7
Engine Power Efficiency, η_{PE} (%)	70.7	73.8	72.9	75.4	76.2	78.1	73.3	76.7	79.1	78.9	69.4	77.4	79.6	80.2	90.5
System Power Efficiency, η_{PS} (%)	66.9	68.6	69.8	71.2	73.5	77.6	73.4	73.6	76.2	76.1	66.2	73.9	75.9	77.8	89.5
Engine Mass Efficiency, η_{ME} (%)	89.5	86.3	87.6	89.4	92.5	86.9	84.8	91.0	89.0	92.0	91.0	89.8	91.0	92.3	94.1
System Mass Efficiency, η_{MS} (%)	88.5	85.3	86.6	88.4	91.5	85.9	83.8	90.0	88.0	91.0	90.0	88.8	90.0	91.3	93.1
Overall Engine Efficiency, η_E (%)	63.3	63.7	63.9	67.4	70.5	67.9	66.4	69.8	70.4	72.6	63.2	69.5	72.4	74.0	85.2
Overall System Efficiency, η_S (%)	59.2	58.5	60.5	62.9	67.3	66.7	61.5	66.2	67.0	69.3	59.6	65.6	68.3	71.0	83.3
Engine Specific Impulse, I_{SPE} (sec)	3473	3818	3875	3955	4093	4130	4162	4324	4368	4371	4372	4407	4467	4530	7624
System Specific Impulse, I_{SPS} (sec)	3440	3780	3840	3920	4050	4090	4120	4280	4320	4330	4330	4360	4420	4480	7550
Ratio of Drain Current, I_-/I_B (%)	1.80	2.09	4.70	1.40	2.54	1.87	2.14	1.88	2.70	1.82	3.06	4.04	1.78	2.03	2.17
Source Energy per Ion, P_A/I_B (keV/ion)	0.354	0.390	0.331	0.352	0.326	0.348	0.371	0.380	0.325	0.330	0.333	0.353	0.340	0.325	0.346
Total Cesium Flowrate, I (amp)	0.458	0.255	0.485	0.341	0.638	0.259	0.254	0.440	0.478	0.537	0.538	0.358	0.346	0.639	0.760

TABLE XV

CORRECTED AND REDUCED PERFORMANCE DATA (contd)

	30	38	43	60	46	1	9	31	37	47	61	40	57	75	17
Positive High Voltage, V_+ (kV)	2.00	2.00	2.00	2.00	2.00	2.00	2.0	2.39	2.39	2.35	2.39	2.39	2.39	2.39	4.92
Negative High Voltage, V_- (kV)	0.100	0.300	0.700	0.410	0.680	0.90	1.10	0.100	0.050	0.460	0.220	0.400	0.530	1.30	0.500
Negative HV Current, I_- (amp)	0.0049	0.0110	0.0088	0.0057	0.0059	0.0080	0.0092	0.0080	0.0080	0.0058	0.0058	0.0069	0.0062	0.0090	0.0320
Beam Current, I_B (amp)	0.218	0.325	0.425	0.308	0.405	0.490	0.595	0.218	0.325	0.405	0.310	0.420	0.420	0.710	0.730
Arc Voltage, V_A (volts)	6.6	6.6	7.3	6.8	7.1	7.1	7.1	6.6	6.6	7.5	6.7	7.7	6.9	7.2	7.3
Arc Current, I_A (amp)	17.2	17.6	19.5	16.0	19.5	22.5	29.0	12.0	17.1	19.0	16.0	19.0	21.2	37.3	35.1
Magnet Voltage, V_M (volts)	3.6	4.0	4.3	4.4	3.9	4.4	4.7	3.7	3.9	3.9	4.2	4.3	4.2	4.1	4.6
Magnet Current, I_M (amp)	2.0	2.1	2.1	2.15	2.1	2.1	2.2	2.05	2.1	2.1	2.1	2.1	2.1	2.20	2.1
Beam Power, P_B (kW)	0.438	0.650	0.850	0.6160	0.8100	0.9800	1.190	0.540	0.7768	0.9680	0.7409	1.004	1.004	1.697	3.592
Drain Power, P_D (kW)	0.0098	0.0253	0.238	0.0139	0.0158	0.0232	0.0285	0.0199	0.0195	0.0165	0.0151	0.0193	0.0181	0.0227	0.1734
Magnet Power, P_M (kW)	0.0070	0.0082	0.0088	0.0092	0.0080	0.0090	0.0101	0.0074	0.0080	0.0080	0.0086	0.0088	0.0086	0.0088	0.0094
Arc Power, P_A (kW)	0.0805	0.1162	0.1424	0.1088	0.1385	0.1598	0.2059	0.0702	0.1129	0.1425	0.1072	0.1453	0.1463	0.2686	0.2562
Total Engine Power, P_E (kW)	0.5333	0.7997	1.025	0.7479	0.9723	1.172	1.485	0.6275	0.4172	1.274	0.8718	1.178	1.177	1.997	4.031
Feed System Power, P_F (kW)	0.0202	0.0223	0.0248	0.0220	0.0237	0.0252	0.0271	0.0202	0.0223	0.0237	0.0220	0.0240	0.0240	0.0293	0.0296
Neutralizer Power, P_N (kW)	0.0090	0.0091	0.0092	0.0091	0.0091	0.0092	0.0093	0.0090	0.0091	0.0091	0.0091	0.0091	0.0091	0.0093	0.0094
System Power, P_S (kW)	0.5625	0.8311	1.058	0.7790	1.005	1.206	1.471	0.6567	0.9203	1.307	0.9029	1.211	1.210	2.036	4.070
Thrust, T (mlb)	3.64	5.42	7.04	5.14	6.76	8.18	9.92	3.98	5.93	7.39	5.65	7.67	7.67	13.0	19.1
Engine Power-to-Thrust Ratio, P_E/T (kW/lb)	146.5	147.4	144.6	145.6	143.8	143.3	144.7	157.7	154.7	172.4	154.2	153.7	153.6	153.7	210.7
System Power-to-Thrust Ratio, P_S/T (kW/lb)	154.5	153.3	149.2	151.6	148.7	147.5	148.3	165.0	155.2	176.9	159.8	157.9	157.8	156.6	213.1
Engine Power Efficiency, η_{PE} (%)	81.8	81.3	82.9	82.4	83.3	83.6	82.9	83.0	84.7	76.0	85.0	85.2	85.3	85.0	89.1
System Power Efficiency, η_{PS} (%)	77.5	78.2	80.3	79.1	80.6	81.3	80.9	79.3	84.4	74.1	82.1	82.9	83.0	83.3	88.3
Engine Mass Efficiency, η_{ME} (%)	85.5	89.9	90.2	91.9	92.5	92.7	92.8	86.5	89.7	91.1	91.2	92.0	92.0	92.4	92.5
System Mass Efficiency, η_{MS} (%)	84.5	88.9	89.2	90.9	91.5	91.7	91.8	85.5	88.7	90.1	90.2	91.0	91.0	91.4	91.5
Overall Engine Efficiency, η_E (%)	69.9	73.1	74.8	75.7	77.1	77.5	76.9	76.2	76.0	69.7	77.5	78.4	78.5	78.5	82.4
Overall System Efficiency, η_S (%)	65.5	69.5	71.7	71.9	73.7	74.6	74.3	67.8	74.9	66.7	74.1	75.4	75.5	76.1	80.8
Engine Specific Impulse, I_{SPE} (sec)	4641	4933	4950	5043	5075	5085	5092	5188	5381	5465	5470	5518	5518	5592	7961
System Specific Impulse, I_{SPS} (sec)	4640	4880	4900	4990	5020	5030	5040	5140	5330	5410	5420	5460	5460	5490	7880
Ratio of Drain Current, I_-/I_B (%)	2.25	3.38	2.07	1.85	1.46	1.63	1.55	3.67	2.46	1.43	1.87	1.64	1.48	1.27	4.38
Source Energy per Ion, P_A/I_B (keV/ion)	0.369	0.357	0.335	0.353	0.342	0.326	0.346	0.363	0.347	0.352	0.346	0.348	0.348	0.378	0.351
Total Cesium Flowrate, I (amp)	0.255	0.361	0.462	0.335	0.438	0.528	0.641	0.252	0.362	0.445	0.340	0.457	0.456	0.710	0.789

TABLE XV

CORRECTED AND REDUCED PERFORMANCE DATA (contd)

	4	58	8	32	35	36	41	12	48	13	49	42	6	73	72
Positive High Voltage, V_+ (kV)	2.39	2.39	2.39	2.87	2.87	2.87	2.87	2.87	2.80	3.33	3.33	3.33	3.33	3.33	4.92
Negative High Voltage, V_- (kV)	0.600	0.600	0.800	0.050	0.050	0.050	0.200	0.400	0.220	0.350	0.220	0.100	0.400	0.575	0.330
Negative HV Current, I_- (amp)	0.0068	0.0067	0.0082	0.0126	0.0081	0.0088	0.0088	0.0083	0.0080	0.0091	0.0136	0.0120	0.0120	0.0089	0.0238
Beam Current, I_B (amp)	0.490	0.420	0.590	0.215	0.310	0.318	0.408	0.600	0.400	0.600	0.430	0.428	0.485	0.700	0.715
Arc Voltage, V_A (volts)	7.1	6.9	7.1	6.7	6.6	6.1	7.7	7.1	7.4	7.1	7.3	7.8	7.2	7.2	7.5
Arc Current, I_A (amp)	23.2	22.0	30.8	12.0	15.3	17.0	17.7	27.6	19.5	27.1	20.0	18.1	23.2	33.0	34.2
Magnet Voltage, V_M (volts)	4.4	4.2	4.4	3.8	3.9	3.9	4.3	4.7	3.9	4.7	3.9	4.3	4.4	5.2	4.6
Magnet Current, I_M (amp)	2.1	2.1	2.1	2.05	2.1	2.1	2.1	2.2	2.05	2.2	2.05	2.1	2.1	2.24	2.1
Beam Power, P_B (kW)	1.171	1.004	1.410	0.8897	0.8897	0.9127	1.171	1.722	1.148	1.998	1.432	1.425	1.615	2.331	3.518
Drain Power, P_D (kW)	0.0203	0.0200	0.0262	0.0368	0.0293	0.0257	0.0270	0.0271	0.0247	0.0335	0.0483	0.0412	0.0448	0.0348	0.1273
Magnet Power, P_M (kW)	0.0090	0.0086	0.0090	0.0076	0.0080	0.0080	0.0080	0.0101	0.0078	0.0101	0.0078	0.0088	0.0090	0.0114	0.0094
Arc Power, P_A (kW)	0.1647	0.1518	0.287	0.0804	0.1010	0.1122	0.1363	0.1960	0.1404	0.1924	0.1460	0.1412	0.1670	0.2376	0.2565
Total Engine Power, P_E (kW)	1.365	1.184	1.664	1.015	1.028	1.059	1.343	1.955	1.321	2.234	1.634	1.616	1.836	2.615	3.911
Feed System Power, P_F (kW)	0.0252	0.0240	0.0270	0.0200	0.0220	0.0220	0.0238	0.0272	0.0236	0.272	0.242	0.0241	0.0251	0.0290	0.0293
Neutralizer Power, P_N (kW)	0.0092	0.0091	0.0093	0.0090	0.0091	0.0091	0.0091	0.0093	0.0091	0.0093	0.0092	0.0092	0.0092	0.0093	0.0093
System Power, P_S (kW)	1.399	1.217	1.700	1.044	1.059	1.091	1.376	1.992	1.359	2.270	1.667	1.649	1.870	2.653	3.950
Thrust, T (mlb)	8.86	7.67	10.8	4.29	6.20	1.36	8.16	12.0	7.99	12.9	9.26	9.21	10.4	15.1	18.7
Engine Power-to-Thrust Ratio, P_E/T (kW/lb)	154.0	154.5	154.0	236.4	197.5	166.6	164.6	158.8	165.3	173.3	176.4	175.5	176.4	173.5	208.7
System Power-to-Thrust Ratio, P_S/T (kW/lb)	157.9	158.7	157.5	243.4	170.8	171.5	168.6	166.0	169.5	176.0	180.0	179.1	179.8	175.7	211.2
Engine Power Efficiency, η_{PE} (%)	85.8	84.8	84.7	87.7	86.5	86.2	87.2	87.9	86.0	89.4	87.6	88.2	88.0	89.1	90.0
System Power Efficiency, η_{PS} (%)	83.7	82.5	82.9	85.2	84.0	83.7	85.1	86.4	84.8	88.0	85.9	86.4	86.4	87.9	89.1
Engine Mass Efficiency, η_{ME} (%)	92.7	92.7	92.6	86.9	88.6	90.9	92.1	92.7	92.9	92.3	92.3	92.4	92.5	92.8	94.8
System Mass Efficiency, η_{MS} (%)	91.7	91.7	91.6	85.4	87.6	89.9	91.1	91.7	91.9	91.3	91.3	91.4	92.5	92.8	93.8
Overall Engine Efficiency, η_E (%)	79.5	78.6	78.4	76.2	76.6	78.4	80.3	81.5	80.7	82.5	80.9	81.5	82.3	83.6	85.3
Overall System Efficiency, η_S (%)	76.8	75.7	75.9	73.2	73.6	75.2	77.5	79.2	77.9	80.3	78.4	79.0	79.9	81.6	83.6
Engine Specific Impulse, I_{SPE} (sec)	5560	5560	5602	5712	5824	5901	6054	6094	6107	6526	6535	6542	6620	6641	8159
System Specific Impulse, I_{SPS} (sec)	5500	5500	5550	5650	5770	5840	5990	6030	6050	6460	6470	6480	6550	6570	8080
Ratio of Drain Current, I_-/I_B (%)	1.39	1.60	1.39	5.86	2.81	2.76	2.16	1.38	2.00	1.52	3.16	2.80	2.47	1.27	3.33
Source Energy per Ion, P_A/I_B (keV/ion)	0.336	0 0.361	0.371	0.374	0.326	0.353	0.334	0.377	0.351	0.321	0.340	0.330	0.344	0.339	0.359
Total Cesium Flowrate, I (amp)	0.529	0.453	0.636	0.247	0.350	0.350	0.443	0.647	0.431	0.650	0.466	0.463	0.518	0.746	0.754

TABLE XV

CORRECTED AND REDUCED PERFORMANCE DATA (contd)

	5	74	33	50	34	69	52	51	59	7	14	18	70	15
Positive High Voltage, V_+ (kV)	2.87	2.87	3.33	3.33	3.33	3.59	3.79	3.79	3.79	3.79	3.79	3.79	3.79	4.36
Negative High Voltage, V_- (kV)	0.300	0.900	0.050	0.0220	0.050	0.100	0.120	0.120	0.330	0.300	0.350	0.400	0.320	0.400
Negative HV Current, I_- (amp)	0.0070	0.0084	0.0207	0.0136	0.015	0.0175	0.0205	0.0240	0.0215	0.0210	0.0144	0.0143	0.0105	0.0270
Beam Current, I_B (amp)	0.490	0.665	0.215	0.410	0.305	0.685	0.420	0.410	0.425	0.485	0.600	0.730	0.690	0.595
Arc Voltage, V_A (volts)	7.2	7.1	6.8	7.6	6.6	6.6	7.6	7.5	6.9	7.2	7.1	7.3	6.1	7.1
Arc Current, I_A (amp)	23.0	32.6	12.0	18.1	16.2	32.5	30.0	19.1	22.0	23.9	29.4	36.1	34.1	29.0
Magnet Voltage, V_M (volts)	4.4	4.8	3.8	4.2	3.9	4.2	4.2	4.2	4.2	4.4	4.7	4.9	4.2	4.7
Magnet Current, I_M (amp)	2.1	2.23	2.05	2.1	2.1	2.15	2.1	2.1	2.1	2.1	2.2	2.2	2.1	2.2
Beam Power, P_B (kW)	1.406	1.909	0.7160	1.365	0.016	2.459	1.592	1.544	1.611	1.838	2.279	2.767	2.615	2.594
Drain Power, P_D (kW)	0.0220	0.0317	0.0700	0.0483	0.0507	0.0646	0.0802	0.438	0.0886	0.0859	0.0596	0.0742	0.0432	0.1285
Magnet Power, P_M (kW)	0.0090	0.0105	0.0076	0.0086	0.0080	0.0088	0.0086	0.0086	0.0086	0.0090	0.0101	0.0105	0.0086	0.0101
Arc Power, P_A (kW)	0.1656	0.2315	0.0816	0.1376	0.1069	0.2308	0.1520	0.1433	0.1518	0.1721	0.2087	0.2635	0.2421	0.2059
Total Engine Power, P_E (kW)	1.601	2.183	0.8752	1.560	1.182	2.763	1.833	1.780	1.860	2.105	2.552	3.115	2.909	2.939
Feed System Power, P_E (kW)	0.0252	0.0284	0.0201	0.0238	0.0219	0.0288	0.0240	0.0238	0.0241	0.251	0.272	0.0296	0.0289	0.0271
Neutralizer Power, P_N (kW)	0.0092	0.0093	0.0090	0.0091	0.0091	0.0093	0.0091	0.0091	0.0092	0.0092	0.0093	0.0094	0.0093	0.0093
System Power, P_S (kW)	1.635	2.221	0.9043	1.593	1.213	2.801	1.866	1.813	1.893	2.139	2.588	3.154	2.947	2.875
Thrust, T (mlb)	9.80	13.3	4.62	8.83	6.56	15.3	9.65	9.42	9.65	11.1	13.8	16.8	15.9	14.7
Engine Power-to-Thrust Ratio, P_E/T (kW/lb)	163.4	164.3	189.0	176.8	180.2	180.9	190.0	189.0	192.8	189.5	184.9	185.9	183.3	200.3
System Power-to-Thrust Ratio, P_S/T (kW/lb)	166.8	167.0	145.3	180.4	184.9	183.1	193.4	192.5	196.2	192.7	187.5	187.7	185.3	202.4
Engine Power Efficiency, η_{PE} (%)	87.8	87.4	81.8	87.6	86.0	89.0	86.7	87.3	86.6	87.3	89.1	88.8	89.9	88.3
System Power Efficiency, η_{PS} (%)	86.0	86.0	79.2	85.7	83.8	87.8	85.3	85.7	85.1	85.9	87.9	87.7	88.7	87.2
Engine Mass Efficiency, η_{ME} (%)	93.2	93.5	88.1	89.8	90.6	92.9	91.2	91.3	92.4	93.4	93.9	94.1	94.4	93.4
System Mass Efficiency, η_{MS} (%)	92.2	92.5	87.1	88.8	89.6	91.9	90.2	90.3	91.4	92.4	92.9	93.1	93.4	92.4
Overall Engine Efficiency, η_E (%)	81.8	81.7	72.1	78.7	77.9	82.7	79.3	79.7	80.0	81.5	83.6	83.6	84.4	82.5
Overall System Efficiency, η_S (%)	79.3	79.6	64.8	76.1	75.1	80.7	76.9	77.4	77.8	79.4	81.7	81.6	82.8	80.6
Engine Specific Impulse, I_{SPE} (sec)	6127	6146	6238	6358	6415	6830	6889	6897	6980	7055	7092	7108	7130	7568
System Specific Impulse, I_{SPS} (sec)	6070	6080	6180	6290	6350	6760	6820	6830	6910	6980	7020	7040	7060	7490
Ratio of Drain Current, I_-/I_B (%)	1.43	1.26	9.63	3.32	4.92	2.55	2.88	5.85	5.06	4.33	2.40	1.96	1.52	4.54
Source Energy per Ion, P_A/I_B (keV/ion)	0.338	0.348	0.380	0.336	0.351	0.337	0.362	0.349	0.357	0.355	0.348	0.361	0.351	0.346
Total Cesium Flowrate, I (amp)	0.526	0.711	0.244	0.451	0.337	0.737	0.461	0.449	0.460	0.519	0.639	0.776	0.731	0.637

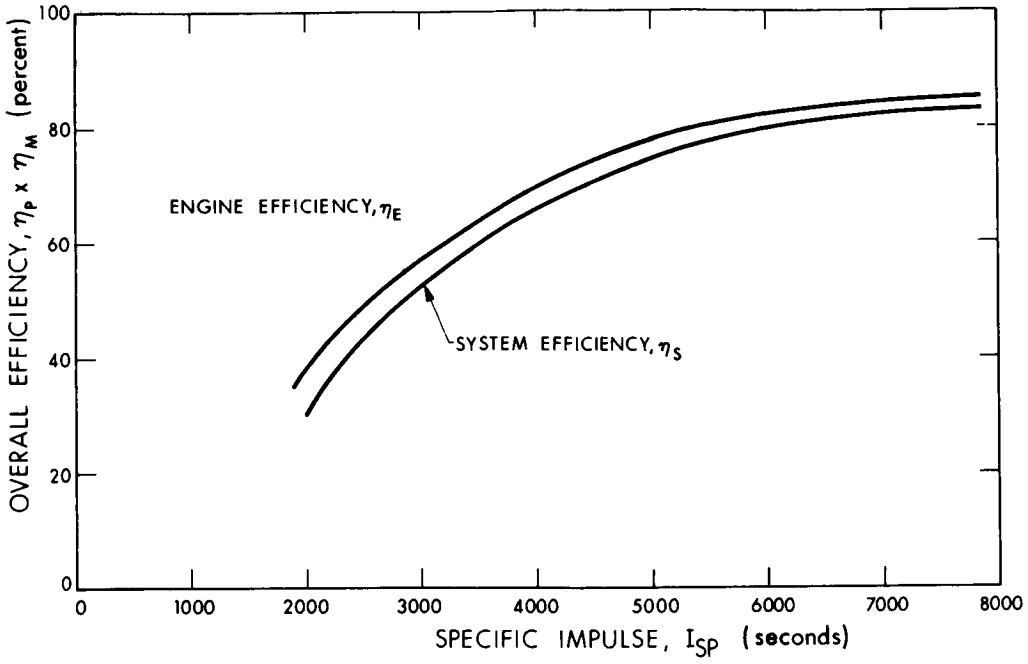

Figure 41. Overall Efficiency versus Specific Impulse

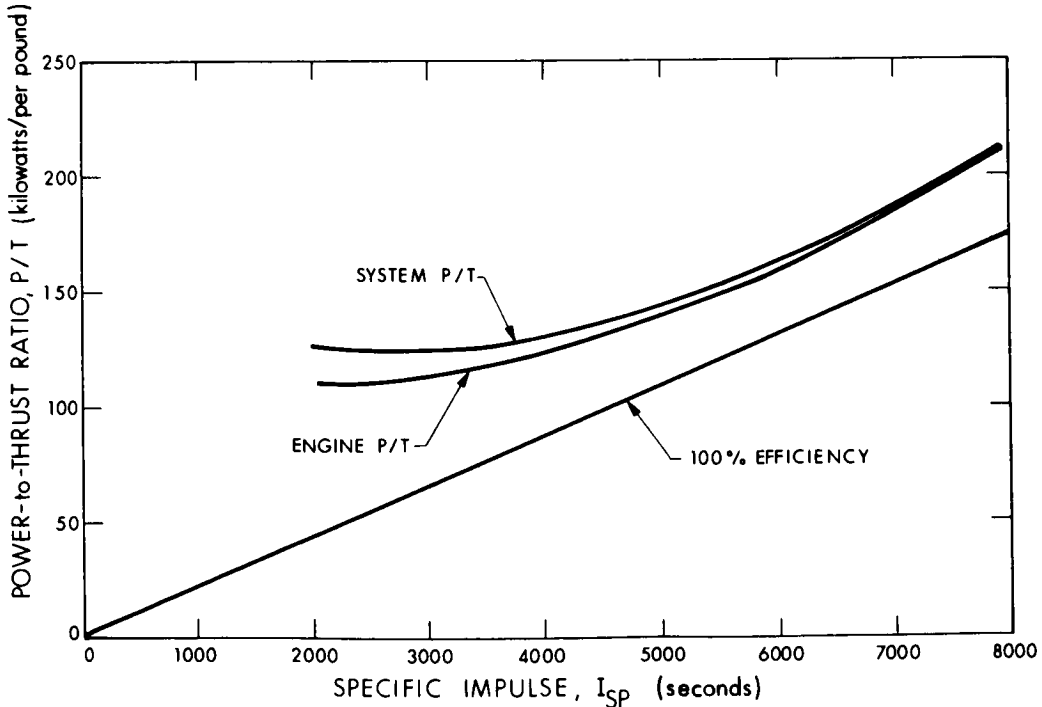

Figure 42. Power-to-Thrust Ratio versus Specific Impulse

Figure 42 shows the minimum power-to-thrust ratio versus specific impulse for the engine and for the system. Power was higher and specific impulse was lower for the system, due to the addition of feed system and neutralizer power and the neutral efflux from the neutralizer, respectively. The DG-2 engine system curve shows that the penalty for the neutralizer and feed system was about 5 kilowatts per pound thrust at 7000 seconds and about 9 kilowatts per pound at 3000 seconds. At the design level of 5000 seconds specific impulse the penalty was about 6 kilowatts per pound of thrust.

To determine optimum operation with respect to accelerator drain current, lines of equal drain current were plotted on a chart of beam current versus positive high voltage (Fig. 43). At every operating point, accelerator electrode potential was adjusted to yield minimum drain.

Figure 44 shows thrust versus system specific impulse. The two distinct curves shown represent the maximum and the optimum thrust. The maximum thrust curve represents a limit imposed by the perveance of the electrode system. The optimum thrust curve was taken from the minimum drain current line since the maximum lifetime is obtained at minimum drain current. This reduction from maximum thrust causes only a one percent loss in system efficiency at 5000 seconds specific impulse.

Conclusions Regarding Engine Performance

The following conclusions were drawn from the performance mapping data:

a. Maximum overall efficiency is obtained at maximum thrust. This was not found during the DG-1 performance mapping, but it is felt that the conclusion is valid since it is based on a wide range of maximum and nonmaximum overall efficiencies.

b. For a given specific impulse, the thrust that will yield the maximum lifetime (the optimum thrust) is usually below the maximum obtainable thrust.

From these conclusions and the performance data at the design point it was predicted that at 5000-second specific impulse the system power-to-thrust ratio would be about 150 kilowatts per pound at an overall system efficiency of about 73 percent. The ratio of drain current to beam current was predicted to be less than 2 percent with an accelerator potential of about 500 volts. Thus on the 4000 hour test both high efficiency and long life were predicted.

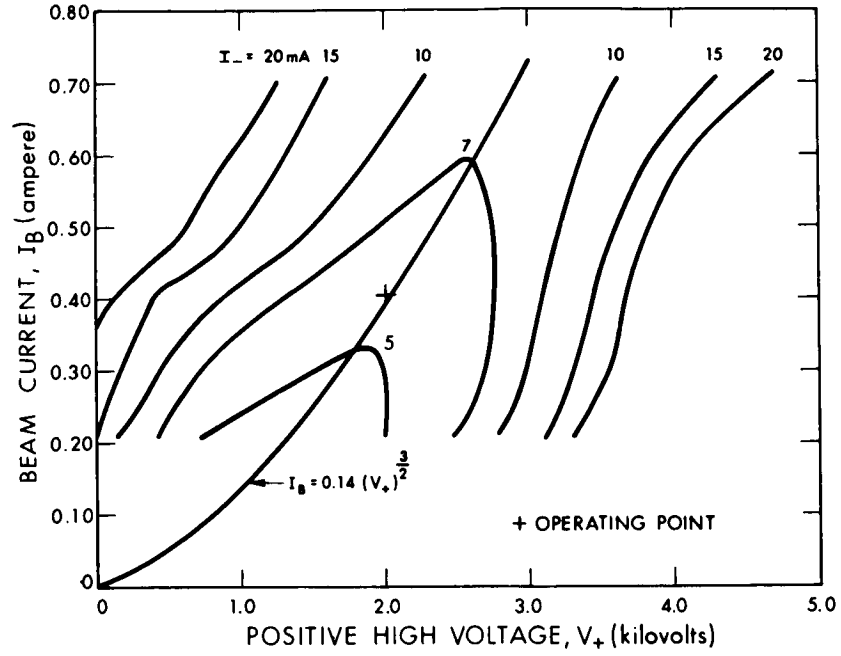

Figure 43. Engine Drain (I_-) Characteristic

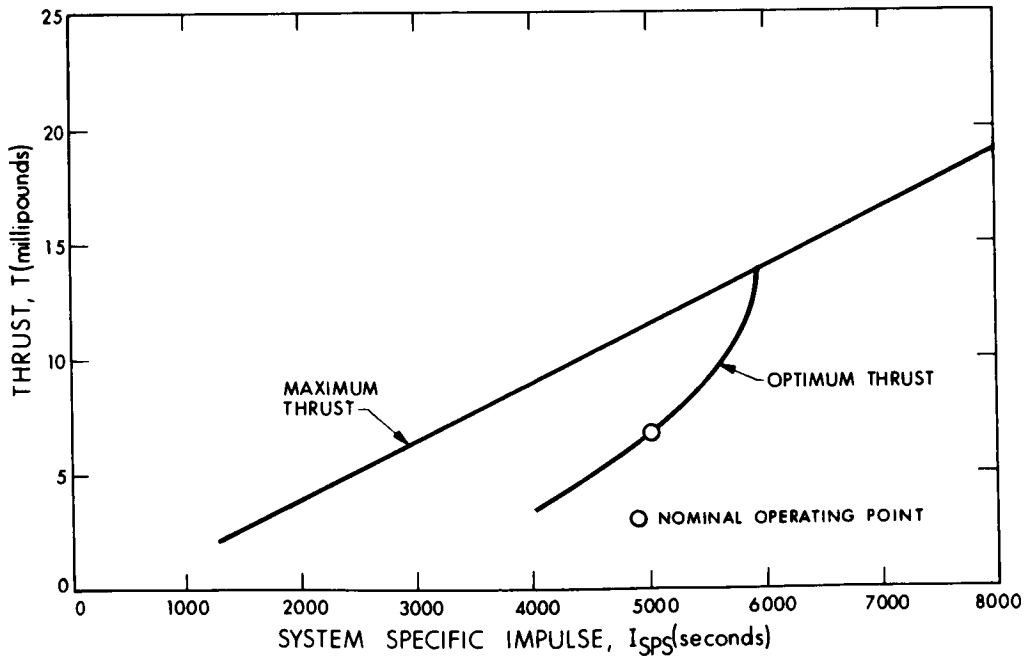

Figure 44. Thrust versus System Specific Impulse

3.2.6 4000-HOUR TEST PERFORMANCE

The objective of the 4000-hour test was operation of the engine system at a power-to-thrust ratio below 160 kilowatts per pound at a nominal 5000-second specific impulse for 4000 hours or more. The 4000-hour feed system was loaded with 18,859 grams of cesium prior to the start of the run. Four hundred and ten grams were used in 160 hours when an initial run was terminated. Deducting 2.0 grams for startup and estimating that 25 grams of cesium remained trapped in the porous wick, 18,422 grams of cesium should have been available for the test. Using the expected 92 percent mass efficiency for the engine this should have been enough for about 8500 hours of testing run time. At 5000 seconds specific impulse a total system power of about one kilowatt and a thrust of 6.67 millipounds would give a system power-to-thrust ratio of about 150 kilowatts per pound. This operating level was chosen on the basis of the performance mapping.

Assembly of the DG-2 engine system and a performance check for the 4000-hour test was completed and on 1 November 1965 the test was begun. Performance through the first 125 hours was excellent, but at about 130 hours the drain current started to increase, after which low drain currents could only be held with abnormally low accelerator potentials. At 163.7 hours the engine system was shut off because of the increase in drain current, the lower negative high voltage requirement, and violent interelectrode arcing. The engine system was removed from the vacuum chamber to check the electrode gap and alignment. The gap was found to be unchanged, but the accelerating electrode was loose on the support insulators, causing severe electrode misalignment. This had caused high drain currents and local heating which resulted in thermal bowing of the screen electrode during the last hours of the test.

In addition, the neutralizer vaporizer ran 30 to 40°C higher than the nominal value throughout the test. A flow rate of 2 percent of the engine flow rate was measured by weight loss after 163.7 hours. An adjustment was required in the geometric relationship between the neutralizer and the ion beam to reduce the cesium flow required for efficient coupling of electrons into the beam.

The engine was disassembled, cleaned, and reassembled with a new accelerator electrode. The neutralizer used in the test was disassembled, cleaned, reassembled, and loaded with 214.4 grams of cesium. Both neutralizers were remounted on the engine with an angle of 68° between the neutralizer and beam axes instead of the previous 60°. Since 40.6 pounds of cesium remained in the 40-pound reservoir after the first test it was not necessary to reload the reservoir prior to restart of the test.

The system was reassembled with an electrode gap of 0.053 inch and after complete system tests, placed in the vacuum chamber for the 4000-hour test. Engine operation was checked by repeating performance points at beam levels of 0.200, 0.300, 0.355, 0.400, 0.500, and 0.600 ampere. Engine operation was found to be identical to that obtained during the performance mapping. The reduced neutralizer angle did lower the neutralizer vaporizer temperature to the proper level. After these performance checks the 4000-hour test was begun on 19 November 1965. Table XVI gives the system performance throughout the duration of the test. After a few hours of operation a high voltage rest cycle occurred and a relay stuck which kept the high voltage supplies off for 20 minutes. The relay stuck on two other occasions with similar high voltage off periods. This relay circuit was replaced with a more reliable one during a later shutdown.

After 33 hours of operation the arc discharge went into violent oscillations that could not be overcome. The system was shut down twice to find the source of the oscillations.

During the first few hours of the test the collector and liner had developed an intermittent short to ground, so that the neutralizer had to be biased negatively. This short was partly responsible for the oscillations, but they were eliminated after about 55 hours by applying more power to the manual valve which had been condensing cesium. This cesium was then forced into the engine in liquid form causing arcing in the discharge chamber.

Figures 45 and 46 show component temperatures and engine system operating parameters versus run time for the duration of the test. After the first 80 hours of the test, the reservoir and vaporizer temperatures had become very stable. The cathode body and accelerator electrode temperatures rose slowly during the first 1500 hours of operation due to a gradual increase in arc power of about 10 percent. This increase in arc power was required to minimize the accelerator drain current, an essential condition for long lifetime. As the arc power was increased, the arc current remained essentially constant, suggesting that either a series lead impedance developed or a change in the cathode emitter surface condition occurred, thereby causing the increase in arc impedance. This arc impedance change was identical to the first 1000 hours of the 2000-hour test.

The bottom plot of Fig. 46 shows the number of high voltage rest periods counted between successive data points, each of which was initiated by a high voltage arc. At the start of the run the maximum rest period was 1 minute, which was too short to provide a sufficient lowering of the plasma density in the engine to allow the high voltage supplies to turn on. Therefore, one high voltage arc would invariably initiate two or three 1-minute rest periods. The 1-minute timer was replaced with a

TABLE XVI

DG-2 ENGINE SYSTEM PERFORMANCE ON LIFE TEST

Time (hours)	0.8	31.9	104.9	303.2	514.0	1008.2	1502.9	2280	5823	6629	7870	8109	3008	4502
Positive High Voltage, V_+ (kV)	2.03	2.01	2.03	2.04	2.01	2.02	2.02	2.01	2.03	2.03	2.01	2.03	2.01	2.02
Negative High Voltage, V_- (kV)	0.54	0.54	0.55	0.54	0.52	0.54	0.53	0.52	0.52	0.52	0.51	0.51	0.52	0.51
Negative HV Current, I_- (amp)	0.0060	0.0050	0.0052	0.0061	0.006	0.0054	0.0055	0.0051	0.0052	0.0052	0.0049	0.0049	0.0049	0.0052
Beam Current, I_B (amp)	0.421	0.421	0.421	0.420	0.420	0.421	0.420	0.420	0.421	0.420	0.411	0.391	0.421	0.421
Arc Voltage, V_A (volts)	6.8	6.3	6.45	6.75	6.9	7.2	7.3	7.0	7.35	7.25	7.25	7.25	7.25	7.2
Arc Current, I_A (amp)	19.1	19.1	21.9	20.8	19.9	21.2	21.6	22.9	22.3	22.8	23.7	23.9	22.8	22.3
Magnet Voltage, V_M (volts)	4.7	4.6	4.4	4.7	4.6	4.8	4.8	4.9	5.0	5.1	5.0	5.1	4.8	4.95
Magnet Current, I_M (amp)	2.12	2.12	2.02	2.1	2.1	2.16	2.14	2.18	2.2	2.2	2.2	2.2	2.13	2.18
Beam Power, P_B (kW)	0.855	0.846	0.855	0.857	0.844	0.850	0.848	0.844	0.855	0.853	0.826	0.794	0.846	0.850
Drain Power, P_D (kW)	0.013	0.013	0.013	0.016	0.015	0.014	0.014	0.013	0.013	0.013	0.012	0.011	0.012	0.013
Magnet Power, P_M (kW)	0.010	0.010	0.009	0.010	0.010	0.010	0.010	0.011	0.011	0.011	0.011	0.011	0.010	0.011
Arc Power, P_A (kW)	0.130	0.120	0.141	0.140	0.137	0.153	0.158	0.160	0.164	0.165	0.172	0.173	0.165	0.161
Total Engine Power, P_E (kW)	1.008	0.989	1.018	1.023	1.006	1.027	1.030	1.028	1.043	1.092	1.021	0.989	1.033	1.035
Feed System Power, P_F (kW)	0.030	0.023	0.018	0.018	0.015	0.017	0.017	0.016	0.016	0.016	0.015	0.015	0.018	0.016
Total Neutralizer Power, P_N (kW)	0.010	0.010	0.010	0.010	0.010	0.010	0.010	0.010	0.010	0.010	0.010	0.010	0.010	0.010
Total System Power, P_S (kW)	1.048	1.022	1.046	0.051	1.031	1.054	1.057	1.034	1.069	1.068	1.046	1.014	1.059	1.061
Thrust, T (mlb)	7.10	7.06	7.10	7.10	7.04	7.08	7.06	7.04	7.10	7.08	6.90	6.59	7.06	7.08
Engine Power-to-Thrust Ratio, $P_{E/T}$ (kW/lb)	142.0	140.1	143.4	144.1	142.9	145.1	145.9	146.0	146.9	147.2	148.0	150.1	146.3	146.2
System Power-to-Thrust Ratio, $P_{S/T}$ (kW/lb)	147.6	144.8	147.3	148.0	146.4	148.9	149.7	146.9	150.6	150.8	151.6	153.9	150.0	149.9
Engine Power Efficiency, η_{PE} (%)	84.9	85.6	83.9	83.7	83.9	82.8	82.4	82.1	81.9	81.8	80.8	80.3	81.8	82.1
System Power Efficiency, η_{PS} (%)	81.6	82.9	81.7	81.5	81.8	80.6	80.4	81.6	79.9	79.8	79.0	78.2	79.9	80.2
Engine Mass Efficiency, η_{ME} (%)	92.0	92.0	92.0	92.0	~ 92.0	~ 92.0	~ 92.0	~ 92.0	92.0	92.0	92.0	92.0	92.6	~ 92.0
System Mass Efficiency, η_{MS} (%)	91.0	91.0	91.0	91.0	~ 91.0	~ 91.0	~ 91.0	~ 91.0	91.0	91.0	91.0	91.0	~ 91.6	~ 91.0
Overall Engine Efficiency, η_E (%)	78.1	78.7	77.2	77.1	77.2	76.2	75.7		75.4	75.4	74.4	73.8	75.7	75.5
Overall System Efficiency, η_S (%)	74.4	75.5	74.4	74.2	74.5	73.4	73.2		72.6	72.6	71.9	71.2	73.2	72.9
Engine Specific Impulse, I_{spE} (sec)	5075	5055	5075	5085	5060	5057	5057	5055	5075	5057	5055	5075	5085	5065
System Specific Impulse, I_{spS}	5020	5000	5020	5030	5006	5000	5000	5000	5020	5020	5000	5020	5030	5010
Ratio of Drain Current to Beam Current I_-/I_B	1.4	1.2	1.2	1.4	1.4	1.3	1.3	1.2	1.2	1.2	1.2	1.2	1.2	1.2
Source Energy per Ion, P_A/I_B (keV/ion)	309	285	335	333	326	364	376	381	0.390	0.393	0.419	0.442	393	383

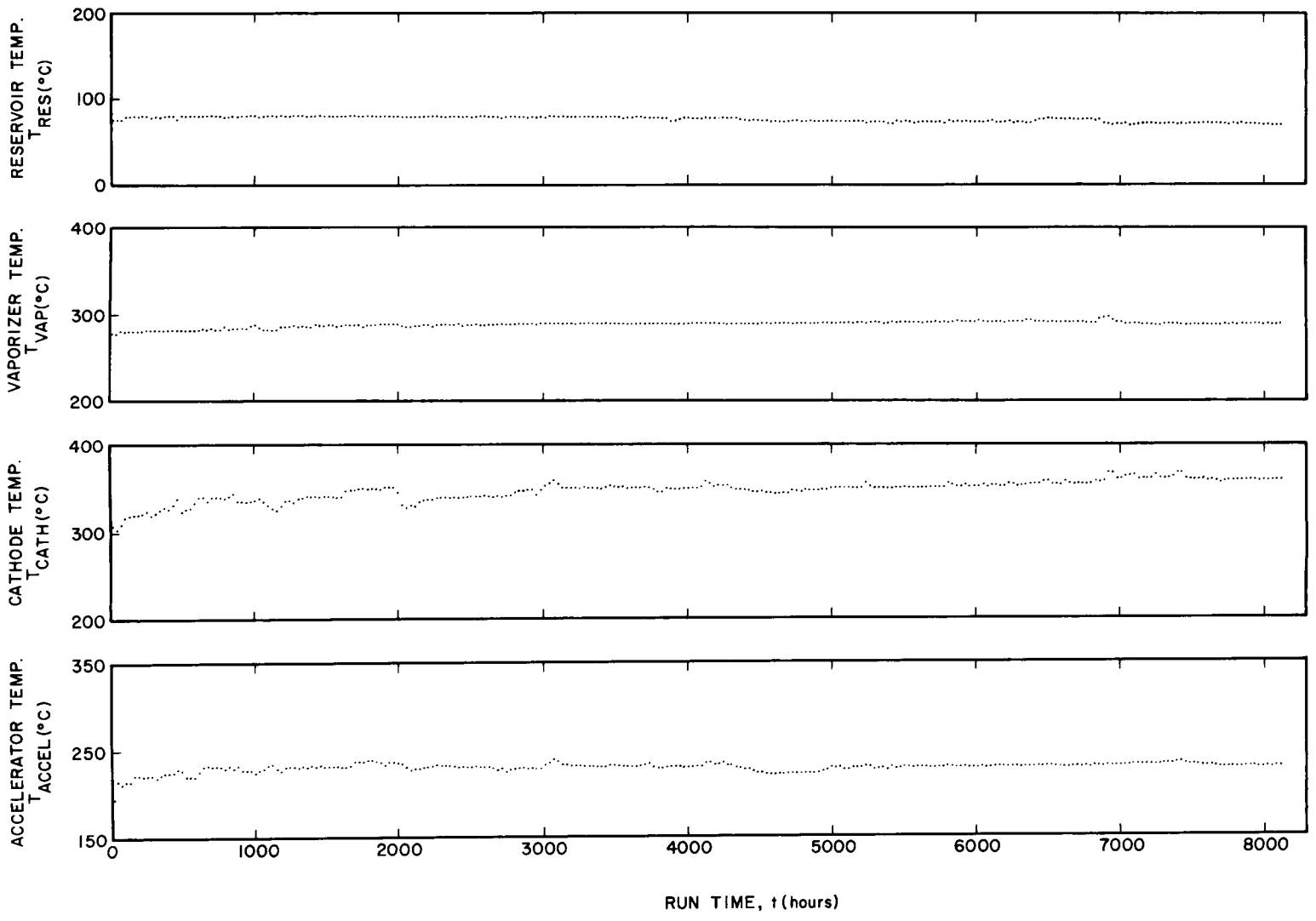

Figure 45. DG-2 Component Operating Temperatures

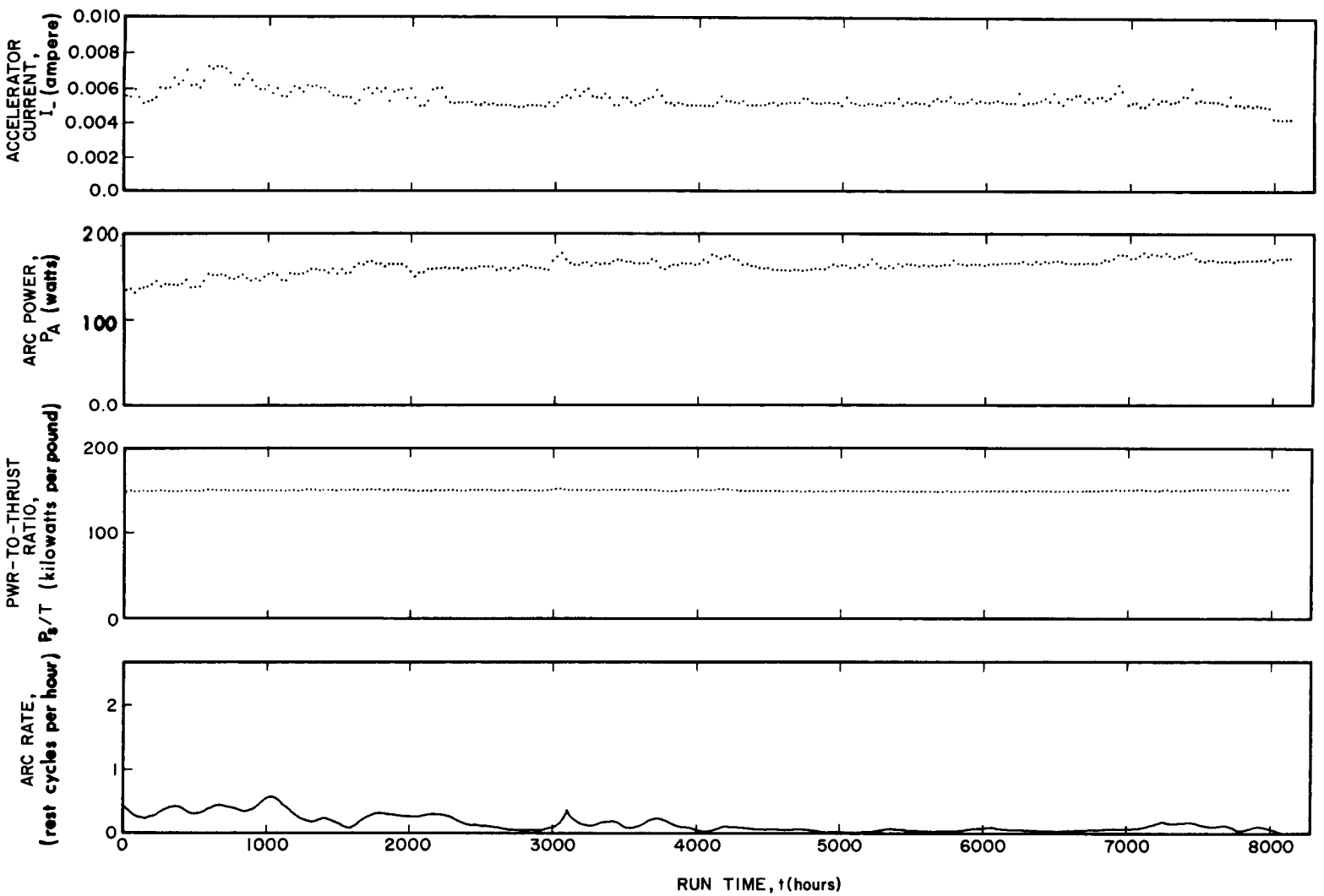

Figure 46. DG-2 System Operating Parameters

timer that could be set for a more adequate rest period of about 3 minutes. With the longer rest period only one high voltage rest was then required to reset the high voltage supplies after an arc. For this reason consecutive short rests initiated by a single arc during early portions of the test have been counted as one rest period on the graph.

At 1045 hours into the DG-2 test an electronics failure caused a loss of feed system power and the engine beam current dropped to zero. After correction of the control system failure and upon restart of the engine it was observed that the cathode heater was open-circuited. The discharge was therefore initiated by applying high voltages and arc voltage to the engine.

The system was performance mapped at 1000, 2000 and 3000 hours. The procedure followed in each case was similar to the prerun performance mapping except that fewer data points were taken. Since several hours would have been needed to bring the feed system to thermal equilibrium at each new flowrate, the feed system powers listed were taken from the lower curve of Fig. 47. This curve was derived by assuming that the 30 percent power reduction observed at the test point since the start of the test would occur at all levels. During the mapping the neutralizer was not operated to give optimum performance. The neutralizer power was assumed to be 10 watts for each point since it was found during the first performance mapping not to vary over the emission current range by more than 1 watt. The neutral cesium detector discussed in Subsection 3.2.2 of this report was lowered into the test chamber to obtain the neutral efflux data for determination of mass efficiency. Performance data for the three checks are given in Tables XVII, XVIII, and XIX.

The system power-to-thrust ratio versus system specific impulse curve at the start of the test is compared in Fig. 48 to the data taken at 1000 hours, at 2000 hours, and at 3000 hours. A slight increase since the start of the test can be seen, and this was due solely to the gradual increase in arc power. However, after 2000 hours the arc power required for optimum performance for each point mapped dropped slightly. At the 5000-second specific impulse test point, the power-to-thrust increase during the first 2000 hours was 4 kilowatts per pound, from 148 to 152 kilowatts per pound. After 2000 hours, however, lower arc power maintained the average system power-to-thrust ratio below 151 kilowatts per pound. The effect of the lower arc power can be seen more clearly from the graphs of Figs. 50 and 51 which show, respectively, the engine mass efficiency and the discharge energy per ion plotted versus beam current for the four performance mappings at 0, 1000, 2000 and 3000 hours.

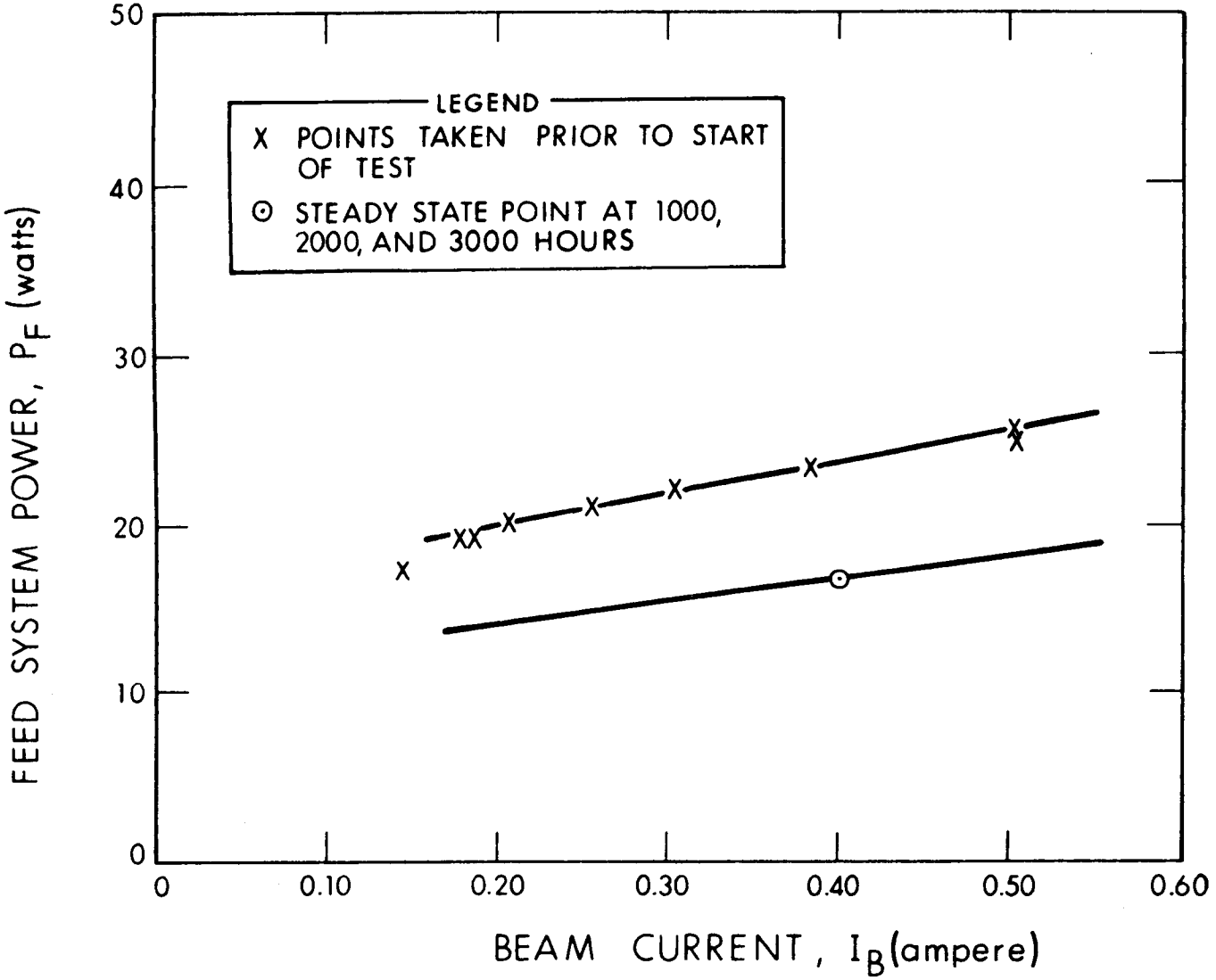

Figure 47. DG-2 Feed System Power Projection

TABLE XVII

DG-2 SYSTEM PERFORMANCE MAPPING DATA AT 1000 HOURS

Point	1	2	3	4	5
Positive High Voltage, V_+ (kV)	1.01	1.32	1.62	2.03	2.43
Negative High Voltage, V_- (kV)	1.00	0.80	0.74	0.56	0.50
Negative HV Current, I_- (amp)	0.0043	0.0043	0.0050	0.0057	0.0062
Beam Current, I_B (amp)	0.199	0.300	0.355	0.401	0.500
Arc Voltage, V_A (volts)	7.0	6.8	6.9	6.8	7.05
Arc Current, I_A (amp)	12.2	14.6	16.8	18.8	23.9
Beam Power, P_B (kW)	0.201	0.396	0.575	0.814	1.215
Drain Power, P_D (kW)	0.009	0.009	0.012	0.015	0.018
Magnet Power, P_M (kW)	0.009	0.010	0.010	0.010	0.010
Arc Power, P_A (kW)	0.085	0.099	0.116	0.129	0.168
Feed System Power, P_F (kW)	0.021	0.022	0.023	0.024	0.026
Neutralizer Power, P_N (kW)	0.010	0.010	0.010	0.010	0.010
System Power, P_S (kW)	0.335	0.546	0.746	1.002	1.447
Thrust, T (mlb)	2.38	4.07	5.27	6.76	9.25
System Power-to-Thrust Ratio, P_S/T (kW/lb)	140	135	142	148	156
Engine Mass Efficiency, η_{ME} (%)	82.9	84.7	89.5	91.8	94.4
System Mass Efficiency, η_{MS} (%)	81.9	83.7	88.5	90.8	93.4
Overall System Efficiency, η_S (%)	49.3	60.5	68.2	73.7	78.5
System Specific Impulse, I_{spS} (sec)	3185	3725	4365	5010	5640
Source Energy per Ion, P_A/I_B, (keV/ion)	0.427	0.330	0.327	0.322	0.336

TABLE XVIII

DG-2 PERFORMANCE MAPPING DATA AT 2000 HOURS

Point	1	2	3	4	5
Positive High Voltage, V_+ (kV)	1.02	1.32	1.62	2.01	2.48
Negative High Voltage, V_- (kV)	1.00	0.80	0.70	0.52	0.50
Negative HV Current, I_- (amp)	0.0039	0.0044	0.005	0.0056	0.0081
Beam Current, I_B (amp)	0.194	0.292	0.343	0.400	0.485
Arc Voltage, V_A (volts)	7.55	7.5	7.55	7.55	7.7
Arc Current, I_A (amp)	12.4	16.7	20.0	21.9	29.1
Beam Power, P_B (kW)	0.198	0.385	0.556	0.804	1.203
Drain Power, P_D (kW)	0.008	0.009	0.012	0.014	0.024
Magnet Power, P_M (kW)	0.011	0.010	0.010	0.011	0.011
Arc Power, P_A (kW)	0.094	0.125	0.151	0.165	0.224
Feed System Power, P_F (kW)	0.014	0.015	0.016	0.017	0.018
Neutralizer Power, P_N (kW)	0.010	0.010	0.010	0.010	0.010
System Power, P_S (kW)	0.335	0.554	0.755	1.021	1.490
Thrust, T (mlb)	2.32	3.98	5.17	6.74	9.06
System Power-to-Thrust Ratio, P_S/T(kW/lb)	144	139	146	151	164
Engine Mass Efficiency, η_{ME} (%)	83.0	84.0	88.5	92.0	94.5
System Mass Efficiency, η_{MS} (%)	82.0	83.0	87.5	91.0	93.5
Overall System Efficiency, η_S (%)	48.5	57.7	64.4	71.7	75.5
System Specific Impulse, I_{spS} (sec)	3210	3700	4320	5000	5700
Source Energy per Ion, P_A/I_B (keV/ion)	0.485	0.428	0.440	0.413	0.462

TABLE XIX

DG-2 PERFORMANCE MAPPING DATA AT 3000 HOURS

Point	1	2	3	4	5
Positive High Voltage, V_+ (kV)	1.01	1.31	1.63	2.01	2.45
Negative High Voltage, V_- (kV)	1.00	0.80	0.70	0.520	0.50
Negative HV Current, I_- (amp)	0.0039	0.0041	0.0044	0.0049	0.0064
Beam Current, I_B (amp)	0.200	0.300	0.350	0.400	0.497
Arc Voltage, V_A (volts)	7.35	7.30	7.28	7.25	7.60
Arc Current, I_A (amp)	12.7	17.1	20.0	22.8	29.9
Beam Power, P_B (kW)	0.202	0.393	0.571	0.804	1.233
Drain Power, P_D (kW)	0.008	0.009	0.010	0.012	0.019
Magnet Power, P_M (kW)	0.010	0.010	0.010	0.010	0.010
Arc Power, P_A (kW)	0.093	0.125	0.148	0.165	0.227
Feed System Power, P_F (kW)	0.014	0.015	0.015	0.016	0.018
Neutralizer Power, P_N (kW)	0.010	0.010	0.010	0.010	0.010
System Power, P_S (kW)	0.337	0.562	0.764	1.017	1.517
Thrust, T (mlb)	2.39	4.24	5.15	6.69	9.31
System Power-to-Thrust Ratio, P_S/T(kW/lb)	141	133	148	152	163
Engine Mass Efficiency, η_{ME} (%)	81.8	87.0	90.7	92.6	95.2
System Mass Efficiency, η_{MS} (%)	80.8	86.0	89.7	91.6	94.2
Overall System Efficiency, η_S (%)	48.4	60.1	67.0	72.4	76.6
System Specific Impulse, I_{spS} (sec)	3140	3820	4440	5030	5750
Source Energy per Ion, P_A/I_B (keV/ion)	0.465	0.417	0.418	0.413	0.455

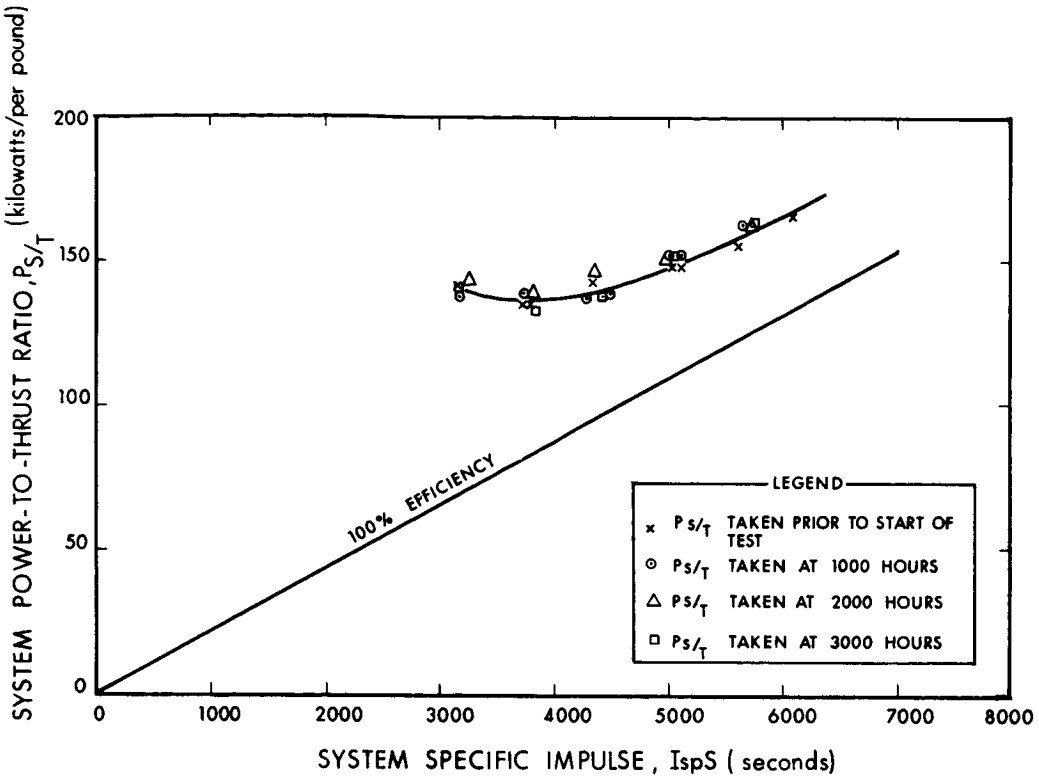

Figure 48. DG-2 System Performance Mapping During Test

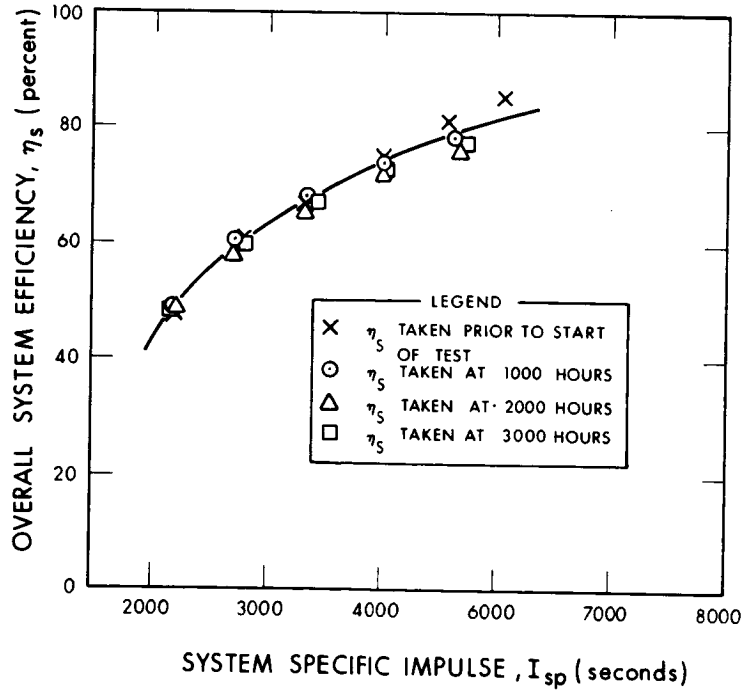

Figure 49. DG-2 System Efficiency During Test

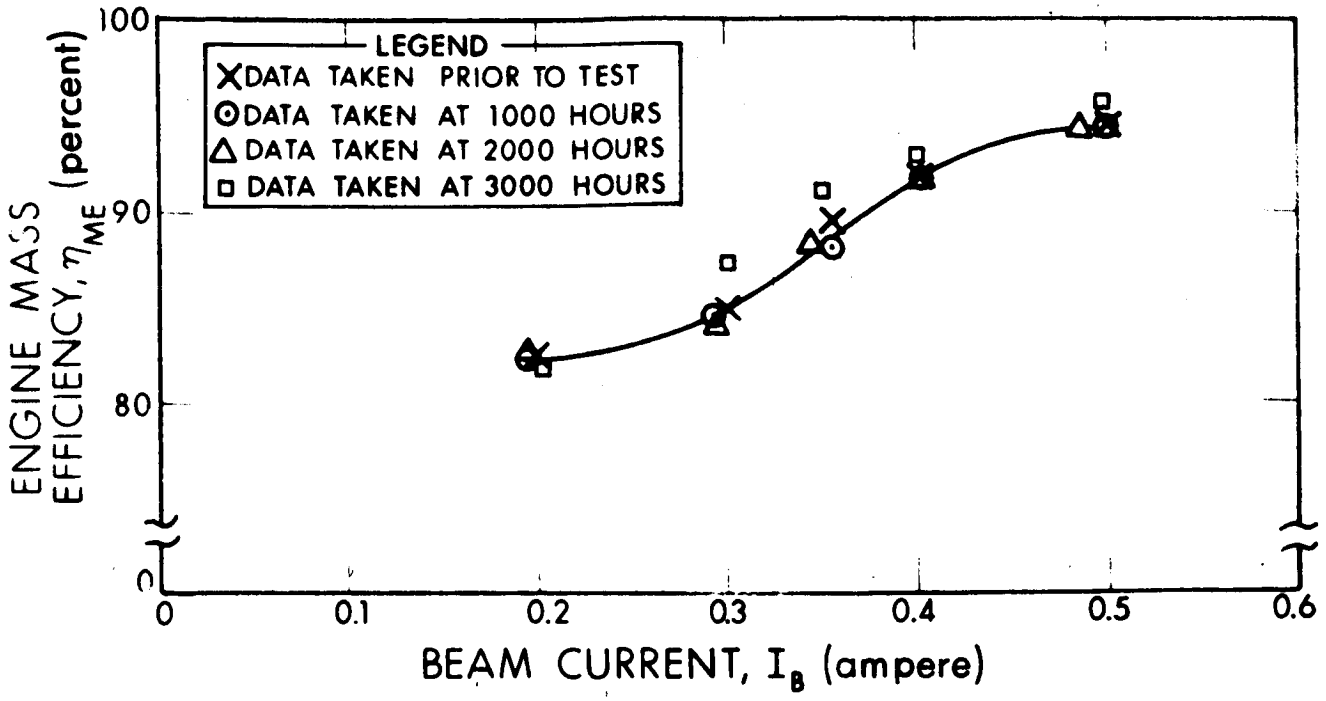

Figure 50. DG-2 Engine Mass Efficiency During Test

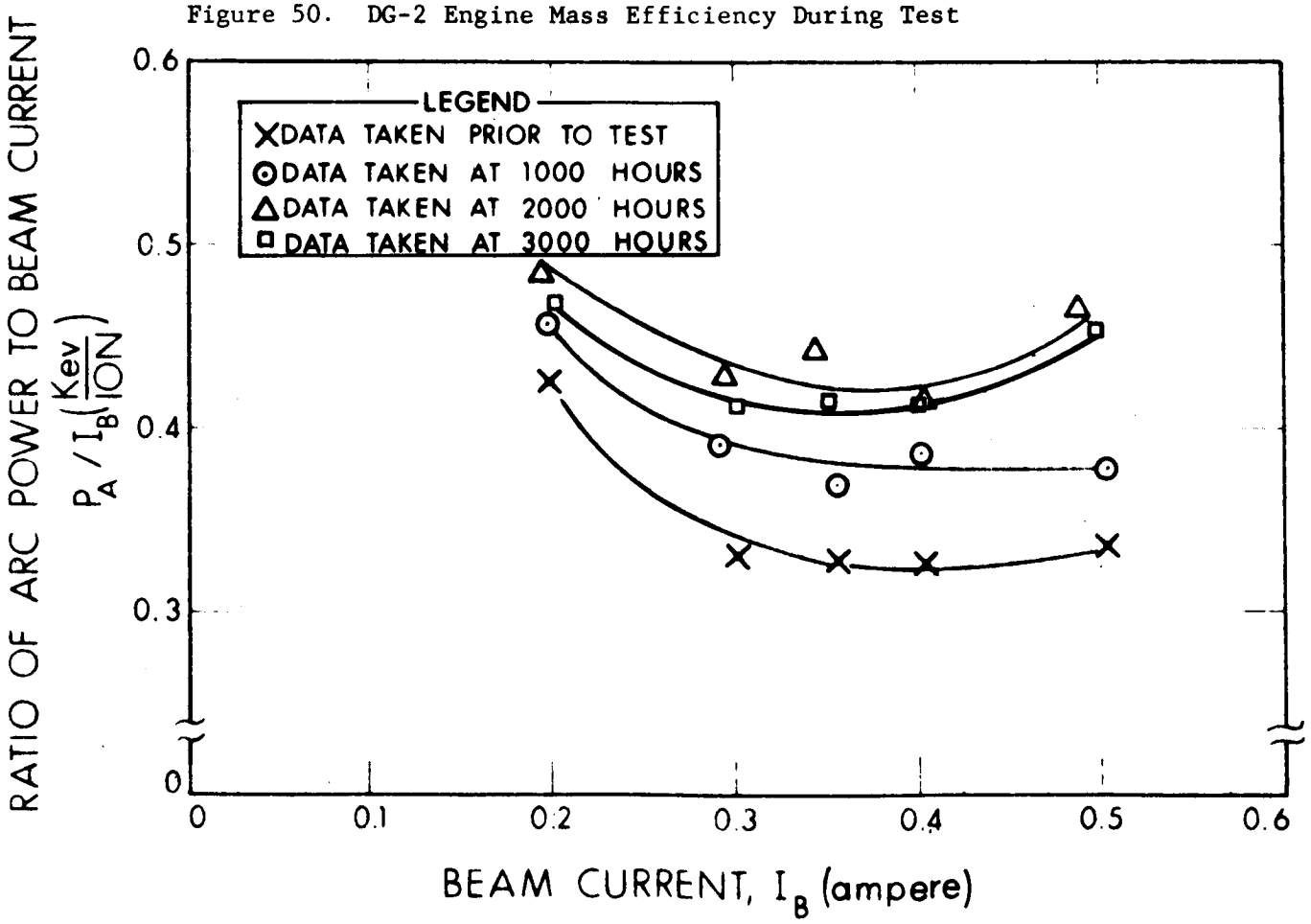

Figure 51. Discharge Energy Per Beam Ion During Test

Upon the completion of each performance mapping during the long test the system operation was returned to the design point. In raising the neutral detector back into its well after the 2000-hour performance mapping a chamber leak was caused, raising the vacuum system to 70 microns and initiating a high voltage rest cycle. The facility was immediately pumped back down and at the end of the first rest cycle the pressure was back down to the 10^{-6} torr range so that engine operation at full thrust was obtained. Within a few minutes the chamber pressure was down to 1×10^{-7} torr and it remained there to the end of the test (Fig. 52). The number of high voltage rest cycles was above average for about 60 hours after the performance mapping and subsequent pressure burst, and then it returned to normal. It is not clear whether the performance mapping or the pressure burst was the cause for the higher arcing rate. Although the pressure burst probably had some adverse effect, it is felt on the basis of similar operation after the 1000-hour mapping that the higher arcing rate was due primarily to the performance mapping.

An effect of both the 1000- and 2000-hour performance mappings was to make a significant drop in the arc voltage required to give optimum efficiency. After the 1000-hour mapping the arc voltage changed from about 7.1 volts to 6.6 volts in about 60 hours. At 2000 hours the arc voltage was still 7.5 volts. After the 3-minute high voltage rest cycle initiated by the pressure burst, the arc voltage was down to 7.0 volts. The decrease in arc voltage was attended by a drop in cathode temperature due to the lowered energy expended in the discharge. During the 100 hours immediately following the 3000-hour performance mapping an arc power of about 6 percent higher than normal was required for optimum operation. The arc power increase caused the slightly higher cathode and accelerator temperatures and was accompanied by a small increase in the arcing frequency, although there was no increase in drain current. It was assumed that feed rate fluctuations during the performance mappings affected cathode deposits which built up slowly during the test. Such deposits determined cathode emissivity, and hence the cathode temperature needed for design point emission. Since an autocathode was used the arc power which heated it was also affected.

After about 6900 hours of engine system operation, there was a major failure in the laboratory supplies which left the engine off for an hour and a half. The arc power and drain current were slightly higher for about 60 hours after this occurrence. Subsequently, the drain current returned to normal. The arc power, however, remained somewhat higher.

At 7448 hours the accelerator current rose to 0.007 ampere and seven arcs were recorded within an hour. Smooth operation was regained by lowering the beam current from 0.421 to 0.411 ampere and by lowering the negative high voltage to 0.44 kilovolt. These changes resulted in

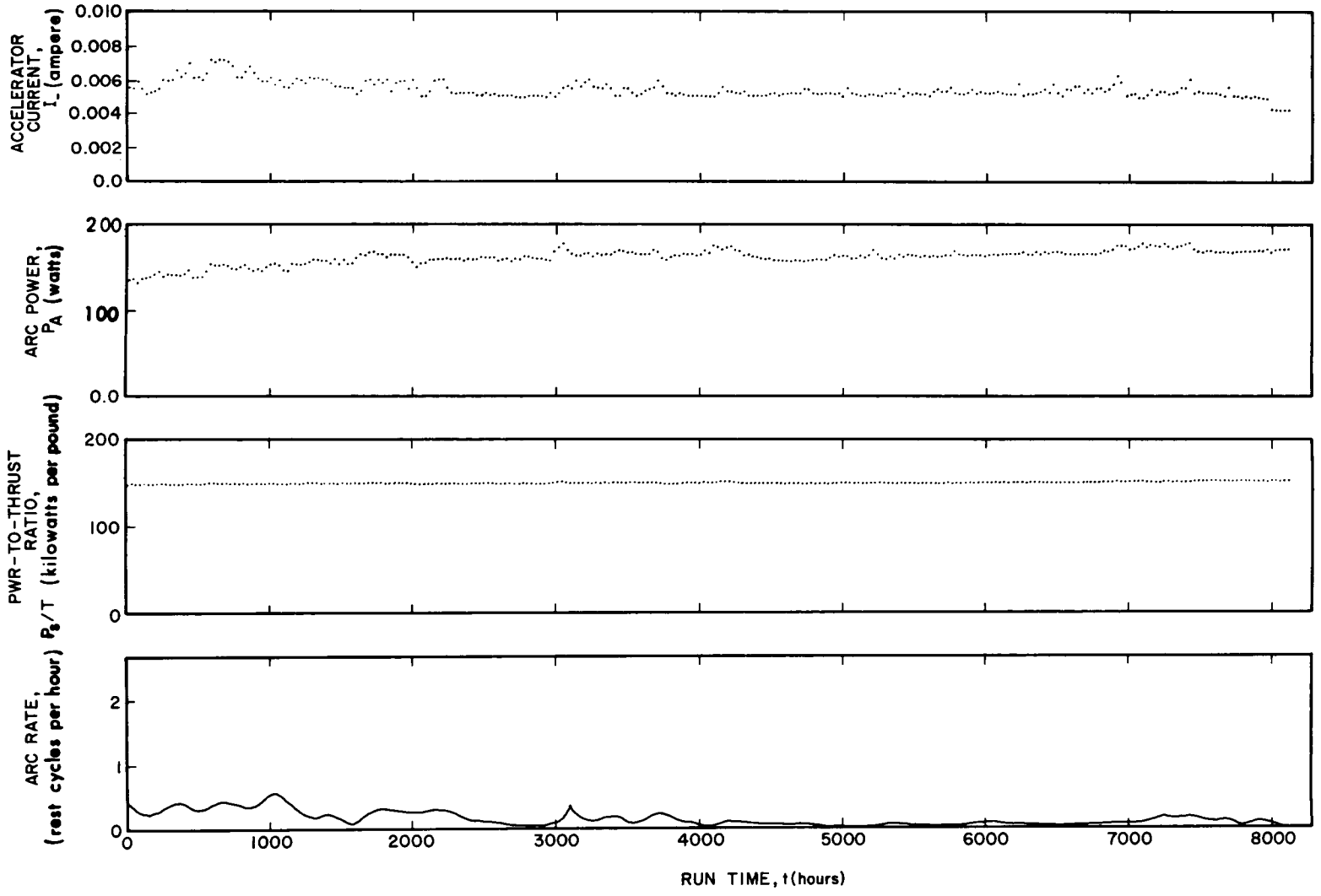

Figure 52. DG-2 System Operating Parameters

a lowering of thrust of 2.5 percent, but the specific impulse and system power-to-thrust ratio remained unchanged at 5000 seconds and 152 kilowatts per pound, respectively. At 7975 hours the plasma bridge neutralizer went off and could not be restarted. The neutralizer had been biased negative because of a short between the facility collector and system ground, so it was in continuous operation from the start of the test, running through all high voltage rest cycles for a total neutralizer run time of 8100 hours. Attempts to start the spare neutralizer were not successful. Backsputtered aluminum had coated both neutralizer orifices. To calculate the system power-to-thrust ratio after the neutralizer stopped, the average neutralizer power, 10 watts, was added to the system power.

The extended test of the DG-2 engine system terminated on 1 November 1966 after 8149 hours of continuous operation due to complete exhaustion of the cesium supply in the engine feed system. A test goal of over 8500 hours had been set based on the calculated duration at 92 percent mass efficiency for the initial cesium load. The reason for the premature end of the test was found to be an error in the beam current metering circuit. At the beginning of the test it was believed that because of ground loops the effect of the neutralizer emission current from the biased neutralizer was to introduce an error in the beam current measurement of 12 milliamperes. Throughout the test correction was made for this, but calibration after the test revealed that the error was actually +9 milliamperes. Therefore, the beam current was actually 421 milliamperes instead of 400 milliamperes.

3.2.7 POST RUN ANALYSIS

The DG-2 engine performed excellently on the 4000-hour test. A summary of its average performance during 8149 hours at design level thrust is given in Table XX. These results include only the time accumulated while the engine was under unbroken vacuum. The engine logged about 200 hours of run time during prerun performance mapping and during a first run terminated after 160 hours, as mentioned in Subsection 3.2.6. These times are not included in the 8149 hours of run time summarized in the table. Using the correct beam current, the mass efficiency calculated by weight loss of cesium was 92.3 percent, very close to the estimated 92 percent. The mass efficiency found by weight loss agrees with mass efficiency measurements of 92 $\pm 1/2$ percent taken with a neutral cesium detector during performance mappings at 0, 1000, 2000, and 3000 hours. Making the proper beam current corrections, the average system performance parameters are summarized in Table XXI. Efficiency of the DG-2 engine system was approximately 1 percent better than that of the DG-1 engine system.

TABLE XX

DG-2 TEST RESULTS

A.	Results of Continuous Test	
	Test duration	8252 hours
	Time at 7.05 mlb average thrust	8149 hours
	Duty cycle	98.8 percent
	Cs consumed by engine	18,455 grams
	Initial load	18,459 grams
	Fraction consumed	99.98 percent
	Cs consumed by neutralizer	145.7 grams
	Initial load	202.6 grams
	Fraction consumed (11,000-hour capacity)	71.9 percent
	Neutralizer-to-engine flow rate ratio	0.0080
	Specific impulse	5000 seconds
	Specific impulse $\left(\frac{\text{thrust x time}}{\text{total weight loss}}\right)$	
	Maximum power-to-thrust ratio	155.0 kW/lb
	Average power-to-thrust ratio	150.7 kW/lb
	Minimum power-to-thrust ratio	147.0 kW/lb
B.	Total Operating Times (including performance mapping)	
	Engine and feed system	8192 hours
	Neutralizer	8080 hours

TABLE XXI

DG-2 ENGINE SYSTEM AVERAGE PERFORMANCE

Positive high voltage, V_+ (kV)	1.99
Negative high voltage, V_- (kV)	0.51
Negative HV current, I_- (amp)	0.0055
Beam current, I_B (amp)	0.421
Arc voltage, V_A (volts)	7.3
Arc current, I_A (amp)	23.2
Magnet voltage, V_M (volts)	5.0
Magnet current, I_M (amp)	2.2
Beam power, P_B (kW)	0.838
Drain power, P_D (kW)	0.014
Magnet power, P_M (kW)	0.011
Arc power, P_A (kW)	0.169
Total Engine Power, P_E (kW)	1.032
Feed system power, P_F (kW)	0.016
Total neutralizer power, P_N (kW)	0.010
Total system power, P_S (kW)	1.058
Thrust, T (mlb)	7.07
Engine power-to-thrust ratio, $P_{E/T}$ (kW/lb)	146.0
System power-to-thrust ratio, $P_{S/T}$ (kW/lb)	149.6
Engine power efficiency, η_{PE} (%)	81.2
System power efficiency, η_{PS} (%)	79.2
Engine mass efficiency, η_{ME} (%)	92.3
System mass efficiency, η_{MS} (%)	91.4
Overall engine efficiency, η_E (%)	74.9
Overall system efficiency, η_S (%)	72.4
Engine specific impulse, I_{spE} (sec)	5050
System specific impulse, I_{spS} (sec)	5000
Ratio of drain current, I-/IB (%)	1.31
Source energy per ion, P_A/I_B (keV/ion)	0.401
Total cesium flowrate, I_o (amp)	0.461

It was necessary during both tests to manually adjust the arc power to maintain high mass efficiency. Since even a change of 30 watts in arc power was but 3 percent of the system power, such adjustments did not noticeably decrease the power-to-thrust ratio or power efficiency. For future systems, some form of arc feedback control could be incorporated to allow automatic control of mass efficiency. One such control system is described in Section 6.

The average system mass efficiency given in Table XXI was corrected for the neutralizer cesium flow rate determined by weight loss measurements. Upon completion of the test it was found that 56.9 grams of cesium were left in the neutralizer reservoir. Thus the average neutralizer cesium flow rate was 0.018 gram per hour or 0.80 percent of the engine flow rate, and the average system mass efficiency determined by total cesium weight loss was 91.4 percent.

At the end of the test the engine system was removed from the vacuum chamber. Two overall photographs, Figs. 53 and 54, show the generally unchanged condition of the system. An electrical check was performed, at which time the beam error was found. Aside from this, all other electrical characteristics of the system, except for the cathode heater which will be discussed below, showed no deterioration over the duration of the test.

Upon disassembly of the engine system, a detailed inspection of the components was performed. Figures 55 and 56 show the downstream and upstream sides of the accelerator electrode, respectively. Very uniform erosion over the whole accelerator on the downstream side can be seen both in the enlargement of the apertures due to direct ion interception and in the pattern of pits in the webs left by charge exchange ions. There was no damage to the upstream side so that the electrode optics were not affected.

Figures 57 and 58 show the deposition of foreign material found inside the cathode and on the inside of the cathode orifice plate. This material was very similar in appearance to that found in the DG-1 cathode after the 3700-hour test. While the exact mechanisms producing the contamination are not known, analyses showed the major constitutent to be cesium with about 3 percent each of molybdenum and tantalum from the cathode body and emitter, respectively. No visible damage to the orifice plate was apparent.

After cleaning, the tantalum emitter was found to have been pitted due to chemical attack. The exact mechanism of this attack is not known. It is estimated that less than 2 percent of the emitter mass was lost during the test.

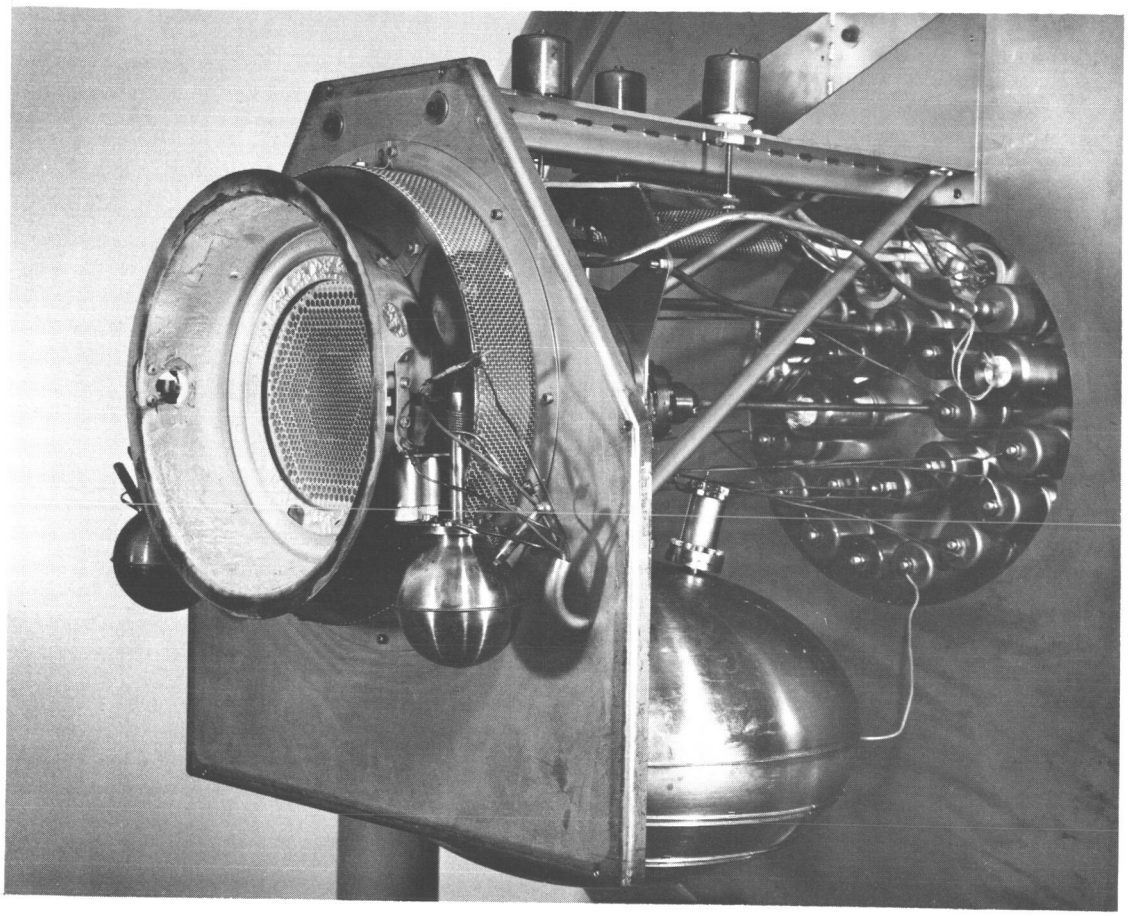

Figure 53. DG-2 Engine System After 8149-Hour Test

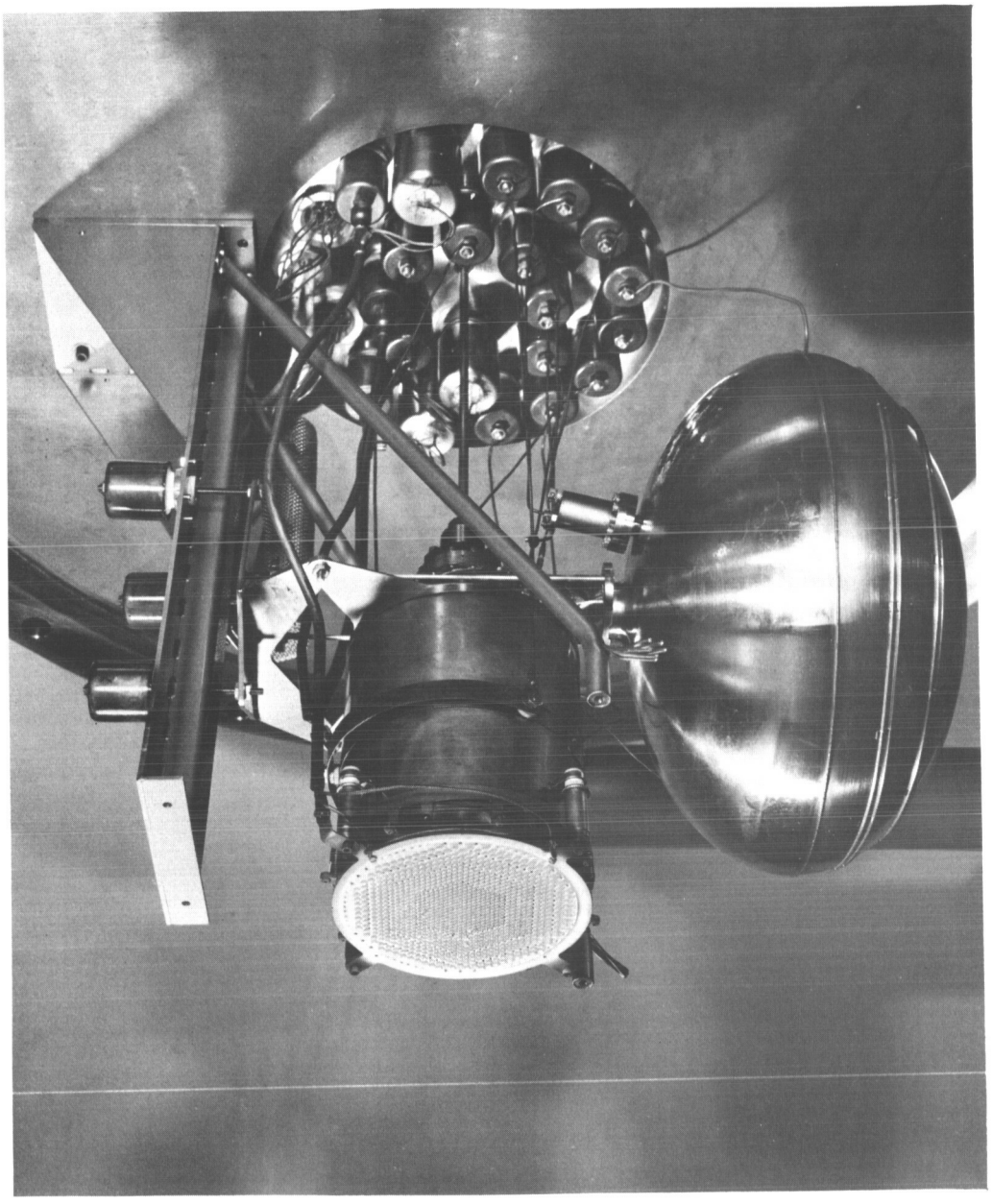

Figure 54. DG-2 Engine and Feed System After 3149-Hour Test

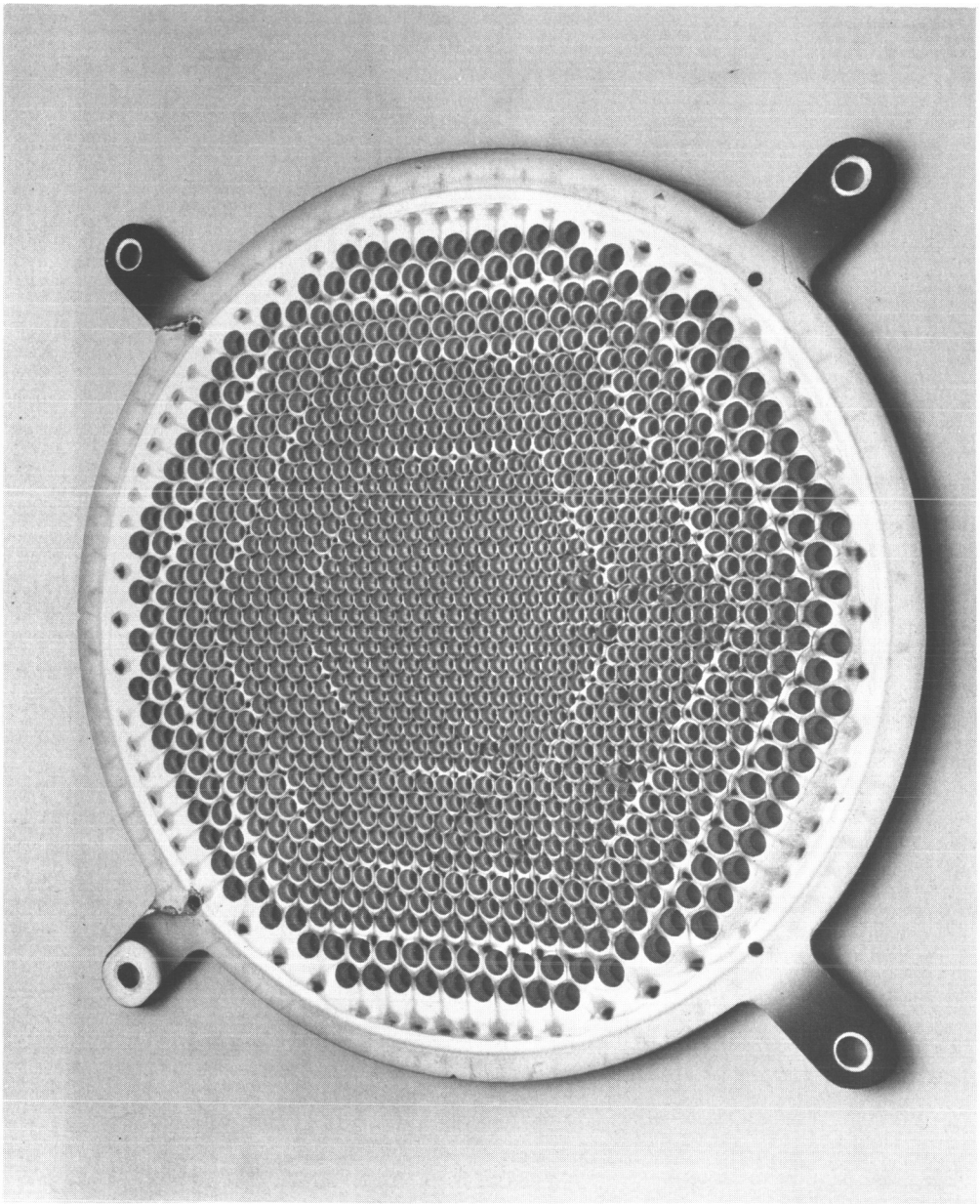

Figure 55. Downstream Side of DG-2 Accelerator After 8149-Hour Test

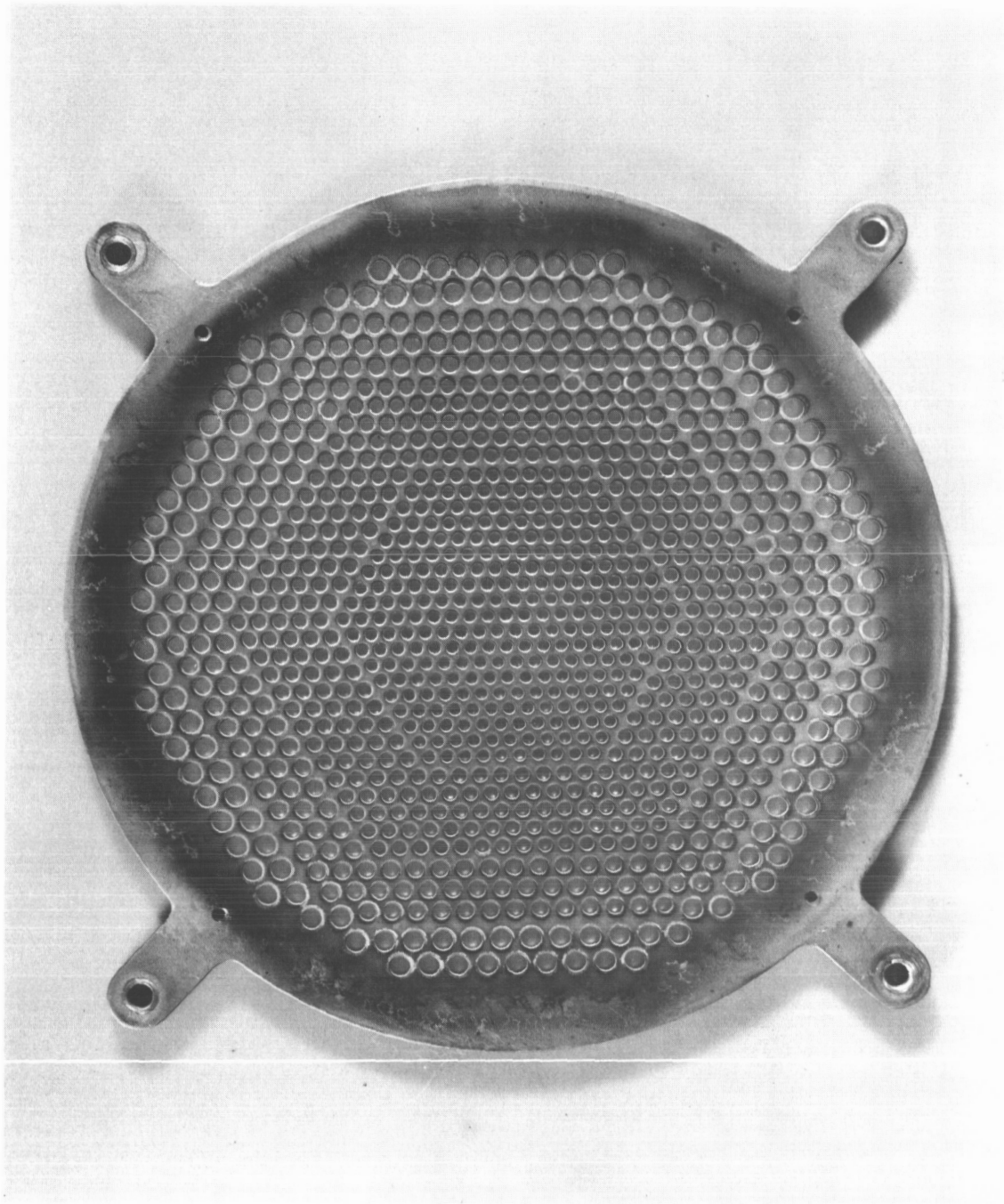

Figure 56. Upstream Side of DG-2 Accelerator After 8149-Hour Test

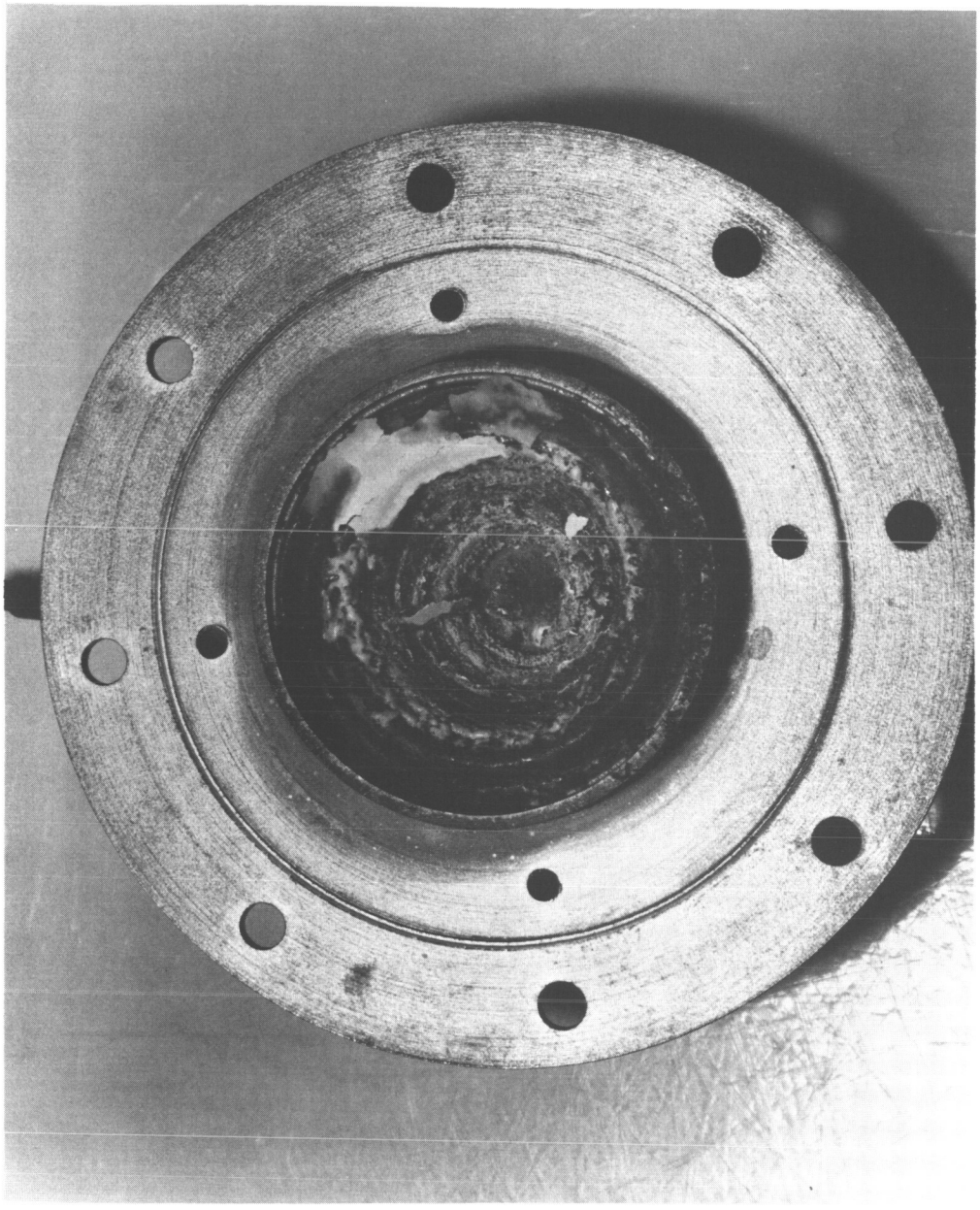

Figure 57. DG-2 Cathode After 8149-Hour Test

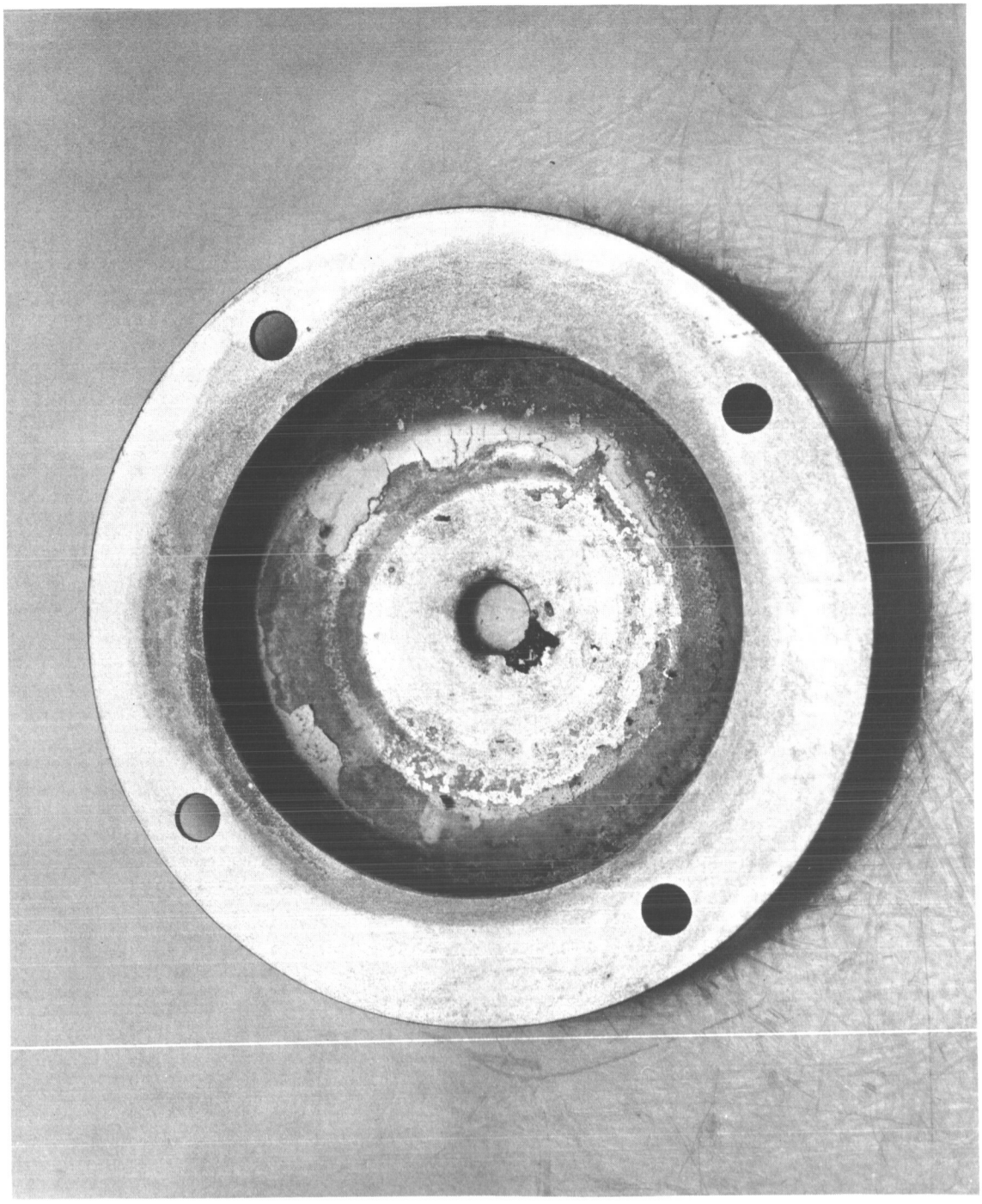

Figure 58. DG-2 Orifice Plate After 8149-Hour Test

Careful examination of the cathode heater terminal and the grounded end of the heater wire showed that the open circuit that was observed at 1045 hours was not at either end of the coil. The cathode was then sectioned so that individual half turns could be probed to find the failure. The open circuit was found in the outermost turn. The sheath of this half turn was then ground away and the insulation removed to reveal a crack in the core conductor. The crack is shown at twenty power in Fig. 59. There was apparently no cause for this failure other than its being a random material failure. A new x-ray inspection technique has been formulated and will be used in an attempt to identify future heater wire defects when the material is received.

The engine shell was found to be in excellent condition. One small bright area was found in the front magnet cover made of titanium. This is shown in Fig. 60. Measurement of the thickness of the foil in this area showed that less than 0.0004 inch out of the original 0.0030 inch thickness had been lost. The most probable cause of this spot was electron bombardment from the neutralizer. Calculations show that evaporation of the titanium because of electron bombardment could have occurred continuously during the whole test, but the severity of the distortion indicates evaporation due to a very high temperature for a short time. The most probable time for such an event would have been during a malfunction when abnormal performance occurred. For example, at 4300 hours the negative high voltage supply failed so that electrons could have backstreamed to the shell. There were several other possible times that the evaporation could have happened, so the exact time and circumstances are not known. This damage is not serious; no degradation of performance was seen, and it cannot be considered a failure mode since less than 15 percent of the cover was lost in that area during the whole test. All other parts of the engine were in excellent condition. No damage to the screen electrode, anode, cathode plate, or electrode insulator support assembly was found.

The reason for the loss of neutralizer emission current after 8100 hours of neutralizer run time was found to be clogging of the neutralizer orifice. To establish the nature of the clogging the orifice cap was removed from the neutralizer and examined on the inside, where the plugging material was found as a buildup only in the near vicinity of the orifice. This is shown at thirty power in Fig. 61. The outer part of the orifice plate was quite clean. The origin of the plugging material is not known exactly, but because of the highly localized buildup around the orifice, it is suspected that it came from outside the neutralizer.

Figure 62 is a closeup view of the spare neutralizer orifice cap and the large amount of aluminum backsputtered onto it from the facility collector and liner. This aluminum completely plugged the orifice so that it could not be started after the first neutralizer ceased emission. More careful shielding from backstreaming material would alleviate this problem, which is a product of the test environment.

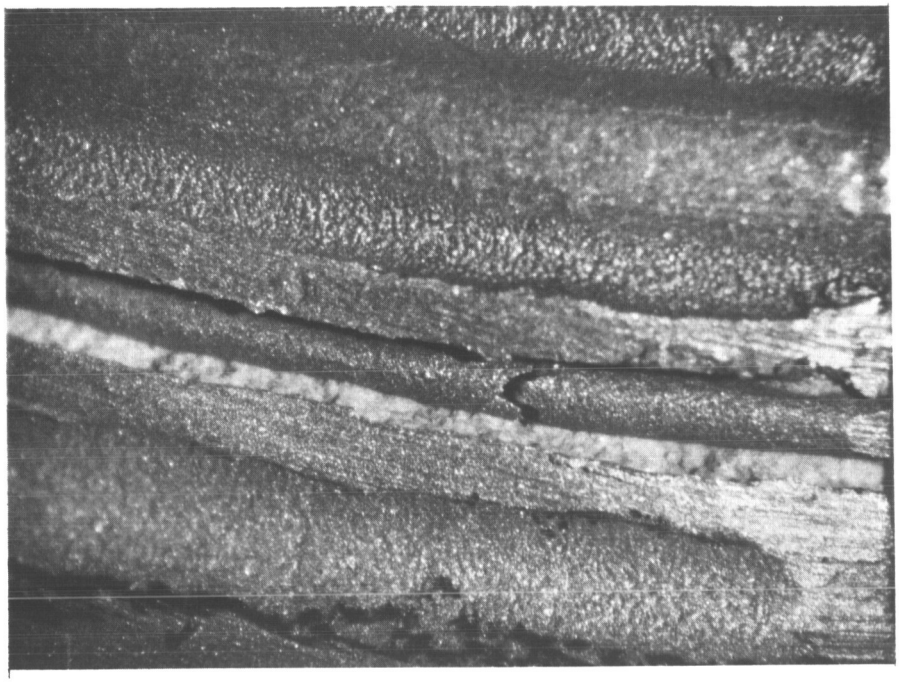

Figure 59. Twenty-Power Photograph of Heater Wire Crack

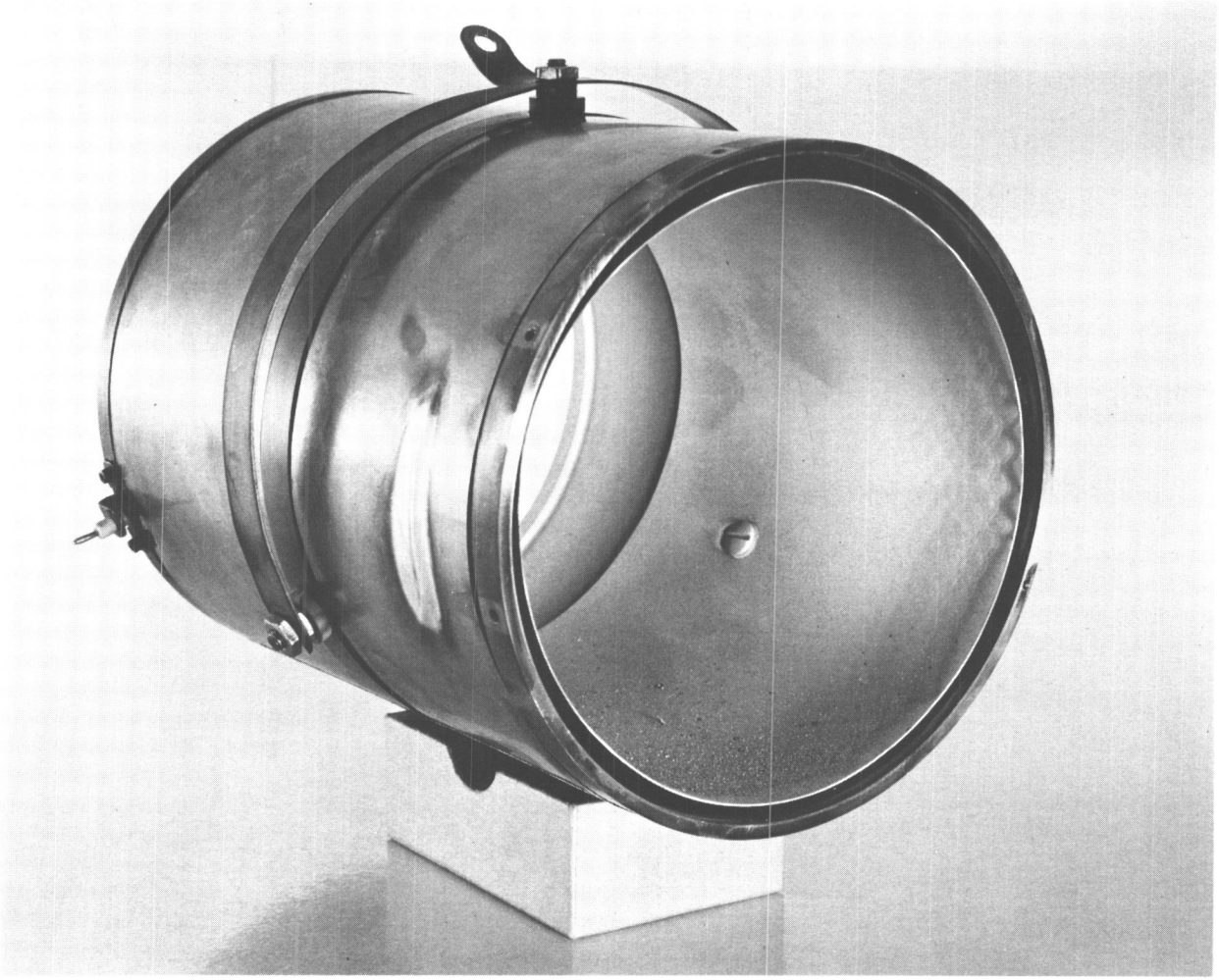

Figure 60. DG-2 Engine Shell After 3149-Hour Test

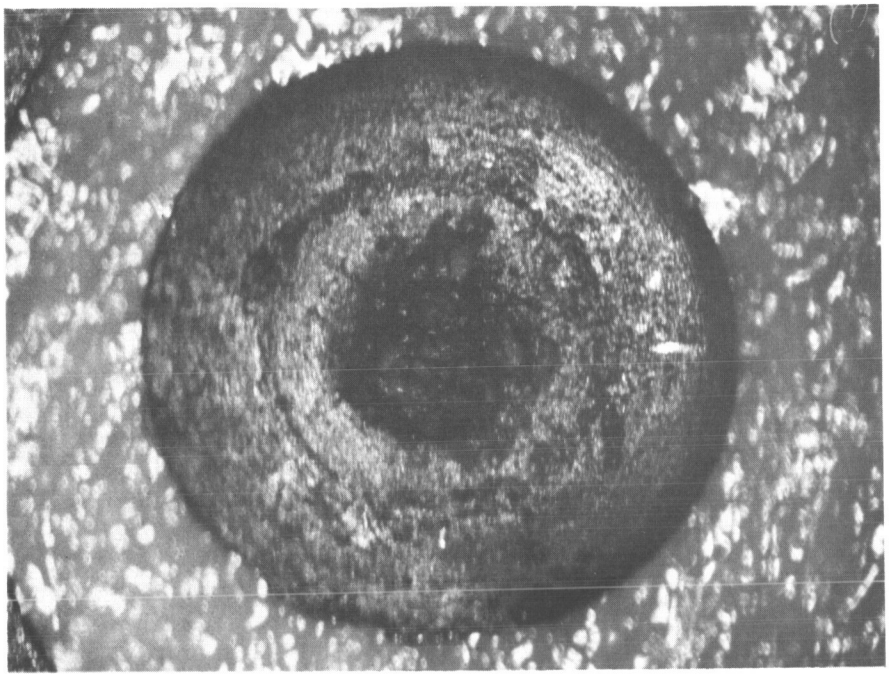

Figure 61. Thirty-Power Photograph of Inside Neutralizer Orifice Cap

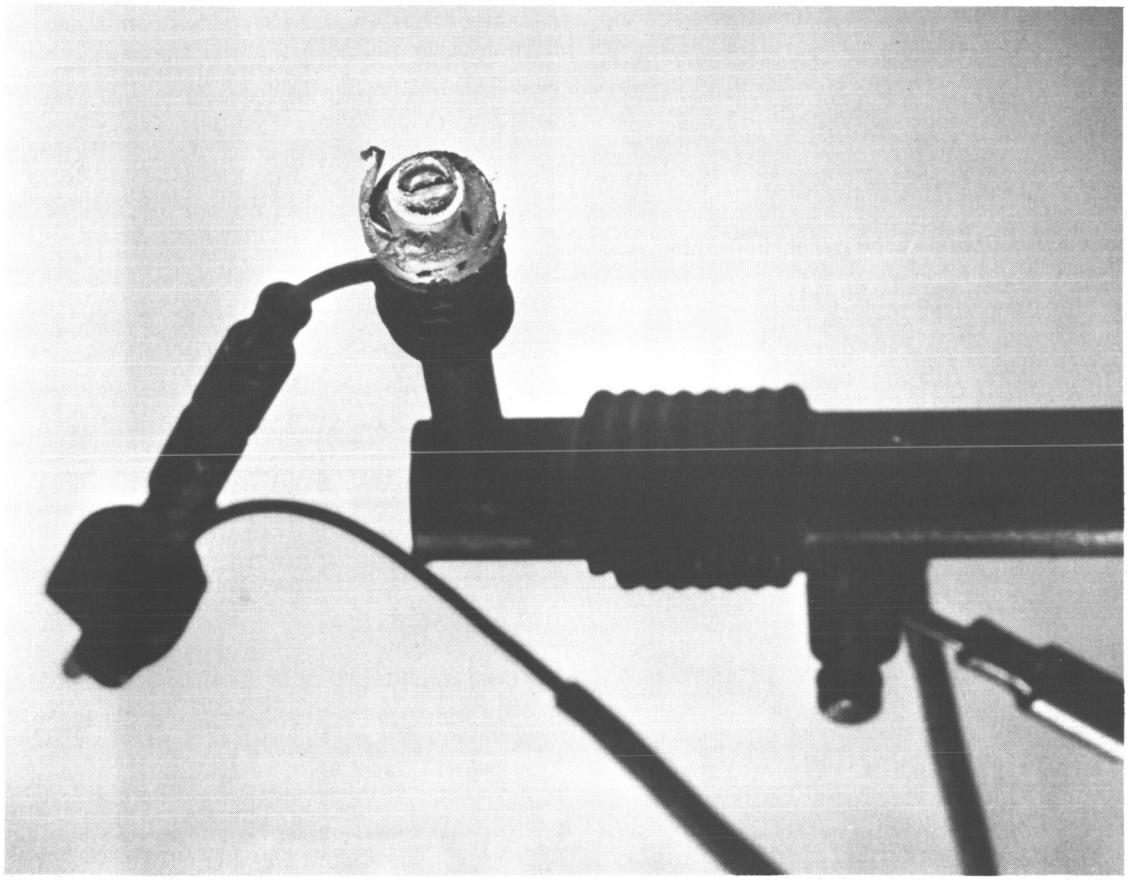

Figure 62. Spare Neutralizer Orifice Cap

Twelve samples of forign material were taken for spectrographic analysis from various engine components. In addition the tantalum emitter was removed from the neutralizer used on the test and analyzed. Table XXII gives the results of the analysis. Aluminum, backsputtered from the collector, was found to be the major constituent of all the samples except those taken from inside the engine cathode and from inside the neutralizer cathode (sample numbers 7, 8, 11, 12, and 13, respectively). The three samples taken from inside the cathode show the major constituents to be molybdenum and tantalum which come from the cathode body and orifice plate and from the emitter, respectively.

Figures 55 and 56 show the material deposited inside the cathode. There was a large amount of cesium in this material, but cesium cannot be detected by the analysis process used. The major constituent of the sample taken from between the vaporizer and cathode in the neutralizer was found to be gold. No satisfactory explanation has been found for a large presence of gold in this region. There may have been an error in the analysis.

Engine component weights were taken and compared to the values obtained before the test. Table XXIII summarizes these results. All of the components show a net weight gain due to backsputtered aluminum from the collector and collection of other foreign material except the accelerator, which lost nearly 6 percent its weight by erosion.

Based on the test results a lifetime in excess of 20,000 hours for the DG type engine can be predicted in parallel to the results from the test of DG-1. As before, the only component deteriorating during the test was the accelerator electrode and its lifetime is the basis for the prediction. The cathode failure was random material failure and can be avoided. The clogging of the neutralizer also appears easy to avert in a space environment, free from backsputtered metal.

40-Pound Feed System Analysis

After removal from the engine the feed system was weighed. The weight difference between the weight before loading and that after the run was approximately 4 grams. This is less than the amount required to fill the porous rod and there was no liquid cesium available for chemical analysis. During the test more than 99.9 percent of the cesium loaded was exhausted.

The feed system was disassembled in the dry box. Photographs and samples for chemical analysis were taken of various components and unusual deposits found during the disassembly.

TABLE XXII

ANALYSIS OF FOREIGN MATERIALS*

Origins of Samples	Peeling from Downstream Side of Ground Shield	Peeling from Upstream Side of Ground Shield	Peeling from Side of Ground Cone	Backsputtered Material Over Spare Neutralizer Cap	Peeling from Downstream Side of Screen	Peeling from Outside of Cathode Orifice Plate	Scrapings from Inside Cathode Around Periphery
	No. 1	No. 2	No. 3	No. 4	No. 5	No. 6	No. 7
Element	%	%	%	%	%	%	%
Zn	< .05	< .05	< .05	1.0	< .05	< .05	< .05
Mn	.01	.01	< .05	.02	.01	< .01	< .01
Si	.1	.2	.1	.1	.1	.1	.05
Cu	.1	.1	.1	.2	.2	.2	.01
Fe	.5	.5	.5	.5	.5	.5	.01
Ni	.005	.005	.005	.05	< .005	< .005	< .005
Ti	.005	.005	.005	.01	.01	.01	.005
Cr	.005	< .005	.005	.03	< .005	< .005	< .005
Sn	.005	< .005	.005	.005	< .005	.005	< .005
Al	1	1	1	1	1	1	1.0
Mo	< .005	.005	< .005	< .005	.5	1.0	1
Au	-	-	-	-	-	-	-
Ag	-	-	-	.001	.005	.005	-
B	-	-	-	.005	-	-	.002
Cd	-	-	.01	-	-	-	-
Co	-	-	-	-	-	-	.5
Ta	-	-	-	-	-	.1	1

*See Note, page 55 , for explanation.

TABLE XXII (contd)

ANALYSIS OF FOREIGN MATERIALS*

Origins of Samples	Scrapings from Inside Cathode Near Center	Peeling from Inside Anode	Scrapings from Inside Anode	Scrapings from Inside Orifice Plate	Inside Spare Neutralizer Tube Below Emitter	Neutralizer Emitter Used On Test
	No. 8	No. 9	No. 10	No. 11	No. 12	No. 13
Element	%	%	%	%	%	%
Zn	< .05*	< .05*	< .05*	< .05*	< .05*	< .05*
Mn	.01	.01	.01	< .01*	.02	.01
Si	.1	.1	.2	.05	.2	.2
Cu	.1	1	1	.02	.005	.05
Fe	.01	.2	.5	.008	.3	.3
Ni	< .005*	< .005*	.005	< .005*	.005	.03
Ti	< .005*	.01	.05	< .005*	.005	< .005*
Cr	.005	< .005*	.005	.01	.3	.3
Sn	< .005*	< .005*	< .005*	< .005*	.005	< .005*
Al	2.0	1	1	.5	.003	.005
Mo	1	.5	1.0	1	< .005*	.7
Au	.005	-	-	-	1	.01
Ag	-	.002	.002	-	.01	-
B	.005	-	-	-	-	.03
Cd	.01	-	-	-	-	.01
Co	3.0	-	-	.5	-	-
Ta	1	.05	.1	1	-	1

*See Note, page 55, for explanation.

TABLE XXIII

DG-2 ENGINE COMPONENT WEIGHTS

Component	Weight Before Test (grams)	Weight After Test (grams)	Weight Change (grams)
Anode	228.056	230.063	+2.007
Cathode Assembly	213.345	217.303	+3.958
Cathode Plate	160.383	161.793	+1.410
Screen Electrode	48.5826	50.8149	+2.2323
Accelerator	100.40	94.44	-5.96

The manual valve was found to be in generally the same condition as in previous tests. Light-colored thin films coated the upstream face of the valve and the diaphragm. These were in such small quantities that samples for chemical analysis could not be obtained.

The valve stem was found to have been broken away from the diaphragm. This was probably caused by foreign deposits between the bearing screw and the bearing stud. During the shutdown of the engine system, prior to removal of the system from the vacuum chamber, the valve was closed. At this time, when the valve was operated, the stem was twisted and pulled loose from the diaphragm.

Because of the valve failure, air was allowed to reach the porous rod and reacted with the residual cesium. Deposits of reacted cesium were found on the vaporizer surface. These deposits were spectrographically analyzed. The results are shown in Table XXIV. The high percentage of silicon found can most likely be attributed to a glass container used in storing the sample before analysis. The chrome, nickel and iron are constituents of the stainless steel and are present in the analysis of the porous rod. The titanium and aluminum are as yet not explained.

The porous nickel rod was removed from the vaporizer and sectioned. Figure 63 shows the position from which samples were taken. These samples were spectrographically analyzed. The results are shown, compared with the analysis of a sample taken during assembly, in Table XXV. The iron found in the analysis can be attributed to dissolved iron from the stainless steel carried in the cesium to the porous rod and also to the tool used for sawing the samples. Most other elements are in small quantities except for a high percentage of zinc found after the run. Zinc is a constitutent of some braze alloys but is hard to explain in this area. The rod at first appeared to be dry except for a small portion near the interface between the vaporizer and the reservoir. When the rod was sectioned however the rod was found to be wet with cesium along the entire length.

The vaporizer was found to be in very good condition with no pits or erosion. Because of the obvious good condition of the vaporizer it was not sectioned.

The port valve was found to be frozen in the closed position. The cause was determined to be cesium deposited on the seal surface and after manually breaking this deposit the valve operated normally. The O-ring seal appeared to be in usable condition.

All heater resistances and the port valve opening and holding current were within normal tolerances. Various weights and measurements were taken before and after the test. These are shown in Table XXVI.

TABLE XXIV

FOREIGN MATERIAL ANALYSIS 40-POUND FEED SYSTEM VAPORIZER

Element	%
Silicon	7.0
Titanium	0.4
Chromium	3.0
Nickel	2.0
Iron	0.9
Aluminum	0.8
Lead	0.3
Silver	0.3
Manganese	0.01
Tin	0.02
Calcium	0.02
Copper	0.07
Vanadium	0.02
Molybdenum	0.05
Columbium	0.04
Magnesium	0.005

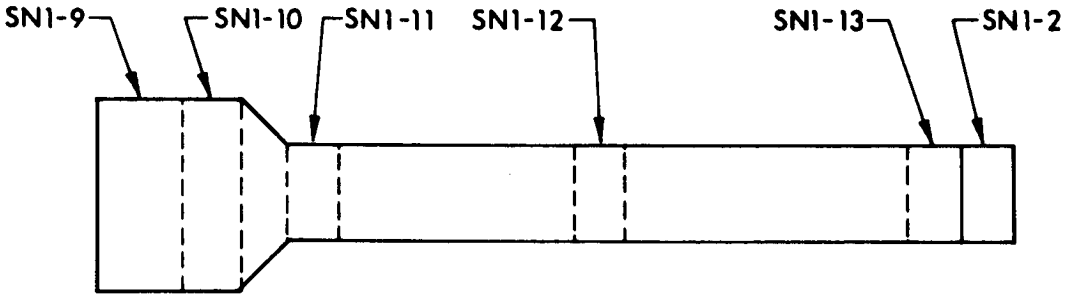

Figure 63. Position of Porous Rod Samples

TABLE XXV

POROUS ROD ANALYSIS (%), 40-POUND FEED SYSTEM*

	Before	After				
Element	SN1-2	SN1-9	SN1-10	SN1-11	SN1-12	SN1-13
Nickel	Rem	Rem	Rem	Rem	Rem	Rem
Iron	0.12	0.23	0.39	0.21	0.19	0.21
Manganese	< 0.05	0.02	0.03	0.04	0.02	0.02
Silicon	0.10	0.03	0.04	0.04	0.07	0.08
Aluminum	—	0.01	0.01	0.011	0.014	0.014
Copper	0.05	0.06	0.05	0.05	0.05	0.05
Titanium	< 0.003	0.005	< 0.005	< 0.005	< 0.005	< 0.005
Cobalt	< 0.03	0.15	0.13	0.15	0.15	0.14
Chromium	—	< 0.01	< 0.01	< 0.01	< 0.01	< 0.01
Magnesium	< 0.004	0.002	0.002	0.001	0.001	0.001
Zinc	—	5.2	5.0	5.3	6.2	3.4
Tin	—	0.01	< 0.005	< 0.005	< 0.005	< 0.005

*See Note, page 55, for explanation.

TABLE XXVI

POST RUN WEIGHT ANALYSIS 40-POUND FEED SYSTEM

	Before	After	Change
Weights	(grams)	(grams)	(grams)
Control Fin	24.69785	24.6277	-0.07015
Fin Assembly	2310.	2295.	-15.0
Reservoir Assembly	3700.	3690.	-10.0
Port Valve Flange	33.38085	33.37975	-0.0011
Vaporizer	107.940	103.725	-4.215
Manual Valve Body	234.3746	234.175	-0.1996
Manual Valve Diaphragm Assembly	64.69075	64.68335	-0.0074
Manual Valve Tip	4.77815	4.77125	-0.0069
Copper Seal Weights	(grams)	(grams)	(grams)
Port Valve	1.70045	1.70145	+0.001
Blank Flange	1.76075	1.76205	+0.0013
Reservoir-Vaporizer	1.75835	1.75915	+0.0008
Vaporizer-Valve	2.80435	2.80415	-0.0002
Manual Valve	5.15060	5.15285	+0.00225
Valve-Cathode	1.66085	1.66315	+0.0023
Dimensions	(inch)	(inch)	(inch)
Control Fin Thickness	0.005	0.005	0
Vaporizer Bore	0.998	0.999	+0.001
Top Shell Thickness	0.0230-0.0235	0.0230-0.0235	0
Bottom Shell Thickness	0.0210-0.0220	0.0210-0.0220	0

The weight loss of the fin assembly is greater than the weight loss of the entire reservoir assembly. The difference could be an amount removed from the fin assembly and redeposited on the reservoir shells. Because the weld area around the reservoir was ground away in opening the shells, an accurate weight determination of the shells was not possible.

The analysis of a sample of the control fin is shown in Table XXVII compared to the analysis obtained during assembly of the system.

Table XXVIII shows the results of the cesium analysis performed on the cesium loaded into the system. As previously noted, there was not enough cesium left after the test for a comparison analysis.

All portions of the feed system were in exceptionally good condition with no signs of corrosion. The feed system supplied propellant until the supply was exhausted, and no problems were encountered. It appears that this type of system could be used for periods many times the 8400 hours accumulated on the feed system during the testing.

1/2-Pound Neutralizer Reservoir Analysis

After disassembly from the engine the reservoir was weighed. The difference between the weight before the run and after was 56.9 grams. The total loaded weight of cesium was 202.6 grams; therefore, 145.7 grams of cesium were used during the test. The complete load of cesium was not used due to clogging of the neutralizer orifice.

Upon disassembly the reservoir parts were found to be in excellent condition with no pitting or erosion. Table XXIX lists various weights and dimensions that were recorded both before the run and after.

The reservoir weight change is mostly due to loss of material when the fill tube was cut off for reloading the system. Therefore an analysis of the weight change is not possible. The weight change in the fin assembly and in the control fin agree within 20 percent. No dimensional changes were noted.

Table XXX shows the chemical analysis of the control fin before and after the test. Table XXXI shows the chemical analysis of the cesium before and after the test. Little change in the constituents was noted except in the quantity of copper. This is easily explained as copper dissolved from the reservoir-to-neutralizer seal.

Except for the clogging of the neutralizer orifice the feed system was in excellent condition and appears capable of operating several times the 8100 hours accumulated on this test.

TABLE XXVII

CONTROL FIN ANALYSIS, 40-POUND FEED SYSTEM

Element	Before	After
	(%)	(%)
Manganese	1.89	0.7
Silicon	0.64	0.7
Chromium	19.0	17.5
Nickel	9.0	11.3
Columbium	0.84	1.0
Copper	0.19	0.2

TABLE XXVIII

CESIUM ANALYSIS, 40-POUND FEED SYSTEM*

	1-3 (ppm)	1-4 (ppm)	1-5 (ppm)	1-6 (ppm)	1-7 (ppm)
Cesium	Rem	Rem	Rem	Rem	Rem
Silver	< 1	< 1	< 1	< 1	< 1
Aluminum	< 1	< 1	< 1	< 1	< 1
Boron	< 3	< 3	< 3	< 3	< 3
Barium	< 50	< 50	< 50	< 50	< 50
Beryllium	< 1	< 1	< 1	< 1	< 1
Calcium	< 1	< 1	< 1	< 1	< 1
Cadmium	< 3	< 3	< 3	< 3	< 3
Cobalt	< 3	< 3	< 3	< 3	< 3
Chromium	< 3	< 3	< 3	< 3	< 3
Copper	1	< 1	< 1	< 1	< 1
Lithium	< 30	< 30	< 30	< 30	< 30
Magnesium	< 1	< 1	< 1	< 1	< 1
Manganese	< 1	< 1	< 1	< 1	< 1
Molybdenum	< 3	< 3	< 3	< 3	< 3
Sodium	25	< 5	< 5	20	15
Niobium	< 30	< 30	< 30	< 30	< 30
Nickel	< 1	< 1	< 1	< 1	< 1
Lead	< 3	< 3	< 3	< 3	< 3
Silicon	< 1	< 1	< 1	< 1	< 1
Iron	2	3	< 1	< 1	< 1
Titanium	< 1	< 1	< 1	< 1	< 1
Vanadium	< 3	< 3	< 3	< 3	< 3
Zinc	< 30	< 30	< 30	< 30	< 30
Zirconium	< 10	< 10	< 10	< 10	< 10
Total Other Elements	< 200	< 200	< 200	< 200	< 200
Tin	< 3	< 3	< 3	< 3	< 3

*See Note, page 55, for explanation.

TABLE XXIX

POST RUN HOUR ANALYSIS 1/2 POUND FEED SYSTEM

Weights (grams)	Before	After	Change
Control Fin	0.48865	0.48600	-0.00265
Fin Assembly	49.92615	49.76600	-0.16015
Reservoir Assembly	136.9 (135.7)	135.6	-1.3
Reservoir-Neutralizer Seal	1.73035	1.72055	-0.00980
Dimensions (inches)			
Control Fin	0.002	0.002	0.0
Reservoir Wall Upper	0.0195-0.0205	0.0195-0.0205	0.0
Reservoir Wall Lower	0.0220-0.0225	0.0220-0.0225	0.0

TABLE XXX

CONTROL FIN ANALYSIS

Element	Before (%)	After
Manganese	0.56	0.8
Silicon	0.57	0.7
Chromium	18.0	17.5
Nickel	9.3	10.9
Columbium	0.65	1.0
Copper	0.18	0.2

TABLE XXXI

CESIUM ANALYSIS 1/2-POUND FEED SYSTEM*

Element	Before (ppm)	After (ppm)
Cesium	Rem	Rem
Silver	< 1	< 1
Aluminum	3	< 1
Boron	< 3	< 3
Barium	< 50	< 5
Beryllium	< 1	< 1
Bismuth	< 3	< 3
Calcium	< 1	< 1
Cadmium	< 30	< 1
Cobalt	< 3	< 3
Chromium	< 1	< 1
Copper	< 1	10
Iron	1	2
Lithium	< 30	< 30
Magnesium	< 1	< 1
Manganese	< 1	< 1
Molybdenum	< 1	< 1
Sodium	3	< 5
Niobium	< 30	< 30
Nickel	< 1	< 1
Lead	< 3	< 3
Silicon	< 1	< 1
Tin	< 3	< 3
Titanium	< 1	< 1
Vanadium	< 3	< 3
Zirconium	< 3	< 3
Zinc	—	< 30
Total Other Elements	< 100	—

*See Note, page 55, for explanation.

SECTION 4

THE DG-3 ENGINE SYSTEM

A third engine system (the DG-3 engine system) was built and delivered to the NASA-Lewis Research Center. This system included an engine of the DG design, a 5-pound, "zero gravity" cesium feed system, a "10,000-hour" plasma-bridge neutralizer, a laboratory power supply and control system, a neutral cesium detector, spare parts, and instruction manuals. Upon assembly the engine system was checked out at Electro-Optical Systems, Inc. and used briefly for integration testing with the NASA-LeRC supplied power conditioning equipment prior to delivery. The power conditioning integration tests were successful and only minor problems were encountered.

4.1 ENGINE SYSTEM HARDWARE

The DG-3 engine supplied with the system was of the same DG design as that used for both the 2000-hour and 4000-hour tests.

The 5-pound, zero gravity feed system delivered operated on the same principles as did the 20, 40, and 1/2-pound feed systems. A manually operated feed valve and an electromechanical reservoir pumpout valve were supplied.

The plasma bridge neutralizer delivered also used a zero gravity feed system with a cesium reservoir capacity of about one-half pound. An electromechanical pumpout valve was also used on this reservoir. The neutralizer and plasma bridge probe were mounted on a separate plate and cone assembly which could serve as the front portion of a ground shield.

The DG-3 engine system is shown in Figs. 64 and 65.

4.2 CONTROL SYSTEM

A complete laboratory control system containing all the necessary power supplies and control elements for manual or automatic engine system operation was delivered with the engine system. The control system is shown in Fig. 66. This control system was similar to those developed under a prior program (Ref. 4).

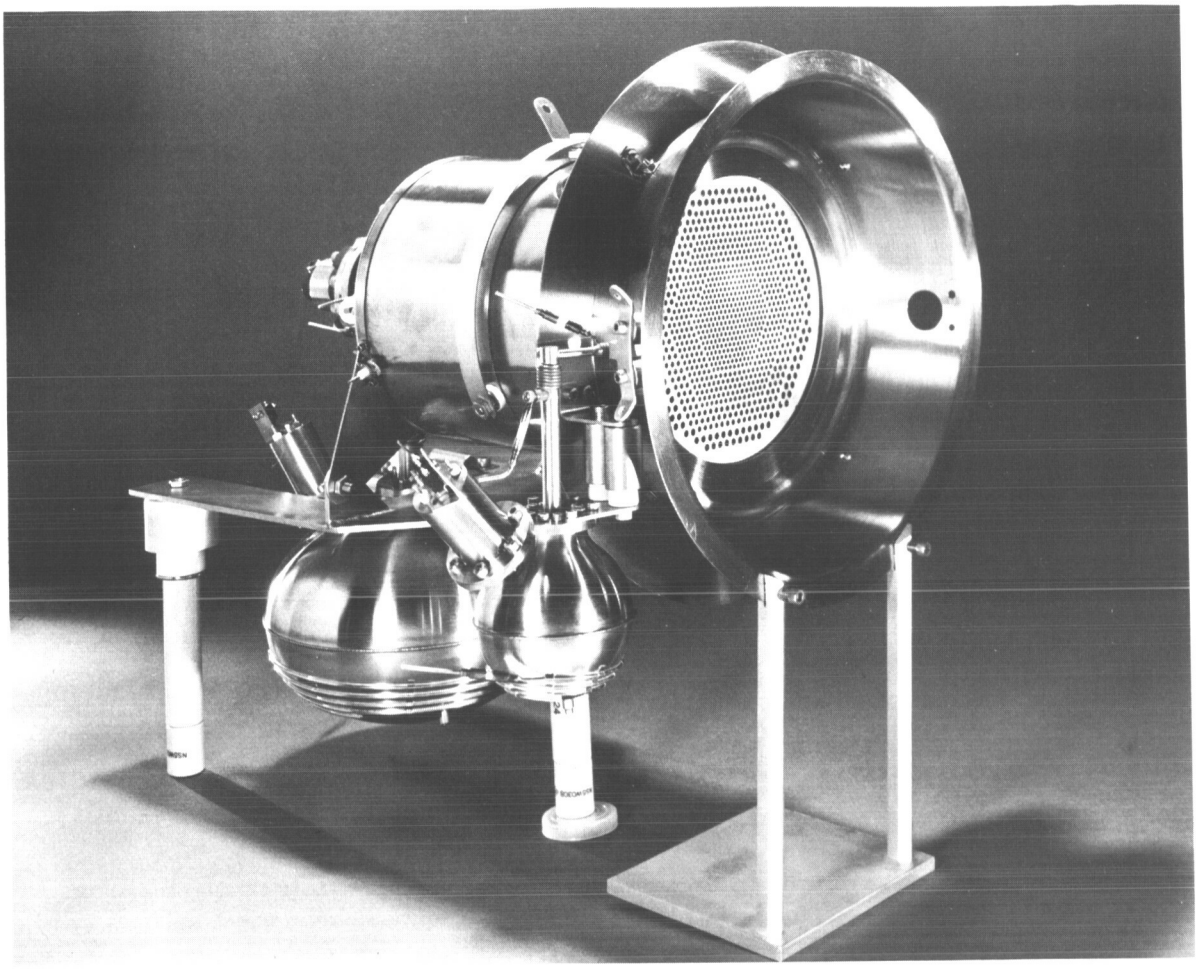

Figure 64. DG-3 Engine System

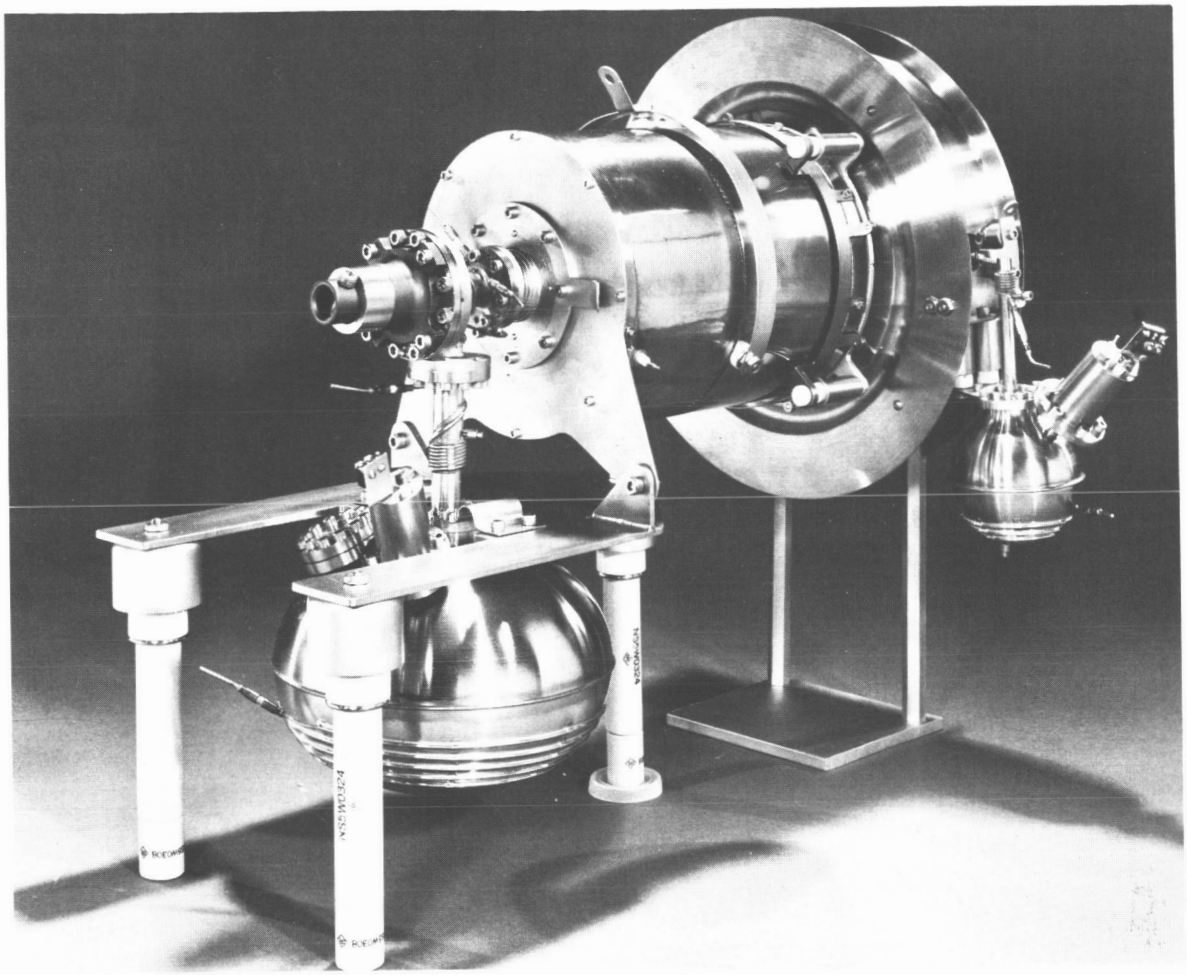

Figure 65. DG-3 Engine System

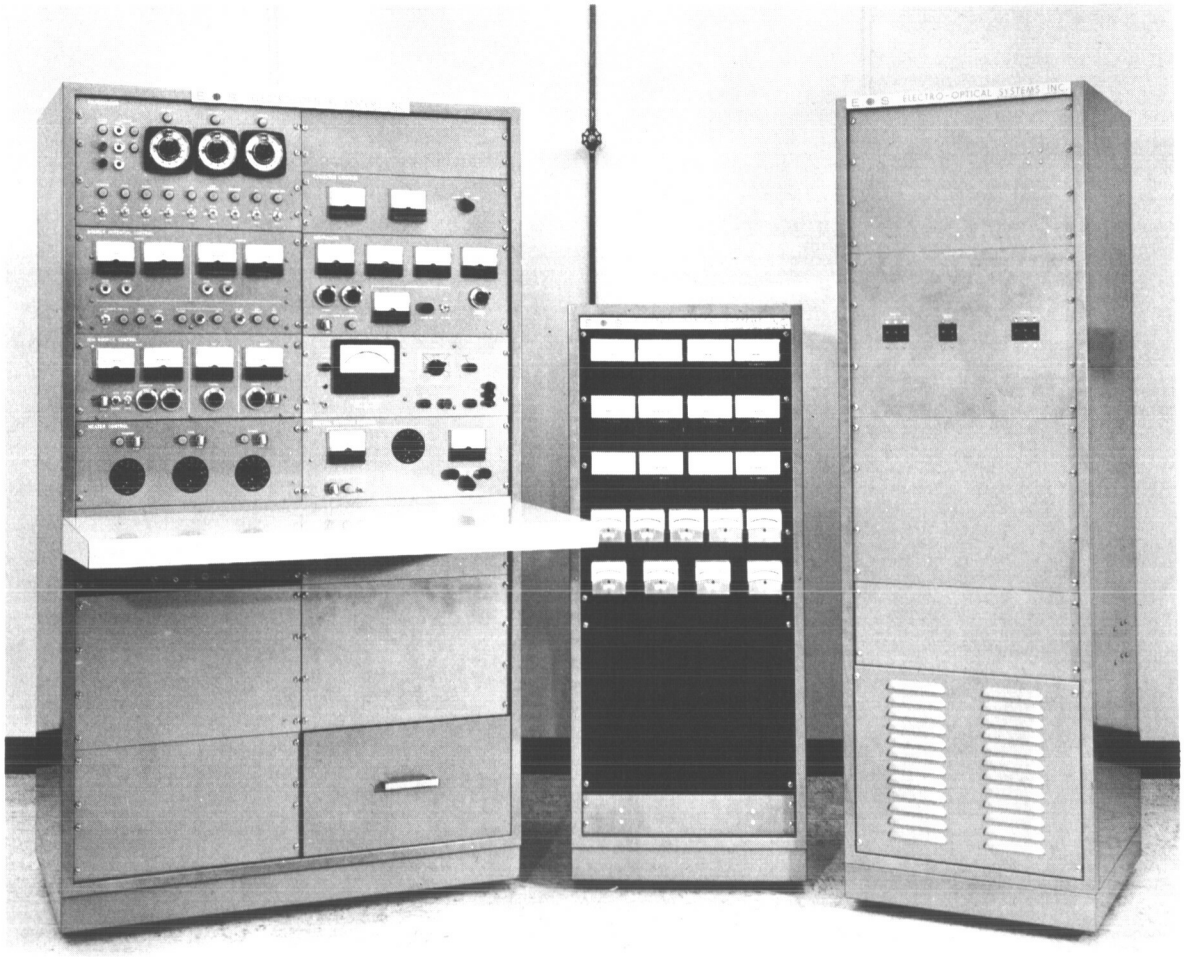

Figure 66. DG-3 Controle, Auxiliary Rack, and High Voltage Rack

4.3 NEUTRAL CESIUM DETECTOR

A neutral cesium detector, Model LM-3, used for engine flow rate determination was also built and delivered. A liquid-nitrogen-cooled shroud was used to condense neutral cesium away from the detector to suppress the background level. The neutral cesium detector with the shroud removed is shown in Fig. 67 while Fig. 68 shows the detector with the shroud in place. Details of the detector operation may be found in Ref. 3.

4.4 POWER-CONDITIONING INTEGRATION TESTS

The DG-3 engine, feed system, and neutralizer were assembled and checked out at Electro-Optical Systems, Inc. with spare laboratory power supplies to insure that all components were functioning normally. Following this checkout, the engine system was operated using flight-type power-conditioning equipment supplied by the NASA-Lewis Research Center. The significant observations of the integration tests are summarized below.

a. The tradeoff between cathode heater power and no-load arc voltage for initiation of the arc was not known in detail. As a result, the specific minimum arc voltage and cathode heater power proved to be insufficient for starting the discharge. An increase in the cathode heater power eliminated this problem.

b. It was expected that any transient loss in extraction voltage would allow the plasma to extrude through the screen electrode causing an effective short between the electrodes. This was found to be true even though the voltage-off period for the breadboard supplies was only a few microseconds long. Addition of filtering to the high voltage supplies prevented high transient currents which otherwise caused shutdown of the power supplies.

c. Recovery of high voltage after a breakdown was accomplished within a few seconds with the breadboard supplies, while the laboratory supplies typically required about three minutes. The "hard, fast" turn-on of the supplies was more compatible with engine response than was the turn-on of the laboratory supplies.

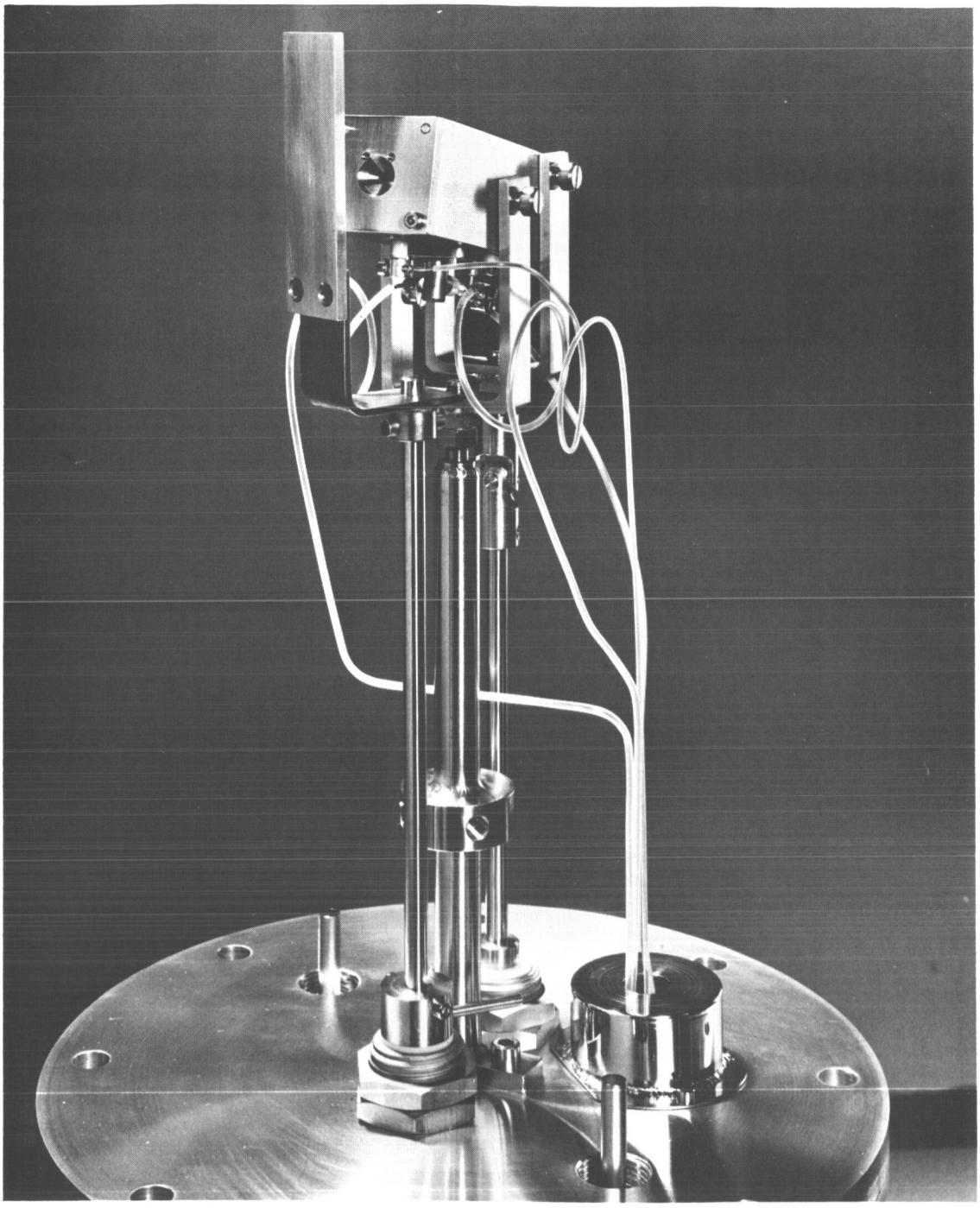

Figure 67. Model LM-3 Neutral Cesium Detector With LN_2 Shroud Removed

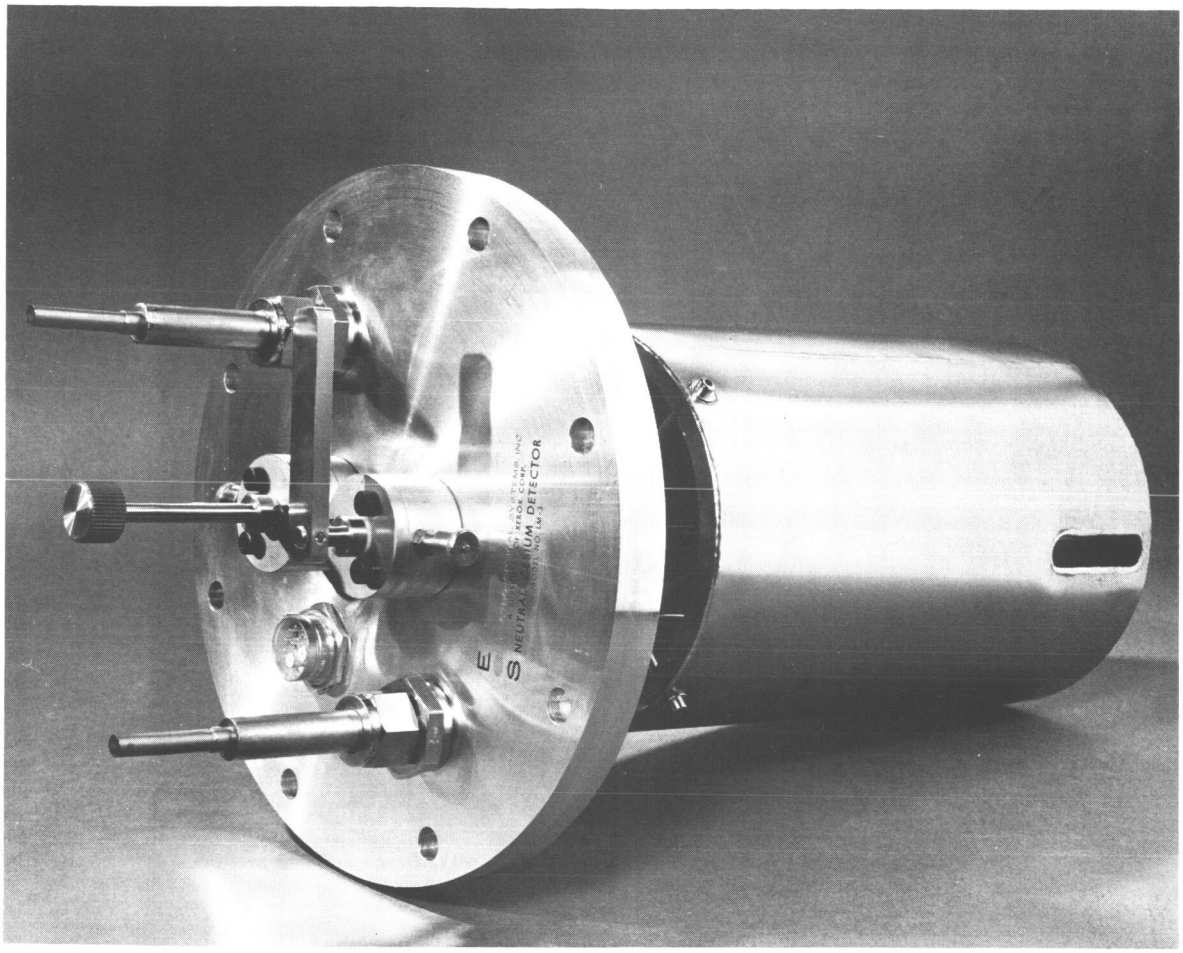

Figure 68. Model LM-3 Neutral Cesium Detector

4.5 SUMMARY

The DG-3 engine system, control system, and neutral cesium detector were delivered to the NASA-Lewis Research Center in February 1966. Technical field support was provided by Electro-Optical Systems, Inc. for initial testing of the systems at the NASA-Lewis Research Center. During these tests performance equivalent to that of the DG-1 and DG-2 systems was obtained.

SECTION 5

PERMANENT MAGNET ENGINE

Development of a permanent magnet version of the DG engine was undertaken at the start of the program. When it became clear that this engine would not be completed in time for life testing, the development was deferred until the life tests had been started. This engine was based on the cylindrical permanent magnet engine described in Refs. 5 and 6. Several magnetic materials were considered including Cunife and Vicalloy. One shell was fabricated from Cunife, but the design was abandoned after its thermal stability was found to be unsatisfactory. A series of tests to evaluate Vicalloy for the shall material was performed, and the material was found to be acceptable so the DGM engine was designed and built using Vicalloy.

An improved accelerator support system was used in the new design. One DGM engine, subjected to vibration tests, showed the design to be very stable. The total engine weight was reduced to 1.6 pounds; however, no operating tests were conducted.

5.1 INITIAL DESIGN CONSIDERATIONS

The feasibility of replacing the engine electromagnet with a permanent magnet circuit was studied at Electro-Optical Systems, Inc. under Contract NAS3-5250. The results of those studies led to the design and construction of two engines, PM-1 and PM-2, utilizing cylindrical shells made from the permanent magnet material, Vicalloy, and an iron cathode mounting plate and screen electrode for pole pieces (Ref. 5).

The new engine design was based on that approach with sufficient magnetic material to provide a minimum axial field to 10 gauss. The design operating point was the same as for the DG engine; 1 kilowatt total input power at 5000 seconds specific impulse. In addition, the design was made for a minimum weight that would be consistent with maximum reliability and lifetime. The magnetic material originally chosen was Cunife, an alloy of 60 percent copper, 20 percent nickel, and 20 percent iron. Cunife was more desirable than Vicalloy, an alloy of 10 percent vanadium, 52 percent cobalt, and 38 percent iron used for previous permanent magnet engines, because of its higher coercive force, but was later abandoned since temperature effects are severe enough to make control of the magnetic field at operating temperature extremely

difficult. While a Cunife shell was fabricated and designated PMG (Fig. 69), the lack of control over the magnetic field caused the design to be dropped as a candidate for use on the 4000-hour test. It was decided to incorporate a Vicalloy shell and to use this engine as a test bed for design improvements.

The new engine made with 0.010-inch thick Vicalloy was designated DGM. Design improvements included were a lightweight, externally-heated stainless steel cathode, a lightweight aluminum anode, aluminum anode bus bar, and a superior accelerator mounting structure to facilitate electrode alignment and to improve the accelerator stability by eliminating torques incurred during assembly. The electrode aperture pattern was identical to that of the DG engine.

5.2 SUPPORTING TESTS

In support of the DGM design a set of magnetic material evaluation tests were run. B-H loop tests were run by placing Vicalloy samples in a pickup coil, the output of which was proportional to the time derivative of the magnetic flux through the sample from an external magnetic field. The output of a large second coil around the sample, wired so as not to link the flux through the sample, was proportional to the time derivative of the magnetic flux in the air. This assembly was placed between the poles of a large electromagnet. From the integrals of the outputs of these two coils, B-H loops were displayed on an oscilloscope. The tests showed the following results:

a. Lot-to-lot variation in residual flux density, B_r, and coercive force, H_c, was within ±5 percent.

b. Dependence of B_r on the direction of material rolling was not significant for the hot-rolled material.

c. Higher H_c and lower B_r was obtained with thinner stock.

d. Heat treatment schedules affected the obtainable values of H_c and B_r but not enough to impair reproducibility.

The effect of elevated temperatures on the residual flux density was also studied. A cylindrical test sample 1.6 inches in diameter and 1.6 inches long with a wall thickness of 0.010 inches was fitted with iron end plates. In this sample the Vicalloy operates at a coercive force of 55.60 oersteds and a flux density nearly equal to the residual flux density.

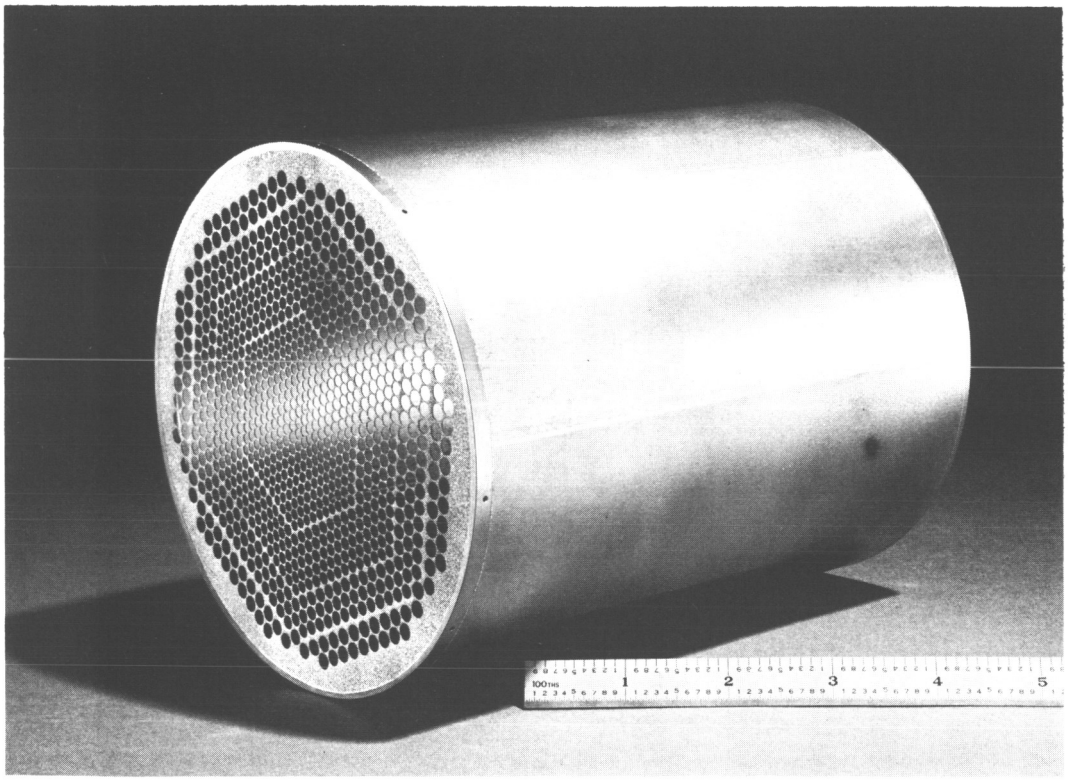

Figure 69. PMG Engine Shell

A spinning coil was inserted through a hole in the side of the sample and the output of this coil provided a signal proportional to the flux in the center of the sample, proportional to the flux in the Vicalloy. This assembly was then placed in a vacuum oven and temperature cycled.

No irreversible loss was apparent up to 330°C and only a small reversible loss was found. The loss of flux density with temperature is shown in Table XXXII. Since earlier permanent magnet engines operated at a temperature of about 200-220°C it should be possible to charge these engines to the desired field strength at room temperature. The material appears to be highly stable and a temperature margin of 100 centigrade degrees exists for the anticipated operating temperatures. Further tests at higher temperatures lead to the following conclusions:

a. Irreversible losses must be stabilized out (at least two cycles to temperature) when operation over 460°C is contemplated.

b. Reversible losses should be corrected for when operation above 300°C is required.

c. Removal of the screen electrode or cathode plate after charging can result in a loss of field strength so the shell should be charged without the end plates to prevent such accidental demagnetization.

TABLE XXXII

REVERSIBLE LOSSES OF VICALLOY AT ELEVATED TEMPERATURES
OPERATING COERCIVE FORCE = 55-60 Oe

Temperature °C	Percentage Loss in B_r
20	0 (reference)
150	0.5
190	1.0
230	2.0
255	3.0
290	5.0
330	8.0

Upon magnetizing the DGM shell it was found that it was possible to reproduce any given field to within 3 percent. Saturation of the shell showed that the magnitude of the required magnetic field was less than 80 percent of the field obtainable. Thus there was an adequate safety margin in the design.

In support of the DGM design, the stainless steel cathode and aluminum anode were tested together on an engine consisting of an old electromagnet engine shell and the prototype DG electrodes. No trouble was encountered in obtaining normal DG performance during startup and operation at thrust.

The last test performed on the permanent magnet engine was vibration testing. Since no specific requirements were available the engine was vibrated in the axial direction and one transverse direction at the arbitrary levels shown in Table XXXIII.

TABLE XXXIII

VIBRATION TEST PROFILE

Direction	Frequency (cps)	Amplitude	Duration (min)
Axial	5-9	1.25 in. p-p	1.5
	9-12	5 g's	0.6
	12-20	0.5 in. p-p	2.8
	20-3000	10 g's	27.2
Transverse	5-9	1.0 in. p-p	1.5
	9-12	5 g's	0.6
	12-19	0.5 in. p-p	2.6
	19-3000	10 g's	28.4

During the vibration testing the engine was observed with a strobe light flashing one-third cycles per second faster than the vibration frequency so that deflections and relative movement of components could be seen in slow motion. The only critical motion seen was the accelerator alternately lifting slightly from the six conical mounting points. The stainless steel spring clips used to hold the accelerator in place were heat treated to develop only about two-thirds their maximum possible hardness. Heat treating to maximum hardness or increasing the thickness of the clip material would eliminate this type of accelerator motion.

After the test the engine assembly and components were examined and no damage was found. Transverse alignment was unchanged but the electrode gap had changed from 0.055 inch to 0.053 inch. Careful examination of the small holes in the accelerator ears, into which the conical mounting points are held by the spring clips, showed the sharp corners had been flattened down slightly allowing the gap to decrease. This problem can be eliminated simply by increasing the contact area between the accelerator and mounting points by countersinking the holes slightly.

Figures 70 and 71 show the complete engine. As shown, the weight is 1.6 pounds and the design operating level the same as that of the DG-1 and DG-2 engines with the exception of magnet power.

5.3 SUMMARY

A permanent magnet engine designed to operate at the DG levels and weighing only 1.6 pounds was designed and built. The permanent magnet material used for the shell was tested, and it was found that good reproducibility of the desired magnetic field can be obtained. No significant variation in field strength can be expected at probable operating temperatures. The completed engine was subjected to vibration testing which showed that only minor design changes are needed.

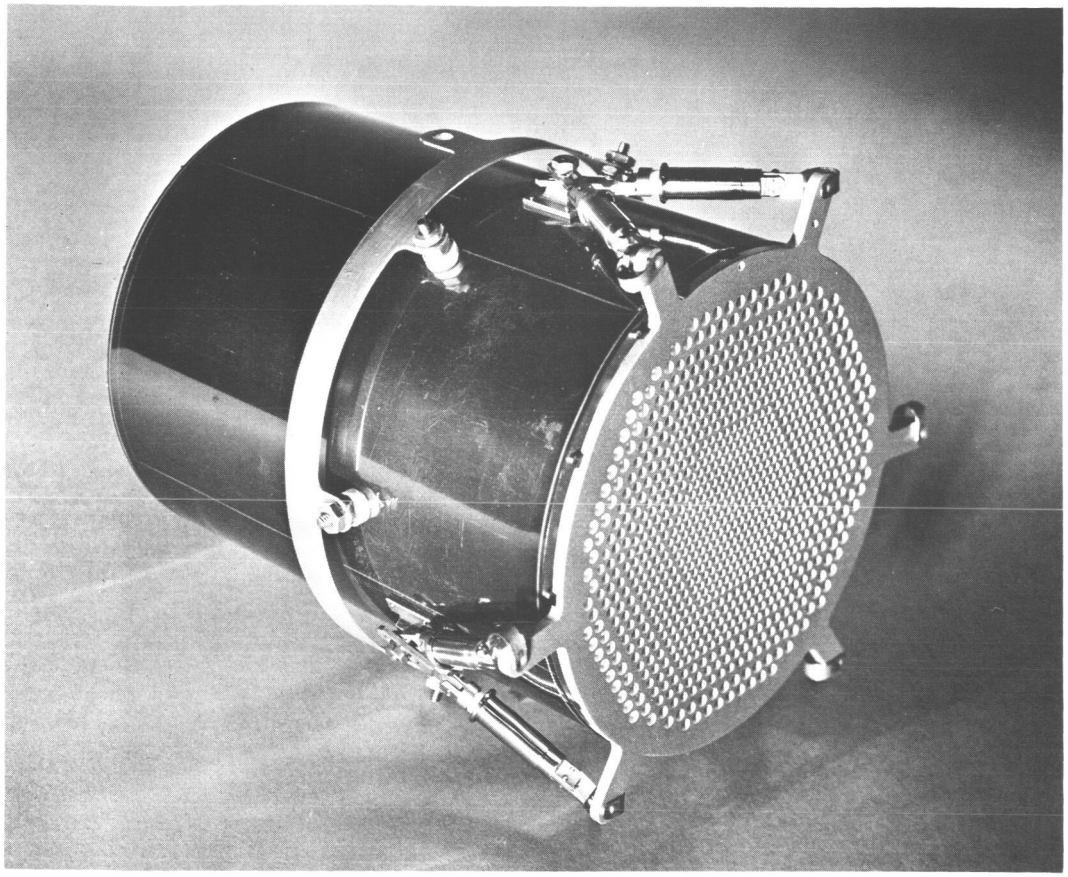

Figure 70. DGM Engine

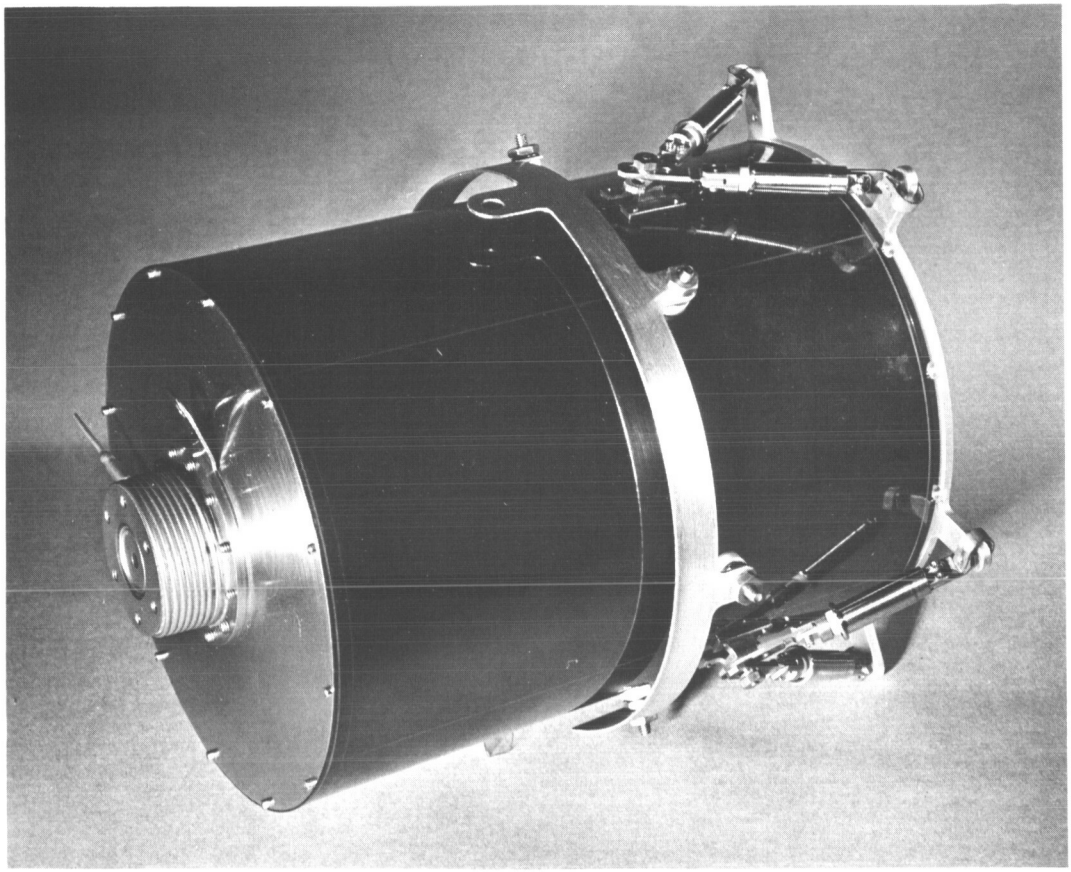

Figure 71. DGM Engine

SECTION 6

AC DISCHARGE ENGINE

6.1 BACKGROUND

This portion of the program was devoted to reevaluation and improvement of an engine which operates in a self-rectifying discharge mode. This concept was initially developed and tested by Electro-Optical Systems, Inc. in 1964. It is based on the fact that a probe immersed in a plasma forms a "rectifying" contact with the plasma; the electron current drawn when the probe is biased positive can exceed, by orders of magnitude, the ion current drawn when the probe is negative.

The engine tested in 1964 was a model DE engine modified by replacing the cylindrical anode with an anode comprised of 18 parallel segments. These segments were driven from a three-phase, full-wave, star-connected transformer with the common point connected to the engine cathode. Alternate segments functioned as the anode when they were positive with respect to the plasma. This maintained the discharge and a continuous ion beam was extracted. Engine performance was not measurably different from that of the DE engine operated with a dc discharge.

The obvious advantage of such a system, and the impetus for its initial development, is the elimination of the high current rectifiers and their losses from the discharge power supply. Disadvantages include increased engine complexity, sputtering of the negative-biased anodes if a high voltage discharge is used, and some power loss to the negatively biased anodes. The engine structure for this type of operation can easily be realized, however. Sputtering was expected to be negligible at the peak negative voltage of about 15 volts. The reverse current was expected to be about two percent of the forward current. A reevaluation was necessary since the efficiency of the basic engine had been increased so significantly during 1965 through incorporation of a gradient in the magnetic field.

6.2 ENGINE DESIGN

The new ac discharge engine was based on the DG design and designated DGA. All components were identical to those of the DG-1 and DG-2 engines with the exception of the engine shell and anode assembly. Twelve anode

segments were used; alternate segments were connected together to form two interleaved sections. The DGA shell and anode assembly are shown in Fig. 72. The anode segments were supported by two insulators each and were connected together outside the discharge chamber as shown. To provide for the additional insulators, a second feedthrough band was added to the chamber. This divided the magnet winding into three coils instead of two as used on the DG engines. The shape of the magnetic field achieved was similar to that of the DF and DG engines as shown in Fig. 73.

The electrical connections between the inverter output transformer and the engine are shown in Fig. 74. A high frequency wattmeter was used to measure the power delivered to the discharge chamber. This allowed a direct comparison between discharge efficiencies in the ac mode and when the anodes were connected together and operated in the dc mode.

The inverter used was an oscillator-power amplifier combination. Separate power supplies for the oscillator and power amplifier provided independent control of the frequency and output voltage. Test frequencies of 1000, 2000, 4000, and 8000 cycles per second were used. Because of the wide frequency range and broad output voltage and power capability, the inverter was not particularly efficient at all levels; efficiency varied from 70 to 95 percent.

6.3 ENGINE PERFORMANCE

The performance of the DGA engine was first mapped over the range of specific impulse from 2000 to 8000 seconds at the four test frequencies and dc. The reduced data are presented in Table XXXIV. No filter was used while these data were obtained. The overall engine efficiency and power-to-thrust ratio are plotted versus specific impulse in Figs. 75 and 76, respectively, for both ac and dc operation. The ac data points were plotted to show typical performance independent of frequency. The solid curve shown in Figs. 75 and 76 represent the performance obtained with the DG-1 and DG-2 engines prior to the two life tests. No significant difference in performance was observed.

Figure 77 shows the mass utilization efficiency plotted as a function of discharge energy per ion for all test frequencies at four operating levels. The straight line shows the slope of the mass efficiency-source energy tradeoff for constant overall engine efficiency. Two points on this line will yield the same overall engine performance. As can be seen, most of the separations between points were on this slope and did not affect overall operation. Those separations perpendicular to this line were small and inconsistent to the extent that they were probably due to random error. It was concluded that the discharge efficiency was independent of frequency over the range tested.

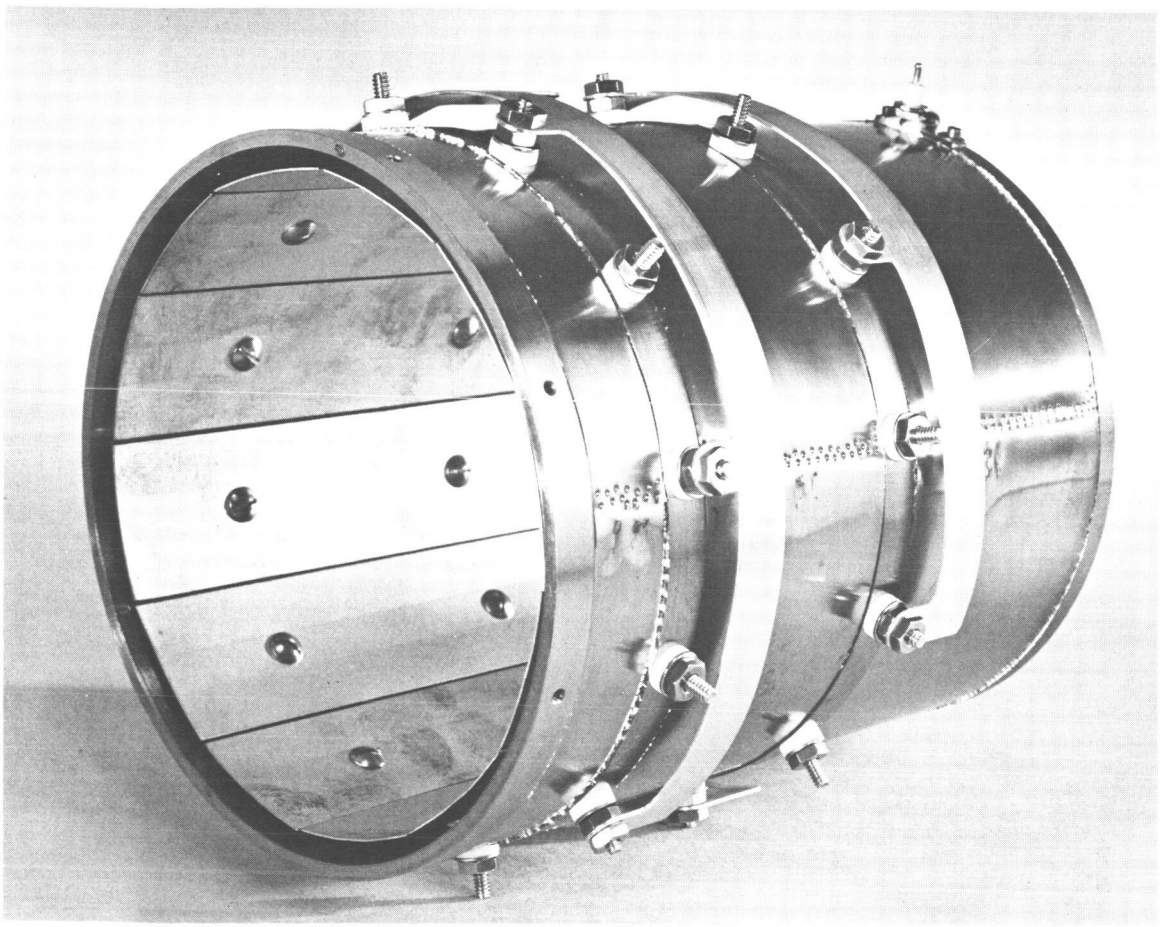

Figure 72. DGA Engine Shell and Anode Assembly

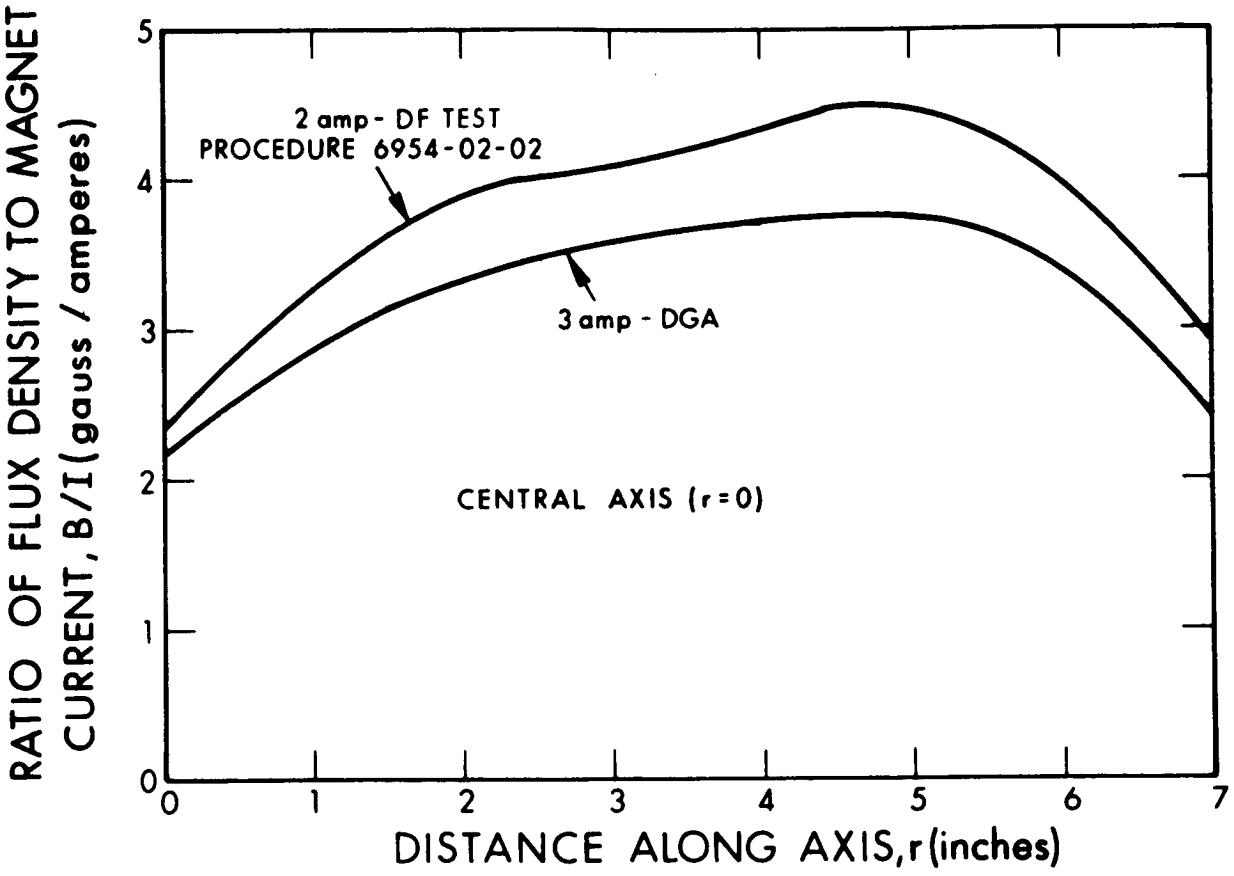

Figure 73. Magnetic Field Plot for the DGA Engine

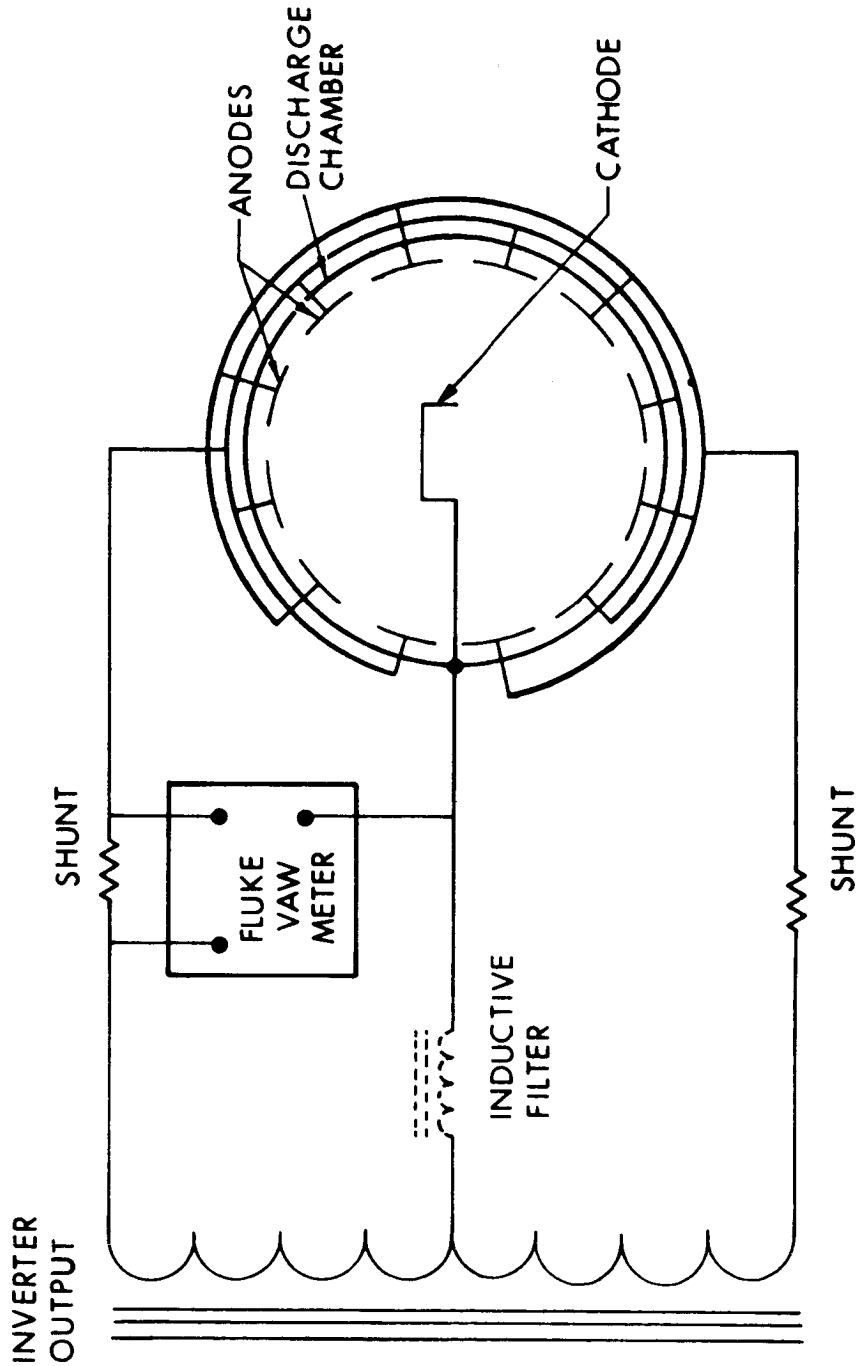

Figure 74. Ac Discharge Engine - Inverter Output Connection

TABLE XXXIV

AC DISCHARGE ENGINE PERFORMANCE

Point	Frequency (kHz)	Positive High Voltage, V_+ (kV)	Negative High Voltage, V_- (kV)	Beam Current, I_B (amp)	Negative HV Current, I_- (mA)	Magnet Voltage, V_M (volt)	Magnet Current, I_M (amp)	Beam Power, P_B (kW)	Drain Power, P_D (kW)	Arc Power, P_A (kW)	Magnet Power, P_M (kW)	Total Engine Power, P_T (kW)	Thrust, T (mlb)	Engine Power-to-Thrust Ratio P_T/T (kW/lb)	Engine Mass Efficiency, η_M (%)	Engine Power Efficiency, η_P (%)	Overall Engine Efficiency, η_E (%)	Engine Specific Impulse, Isp (sec)	Source Energy per Ion P_B/I_B (keV/ion)
1	1.0	0.345	1.68	0.241	9.5	6.7	2.37	0.083	0.019	0.090	0.016	0.208	1.7	122	88.3	40.0	35.3	2020	373
2	2.0	0.345	1.68	0.241	9.1	6.7	2.37	0.083	0.018	0.084	0.016	0.201	1.7	118	87.7	41.3	36.2	2000	348
3	4.0	0.345	1.63	0.244	9.5	6.7	2.37	0.084	0.019	0.084	0.016	0.203	1.7	119	85.6	41.5	35.5	1950	344
4	8.0	0.345	1.66	0.245	10.5	6.7	2.37	0.085	0.021	0.084	0.016	0.206	1.7	121	85.5	41.2	35.3	1950	352
5	1.0	0.525	1.60	0.249	5.0	6.7	2.37	0.131	0.011	0.086	0.016	0.244	2.2	111	91.6	53.7	49.3	2580	345
6	2.0	0.540	1.55	0.262	5.8	6.4	2.33	0.141	0.012	0.094	0.016	0.263	2.3	114	90.1	53.6	48.4	2565	358
7	4.0	0.545	1.51	0.259	5.4	6.4	2.33	0.141	0.011	0.090	0.016	0.258	2.3	112	90.0	54.6	49.6	2600	347
8	8.0	0.545	1.49	0.250	5.4	6.6	2.33	0.136	0.011	0.090	0.015	0.252	2.2	115	90.6	54.0	49.0	2595	360
9	1.0	0.725	1.59	0.315	5.4	6.6	2.33	0.228	0.013	0.108	0.016	0.365	3.2	114	92.2	62.5	57.5	3040	343
10	2.0	0.710	1.65	0.339	6.0	7.0	2.33	0.240	0.014	0.112	0.016	0.382	3.4	112	92.4	62.9	58.0	3020	330
11	4.0	0.750	1.70	0.340	5.8	7.0	2.33	0.255	0.014	0.122	0.016	0.407	3.5	116	93.2	62.9	58.4	3125	358
12	8.0	0.745	1.62	0.350	6.0	7.0	2.33	0.261	0.014	0.114	0.016	0.405	3.6	113	92.4	64.5	59.5	3090	325
13	1.0	0.950	1.52	0.358	5.5	6.7	2.35	0.340	0.014	0.118	0.016	0.488	4.1	119	93.0	69.7	64.8	3515	330
14	2.0	0.950	1.68	0.353	5.5	6.7	2.35	0.337	0.014	0.120	0.016	0.487	4.1	119	94.0	69.2	65.0	3545	340
15	4.0	0.970	1.50	0.347	5.2	6.7	2.35	0.336	0.013	0.116	0.016	0.481	4.1	118	93.4	69.8	65.2	3560	334
16	8.0	0.960	1.52	0.341	5.3	6.7	2.36	0.328	0.013	0.114	0.016	0.471	4.0	118	93.4	69.7	65.0	3540	334

TABLE XXXIV

AC DISCHARGE ENGINE PERFORMANCE (contd)

Point	f (kHz)	V_+ (kV)	V_- (kV)	I_B (amp)	I_- (mA)	V_M (volt)	I_M (amp)	P_B (kW)	P_D (kW)	P_A (kW)	P_M (kW)	P_T (kW)	T(mlb)	P_T/T (kW/lb)	η_M (%)	η_P (%)	η_E (%)	I_{sp} (sec)	P_A/I_B (keV/ion)
17	1.0	1.20	1.62	0.365	5.5	6.7	2.35	0.438	0.013	0.122	0.016	0.589	4.8	123	93.7	74.5	69.8	3980	334
18	2.0	1.2	1.60	0.370	5.5	6.7	2.35	0.444	0.015	0.122	0.016	0.597	4.8	124	93.5	74.4	69.5	3970	330
19	4.0	1.2	1.68	0.375	5.6	6.7	2.36	0.450	0.016	0.124	0.016	0.606	4.9	124	93.5	74.2	69.4	3970	330
20	8.0	1.2	1.57	0.375	6.0	6.7	2.36	0.450	0.017	0.124	0.016	0.607	4.9	124	93.5	74.2	69.4	3970	330
21	1.0	1.53	1.10	0.386	5.0	6.7	2.37	0.588	0.013	0.130	0.016	0.747	5.6	133	93.7	78.8	73.8	4495	337
22	2.0	1.53	1.18	0.384	5.0	6.75	2.37	0.588	0.014	0.128	0.016	0.746	5.6	133	94.0	78.8	74.0	4500	334
23	4.0	1.53	1.13	0.380	5.0	6.7	2.35	0.582	0.013	0.130	0.016	0.741	5.5	135	94.4	78.7	74.2	4520	342
24	8.0	1.53	1.17	0.379	5.0	6.7	2.35	0.580	0.014	0.130	0.016	0.740	5.5	135	94.0	78.4	73.6	4500	343
25	1.0	1.90	0.98	0.406	5.0	6.75	2.37	0.772	0.014	0.134	0.016	0.936	6.6	139	93.9	82.5	77.4	5010	330
26	2.0	1.90	0.98	0.408	5.0	6.75	2.37	0.776	0.014	0.136	0.016	0.942	6.7	140	94.1	82.4	77.6	5025	333
27	4.0	1.90	0.90	0.412	5.1	6.75	2.37	0.783	0.014	0.134	0.016	0.947	6.5	139	93.8	82.7	77.6	5005	325
28	8.0	1.90	0.94	0.415	5.2	6.75	2.37	0.789	0.015	0.136	0.016	0.956	6.8	140	93.6	82.5	77.2	5000	328
29	1.0	2.75	0.275	0.432	5.2	7.6	2.63	1.188	0.015	0.146	0.020	1.369	8.5	161	93.1	86.9	80.9	6000	315
30	2.0	2.75	0.280	0.446	5.1	7.6	2.63	1.228	0.015	0.150	0.020	1.413	8.8	161	93.0	86.8	80.8	5980	336
31	4.0	2.75	0.260	0.418	4.9	7.6	2.63	1.150	0.015	0.148	0.020	1.333	8.3	161	93.7	86.2	80.8	6020	354
32	8.0	2.75	0.230	0.415	5.0	7.6	2.63	1.132	0.015	0.142	0.020	1.309	8.2	160	93.6	86.8	81.2	6020	342
33	1.0	3.25	0.20	0.439	6.3	6.9	2.44	1.428	0.022	0.150	0.017	1.617	9.4	172	93.7	88.3	82.7	6550	342
34	2.0	3.25	0.20	0.440	6.1	7.0	2.43	1.430	0.021	0.150	0.017	1.628	9.4	173	94.0	88.9	83.6	6565	341
35	4.0	3.25	0.20	0.439	6.0	7.0	2.43	1.428	0.021	0.150	0.017	1.618	9.4	172	93.7	88.6	83.0	6560	342

TABLE XXXIV

AC DISCHARGE ENGINE PERFORMANCE (contd)

Point	f (kHz)	V_+ (kV)	V_- (kV)	I_B (amp)	I_- (mA)	V_M (volt)	I_M (amp)	P_B (kW)	P_D (kW)	P_A (kW)	P_M (kW)	P_T (kW)	T (mlb)	P_T/T (kW/lb)	η_M (%)	η_P (%)	η_E (%)	I_{sp} (sec)	P_A/I_B (keV/ion)
36	8.0	3.25	0.20	0.439	5.6	7.0	2.43	1.428	0.019	0.148	0.017	1.612	9.4	172	93.7	88.4	82.8	6550	338
37	1.0	3.70	0.20	0.445	7.2	7.3	2.42	1.649	0.028	0.156	0.018	1.851	10.2	182	94.9	89.2	84.5	7070	350
38	2.0	3.71	0.020	0.440	7.0	7.2	2.41	1.631	0.027	0.144	0.018	1.820	10.1	180	94.9	89.7	85.1	7080	328
39	4.0	3.70	0.20	0.465	6.9	7.2	2.42	1.720	0.027	0.144	0.018	1.909	10.6	180	95.4	90.1	86.0	7110	309
40	8.0	3.71	0.20	0.450	7.1	7.2	2.42	1.670	0.027	0.145	0.018	1.860	10.3	181	94.8	89.8	85.1	7080	333
41	1.0	4.22	0.20	0.445	10.2	7.2	2.42	1.880	0.045	0.140	0.018	2.083	10.9	191	95.3	90.2	86.1	7590	315
42	2.0	4.22	0.20	0.443	10.5	7.2	2.42	1.870	0.046	0.142	0.018	2.076	10.8	192	95.2	90.2	85.7	7580	380
43	4.0	4.20	0.20	0.464	9.5	7.2	2.42	1.949	0.042	0.140	0.018	2.149	11.4	188	95.1	90.6	86.1	7550	302
44	8.0	4.20	0.20	0.458	9.8	7.2	2.42	1.923	0.043	0.140	0.018	2.124	11.2	190	95.5	90.7	86.5	7580	306
1	DC	0.52	1.60	0.270	5.5	6.8	2.3	0.140	0.012	0.087	0.016	0.255	2.3	111	89.5	54.9	48.5	2500	354
2	DC	0.80	1.91	0.340	7.0	7.3	2.50	0.272	0.019	0.114	0.018	0.423	3.62	117	88.0	64.3	56.6	3050	335
3	DC	1.00	1.47	0.295	4.5	6.8	2.3	0.295	0.011	0.104	0.016	0.426	3.5	122	93.0	69.3	64.4	3600	352
4	DC	1.32	1.69	0.428	7.0	7.4	2.51	0.565	0.021	0.158	0.018	0.762	5.85	130	93.6	74.1	69.4	4170	369
5	DC	1.62	1.40	0.430	6.1	7.4	2.51	0.696	0.013	0.158	0.018	0.885	6.5	136	94.1	78.7	74.0	4650	378
6	DC	2.0	1.0	0.430	5.5	7.4	2.51	0.860	0.016	0.145	0.018	1.039	7.2	144	93.9	82.7	77.6	5140	337
7	DC	2.40	0.75	0.445	6.2	7.4	2.5	1.070	0.019	0.152	0.018	1.259	8.2	153	93.2	85.0	79.2	5600	341
8	DC	2.62	0.20	0.440	5.0	6.0	2.1	1.152	0.015	0.150	0.013	1.330	8.5	156	93.6	86.7	81.1	5875	340
9	DC	3.20	0.20	0.450	6.0	7.2	2.48	1.440	0.020	0.153	0.018	1.631	9.7	168	95.4	88.5	84.4	6610	340
10	DC	4.22	0.20	0.445	11.0	6.0	2.1	1.880	0.013	0.141	0.013	2.083	10.8	194	95.2	90.1	85.8	7580	317

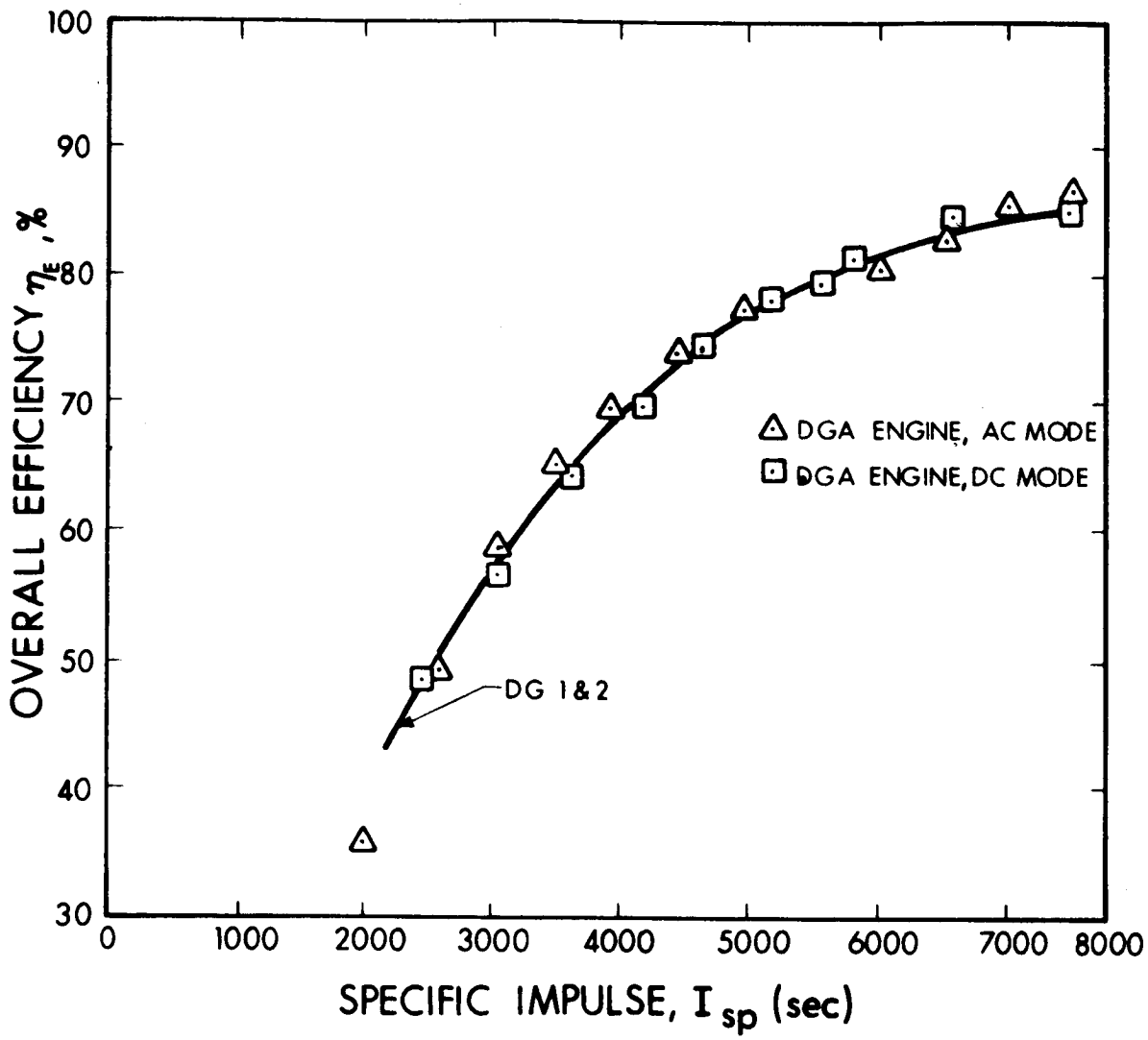

Figure 75. Overall Efficiency versus Specific Impulse, DGA

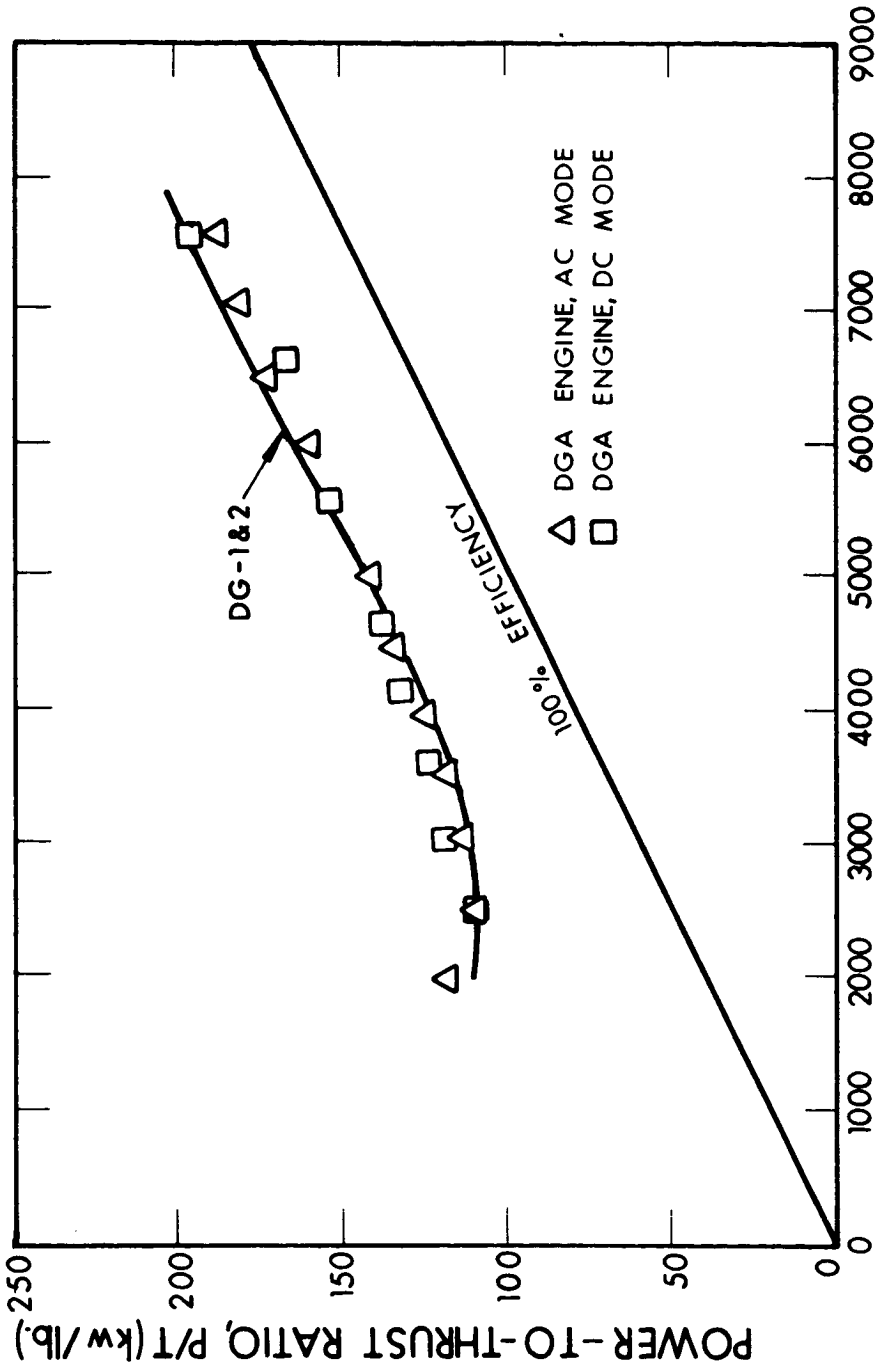

Figure 76. Power-to-Thrust Ratio versus Specific Impulse - DGA

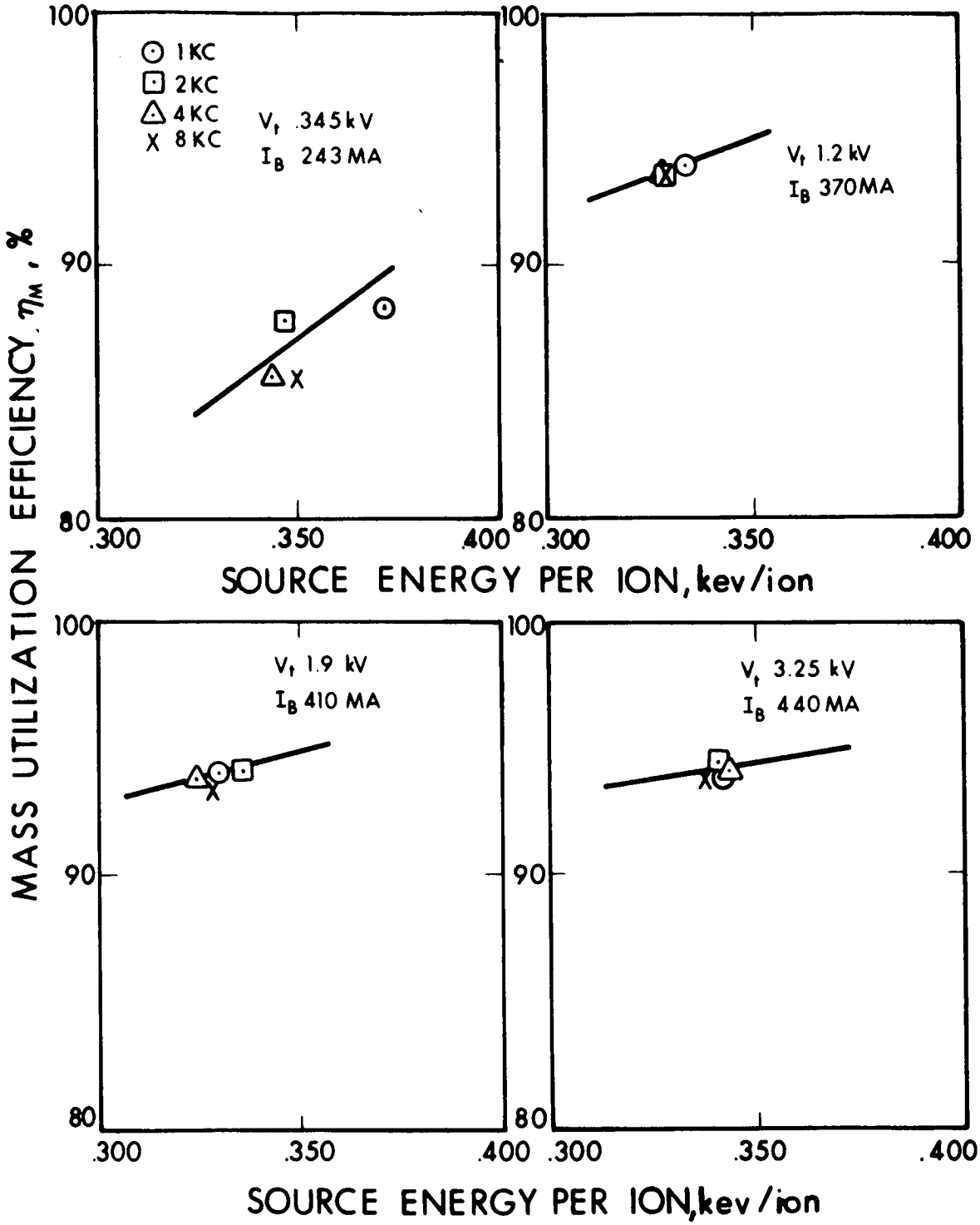

Figure 77. Mass Efficiency versus Discharge Energy Expenditure per Ion for DGA Engine (line shows slope of constant engine efficiency)

No anode weight loss was found at the conclusion of these tests, verifying the expectation that the bombarding ion energies would be below the sputtering threshold.

The reverse anode currents during the negative half cycle were measured using an oscilloscope and found to be less than 3 percent of the forward currents. No significant transient effects were observable on the beam, discharge, and accelerator drain currents using an oscilloscope.

Inductive filtering was then tested to determine whether any improvement in performance could be realized. Three chokes, 100, 350, and 1000 microhenrys, were placed in series with the cathode return line to the inverter as shown in Fig. 74. A bypass switch was connected to each choke to allow adjustment of the total inductance. Data obtained at low and high frequencies are shown in Table XXXV. For each frequency the high voltages, beam current, and discharge power were held constant. There was no apparent effect at 1000 cycles per second but a slight reduction in drain current with inductance was apparent at 8000 cycles per second where transients should have eight times more effect. The slight effect found would not justify the use of inductive filtering.

One significant difference in engine response was noticed; it was difficult to start the discharge. The physical symmetry of the positive and negative anode segments resulted in cancellation of the electric field within the discharge chamber. In addition, the high voltage at no load normally provided for starting in the dc discharge mode was not present. Cathode temperatures of 450 to 500°C were required to start the discharge as opposed to 300 to 350°C for the DG-1 and DG-2 engines. The solution developed for this problem is described in the following section.

6.4 DISCHARGE STARTING

The electric field requirement for starting was defined from experience as that due to the normal dc anode at a potential of about 25 volts, maintained just long enough for initiation of the discharge. It appeared that this requirement might be met on a transient basis rather than continuously. A circuit, shown in Fig. 78, was constructed to provide a positive transient for both anodes once each cycle. This system required the use of an inductive filter but did not stress the inverter output transistors. The need for inductive filtering will be shown in Subsection 6.5. With this circuit, the discharge started smoothly at cathode temperatures of 320°C.

The start-run switch was subsequently interlocked with the cathode turn-off. The "run" position of the switch was eliminated and a base-to-emitter resistor was added to hold the transistor off during normal operation.

TABLE XXXV

EFFECT OF INDUCTIVE FILTERING

Frequency (cycles per second)	Inductance (microhenry)	Drain Current (milliampere)
1000	0	4.4
1000	100	4.9
1000	350	4.3
1000	1000	4.4
8000	0	4.9
8000	100	4.5
8000	350	4.4
8000	1000	4.4

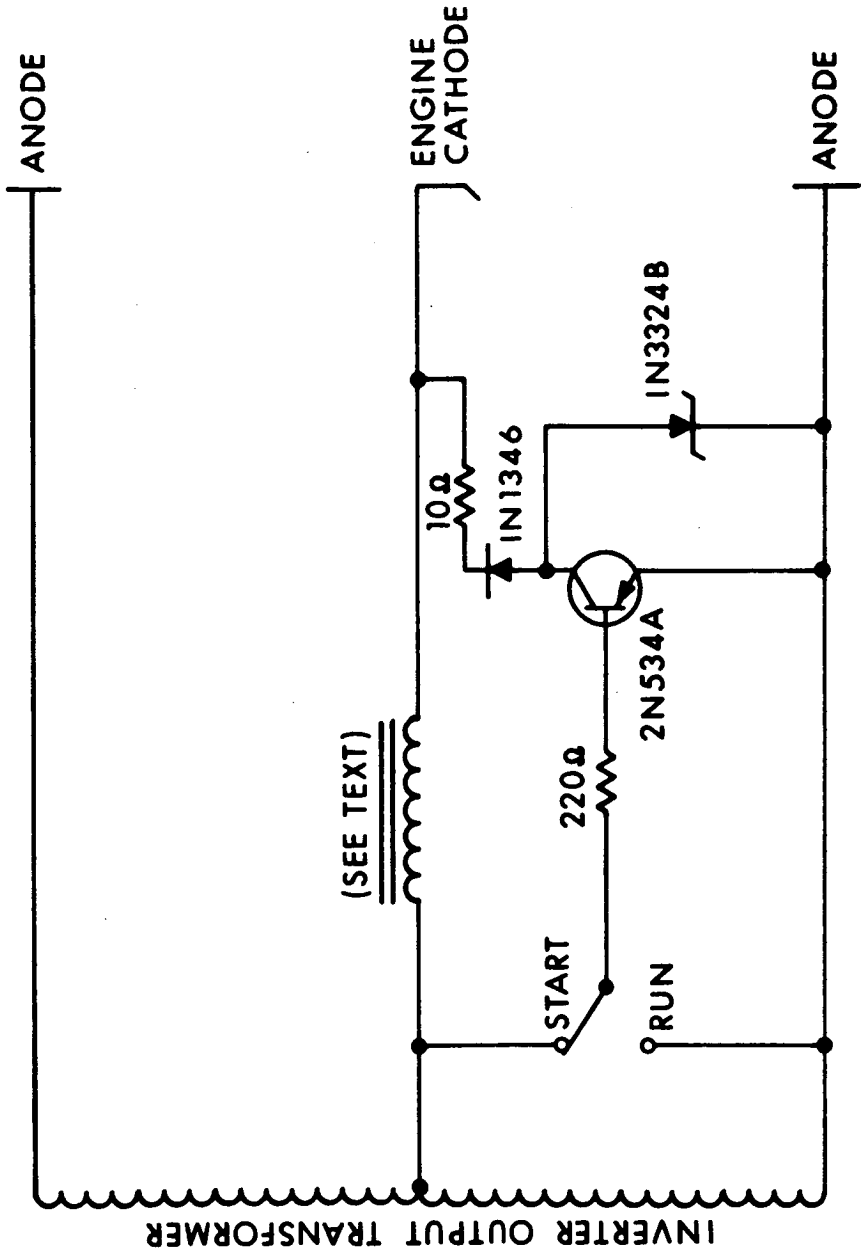

Figure 78. Starting Circuit for the DGA Engine

A high-impedance cathode heater was built for operation directly from the inverter output. Both the cathode heater and the starting circuit were disconnected when the discharge current exceeded 10 amperes. A completely automatic start using this system will be described in Subsection 6.6.

6.5 DISCHARGE POWER CONTROL

For laboratory operation the dc input voltage to the inverter power amplifier was varied to control the inverter output voltage. This could not easily be implemented in a flight system, however, because it would require an additional high power regulator. A more efficient method would be to use pulse-width modulation; this approach was pursued.

A magnetic amplifier was installed between the oscillator and power amplifier to control the pulse width. The inductive filter was then used to smooth the discharge power. Figure 79 shows an electrical schematic of the inverter configuration used.

Data were taken to verify the need for inductive filtering. Performance was checked for different values of inductance and pulse width while the high voltages and beam current were held constant. The discharge power was held constant by increasing the power amplifier input voltage as the pulse width was reduced. The data, shown in Table XXXVI, clearly demonstrate the need for and effectiveness of the inductive filtering.

Engine efficiency did not change when operated in this manner so this method of power control was considered valid as well as simple. Attention was then turned to the one most important remaining problem, that of automatic discharge power control.

6.6 AUTOMATIC CONTROL

A number of different discharge power supply output characteristics had been considered to maintain optimum performance over long periods of time. While attributable in part to environmental effects, discharge characteristics for the DG-1 and DG-2 engines varied throughout the two life tests. Voltage, current, and power varied and adjustments were made manually to the discharge supply. Some automatic control would obviously be required. Such a control would ideally control the discharge on the basis of overall engine performance.

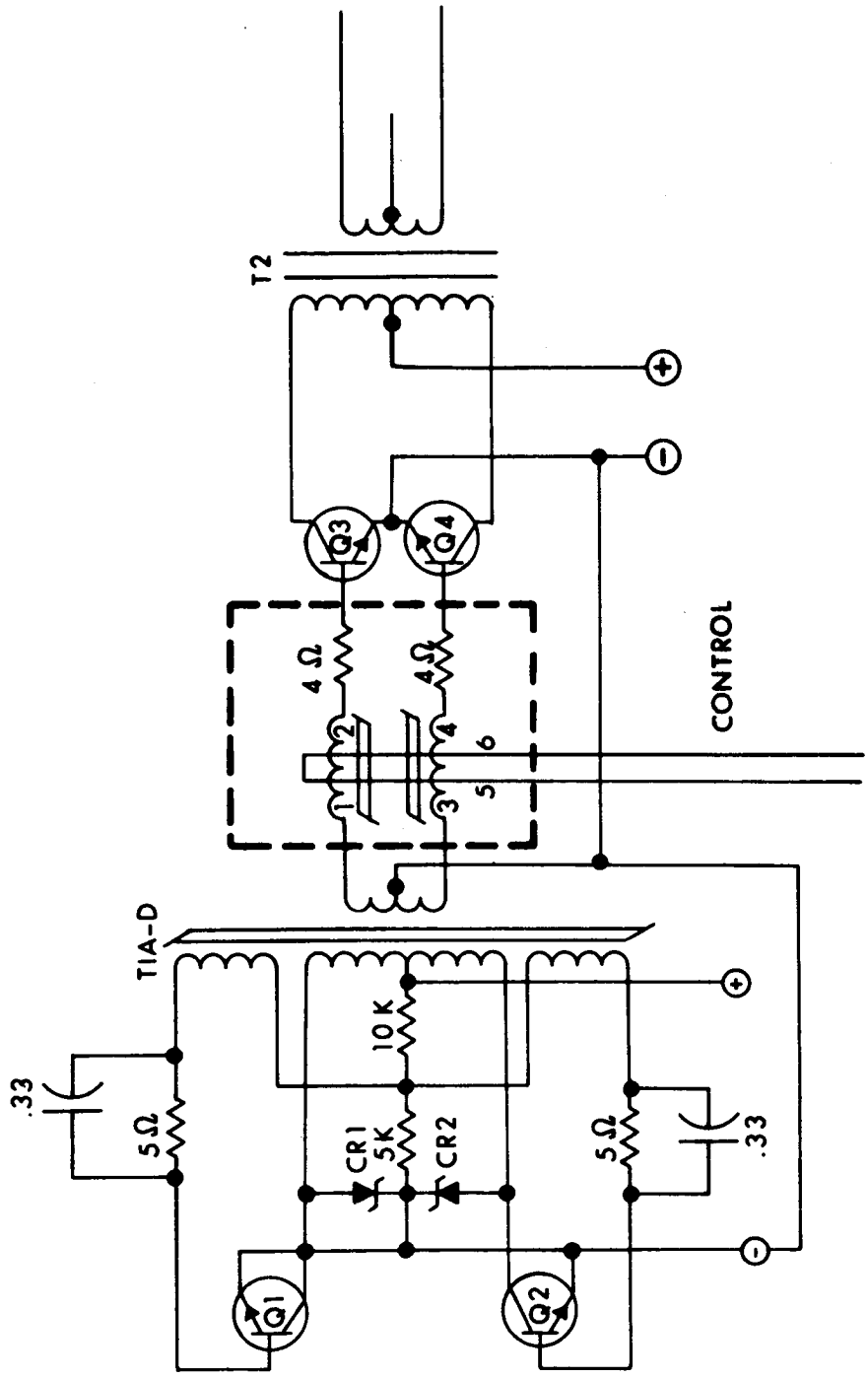

Figure 79. Inverter Schematic

TABLE XXXVI

EFFECT OF INDUCTIVE FILTERING ON
PULSE-WIDTH MODULATED OPERATION

Frequency (cycles per second)	Inductance (microhenry)	Pulse Width (percent of 1/2 cycle)	Drain Current (milliampere)
2000	0	100	5.3
2000	0	50	13.0
2000	100	100	4.3
2000	100	50	5.0
8000	0	100	4.7
8000	0	50	6.0
8000	100	100	4.5
8000	100	50	4.5

Two characteristics which guided manual adjustments during life testing are shown in Figs. 80 and 81. By varying the discharge power slightly, it was possible to determine where on these characteristics the engine was operating. The discharge power was then adjusted for minimum drains and/or the knee of the beam versus discharge power curve. Validity of these adjustments was verified by performance mapping the DG-2 engine at 1000-hour intervals during the first half of the 8200-hour test. The accelerator drain current increase at low powers is due to increased neutral efflux resulting in increased charge exchange in the accelerating region. The drain increase at high powers is apparently due to discharge instabilities; the drain current is not steady in this region of operation. The characteristic of Fig. 81 shows that the beam current stops increasing when the mass utilization approaches 100 percent.

Dynamic measurements of these characteristics were made to determine whether an automatic variation of discharge power could generate a signal in the drain current or beam current sufficient to identify the operating condition. (Static measurements could not be used since the drain characteristic is double valued and the beam current is regulated by the feedrate control loop.) An oscillator was connected to the pulse width control input and a lock-in amplifier was used to measure the signal resulting in the drain and beam currents. No signal could be found in the drain current but a small signal was detected in the beam current. A synchronous detector was built using laboratory operational amplifiers and a synchronizing system was assembled with reed relays. With this detector, stronger signals were obtainable so a feedback control loop was synthesized.

This feedback loop was designed to measure the 8 cycles per second ripple on the beam current resulting from an 8 cycles per second pulse-width modulation superimposed on the pulse-width modulation used to adjust the discharge power. If the signal was larger than some reference value the discharge power would be increased and vice versa. In this way the engine would be operated at the knee of the beam current versus discharge power curve which is the point of maximum efficiency for given high voltages and flow rate.

Figure 82 shows a block diagram of this control loop. By inverting the signal each half cycle and integrating over a full cycle, both high and low frequency noise is integrated out and only the integral of the desired signal appears at the output of the integrator at the end of each cycle. By simultaneously integrating a dc reference, only an error will appear at the output. At the end of each cycle this error is added to a holding circuit which holds the control pulse width during the following integration cycle. The modulation signal or "dithering" signal from the clock is added at the magamp.

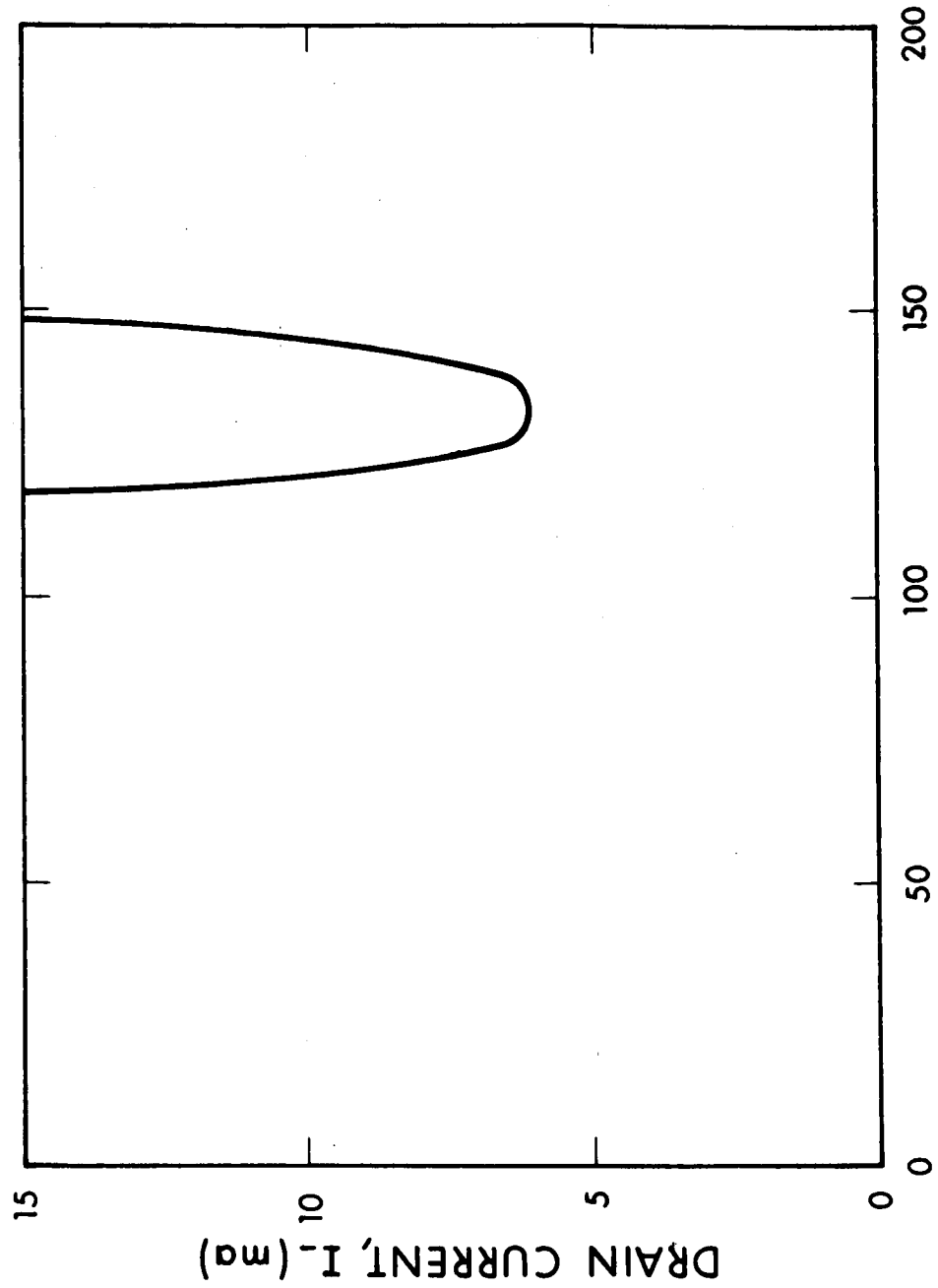

Figure 80. Typical Drain Current Characteristics

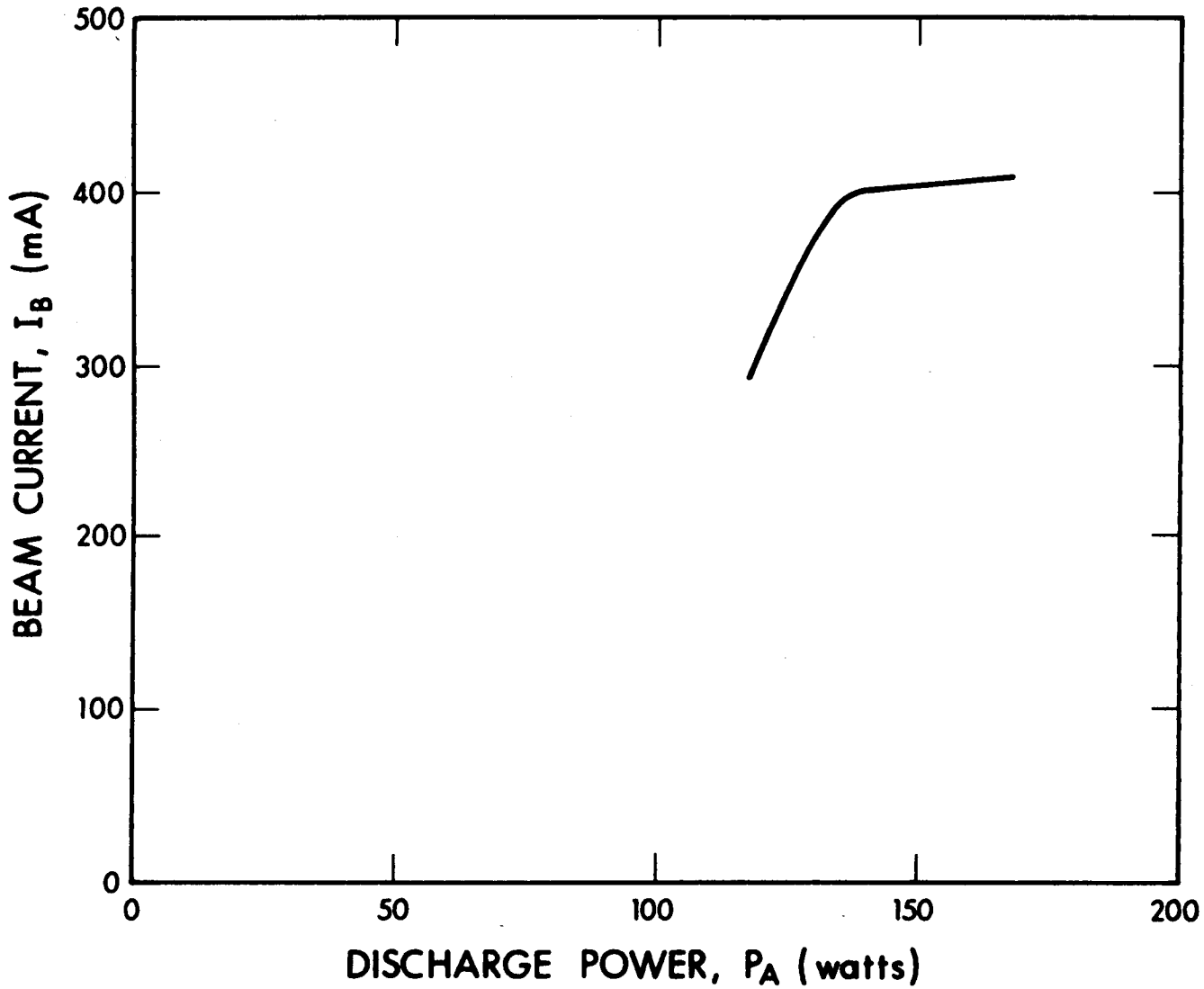

Figure 81. Typical Beam Current versus Discharge Power Characteristics with Constant Flow Rate

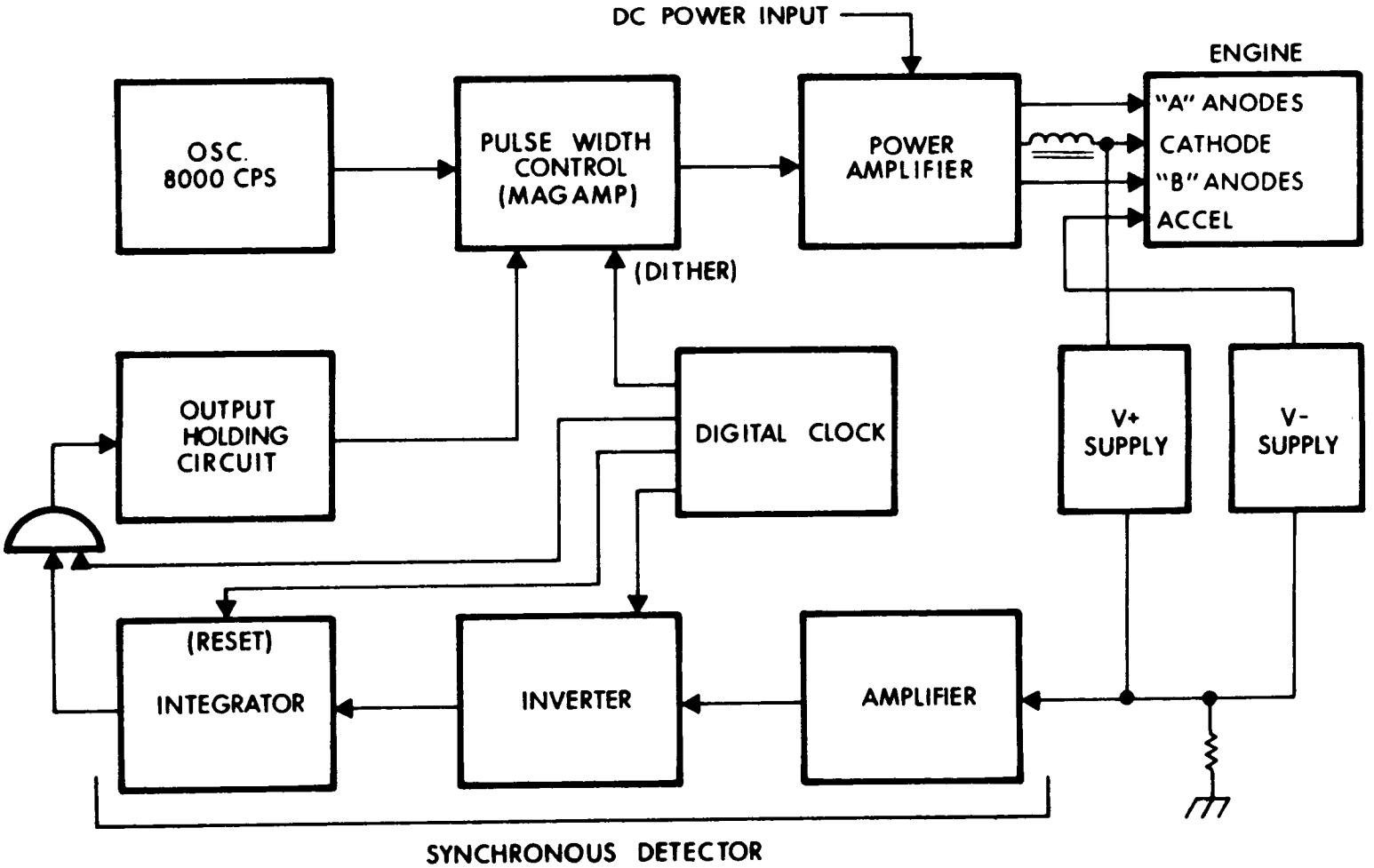

Figure 82. Block Diagram of Automatic Discharge Power Control System for the AC Discharge Engine

This system was connected to the engine after steady-state operation was achieved and data were taken as the reference was adjusted. The data from this test are shown in Fig. 83. Coherent data were obtained as shown, indicating successful control. Wide fluctuations in power to the vaporizer were observed due to regulation by the beam control loop; however, the flow rate did not appear to be significantly affected. A reasonably broad range of reference values could be used which indicated that the knee of the beam current versus discharge power curve was adequately defined. The control loop was stable at steady state but could not handle step-function perturbations. The control loop circuitry was then upgraded for further tests.

The relay clock was replaced with an integrated circuit ripple counter and appropriate logic gates. Diode-transistor logic circuits were used. The schematic for the new digital clock is shown in Fig. 84. The manual switches shown were used to adjust the phase angle between the modulation signal and the synchronous detector. By sending both set and reset signals to the modulation generating flip flop, synchronism is achieved within one half cycle and sense (±) is maintained. Power input to the clock was +5 volts dc.

Figure 85 shows a schematic of the synchronous detector and holding circuitry used to replace the first version. The operational amplifiers used were Motorola MC 1531G integrated circuits operated from ±5 volts dc. The input amplifier was tuned to aid in rejecting the large 120 cycles per second signal imposed on the beam current by the laboratory high voltage supplies and to reduce sensitivity to slow exponentially decaying transients which did not integrate to zero. The output holding circuit was designed to add one tenth of the error signal to the output each cycle. This reduced the effect of spurious error signals. Switching for the synchronous inverter, integrator reset, and output transfer functions was accomplished with N-channel junction, field-effect transistors. The gates were connected through a 10-megohm resistor to +5 or -15 volts dc to turn the transistors on or off.

A 20-volt power supply with a bleeder resistor and two 5-volt zener diodes provided the necessary voltages to run the control system. Approximately 6 watts of power was drawn from the supply, over half of which was dissipated by the bleeder and zeners.

The interlock shown in Fig. 85 was closed whenever the beam current fell below 200 milliamperes and opened above 300 milliamperes. This prevented complete turn-off of the discharge power during start-up when the slope of the beam current versus discharge power curve is very low and the control loop would always try to reduce the discharge power.

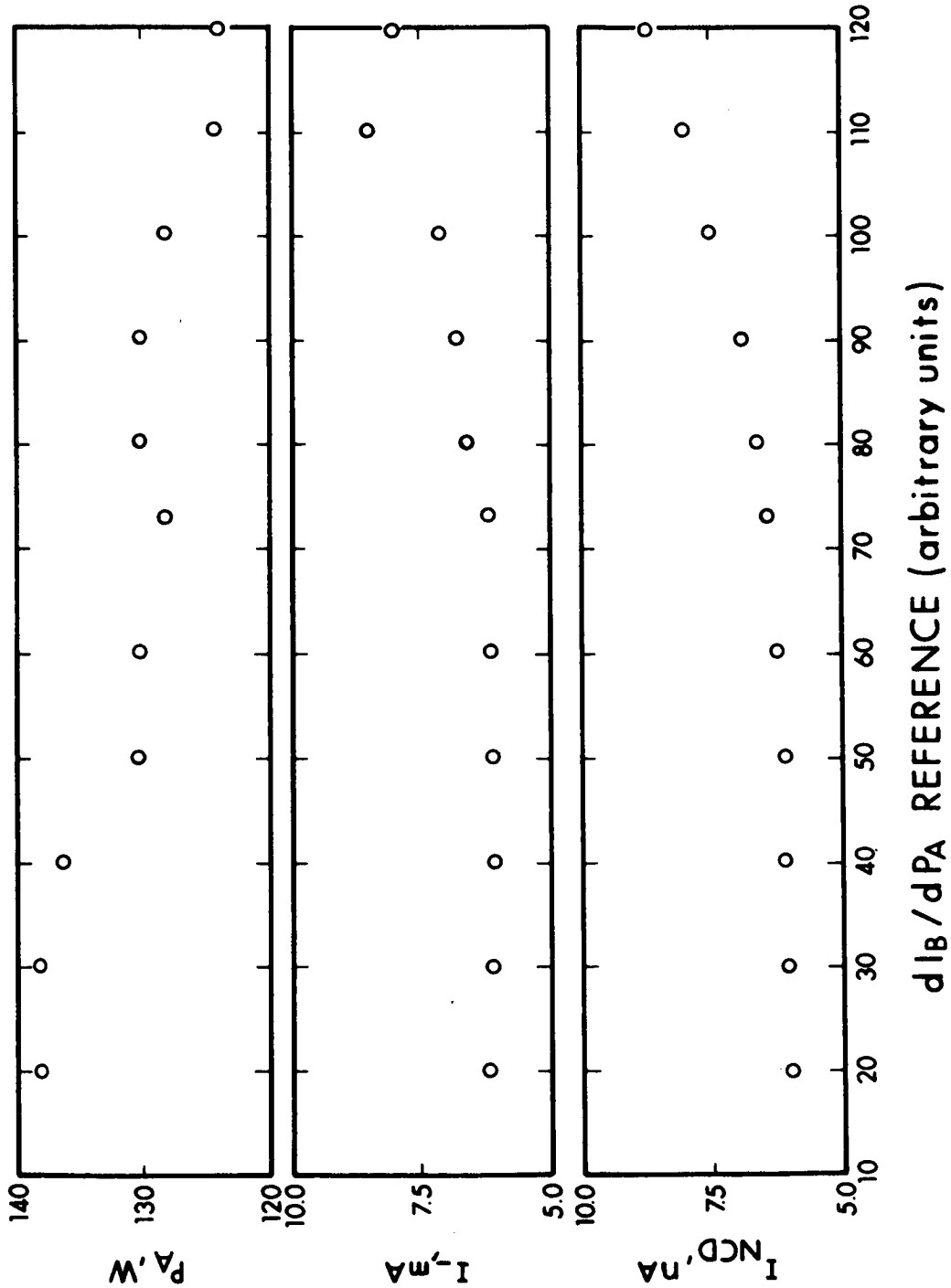

Figure 83. Initial Arc Control Operation

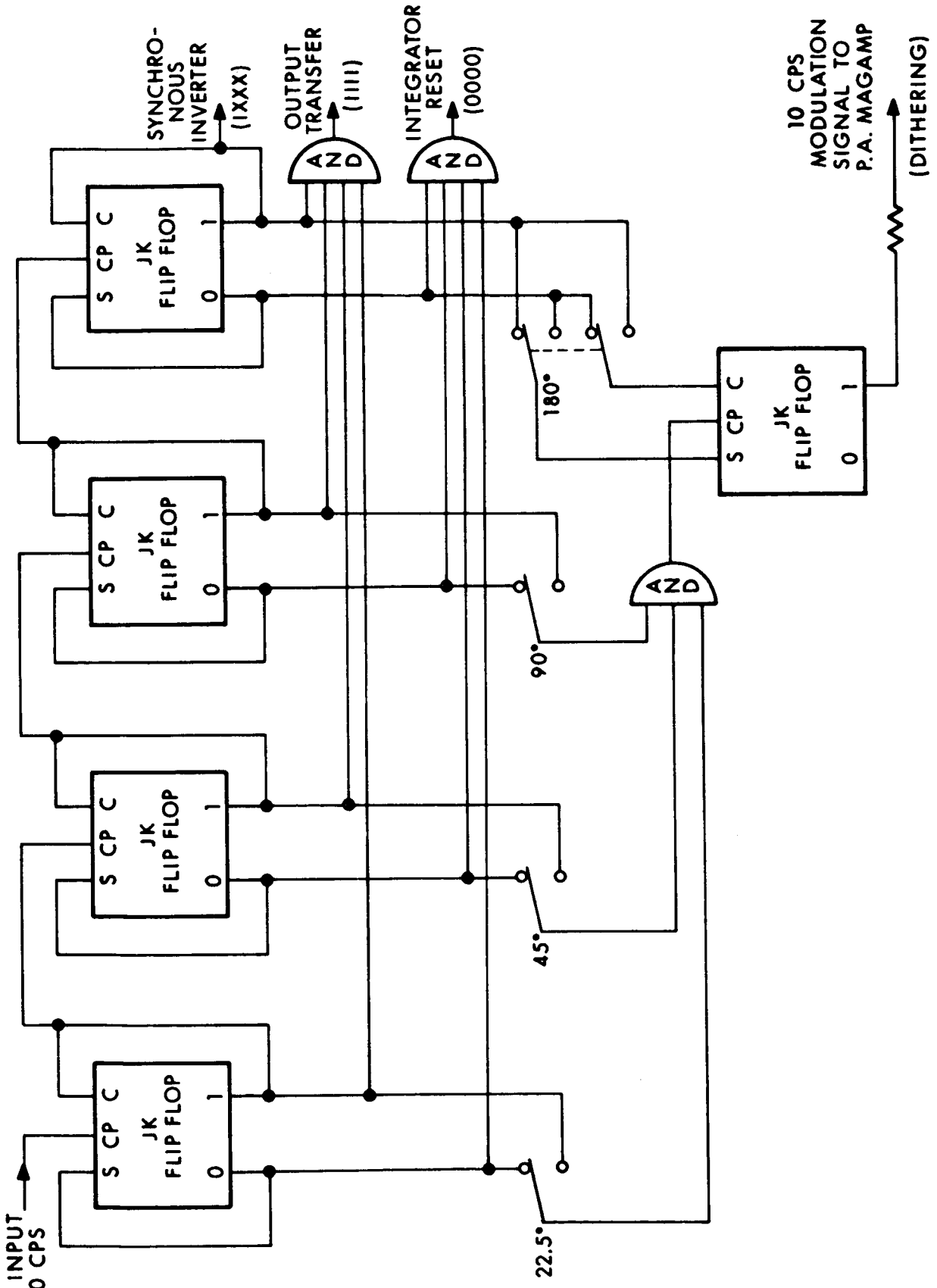

Figure 84. Digital Clock Schematic

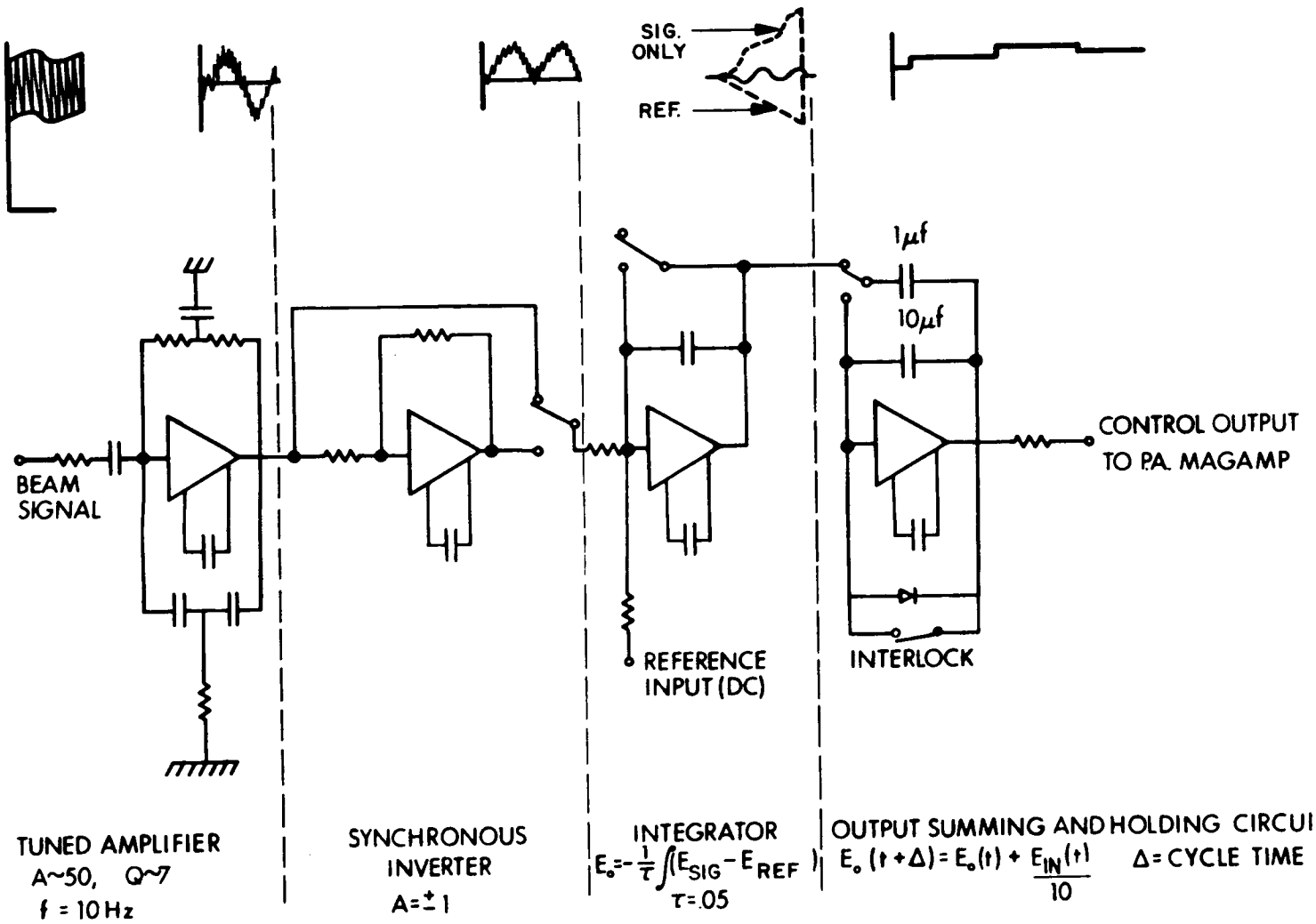

Figure 85. Synchronous Detector Comparator and Output Schematic

The engine was started manually and brought to steady-state operation before closing the discharge control loop. Once the loop was closed, five volt step changes in the dc input to the power amplifier were used to perturb the system and check its stability. Figure 86 shows the inverter input voltage and current as a function of time during one check. In this case, the voltage was raised from 50 volts to 55 volts and then dropped to 45 volts. The control loop, detecting the shift from the knee of the beam current versus discharge power curve, corrected the power by changing the pulse width from 71.5 percent to 63 percent and then to 81 percent. The power was not held perfectly constant due to the fact that the 10 cycles per second modulation signal varied the pulse width by ±1.3 percent of the half cycle time rather than the duty cycle time. This caused some reduction in the percentage discharge power change as the pulse duty cycle increased for low input voltages. The resultant reduction in the beam signal caused the control loop to reduce the power.

The input voltage, reference setting, clock frequency, and phasing were then varied one at a time while input steps were generated to test the range of control loop stability. The system was stable and held the discharge power constant to within ±2 percent for input voltages from 45 to 60 volts, reference settings over a 4-to-1 range, input frequencies from 150 to 180 cycles per second, and phase changes of ±22.5 degrees. The frequency limits were a result of the tuned input amplifier so the system was stable when the frequency and phase were varied together. For example, at a frequency of 190 cycles per second and a phase shift of 45 degrees the system was stable.

While input voltage variations were used here as perturbations to check stability, this type of variation can be expected and is accommodated easily. While not the initial object of this effort, this accommodation is perhaps as significant as the success achieved in controlling maximum overall efficiency in that it eliminates the need for line regulation.

The beam control loop reference was then set to 300 mA from 400 mA. The optimum reference setting was found to be 74 percent of the optimum reference setting for operation at 400 mA. The use of one reference adjustment for both the beam current and discharge power control loops would appear to allow simple throttling. As a final perturbation from steady state, the 100-microhenry choke was shorted out. While the discharge power increased only slightly, the accelerator drain current doubled. The engine continued to run however, and normal operation was recovered when the short was removed.

The vaporizer was then shut off until the discharge went out and the cathode heater turned on. After about ten minutes the vaporizer was turned back on and the engine restarted automatically. Recorder traces from this turn-on are shown in Fig. 87. The inverter input current was nonzero at the start because the cathode heater was on. There was also some neutral flow as shown in the third trace and some accelerator leakage current.

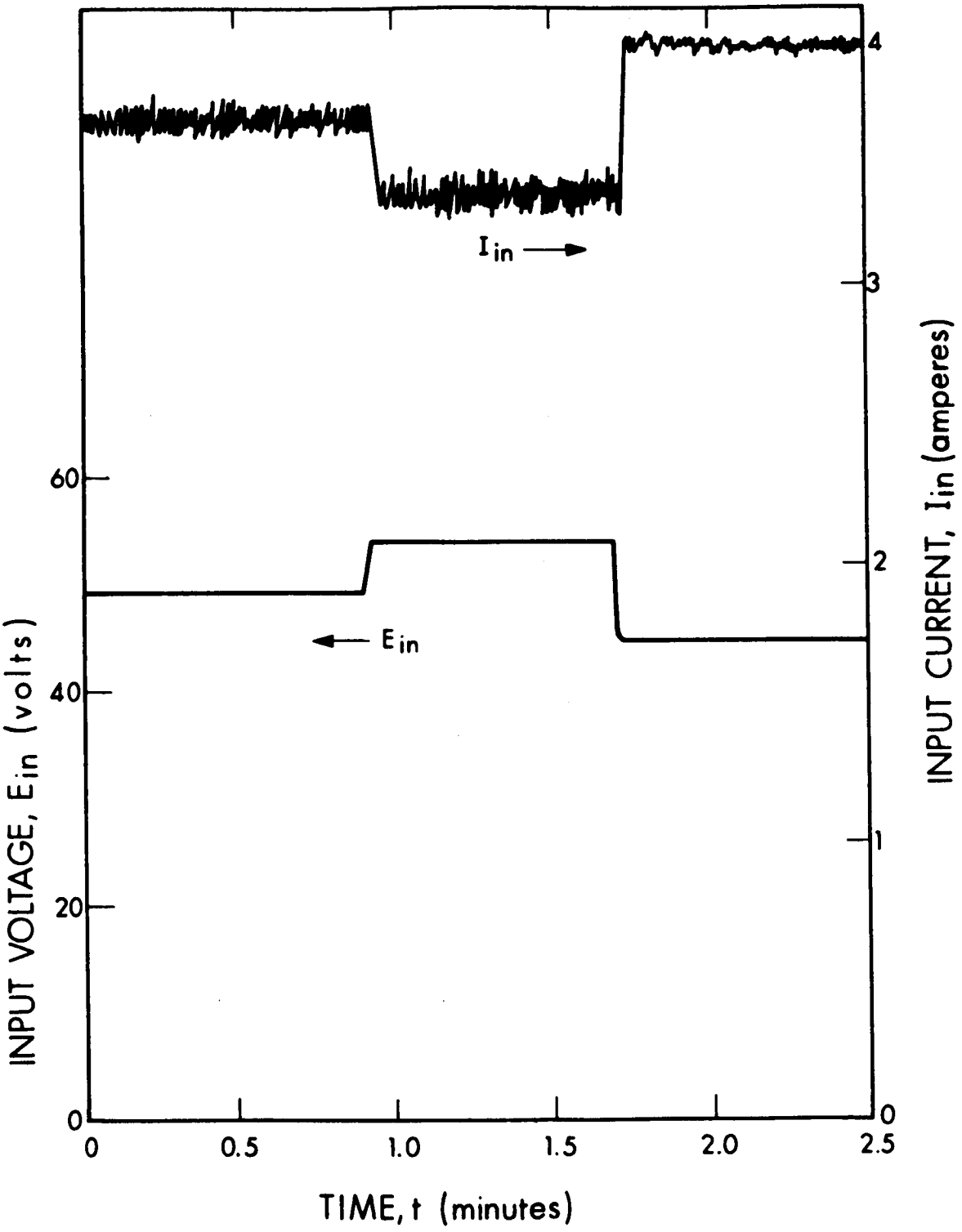

Figure 86. Response to Input Voltage Changes

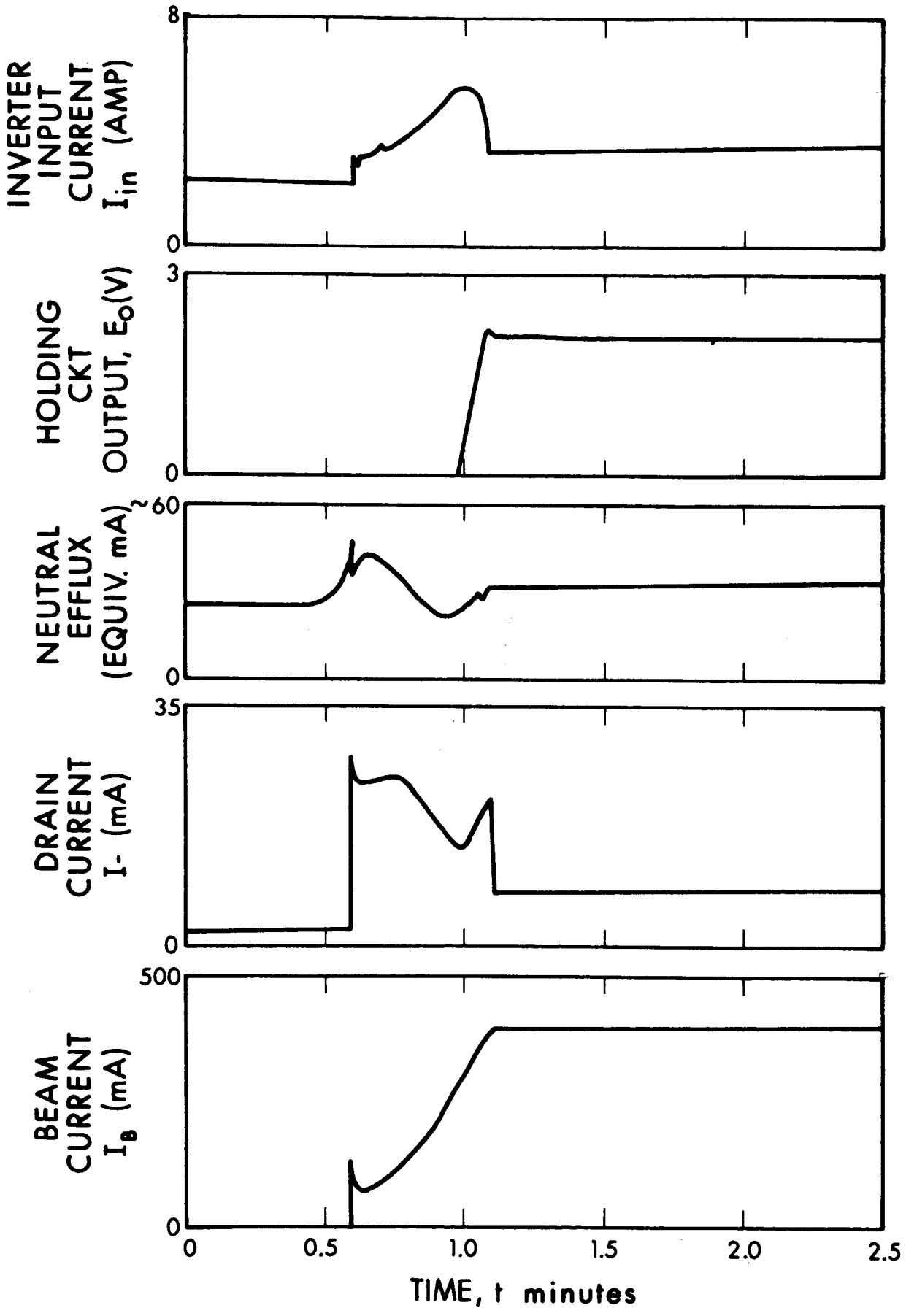

Figure 87. Automatic Startup Responses

The vaporizer was turned on at t = 0.3 minute, whereupon the flow rate began to increase as shown by the neutral efflux. At t = 0.6 minute the discharge started and the cathode heater and starting circuit turned off. At t = 1.0 minute the beam current passed 300 milliamperes causing the arc control interlock to open and at t = 1.1 minutes stable operation was achieved. Start-ups were made subsequently by heating only the cathode until thermal equilibrium was achieved before turning on the vaporizer. These starts were equally successful.

6.7 CONCLUSIONS

The efficiency of the ac discharge engine was found to be identical to that of the DG engines used on the life tests. The necessary circuitry for starting and power control was determined and a method for automatic discharge power control was developed which maintains engine operation at maximum efficiency. This control system was capable of correcting for input line voltage variations as well as shifts in engine performance. This system should be adopted for engines of this (1 kilowatt) size and larger. The value of this approach may be reduced on smaller engines where such high efficiency has not yet been shown (Ref. 10).

SECTION 7

QUALITY ASSURANCE

The quality assurance system employed to service the needs of NASA-Lewis Contract NAS3-7112 evolved during the early phases of NASA-Lewis Contract NAS3-2516 and was also utilized on NASA-Lewis Contract NAS3-5250. Close cooperation between technical and product assurance personnel resulted in a flexible, efficient system.

The system is based on extensive use of the shop traveler. Quality information pertaining to fabricated articles and assemblies is entered on the traveller while work is in process. The traveller is ultimately placed in a permanent file as a record of actual detail part history. Supplementing shop traveller information are laboratory log books containing test data, log books containing calibration records, and material certification files at receiving inspection. The shop travellers are instrumental in establishing quality criteria; engineering drawings, test procedures, material and process specifications, and their respective revisions are prepared with the aid of the accumulated quality information.

7.1 PROGRAM REQUIREMENTS

Detailed quality assurance program requirements were specified in NASA-Lewis Document QA-1a, "Quality Assurance Program Provisions for Research, Test, and Development Projects," dated 13 July 1962, in EOS Report 3670-QAP-2, "Quality Assurance Plan - Revised," dated 22 January 1963, and in the clarifications noted under Task II of the work statement for Contract NAS3-7112. A quality program plan meeting these provisions was generated at the beginning of the program. This plan (EOS Report 6954-QAP-1, "Quality Assurance Plan - Revised," dated 3 May 1965) provided the planning function for inspections and tests conducted during the contract effort. Included in the test plan were the equipment log and failure report formats used.

7.2 PROGRAM FUNCTIONS

Quality assurance program functions pertained to the overall project activity and were not intended to be accomplished by any one department or group. Specific quality obligations were imposed on organizational

elements other than the EOS Product Assurance Group which retained responsibility for the execution of product assurance policies and programs. A representative from Product Assurance was assigned to the project to work together with these other organizational elements. The representative assisted these groups in performing their quality assurance assignments. In this manner project and quality activity were continuously integrated.

Appendix A of Reference 4 describes these quality assurance program functions in detail.

7.3 PERFORMANCE

DG-3 final inspection report was prepared for the delivered thrustor system. This system included a thrustor, rack-mounted power supplies and automatic control system, a plasma bridge type neutralizer, and a zero gravity cesium feed system.

Equipment logs, including test and calibration data, were also prepared and maintained for each of the following:

DG-1 engine
DG-2 engine
40 pound feed system S/N 1
20 pound feed system S/N 1
5 pound feed system S/N 1
705210 neutralizer assembly S/N 1
705210 neutralizer assembly S/N 2
705210 neutralizer assembly S/N 3
705269 neutralizer assembly S/N 1
705269 neutralizer assembly S/N 2
1/2 pound feed system S/N 1
1/2 pound feed system S/N 2
1/2 pound feed system S/N 3
1/2 pound feed system S/N 4
1/2 pound feed system S/N 5
GFE control system S/N 1
GFE control system S/N 2

Over four hundred and fifty shop travellers were processed during the program. Quality information contained on completed travellers was reviewed. Engine and feed system drawings were revised in accordance with pertinent data contained on the travellers.

Special processing instructions were issued for the following:

a. Tungsten inert gas welding of O.F.H.C. copper.

b. Vacuum brazing of copper to stainless steel with silver-copper-nickel filler material.

c. Torch brazing of nickel or stainless steel to nickel plated mild steel heater connectors with silver-copper-indium filler material.

d. Vacuum brazing of stainless steel sheathed Tophet "C" heater wire to stainless steel with copper-nickel filler material.

e. Vacuum brazing of stainless steel to stainless steel with filler brazing alloys having melting points in the range from 700 to 1320°C.

f. Vacuum brazing of stainless steel to dissimilar materials with filler brazing alloys having melting points in the range from 700 to 1320°C.

g. Vacuum brazing of tantalum to tantalum with filler brazing alloys having melting points in the range from 700 to 2650°C.

h. Vicalloy processing.

i. Cadmium seal on DG neutralizer orifice.

j. Coil potting on feed system port valve part number 705672.

k. Preparation of coaxial heater for electron beam welding core to sheath.

The following test procedures were released:

6954-02-1)	Magnet Coil Check, Air
6954-02-2)	Cathode Check, Air
6954-02-3)	Reliability Engine Component Weights
6954-02-4)	Electrode System Check, Air
6954-02-5)	Neutralizer Inspection and Test Procedure
6954-02-6)	705221 Engine/Neutralizer System Electrical Check, Air
6954-02-7)	Test Procedure for 2000 Hour Run
6954-02-8)	Cathode Check, Air
6954-02-9)	Test Procedure for 4000 Hour Run
6954-03-1)	Feed System Assembly and Test Procedure
6954-05-01)	Programmer Electrical Check and Test (D705638)
6954-05-02)	Source Potential Control Check and Test (E705854)
6954-05-03)	Ion Source Control Check (D705853)

6954-05-04) Heater Control Check and Test (C705640)
6954-05-05) Collector Control Check and Test (C705641)
6954-05-06) Neutralizer Control (E705851) Check and Test
6954-05-07) Neutral Detector Control Check and Test (C705639)
6954-05-08) Junction Box (E705884) Wiring Check
6954-05-09) Auxiliary Rack Individual Chassis Checks
6954-05-10) Source Potential Power Supply Check and Test (E705885)
6954-05-11) Port Valve Actuator (E705887) Check and Test
6954-05-12) Engine Control System Electronic Checkout
6954-05-13) Electric Instruments Used on 6954-05 Check and Test Procedure

7.4 FAILURES

Three failures were reported during the contract period. These are summarized below.

a. On 8 November 1965, DG-2 endurance testing was terminated at 164 hours because engine performance was deteriorating. Drains had increased to 6 mA and approximately 5 arcs per hour were being observed. Upon removal from the test chamber, the accelerating electrode attachment screws were found to be loose. The electrode had slipped sideways out of alignment. These screws had not been tightened at assembly. The assembly technician involved was notified of the failure. Specific corrective action was not taken beyond the exercise of more care during assembly and checkout.

b. On 7 January 1966, an open circuit developed in the DG-2 engine cathode heater after 1045 hours. Since this heater was not required during normal operation, the test was allowed to continue. At the completion of the test the failure was found to be due to a fracture of the coaxial heater wire core. The heater wire core open circuit apparently was due to defective raw material. Print 705216, Revision C, was released, requiring heater wire x-ray per Parts Processing Instruction No. 24.

c. On 25 October 1966, 705269 S/N 1 neutralizer emission went to zero after 8100 hours operation with DG-2 engine. Foreign material, probably sputtered from the test chamber, plugged the neutralizer orifice. Further life testing will require greater care in shielding the neutralizer from chamber beam targets. No other corrective action can be taken on this failure since it was related to the ground test environment.

7.5 SUMMARY

The quality assurance program was primarily intended to support extended lifetime testing of the ion engine system. As each life test engine was being fabricated and assembled, shop travellers (consisting of work orders, purchase requests, blueprints, specifications, and inspection and test reports) were processed. In addition, all parts and assemblies were continuously identified by part and serial number in such a manner that traceability to raw material certifications was maintained. These shop travellers now serve as a permanent record of fabrication history.

Prior and subsequent to lifetime testing, all data gathering equipment was calibrated using standards traceable to the National Bureau of Standards. Critical components were weighed before and after testing in order to better evaluate deterioration trends. System checkout tests performed before and after testing were also compared.

Data were monitored at 36 second intervals on a strip chart recorder, Two channels for beam and drain current were continuously monitored on another strip chart recorder. In addition, data were manually recorded in an equipment log book by cognizant test operators at least twice daily. These equipment log books also contained pretest and posttest observations.

Particular attention was given to observed failures. As reported in Subsection 7.4 above, these failures did not seriously impair system performance. The adequacy of the quality assurance program is best indicated by the low failure rates encountered during life testing.

REFERENCES

1. H. R. Kaufman and P. D. Reader, "Experimental Performance of Ion Rockets Employing Electron-Bombardment Ion Sources," ARS Preprint 1374-60, 1960

2. Paul D. Reader, "Investigation of a 10-Centimeter Diameter Electron-Bombardment Ion Rocket," NASA TN D-1163, Lewis Research Center, 1962

3. R. C. Speiser et al, "Study of a Gas Discharge Cesium Ion Source," EOS Report No. 2120-Final, Jan 1963

4. R. C. Speiser, R. M. Worlock, F. A. Barcatta, G. C. Reid, and G. Sohl, "Ion Rocket Engine System Research and Development," EOS Report 3670-Final (NASA CR-54067), Pasadena, California, 28 Jun 1964

5. G. Sohl, G. C. Reid, F. A. Barcatta, S. Zafran, and R. C. Speiser, "Ion Rocket System Research and Development," EOS Report 4920-Final (NASA CR-54323), Pasadena, California, 30 Dec 1965

6. G. Sohl, G. C. Reid, and R. C. Speiser, "Cesium Electron Bombardment Ion Engines," J. Spacecraft Rockets 3, 1093-1098 (1966)

7. Technical Documentary Report No. APL-TDR-64-52, Vol. I, May 1964

8. A. Theordore Forrester and F. A. Barcatta, "Surface Tension Storage and Feed Systems for Ion Engines," J. Spacecraft Rockets 3, 1080-1085 (1966)

9. M. P. Ernstene, A. T. Forrester, E. L. James, G. W. Purmal, and R. M. Worlock, "Surface Ionization Engine Development," AIAA Preprint 65-375 (1965)

10. G. Sohl, V. V. Fosnight, and S. J. Goldner, "Cesium Electron Bombardment Ion Microthrustors," AIAA Preprint 67-81 (1967)